VOLUME 106 PART C NUMBER 9 MARCH 1959

The Proceedings

OF

THE INSTITUTION OF ELECTRICAL ENGINEERS

FOUNDED 1871: INCORPORATED BY ROYAL CHARTER 1921

PART C

MONOGRAPHS Nos. 310–326

SAVOY PLACE · LONDON W.C.2

Price Fifteen Shillings

The Institution of Electrical Engineers

FOUNDED 1871
INCORPORATED BY ROYAL CHARTER 1921

PATRON: HER MAJESTY THE QUEEN

COUNCIL 1958–1959

President

S. E. GOODALL, M.Sc.(Eng.).

Past-Presidents

W. H. ECCLES, D.Sc., F.R.S.
The RT. HON. THE EARL OF MOUNT EDGCUMBE, T.D.
J. M. DONALDSON, M.C.
PROFESSOR E. W. MARCHANT, D.Sc.
H. T. YOUNG.
SIR GEORGE LEE, O.B.E., M.C.
SIR ARTHUR P. M. FLEMING, C.B.E., D.Eng., LL.D.
J. R. BEARD, C.B.E., M.Sc.
SIR NOEL ASHBRIDGE, B.Sc.(Eng.).
COLONEL SIR A. STANLEY ANGWIN, K.C.M.G., K.B.E., D.S.O., M.C., T.D., D.Sc.(Eng.).
SIR HARRY RAILING, D.Eng.
P. DUNSHEATH, C.B.E., M.A., D.Sc.(Eng.).
SIR VINCENT Z. DE FERRANTI, M.C.
T. G. N. HALDANE, M.A.
PROFESSOR E. B. MOULLIN, M.A., Sc.D., LL.D.
SIR ARCHIBALD J. GILL, B.Sc.(Eng.).
SIR JOHN HACKING.
COLONEL B. H. LEESON, C.B.E., T.D.
SIR HAROLD BISHOP, C.B.E., B.Sc.(Eng.).
SIR JOSIAH ECCLES, C.B.E., D.Sc.
SIR GEORGE H. NELSON, Bart.
SIR GORDON RADLEY, K.C.B., C.B.E., Ph.D.(Eng.).
T. E. GOLDUP, C.B.E.

Vice-Presidents

SIR WILLIS JACKSON, D.Sc., D.Phil., Dr.Sc.Tech., F.R.S.
G. S. C. LUCAS, O.B.E.
SIR HAMISH D. MACLAREN, K.B.E., C.B., D.F.C., LL.D., B.Sc.
C. T. MELLING, C.B.E., M.Sc.Tech.
A. H. MUMFORD, O.B.E., B.Sc.(Eng.).

Honorary Treasurer

E. LEETE.

Ordinary Members of Council

J. A. BROUGHALL, B.Sc.(Eng.).
PROFESSOR M. W. HUMPHREY DAVIES, M.Sc.
SIR JOHN DEAN, B.Sc.
B. DONKIN, B.A.
J. M. FERGUSON, B.Sc.(Eng.).
D. C. FLACK, B.Sc.(Eng.), Ph.D.
J. S. FORREST, D.Sc., M.A.
R. J. HALSEY, C.M.G., B.Sc.(Eng.).
E. M. HICKIN.
J. B. HIGHAM, Ph.D., B.Sc.
F. C. MCLEAN, C.B.E., B.Sc.
B. L. METCALF, B.Sc.(Eng.).
J. R. MORTLOCK, Ph.D., B.Sc.(Eng.).
R. H. PHILLIPS, T.D.
H. V. PUGH.
J. R. RYLANDS, M.Sc., J.P.
D. P. SAYERS, B.Sc.
C. E. STRONG, O.B.E., B.A., B.A.I.
D. H. TOMPSETT, B.Sc.(Eng.).
H. WATSON-JONES, M.Eng.
H. WEST, M.Sc.

Chairmen and Past-Chairmen of Sections

Measurement and Control:
J. K. WEBB, M.Sc.(Eng.), B.Sc.Tech.
*H. S. PETCH, B.Sc.(Eng.).

Electronics and Communications
G. MILLINGTON, M.A., B.Sc.
*J. S. MCPETRIE, Ph.D., D.Sc.

Supply:
D. P. SAYERS, B.Sc.
*PROFESSOR M. G. SAY, Ph.D., M.Sc., F.R.S.E.

Utilization:
R. A. MARRYAT, B.Sc.(Eng.).
*J. VAUGHAN HARRIES.

Chairmen and Past-Chairmen of Local Centres

East Midland Centre:
D. E. LAMBERT, B.Sc.(Eng.).
*J. D. PIERCE.

Mersey and North Wales Centre:
J. COLLINS.
*T. MAKIN.

North Midland Centre:
J. D. NICHOLSON, B.Sc.
*A. J. COVENEY.

North-Eastern Centre:
A. T. CRAWFORD, B.Sc.
*T. W. WILCOX.

North-Western Centre:
PROFESSOR F. C. WILLIAMS, O.B.E., D.Sc., D.Phil., F.R.S.
*F. R. PERRY, M.Sc.Tech.

Northern Ireland Centre:
D. S. MCILLHAGGER, Ph.D., M.Sc.
*C. M. STOUPE, B.Sc.

Western Centre:
R. W. STEEL.
*J. F. WRIGHT.

Scottish Centre:
R. J. RENNIE, B.Sc.
*E. O. TAYLOR, B.Sc., F.R.S.E.

South Midland Centre:
J. ASHMORE.
*L. L. TOLLEY, B.Sc.(Eng.).

Southern Centre:
G. BISHOP, B.Sc.
*L. G. A. SIMS, M.Sc., Ph.D., D.Sc.

* Past Chairman.

Secretary

W. K. BRASHER, C.B.E., M.A., M.I.E.E.

Deputy Secretary

F. JERVIS SMITH, M.I.E.E.

Principal Assistant Secretary

F. C. HARRIS.

Editor-in-Chief

G. E. WILLIAMS, B.Sc.(Eng.), M.I.E.E.

THE PROCEEDINGS OF
THE INSTITUTION OF ELECTRICAL ENGINEERS

EDITED UNDER THE SUPERINTENDENCE OF W. K. BRASHER, C.B.E., M.A., M.I.E.E., SECRETARY

VOL. 106. PART C. NO. 9. MARCH 1959

DISCUSSION ON
'AN ANALYSIS OF COMMUTATION FOR THE UNIFIED-MACHINE THEORY'*

Dr. T. H. Barton (*communicated*): The unified theory appears, on first acquaintance, to be an aesthetically satisfying method of teaching the theory of rotating machines. However, in its present state of development, a number of difficulties arise, and it will be necessary, if its use in undergraduate courses is to become widespread, to develop reasonably simple approaches to the effects of magnetic saturation, the consideration of leakage inductances, which are far more reliable indicators of machine performance than the total inductances at present used, the treatment of harmonic fields and commutation. Mr. Jones, with his present paper, has admirably removed the latter item from the list of stumbling blocks.

The paper has pointed the way to the solution of a problem which has puzzled me for some time. It seems evident that the impedance of the commutator primitive should be derivable from that of the slip-ring primitive by expansion of the differentials of all products such as $i \cos\theta$ and then equating the rotor angle, θ, to zero. This, however, leads to the erroneous result given below in terms of Mr. Jones's symbols:

1	2	3	4
$R_1 + L_1 p$		$-M_1 w$	$M_1 p$
	$R_2 + L_2 p$	$M_2 p$	$M_2 w$
$-M_1 w$	$M_2 p$	$R_3 + (L_q p)$	$-2L_b w$
$M_1 p$	$M_2 w$	$-2L_b w$	$R_3 + (L_d p)$

Element 13, which gives the voltage induced in the *d*-axis field coil by rotation past it of the flux of the *q*-axis armature coil, should be zero, as should element 24, which gives the voltage induced in the *q*-axis field coil by rotation past it of the flux of the *d*-axis armature coil. Element 34, which gives the voltage induced in the *q*-axis armature coil by virtue of its rotation through the flux of the *d*-axis armature coil should correspond to the total flux L_d and not the second-harmonic component L_b, and similarly element 43 should correspond to the total flux L_q. Mr. Jones's paper makes it evident that the above dilemma arises from the inadequacy of the slip-ring primitive to represent the commutator primitive; two extra rotor coils are required corresponding to the coils undergoing commutation, as shown in Fig. A, where, for clarity, the coils undergoing commutation have been shown outside the armature.

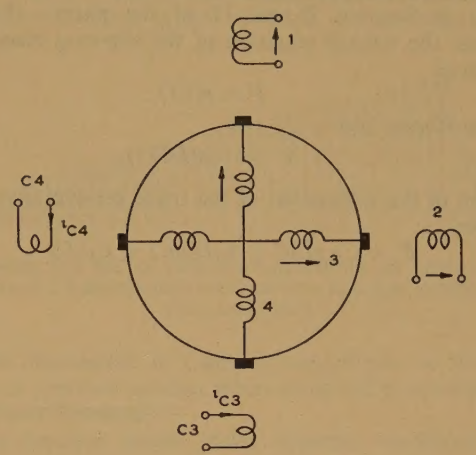

Fig. A

The change in flux provided by the current i_{c3} in the commutating coil C3 must induce a voltage of magnitude $+M_1\omega i_3$ in the *d*-axis field coil 1, thus annulling the effect of the rotation of the flux associated with the *q*-axis armature coil. Similarly, the change in flux produced by the current i_{c4} in the commutating coil C4 must induce a voltage of magnitude $-M_2\omega i_4$ in the *q*-axis field coil. So far, nothing except a change of viewpoint has been added to Mr. Jones's paper; but the next step, the consideration of the mutual interaction between the commutating coils and the main armature coils, does raise a new issue. The coil C3 induces, by transformer action, a voltage in the *d*-axis armature coil 4, whose magnitude must be, by comparison with eqn. (13), $+(L_a + L_b)\omega i_3$, and C4 must induce a voltage in coil 3 of magnitude $-(L_a - L_b)\omega i_4$. Now, although the net voltage induced in the field windings can be justifiably assumed to be zero, the size of the last two voltages is by no means obvious, unless one is prepared to derive eqn. (13) initially, and I put forward the following as a plausible but by no means ideal explanation. The transformer coupling between C3 and 1 results in a voltage $+M_1\omega i_3$ in coil 1. Since we are restricting ourselves to fundamental sinusoidal distributions, and this applies to field current sheets as well as armature current sheets, a voltage $+(n_a/n_f)M_1\omega i_3$ will be induced in

* JONES, C. V.: Monograph No. 302 U, April, 1958 (see 105 C, p. 476).

coil 4, n_a being the number of armature turns and n_f the number of field turns. Now, since M_1 is the mutual inductance between coils 1 and 4, $(n_a/n_f)M_1$ is, except for a small leakage flux, the self-inductance of coil 4, i.e. $L_d = L_a + L_b$. Hence the voltage induced in 4 by C3 is $(L_a + L_b)\omega i_3$, as deduced above from a comparison with eqn. (13). The requirement for the voltage induced in 3 by C4 may be similarly established.

Mr. C. V. Jones (*in reply*): I entirely agree with Dr. Barton that an adequate treatment of such subjects as saturation, leakage reactance, harmonic analysis and commutation, to which may be added eddy-current and hysteresis losses, is necessary before the unified-machine theory can be considered a comprehensive one. A full discussion of these subjects would, however, be out of place here.

Although Dr. Barton effectively explains the fallacy he propounds, it is instructive to consider the matter further, since the problem of the relationship between the slip-ring and commutator primitive machines is one of great interest. There are two possible approaches.

Analytically, the appropriate transformation may be used, as described in Sections 2 and 11 of the paper. Neglecting resistances, the voltage equation of the slip-ring machine may be written as

$$V = p(LI)$$

which transforms into

$$V' = C_t p(LCI')$$

Expansion of the differential of the triple product gives for the impedance

$$Z' = C_t(pL)C + C_tL(pC) + C_tLCp$$

Comparison of this impedance with that given by Dr. Barto shows that the error arises from the absence of the second tern It is therefore fallacious simply to expand the term $p(LI)$ an then set $\theta = 0$.

From the physical point of view, the component volta associated with this missing impedance is clearly provided b the reaction of the short-circuited turns. Physically, I shou prefer to derive the four-winding commutator machine accordin to the argument given in the paper with an initial slip-rin primitive of eight windings. This argument, though length would be straightforward, would include all possible interactio and would give useful information about commutation in cros field machines. Nevertheless, the ultimate elimination of th short-circuited turns would involve a process essentially simil to that given by Dr. Barton, and here I cannot understan his reluctance to make use of the result that the transform and generator voltages in the field windings are equal an opposite. This would appear to be fundamental to the pr cess of commutation, and it would seem that Dr. Barto himself uses it in deriving the voltage $+M_1\omega I_3$ in his fin argument.

For coil 1, the generated voltage is $-\omega M_1 I_3$ and the tran former voltage from the short-circuited turns is $M_{1c3}pI_c$ From Section 5.3 the sum of these voltages is zero, and the fore $M_{4c3}pI_{c3}$, which is the corresponding transformer volta in coil 4, must be equal to $+\omega L_d I_3$ if the assumptions used establishing the original slip-ring matrix are retained. Th generator voltage in coil 4 from coil 3 is $-\omega 2L_b I_3$. Additio gives for the total voltage the value $+\omega L_q I_3$. A similar analys applies to coil 3.

DISCUSSION ON 'THE DETERMINATION OF CONTROL SYSTEM CHARACTERISTICS FROM A TRANSIENT RESPONSE'*

Mr. G. Duckworth (*communicated*): Eqn. (12) may be written

$$\sum_{i=0}^{n} Y_{in}Z^i = 0$$

where Y_{in} is the cofactor of element X_{in} in the last, $(n + 1)$th, column of the square matrix of order $(n + 1)$ given by eqn. (11). If this matrix is non-singular, the cofactors are proportional t the elements of the last, $(n + 1)$th, row of the inverse matri This observation provides a method of evaluating the coefficien of eqn. (12) which may be more convenient than the evaluatio of the cofactors separately, especially if an automatic comput is available with an interpretive scheme for handling matrices.

Lanczos† discusses the limitations of this type of curve-fittin

* ELLINGTON, J. P., and MCCALLION, H.: Monograph No. 288 M, February, 1958 (see 105 C, p. 370).

† LANCZOS, C.: 'Applied Analysis' (Pitman, 1957), p. 272.

21.317.61 : 621.382

The Institution of Electrical Engineers
Monograph No. 310 M
Aug. 1958

A METHOD FOR TESTING AND ESTABLISHING THE RATING OF SEMI-CONDUCTOR RECTIFIERS UNDER DYNAMIC CONDITIONS

By J. I. MISSEN, M.Sc.

(*The paper was first received* 21*st January, and in revised form* 21*st May*, 1958. *It was published as an* INSTITUTION MONOGRAPH *in August*, 1958.)

SUMMARY

Owing to the combination of high current density and low forward oltage drop in the rectifying junction of a semi-conductor rectifier, ie physical size and thermal capacity for a given rating are low, so iat the current on overload can be much greater than for other types f rectifier. Consequently, the junction-temperature rise on overload extremely rapid, and in some cases considerable temperature uctuations occur at mains frequency. It is therefore necessary to e able to monitor the junction temperature dynamically (i.e. under orking conditions at mains frequency) and to observe the rise of emperature with time. A further necessity for dynamic testing occurs nce the measurement of the forward characteristic at high current y d.c. methods can result in excessive heating and possible failure. n the apparatus to be described the separation of forward and reverse alf-cycles is secured by means of a synchronous commutator, permitting independent measurement of forward and reverse current and oltage at mains frequency, and hence continuous indication of unction temperature. Operation of the rectifier at full rating without xpenditure of the full power necessary to accomplish this by direct ethods is also possible. This is particularly useful in life testing rge numbers of semi-conductor rectifiers. Limited experience indiates that this method of testing provides operating conditions which are all ways identical to those which a device experiences under full-oad conditions.

LIST OF SYMBOLS

R_L = Load resistance.
θ = Thermal resistance.
ψ = Conduction angle.
T_j = Junction temperature.
T_A = Ambient temperature.
R_F = Forward slope resistance.
P_D = Power dissipation in a rectifier due to forward current flow.
P_R = Power dissipation in a rectifier in the reverse half cycle.
P_0 = Power dissipated by the cooling system.
V_0 = Maximum forward voltage drop for zero forward current.
V_M = Mean forward voltage drop.
I_M = Mean rectified current.
I_P = Peak current.

(1) INTRODUCTION

During recent years the *p–n* junction diode, first in germanium nd secondly in silicon, has developed into a rectifying device of ajor importance. One of its main attractions is its high ficiency, and this, coupled with the fact that the diode can ndle large current densities, has meant that the area of the ctive junction itself is often very small. The extent to which e designer can take advantage of this feature depends largely n the thermal characteristics of both the junction itself and its sociated heat sink. It is therefore very desirable when assessg the potentialities of a given device to be able to apply tests which simulate, as closely as possible, those which will occur in actual use. It is particularly important that the capability of the rectifier to withstand current overloads should be examined in this way, since there are few applications where no overloads occur. Because the area of a junction for a given rating is often comparatively small, its thermal capacity may also be small, and a large transient overload can cause the temperature at the junction to become prohibitively high, sometimes with disastrous consequences.* As a typical example, the envelope in Fig. 1

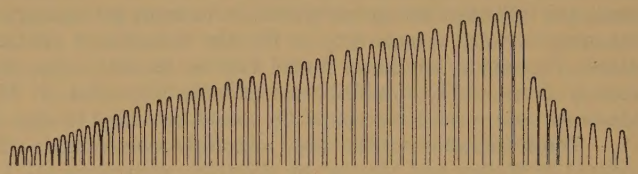

Fig. 1.—Rise and fall of junction temperature on application of a short (1½ sec) current overload to a junction rectifier.
Pulses are at 50 c/s.

shows the fluctuation in junction temperature at 50 c/s for a germanium junction rectifier when subjected to a current overload of short duration.

Testing junction diodes under dynamic conditions is considerably simplified by the fact that both the forward and reverse characteristics vary with the temperature at the rectifying junction, which is usually the most critical part. These variations can be studied at leisure using an oven, hot-plate or oil bath to provide known variations of temperature in the rectifier; in this way the diode can be calibrated and used as its own thermometer. The problem of dynamic testing is then reduced to measuring one of these temperature-sensitive characteristics while the diode is being subjected to conditions which simulate those expected in actual operation. Dynamic testing also shows advantages in making measurements at high currents which might not be possible with direct current, owing to overheating of the semi-conductor junction.

However, apart from the necessity for dynamic testing as a result of the properties of semi-conductor devices, certain dynamic methods have intrinsic advantages. Various methods spring to mind. In general they depend on isolation of the forward and reverse half-cycles by diode circuits or by connecting two synchronous sources of power to the rectifier. The problem then becomes one of measuring the voltage and current at suitable points during the appropriate half cycle.

The basic diode measurement circuit is shown in Fig. 2. If D_1 is the diode under test, V is the applied alternating voltage and R_L is the load resistance, D_1 functions in a half-wave circuit with resistive load. Forward current passes through D_2 and reverse current through D_3. Thus the meter measures the mean reverse current, I_R, and hence the mean junction tempera-

Correspondence on Monographs is invited for consideration with a view to ublication.
The paper is a communication from the Staff of the Research Laboratories of The eneral Electric Company Limited, Wembley, England.

* MORTENSON, K.: 'Transistor Junction Temperature as a Function of Time', *Proceedings of the Institute of Radio Engineers*, 1957, 45, p. 504.

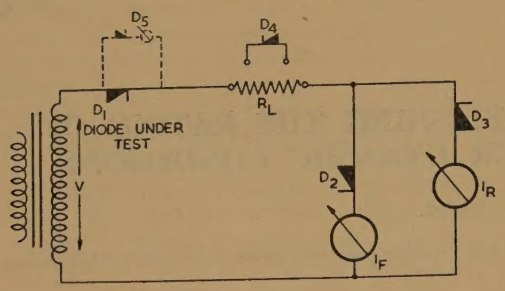

Fig. 2.—Simple dynamic test.

ture for a given mean rectified current I_F. Calibration of junction temperature against mean reverse current is effected by placing D_1 in an oven of known temperature and replacing R_L by D_4 to prevent the flow of forward current. I_R can then be plotted against oven temperature.

The simple circuit possesses several limitations. Thus, if D_2 warms up appreciably, owing to the flow of the forward current of D_1, its reverse impedance may shunt the reverse-current measuring circuit appreciably and introduce errors. The second limitation is the fact that no provision can be made for measuring the mean forward voltage drop in D_1; the inclusion of another diode, D_5, and a voltmeter would not be feasible, since the voltage drop in D_5 would be comparable with that in D_1. Moreover, the reverse current of D_5 would be added to that of D_1. These limitations have been elegantly overcome in the method of Walker and Martin* by effectively converting D_2, D_3 and D_5 to perfect diodes by use of electronic feedback techniques. The modified apparatus provides accurate results but suffers from several limitations of the basic circuit.

Peak inverse voltage and mean rectified current tend to be interdependent, since adjustment of R_L when a high current is to be passed is not readily performed. Variation of the applied alternating voltage to adjust the rectified current involves recalibration of the reverse current against junction temperature, since the reverse current varies somewhat with reverse voltage. The power consumption in testing large rectifiers is considerable, since a high peak inverse voltage and large rectified current require a large power input.

In the method to be described it was found possible to arrange that a semi-conductor device capable of providing a large power output could be tested at full rating without the expenditure of the power necessary to accomplish this by a direct method. The new method is very appropriately called a 'cheater' technique for reasons which will become clearer from the description to follow.

Since multiple switching operations were contemplated it was considered that the 'perfect diode' was best obtained by rather simpler methods, involving mechanical switching. Thus the advantages of the method described by Walker and Martin* were obtained, together with considerable economies in power consumption.

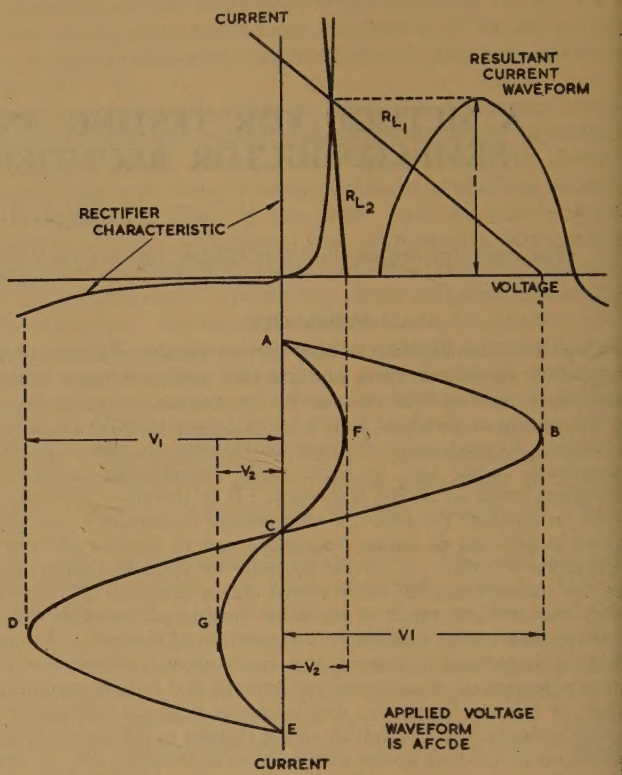

Fig. 3.—Graphical operation of the cheater circuit.

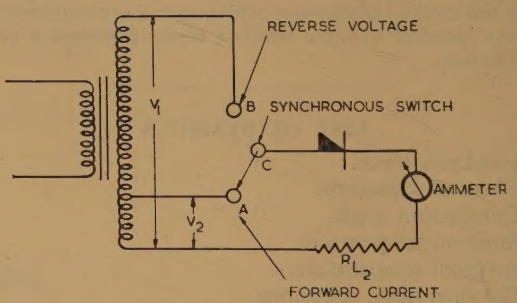

Fig. 4.—Simplified cheater circuit.

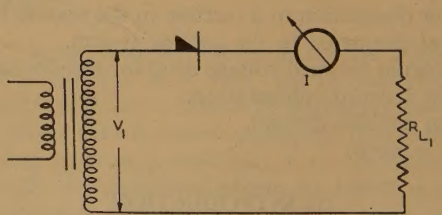

Fig. 5.—Direct half-wave circuit.

(2) PRINCIPLE OF OPERATION OF THE CHEATER CIRCUIT

By reference to Figs. 3–5, the principles of operation of a cheater circuit may be considered.

For normal half-wave operation of a diode into a resistive load, R_{L1}, as shown in Fig. 5, a voltage ABCDE of peak amplitude V_1 is applied, a current I flows, and a peak inverse voltage V_1 is applied as shown graphically in Fig. 3. The same current would flow if a voltage of lower amplitude, V_2, were applied via load resistance R_{L2}. However, the peak inverse volta would then be only V_2.

In the cheater circuit the voltage waveform AFCDE is appli to the rectifier via load R_{L2}. Hence the rectifier is run at f rated conditions of forward current and peak inverse voltage f the expenditure of a relatively small amount of power. In ord to achieve these operating conditions, the rectifier must switched synchronously from low voltage in the forward dir tion to high voltage in the reverse direction.

Fig. 4 gives a simplified diagram of a cheater circuit. If t switch makes contact at A when this point is changing throu

* WALKER, A., and MARTIN, R.: 'Dynamic Methods of Testing Semi-Conductor Rectifier Elements and Power Diodes', *Electronic Engineering*, 1957, **29**, p. 220.

zero to positive potential with respect to the lower end of the winding, the rectifier will pass current in the forward direction, of magnitude dependent on the circuit resistance and applied voltage. Since the only resistance is that due to the diode forward resistance, the ammeter and R_{L2}, the full rated current will flow for a low applied voltage.

As the polarity changes to negative, the switch changes over to the other contact, B, and connects a high voltage in the reverse direction to the diode. This can be made equivalent to the peak inverse voltage V_1. Thus the diode operates at full rating for a power requirement of only V_2/V_1 times the power requirement by the direct method.

Since V_2 need be only a few volts and V_1 is frequently several hundred, a considerable saving in power results. It will be seen that in its simplified form the cheater circuit isolates forward and reverse currents of the rectifier under test and allows independent adjustment of V_1 and V_2. Hence it satisfies the requirements of flexibility, power economy and independent measuring facilities for forward and reverse half-cycles.

(3) SYNCHRONOUS SWITCHING

Of the more readily available switching mechanisms, three types were considered, namely synchronous contactors, ignitrons or thermionic valves and synchronous commutators. Methods using contactors or large relays are possible, since they are essentially contact-rectifier developments, but preliminary investigation indicated that there might be considerable difficulty due to phase errors and contact bounce, and it was not considered desirable to expend the necessary development time.

It is probable that small mercury-arc rectifiers and such devices would function very well as switching elements in a pure cheater, but if measurement of the mean rectifier forward voltage drop is required, they must be rejected because of their arc drop of 10–15 volts.

The third system considered, which is shown in Fig. 6, uses a

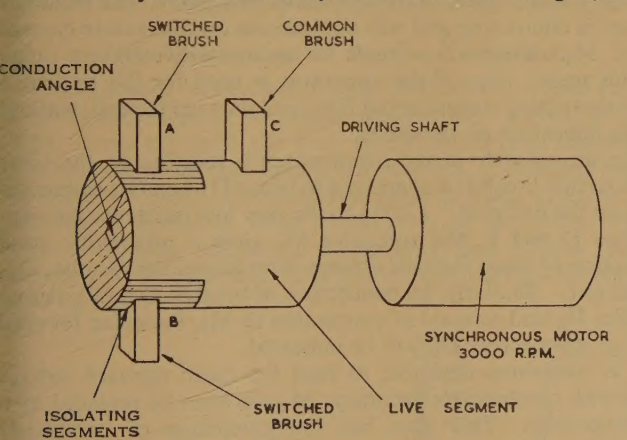

Fig. 6.—Synchronous commutator.

synchronous commutator. This is rotated at 3000 r.p.m. by a synchronous motor and has a live segment which connects the common brush, C, to brushes A and B in turn. By suitable phasing, C is connected to A during a portion of one half-cycle of power supply, and to B during the other half-cycle.

Several methods of commutator construction were tried. Probably the simplest and most convenient consists of four standard commutators such as those used for small d.c. motors, mounted on a common shaft as shown in Fig. 7. By appropriate interconnection of segments on a commutator and cross-connection to segments of an adjacent commutator, the basic design in Fig. 6 may be produced. This has the added facility

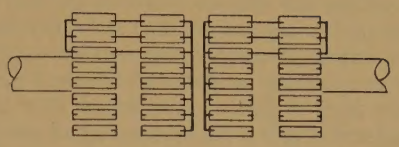

Fig. 7.—Commutator interconnections providing double-pole change-over switching.

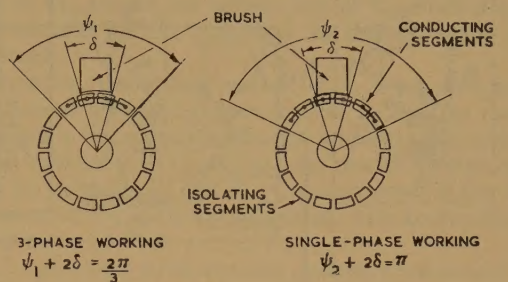

Fig. 8.—Method for adjustment of conduction angle.

of permitting simple variation of conduction angle by connection of the appropriate number of segments. This is represented diagrammatically in Fig. 8, which shows the allowance necessary for the brush width. The method has been adopted in practice with considerable success, and operational experience has shown the choice to be justified in its simplicity and reliability.

(4) THE COMPLETE APPARATUS UTILIZING COMMUTATOR SWITCHING

The basis of the apparatus is the commutator, which normally functions as a double-pole synchronous change-over switch. By suitable connection to the brushes, the following facilities are available:

(*a*) Measurement of mean reverse current, rectified current, peak inverse voltage and mean forward voltage drop.
(*b*) Measurement of junction temperature from prior calibration and observation of mean reverse current or mean forward voltage drop.
(*c*) Rise of junction temperature with time to simulate overload conditions and assess the current overload protection requirements for a rectifier. Observation of thermal runaway.
(*d*) Display of rectifier characteristics under dynamic conditions. Thermal-resistance measurement.
(*e*) Independent life-test operation of a number of rectifiers under full rating conditions at low power consumption.

Since much of the circuit is common to all measurements, it will be described fully in Section 4.1.

(4.1) Measurement of Mean Reverse Current, Rectified Current, Peak Inverse Voltage and Mean Forward Voltage Drop

For purposes of explanation the simplified cheater circuit in Fig. 4(*a*) is shown applying forward voltage via contact A and reverse voltage via contact B. In the actual circuit which was used (Fig. 9), it was found possible to test two rectifiers simultaneously by applying forward voltage only, via the commutator. In operation, the common brush C is connected to brushes A and B in turn, hence connecting the transformer winding to diodes D_A and D_B in turn. If the phasing is correct, D_A will be connected to the transformer, T_1, as the voltage is changing to positive, so that it will conduct in the forward direction. The load R_{L3} acts as a shunt for the ammeter, and is such that the non-linearity of the diode's forward characteristic is swamped, and the current waveform is effectively sinusoidal, although the power dissipation is still low.

When the voltage from T_1 is changing to negative, D_B is con-

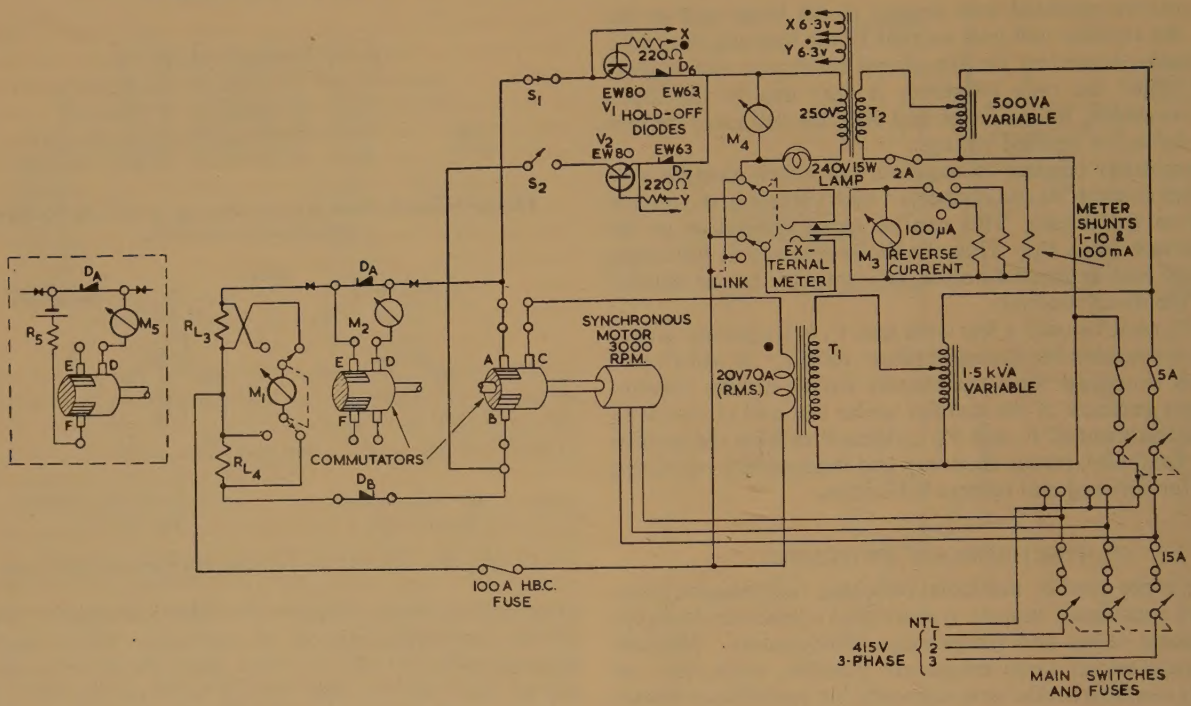

Fig. 9.—Complete circuit for measurement of rectified current mean forward voltage drop, mean reverse current, and peak inverse voltage.

The inset circuit shows the modification required for measuring the junction temperature from the forward characteristic of the rectifier under text.

nected via the commutator and brushes C and B, and passes forward current. Since R_{L4} is of the same order as R_{L3}, the forward currents of D_A and D_B will be almost equal, although the forward characteristics may differ markedly. Rectified current measurement is made by switching a moving-coil d.c. meter M_1 across R_{L3} or R_{L4}. The current is adjusted by a variable auto-transformer feeding T_1.

When D_B is conducting in the forward direction, brush A is running on isolated segments. Reverse voltage may be applied to D_A from the secondary winding of T_2, whose voltage is also adjustable. When reverse voltage is applied to D_A, its reverse current passes through D_6 in the forward direction, and in the event of a breakdown in D_A, current limitation is provided by a tungsten-filament lamp. Owing to the temperature coefficient of resistance of the lamp filament, it provides little limitation at low current and hence does not mask 'runaway' effects. It will be noted that, owing to the phasing of T_1 and T_2 and the directions of D_6 and D_7, reverse voltage is held off from the rectifier which is conducting in the forward direction. However, when a rectifier under test is conducting in the forward direction and the secondary voltage of T_2 is low, it is possible for a small current to flow through its hold-off diode in the forward direction and produce an apparent reverse current. Transistors V_1 and V_2 have been introduced as switching devices which open-circuit the rectifier reverse circuit when the rectifier under test is conducting in the forward direction and thus prevent the flow of this apparent reverse current. The transistors are switched by applying a small alternating voltage via current-limiting resistors between emitters and bases. They are not subjected to the full reverse voltage, since the hold-off diodes in series are of higher reverse resistance and receive a larger share of the reverse voltage. The reverse leakage current is defined by D_6 and D_7, which are small-area silicon junction diodes. Apart from the necessity for their breakdown voltages to exceed the maximum peak inverse voltage of the circuit, their specification is not stringent, since any reverse leakage current will not materially affect the forward current of the rectifier under test, into which it flows.

Switches S_1 and S_2 are provided for isolation of a given reverse voltage circuit, since, if both circuits are made, the resultant current is alternating and will not indicate on the reverse current meter, M_3. Provision is made for an insensitive current range on this meter, since if the apparatus is used for life testing, a large alternating current could flow, and damage the coil, without giving indication on the meter.

The second pole of the commutator is rotating on the same shaft, so that brush E is connected to brush D when C is connected to A on the first pole. Owing to the very low resistance between brushes D and E, the voltmeter M_2 gives a reasonably good indication of mean forward voltage drop across the rectifier, D_A under test. Similarly, by connection of brushes D and F across rectifier D_B and reversal of connection to M_2, the mean forward voltage drop across D_B will be indicated.

It is sometimes desirable to read the mean forward voltage drop with considerable accuracy; M_2 can then be replaced by a potentiometer. This also has the advantage of completely eliminating contact-resistance errors.

The measurement of peak inverse voltage is possible by multiplication of the reading of M_4 by a suitable factor. It may be obtained more accurately by connecting a peak voltmeter across rectifier D_A via brushes D and F or across D_B via brushes D and E.

In order to ensure that the commutator is in phase with the applied voltage waveform, provision is made for selecting the a.c. supply to the transformers T_1 and T_2 between any phase and neutral of the incoming 3-phase supply for the motor. By this means, rough control of phasing is obtained in 60° steps. Fine control of phase is provided by rotation of the motor field with respect to the brushes by rotating the stator, which is fixed in a cradle. The fine phasing mechanism is shown in Fig. 10

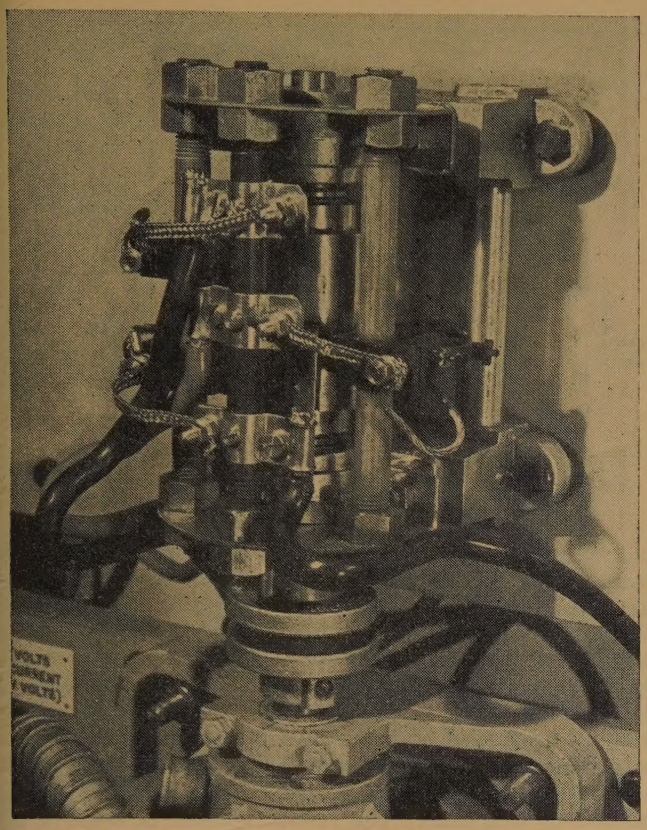

Fig. 10.—Commutator phasing mechanism.

Thus the apparatus in its basic form permits measurement of rectified current, peak reverse voltage, mean reverse current and mean forward voltage drop on two diodes simultaneously.

(4.2) Measurement of Junction Temperature

For a number of semi-conductor rectifiers the reverse current is sufficiently large to be readily measurable. Since this parameter varies exponentially with temperature, prior calibration of mean reverse current against temperature, at constant reverse voltage in an oven, allows determination of mean junction temperature in operation from observation of the mean reverse current. Typical variations of forward and reverse characteristics with temperature for a germanium junction rectifier are given in Fig. 11.

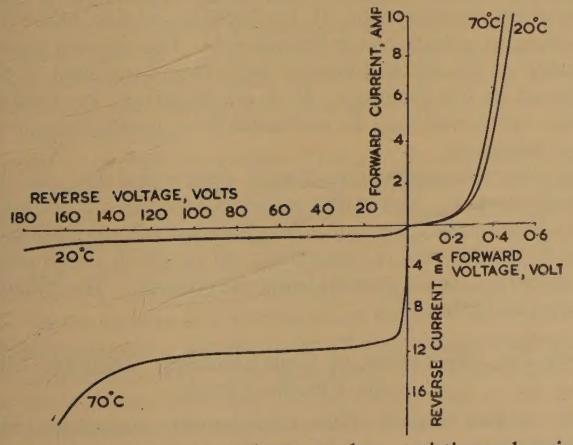

Fig. 11.—Typical forward and reverse characteristics and variation with temperature.

However, in some rectifiers, notably the smaller silicon types, the reverse current is less than the leakage and capacitive currents of the apparatus and may only amount to several microamperes. In these cases it is preferable to rely on the variation of the forward characteristic with temperature. This is most simply accomplished as shown in the inset circuit in Fig. 9; brushes D and F are connected in series with a low-current moving-coil meter, resistor R_5 and rectifier D_A during the 'off' half-cycle. Since the forward characteristic varies with temperature, prior calibration of the reading of M_5 against the temperature of D_A when it is heated in an oven will provide a method for measuring the junction temperature.

In operation the rectified current of D_A is adjusted by means of the variable auto-transformer feeding T_1, and the reading of M_5 is noted in order to determine the junction temperature from the oven calibration. In this test the reverse voltage circuit is opened via switches S_1 and S_2. Measurement of the junction temperature of D_B follows similar lines, with appropriate brush connection.

This is not strictly a full dynamic method, since reverse voltage is not applied to the rectifier under test. However, in view of the useful results which were obtained, it was not considered necessary to modify the circuit to permit the application of full dynamic conditions.

(4.3) Rise of Junction Temperature with Time and Controlled Thermal Runaway

As a consequence of the very small thermal capacity of semi-conductor devices, their rise in junction temperature with time is very rapid compared with other devices. In order to ensure that they will be protected against current overload, it is necessary to measure the rise of junction temperature with time and to compare the resulting curve with the graph of prospective current against breaking time for the protective element. Since appreciable cooling of the junction can occur in a small fraction of a second, dynamic methods are essential.

By employing the standard cheater technique for measuring junction temperature, using the change in either reverse or forward current, junction-temperature rise with time can be plotted. For time intervals in excess of several seconds, a stop-watch can be used. In order to resolve shorter time intervals, a photographic record of the oscillograph trace of the calibrating current can be taken. Time calibration is inherent, since the waveform has a fundamental frequency of 50 c/s.

Typical curves of junction-temperature rise against time for a given rectified current are shown in Fig. 12, and derived isothermals of rectified current against time for a given junction-temperature rise are given in Fig. 13. A similar curve for an h.b.c. protective fuse is superimposed. The intersection of the fuse characteristic and junction-temperature isothermal indicates the junction-temperature rise before the circuit is broken, the

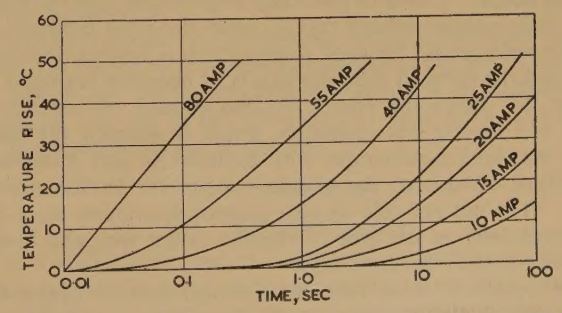

Fig. 12.—Variation of junction temperature with time for dynamic operation.
Current values are for half-wave operation.

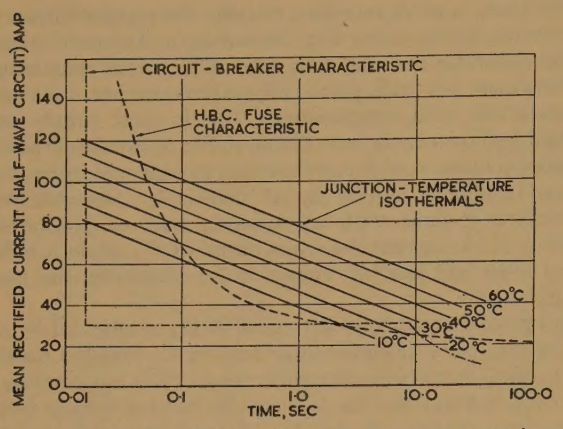

Fig. 13.—Variation of rectified current with time for a given junction-temperature rise, and comparison with curves of breaking time for protective devices.

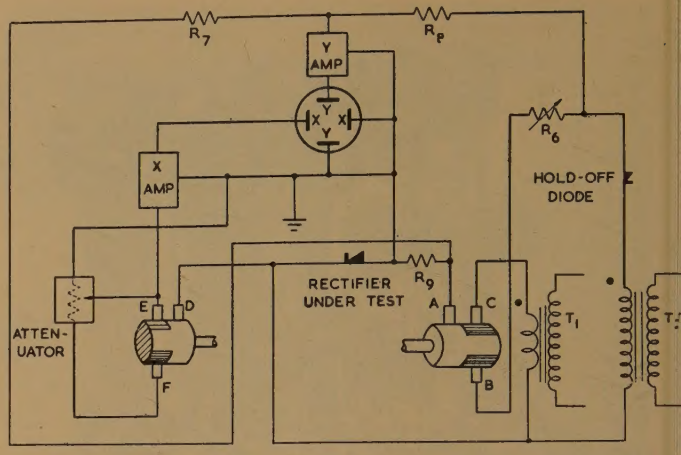

Fig. 14.—Circuit for the display of rectifier characteristics under dynamic conditions with forward voltage expansion.

current flowing and the time for breaking. Although the isothermals given in Fig. 13 follow a straight-line law, this need not be the case. The curves may be adapted to show the excess junction-temperature rise over that produced by the maximum continuous rated rectifier current. In this way they can be used to indicate to the circuit designer whether a given current overload protection device is adequate to maintain the junction temperature within safe limits in the event of overload.

Thermal runaway due to excessive reverse dissipation is a well-known phenomenon in semi-conductor devices, and limiting conditions are readily calculated. It may be further shown (see Section 6.1) that the conditions are less onerous if a limiting resistance is in series with the applied reverse voltage. Since forward and reverse half-cycles are isolated in the cheater, resistance is readily added, and runaway condition is displayed by a large increase in reverse current beyond a given reverse power dissipation.

(4.4) Display of Rectifier Characteristics under Dynamic Conditions and Thermal Resistance Measurement

One disadvantage of the typical oscillograph display of voltage/current characteristics for a semi-conductor rectifier is that the characteristics relate only to the rectifier at some given ambient temperature when it is passing only the small current necessary for the oscillograph display. It does not display characteristics when the device is working at full rating, or on overload, when the current density and peak junction temperature may be very high.

The cheater circuit is simply adapted to this latter requirement. Furthermore, by utilizing the second commutator, the trace can be expanded to display a forward characteristic in greater detail. This is of particular importance with rectifiers of high peak reverse voltage rating, when the ratio between peak inverse voltage and forward voltage drop is several hundred to one, and the forward characteristic is of necessity cramped.

Fig. 14 shows the circuit for the display of rectifier forward and reverse characteristics, which is adapted for display on a standard oscillograph with built-in X- and Y-deflection amplifiers. Much of the circuit is common to the previous tests. It is not possible to give component values, since these are dependent on the type of rectifier under test, and also the available gain of the amplifiers.

The operation is as follows: Forward current passes when brushes A and C are connected. The forward voltage across the rectifier under test, D_A, will appear at the input to the X-amplifier via brushes D and E of the second commutator, and will produce an X-deflection corresponding to the amplifier gain setting. The flow of forward current produces a p.d. across R_9 and the voltage will be amplified by the Y-amplifier via R_7 and will produce a Y-deflection on the tube face. Hence the forward rectifier characteristic will be drawn on the face of the tube to a scale dependent on the amplifier gain settings. In the other half-cycle, reverse voltage is applied to the rectifier from T_2 via R_6 and brushes A and B while brushes D and F are connected. Thus reverse voltage across the rectifier is applied to the attenuator before passing through the X-amplifier and is reduced in amplitude. The reverse current develops a p.d. across R_6 and R_9 which is applied to the Y-amplifier via R_8. Thus the reverse characteristic is drawn.

It will be seen that the first commutator fulfils the function of separating forward and reverse half-cycles, while the second commutator acts as a synchronous short-circuit across the attenuator. By this means the forward and reverse current and voltage may be independently adjusted by the four controls provided by X-gain, Y-gain, attenuator setting and R_6 setting.

The attenuator should present a high impedance, since it shunts the rectifier under test when it is biased in the reverse direction. R_7 and R_8 are to prevent mutual interaction between forward and reverse current deflections at the input to the Y-amplifier. It is important that the commutator should conduct for 180° in order to display the full characteristic. The X- and Y-amplifiers should preferably be d.c.-coupled.

Although the measurement of thermal resistance more properly belongs to Section 4.2, it is included here since a knowledge of the forward characteristic of the rectifier is also required; its measurement is described in Section 4.4. The thermal resistance is defined as the rise in junction temperature per watt of power dissipated in the junction. It is an important parameter for rectifier rating and may be evaluated from measurements taken on the apparatus.

The junction-temperature rise is determined by one of the methods quoted. Power dissipation is calculated from a knowledge of the rectified current, mean forward voltage drop and the shape of the forward characteristic, all of which parameters are available from measurements using the cheater. The calculation is shown in Section 6.2.

(4.5) The Life-Testing of Semi-Conductor Rectifiers Using the Cheater Circuit

The cheater circuit offers considerable advantages in life testing large numbers of high-power rectifiers, since the saving in power becomes attractive. Fig. 15 shows the modification

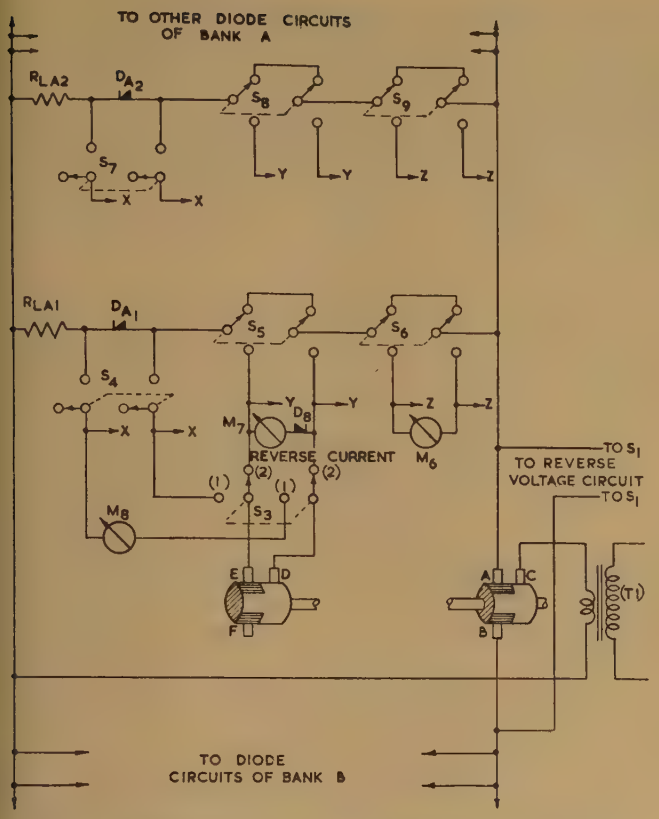

Fig. 15.—Circuit for the quantity life-testing of semi-conductor rectifiers.

to the circuit which permits the monitoring of rectified current, reverse current and forward voltage drop for each individual rectifier. The diodes are run in two banks corresponding to brushes A and B, and utilize every forward half-cycle in the same way as the single rectifiers in the test described in Section 4.1. In a given bank the diodes are effectively in parallel, although each is provided with its own load to ensure that forward-current sharing is secured. By use of the second pole of the commutator, independent measuring facilities are available.

The circuit in Fig. 15 shows the switching arrangements for two rectifiers of bank A. All circuits are identical for a given bank, and the complete parallel combination corresponds to rectifiers D_A or D_B in Fig. 9. Since the circuits are identical in bank B, apart from slight phasing modifications, they are not shown. Common busbar connections are lettered XX, YY, etc. The common circuit is as given in Fig. 9, with the modification that the current-limiting lamp of the reverse-voltage circuit is short-circuited, and the common reverse-current meter is switched to an insensitive range.

In order to explain the action of the circuit, consider measurements on rectifier D_{A2} (Fig. 15). When S_3 closes to the contacts marked (1) and S_7 connects D_{A2} across busbars XX, meter M_8 will read the mean forward voltage across D_{A2} via brushes D and E. If S_3 is then closed to the contacts marked (2) and S_8 is operated to YY, the forward current for D_{A2} will pass through D and E. In the reverse direction they will be open-circuited by the commutator rotation, and the mean reverse current through D_{A2} will be indicated by M_7. The possibility of a reverse deflection on M_7 arising from the small potential difference across D and E due to the flow of forward current is obviated by D_8.

Mean-forward-current indication is provided by operation of S_9, which connects M_6 in the circuit of D_{A2}. This measurement can be made simultaneously with that of mean forward voltage drop or mean reverse current. Switches S_7–S_9, etc., are biased to the non-operative condition shown, in order that only one diode is measured at a time. The meters, M_6, M_7 and M_8 are all of the moving-coil d.c. type.

The total number of rectifiers which may be tested per commutator by this method is obviously dependent on both commutator size and rectifier rating. However, it has been found that this method will operate satisfactorily in testing medium-power rectifiers at full rating, with only 10% of the power which would be required in testing under conventional circuit conditions.

The circuit which has been described is one of several commutator methods which are suitable for life-testing large numbers of rectifiers. For example, one commutator may be used for applying a cheater technique solely to a large number of rectifiers in parallel. Measurement facilities are then provided by switching the rectifier to be tested to a single circuit similar to that described in Section 4.1, and with comparable operating conditions to those provided by the main commutator circuits. Alternatively, multiple-segment commutators with a separate brush for each rectifier under test will also provide independent measuring facilities.

(5) CONCLUSIONS

Although specific reference has not been made to the fact, the apparatus is readily adaptable to temperature measurements of both emitter and collector junctions of transistors. It is probable that dynamic methods of junction-temperature measurement are even more important for a transistor than for a rectifier, owing to the relatively lower thermal capacity as a result of the extremely small spacing between collector and emitter.

Although the apparatus described has produced results which provide a far more realistic picture of the thermal and electrical parameters of a semi-conductor rectifier, it is probably the forerunner of even more versatile measurement circuits.

As will be seen from Fig. 1, even measurements at 50 c/s do not provide a complete indication of the peak junction temperature, although this can be estimated with reasonable accuracy. It is likely that measurements may in future be made at frequencies of up to 10 kc/s. This will necessitate the use of ignitron methods for high-current switching and thermionic-valve techniques similar to those described by Walker and Martin* for measurements of forward and reverse electrical parameters. Another possibility lies in the use of pulses of microseconds duration for strobing the characteristics of the device while it is actually conducting.

However, the satisfactory design of apparatus using higher-frequency measuring techniques is fraught with considerable difficulties, not the least of which being the mutual incompatibility of high (reverse)-resistance measurement and the use of pulses with short rise times and durations, which are readily by-passed by stray capacitance.

The present circuit can be expected to find considerable use in production testing, where the simultaneous indication of forward and reverse test points at maximum rating is of considerable advantage. Its use in the life-testing of large devices can also offer considerable power economies.

(6) APPENDICES

(6.1) Thermal Runaway

It is a well-known fact that the reverse current of a semi-conductor device at constant reverse voltage varies approximately exponentially with junction-temperature rise above ambient. If an excessive reverse power dissipation is applied, the junction

* *Op. cit.*

temperature will rise, causing a further increase in reverse current and hence power dissipation. If the reverse power dissipation is sufficient to cause a certain increase in junction temperature, the temperature will rise extremely rapidly in a condition known as thermal runaway. This can result in device failure. Conditions for thermal runaway are derived below. The application of reverse voltage, V, to a diode of characteristic AB via resistance R, is represented graphically by Fig. 16.

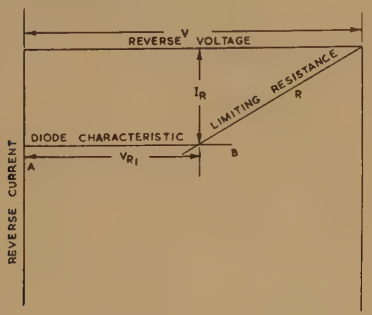

Fig. 16.—The application of reverse voltage via resistor R.

The power dissipation in the rectifier is

$$P_R = (V - I_R R)I_R \quad . \quad . \quad . \quad . \quad . \quad (1)$$

The power dissipated by its cooling system is $P_0 = \Delta T/\theta$ where ΔT is the temperature rise and θ is the thermal resistance; this is merely a restatement of Newton's law of cooling.

Under conditions of thermal equilibrium, i.e. when the rectifier is on the point of runaway,

$$\left.\begin{aligned} P_R &= P_0 \\ \text{and} \quad \frac{dP_R}{dT} &= \frac{dP_0}{dT} \end{aligned}\right\} \quad . \quad . \quad . \quad . \quad . \quad . \quad . \quad (2)$$

Furthermore, $I_R = i\varepsilon^{aT}$ (a is a constant)

Hence $$\frac{\Delta T}{\theta} = (V - I_R R)I_R$$

and $$\frac{1}{\theta} = aI_R(V - 2I_R R)$$

Thus $$\Delta T = \frac{V - I_R R}{a(V - 2I_R R)} \quad . \quad . \quad . \quad . \quad (3)$$

If $R = 0$, $\Delta T = 1/a \simeq 10° - 14°\,\mathrm{C}$

Thus, if a reverse voltage is applied via zero resistance to the rectifier in the reverse direction, thermal runaway will occur if the junction-temperature rise due to reverse power dissipation exceeds approximately 10° C.

It may readily be shown from eqn. (3) that the maximum stable value of ΔT increases with R for constant V and I. For example, if $V = 2I_R R$, $\Delta T = \infty$ and runaway cannot occur. The calculation is given for d.c. conditions for simplicity. The values for V and I_R are modified under a.c. conditions, since reverse power dissipation is applied for a portion of the a.c. cycle only.

In the cheater circuit, 'controlled' thermal runaway is possible by adjustment of the limiting resistance R, independently of the forward current circuit.

(6.2) Calculation of Thermal Resistance from Measurements of Junction Temperature, Rectified Current, Mean Forward Voltage Drop and Forward Characteristic

In order to simplify the calculation, the following assumptions will be made:

(*a*) The forward characteristic is assumed to be of the form $V = V_0 + IR_f$, where R_f is the forward slope resistance of the characteristic over the linear region and V_0 is the value of the intersection on the voltage axis by extrapolation backwards from the linear region. The error involved in taking this characteristic rather than the exponential form is very small.

(*b*) The current waveform is partly sinusoidal, as shown in Fig. 17. This is true so long as the load resistance, R_L, is

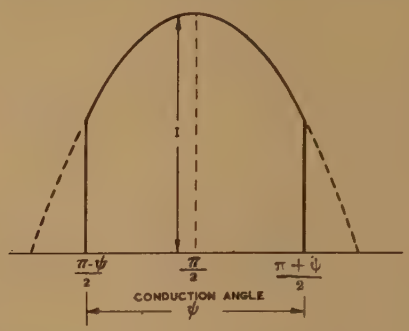

Fig. 17.—Forward current waveform through the rectifier under test

sufficiently high to swamp the non-linearity of the forward characteristic.

The mean power dissipation, P_D, due to a peak forward current I_P and conduction angle ψ is

$$P_D = \frac{1}{\pi}\int_{(\pi-\psi)/2}^{\pi/2}(R_f I_P^2 \sin^2\phi + V_0 I_P \sin\phi)d\phi \quad . \quad . \quad . \quad (1)$$

$$= \frac{I_P}{\pi}\left[R_f I_P\left(\frac{\phi}{2} - \frac{\sin^2\phi}{4}\right) - V_0\cos\phi\right]_{(\pi-\psi)/2}^{\pi/2}$$

$$= \frac{I_P^2 R_f}{4\pi}(\psi + \sin\psi) + \frac{V_0 I_P}{\pi}\sin\frac{\psi}{2} \quad . \quad . \quad . \quad . \quad (2)$$

If moving-coil d.c. meters measure the mean rectified current and mean forward voltage, they will measure I_M and V_M, where

$$I_M = \frac{1}{\pi}\int_{(\pi-\psi)/2}^{\pi/2} I_P \sin\theta d\theta = \frac{I_P}{\pi}\sin\frac{\psi}{2} \quad . \quad . \quad . \quad . \quad (3)$$

and

$$V_M = \frac{1}{\pi}\int_{(\pi-\psi)/2}^{\pi/2}(V_0 + R_f I_p \sin\theta d\theta) = \frac{1}{\pi}\left(V_0\frac{\psi}{2} + R_f I_p \sin\frac{\psi}{2}\right) \quad (4)$$

On substitution from eqns. (3) and (4) for I_p and R_f in eqn. (2),

$$P_D = \frac{I_M\left(V_M\pi - V_0\frac{\psi}{2}\right)(\psi + \sin\psi)}{4\sin^2\frac{\psi}{2}} + V_0 I_M$$

For $\psi = \pi$

$$P_D = \frac{I_M\pi^2\left(V_M - \frac{V_0}{2}\right)}{4} + V_0 I_M \simeq I_M\left(2{\cdot}5V_M - \frac{V_0}{4}\right)$$

For $\psi = 2\pi/3$

$$P_D = I_M\left[\frac{\pi}{3}\left(V_M - \frac{V_0}{2}\right)\left(\frac{4\pi + 3\sqrt{3}}{6}\right) + V_0\right] \simeq 3I_M V_M$$

The thermal resistance, θ, is then $(T_j - T_A)/P_D$, where T_j is the junction temperature, as measured with the apparatus from forward or reverse characteristic change, at a power dissipation P_D in the device, and T_A is the ambient temperature.

621.372.81.09

The Institution of Electrical Engineers
Monograph No. 311 R
Sept. 1958

PROPAGATION AROUND BENDS IN WAVEGUIDES

By Professor H. E. M. BARLOW, Ph.D., B.Sc.(Eng.), Member

(*The paper was first received 29th January, and in revised form 22nd May*, 1958. *It was published as an* INSTITUTION MONOGRAPH *in September*, 1958.)

SUMMARY

When a waveguide supporting a given mode is bent at some point along its length, there is generally a problem in providing for the continuity of the same undisturbed field pattern throughout. The hollow metal rectangular waveguide transmitting the dominant H_{01} mode and bent in the E-plane is an exception to this, but for the most part mode conversion occurs at the bend, which can have serious consequences in multi-mode tubular waveguides or in surface waveguides. To minimize this difficulty in the circular H_{01} waveguide, a proposal was made previously to use an inhomogeneous dielectric in association with the waveguide as a means of accelerating the wave pattern on the outside of the bend and retarding it on the inside, so as to approach much more closely the ideal conditions. In the present paper this idea has been extended to other forms of waveguide, and dielectrics which might find application in this way are briefly discussed.

(1) INTRODUCTION

There are many applications of waveguides in which bends are unavoidable. In some of these the waveguide can be preformed to meet the particular requirements on site, but in others it is essential to be able to adjust the curvature according to the needs as they arise. In a recent paper the author showed[1] that, for the H_{01} wave mode in a metal tube of circular cross-section, a good approximation to undisturbed propagation around a bend in the tube was obtained by suitable variation, with regard to the centre of curvature, of the permittivity and/or the permeability of the medium within the tube. Thus at any radius of curvature, R, the propagation coefficient, γ, should be such that γR is a constant. When the losses are relatively negligible, this requirement resolves itself into providing arrangements for keeping the wavefront, represented by an equiphase plane, radial with respect to the centre of curvature.

In the present paper it is proposed to extend this idea to other forms of waveguide and to show that the proposition is of wide application. The rectangular H_{01} waveguide bent in either the H- or the E-plane will be discussed first on this basis, having in mind an inhomogeneous dielectric filling the guide, and it will be shown that a perfect solution for the bend can be obtained in this way. The fact that rectangular guides bent in the E-plane and filled with air or a homogeneous dielectric will also satisfy the requirements of undisturbed propagation makes the application of the more complicated solution unnecessary in that particular case. There is also the problem of the discontinuity at the transition from a straight to a curved length of waveguide[2] and this may be aggravated when accompanied by a change from air- to solid-dielectric filling.

An example of perhaps greater significance is the single-wire transmission line coated with dielectric, and in considering this from the aspect of maintaining γR constant at a bend, it will be shown that a good approximation to the requirements of undisturbed propagation can thus be achieved. Although the dielectric-coated single-wire waveguide as a flexible link has found a number of applications, comparatively little information seems to be available about the radiation which occurs at bends. Scott[3] has made some theoretical computations based on a homogeneous dielectric surrounding the conductor, and Halford[4] has carried out a few measurements on enamelled copper wires bent into an arc of a circle of 2–3 m radius. The results seem to indicate, in some instances, that the radiation is less than would be expected, and the explanation may lie in the decreasing permittivity with density of the dielectric coating between the inside and the outside of the bend accelerating the wavefront as the radius of curvature increases. With satisfactory arrangements for flexing a surface waveguide of this kind, such as by the use of polythene-coated beryllium-copper wire, there seems to be a good case for its application as the feed to an aerial scanner using the end of the waveguide, suitably modified by introducing discontinuities along its length to act as an end-fire radiator. Such a feed to a parabolic mirror would have the advantage of offering little obstruction to the radiation.

For hollow metal tubes whose cross-sectional dimensions are such that they are restricted to the support of a single wave mode, any discontinuities along the length, including bends, can produce only evanescent field disturbances, which quickly die out. In multi-mode waveguides, however, it is important to provide for a smooth transition from one condition to another, and the bending of such guides is no exception.

(2) HOLLOW METAL WAVEGUIDE OF RECTANGULAR CROSS-SECTION SUPPORTING THE H_{01} MODE

To examine the field distribution at bends we require Maxwell's equations in cylindrical co-ordinates. Thus, referring to Fig. 1(*a*) we have

$$\frac{1}{R}\left(E_\theta + R\frac{\partial E_\theta}{\partial R} - \frac{\partial E_R}{\partial \theta}\right) = -\mu\frac{\partial H_y}{\partial t} \quad . \quad . \quad (1)$$

$$\frac{\partial E_R}{\partial y} - \frac{\partial E_y}{\partial R} = -\mu\frac{\partial H_\theta}{\partial t} \quad . \quad . \quad . \quad . \quad (2)$$

$$\frac{1}{R}\left(\frac{\partial E_y}{\partial \theta} - R\frac{\partial E_\theta}{\partial y}\right) = -\mu\frac{\partial H_R}{\partial t} \quad . \quad . \quad . \quad (3)$$

$$\frac{1}{R}\left(H_\theta + R\frac{\partial H_\theta}{\partial R} - \frac{\partial H_R}{\partial \theta}\right) = \sigma E_y + \epsilon\frac{\partial E_y}{\partial t} \quad . \quad . \quad (4)$$

$$\frac{\partial H_R}{\partial y} - \frac{\partial H_y}{\partial R} = \sigma E_\theta + \epsilon\frac{\partial E_\theta}{\partial t} \quad . \quad . \quad . \quad . \quad (5)$$

and

$$\frac{1}{R}\left(\frac{\partial H_y}{\partial \theta} - R\frac{\partial H_\theta}{\partial y}\right) = \sigma E_R + \epsilon\frac{\partial E_R}{\partial t} \quad . \quad . \quad (6)$$

(2.1) Waveguide Bent in the H-Plane

In order to provide for undisturbed propagation at the bend, the only field components present should be E_y, H_θ and H_R [see Fig. 1(*b*)].

If we assume that we can satisfy Maxwell's equations in terms

Correspondence on Monographs is invited for consideration with a view to publication.

Prof. Barlow is Pender Professor of Electrical Engineering, University College, University of London.

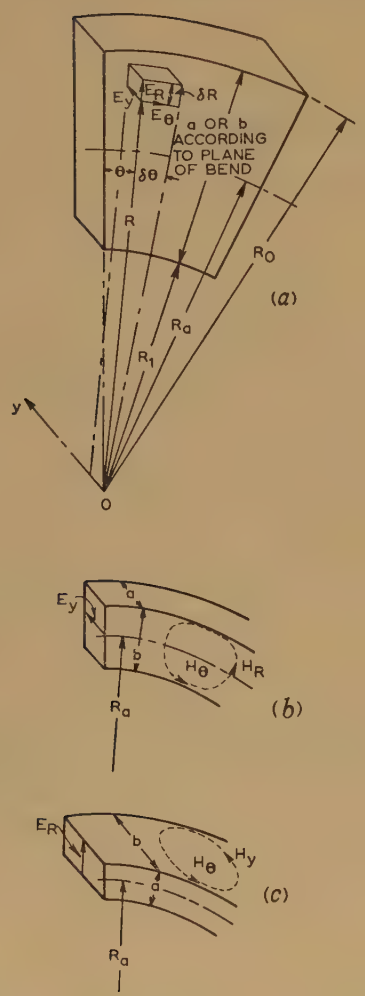

Fig. 1.—Bends in rectangular H_{01} waveguide.
(*a*) Cylindrical co-ordinate system.
(*b*) Bend in H-plane (field components).
(*c*) Bend in E-plane (field components).

of these three components (so that $E_\theta = 0$, $E_R = 0$ and $H_y = 0$) and that the fields vary sinusoidally in time, we find

$$\frac{1}{R}\left(\frac{\partial \mathscr{E}_y}{\partial R} + R\frac{\partial^2 \mathscr{E}_y}{\partial R^2} + \frac{1}{R}\frac{\partial^2 \mathscr{E}_y}{\partial \theta^2}\right) = j\omega\mu(\sigma + j\omega\epsilon)\mathscr{E}_y \quad . \quad (7)$$

together with $\partial \mathscr{H}_R/\partial y = 0$ and $\partial \mathscr{H}_\theta/\partial y = 0$ where script letters are used to represent the field components in space co-ordinates only.

Assuming the usual form of axial distribution of field for a pure travelling wave, we can write

$$\mathscr{E}_y = A_1 \mathscr{E}_{yR} \varepsilon^{-\gamma R\theta} \quad . \quad . \quad . \quad . \quad . \quad (8)$$

$\mathscr{E}_{yR}$ being that part of $\mathscr{E}_y$ dependent upon R with $\gamma = \alpha + j\beta$ as the propagation coefficient. When γR = constant, which provides for the maintenance of a radial wavefront, we get from eqn. (7) the wave equation

$$\frac{\partial^2 \mathscr{E}_{yR}}{\partial R^2} + \frac{1}{R}\frac{\partial \mathscr{E}_{yR}}{\partial R} - u^2 \mathscr{E}_{yR} = 0 \quad . \quad . \quad . \quad (9)$$

where* $$\gamma^2 - \kappa^2 = -u^2 \quad . \quad . \quad . \quad . \quad . \quad . \quad (10)$$

and $$\kappa^2 = j\omega\mu(\sigma + j\omega\epsilon) \quad . \quad . \quad . \quad . \quad (11)$$

* In Reference 1, P was used instead of κ; the notation has been changed here to conform with accepted practice.

It will be observed that the usual condition γ = constant leads to a much more complicated wave equation which can be reduced to eqn. (9) only when

$$|\gamma R\theta| \ll 1$$

Now for constant values of u the solution to eqn. (9) is

$$\mathscr{E}_{yR} = A_2 J_0(juR) + A_3 Y_0(juR) \quad . \quad . \quad . \quad (12)$$

and for a perfect conductor forming the wall of the waveguide $\mathscr{E}_{yR} = 0$ both when $R = R_0 = (R_a + b/2)$ and when $R = R_1 = (R_a - b/2)$, so that

$$-\frac{A_2}{A_3} = \frac{Y_0(juR_1)}{J_0(juR_1)} = \frac{Y_0(juR_0)}{J_0(juR_0)} \quad . \quad . \quad . \quad (13)$$

Eqns. (12) and (13) can be satisfied exactly, and we therefore conclude that the conditions postulated can, in fact, be met. The essential requirements are γR = constant with $u^2 = \kappa^2 - \gamma^2$ = constant, and we shall see later what this implies.

It is perhaps of interest to observe that when $|juR| \gg 1$ we can rewrite eqn. (13) as

$$-\frac{A_2}{A_3} = \frac{\sin(juR_1 - \pi/4)}{\cos(juR_1 - \pi/4)} = \frac{\sin(juR_0 - \pi/4)}{\cos(juR_0 - \pi/4)}$$

from which $$ju = \left(\frac{n\pi}{R_0 - R_1}\right)$$

where n is an integer.
Thus, neglecting losses, $\gamma = j\beta$ and $\kappa^2 = -\omega^2\mu\epsilon$ so that

$$\beta = \sqrt{\left[\omega^2\mu\epsilon - \left(\frac{n\pi}{R_0 - R_1}\right)^2\right]}$$

and the cut-off wavelength $\lambda_c = 2(R_0 - R_1)/n$ where $n = 1$ for the H_{01} mode as required.

(2.2) Waveguide Bent in the E-Plane

In this case [see Fig. 1(*c*)] the only field components present for undisturbed propagation should be E_R, H_θ and H_y. Again using script letters to designate field components in terms of space co-ordinates and assuming the usual sinusoidal time variation, we get

$$\frac{1}{R^2}\frac{\partial^2 \mathscr{E}_R}{\partial \theta^2} + \frac{\partial^2 \mathscr{E}_R}{\partial y^2} = j\omega\mu(\sigma + j\omega\epsilon)\mathscr{E}_R \quad . \quad . \quad (14)$$

together with $\partial \mathscr{H}_y/\partial R = 0$ and

$$\partial \mathscr{H}_\theta/\partial R = -\frac{1}{R}\mathscr{H}_\theta \quad . \quad . \quad . \quad . \quad (15)$$

Now putting $$\mathscr{E}_R = B_1 \mathscr{E}_{Ry} \varepsilon^{-\gamma R\theta} \quad . \quad . \quad . \quad . \quad . \quad (16)$$

where $\mathscr{E}_{Ry}$ is that part of $\mathscr{E}_R$ which is dependent upon y, we find both for γR = constant and for γ = constant

$$\frac{\partial^2 \mathscr{E}_{Ry}}{\partial y^2} = (\kappa^2 - \gamma^2)\mathscr{E}_{Ry} = u^2 \mathscr{E}_{Ry} \quad . \quad . \quad (17)$$

u and κ having the values given by eqns. (10) and (11) respectively. When u = constant the solution to eqn. (17) is

$$\mathscr{E}_{Ry} = B_2 \cos(juy) + B_3 \sin(juy) \quad . \quad . \quad (18)$$

Inserting the boundary conditions $\mathscr{E}_{Ry} = 0$ when $y = 0$ and $y = b$, so that $B_2 = 0$ and $jub = n\pi$, giving

$$\mathscr{E}_{Ry} = B_3 \sin\left(\frac{n\pi y}{b}\right)$$

with $\beta = \sqrt{[\omega^2\mu\epsilon - (n\pi/b)^2]}$ and $\lambda_c = 2b$ as required for negligible losses and $n = 1$.

If the values of $\mathscr{H}_\theta$ at $R = R_0$ and $R = R_1$ are respectively $\mathscr{H}_{\theta 0}$ and $\mathscr{H}_{\theta 1}$, we also find, from eqn. (15),

$$\frac{\mathscr{H}_{\theta 0}}{\mathscr{H}_{\theta 1}} = \frac{R_0}{R_1} \quad . \quad . \quad . \quad . \quad . \quad . \quad . \quad (19)$$

It is interesting to notice that in this case both the conditions $\gamma R =$ constant and $\gamma =$ constant, together with the general requirement $u =$ constant, yield an exact solution. There is therefore no point in using an inhomogeneous dielectric for the E-plane bend.

For the condition $\gamma R =$ constant it will be observed that the distribution of the transverse components of the electric and magnetic fields over the cross-section of the rectangular waveguide is exactly the same for straight and bent guides only when bending takes place in the E-plane, although the difference in the case of H-plane bends is normally quite small. Since the transition from straight to bent sections of waveguide is a gradual one and corresponds to a change from an infinite value of R to a large finite value, it is reasonable to conclude that at the input and output of the H-plane bend no serious discontinuity will in any event arise, provided that the dielectric filling extends throughout the transition.

The wave impedance $\omega\mu/\beta$ changes over the cross-section of the waveguide in accordance with the change in β.

(3) DIELECTRIC-COATED SINGLE-WIRE WAVEGUIDE

The application of Maxwell's equations to this waveguide requires that they be expressed in toroidal co-ordinates. Thus, referring to Fig. 2, we have

$$\frac{1}{r}\left(E_\phi + r\frac{\partial E_\phi}{\partial r} - \frac{\partial E_r}{\partial \phi}\right) = -\mu\frac{\partial H_\theta}{\partial t} \quad . \quad . \quad (20)$$

$$\frac{1}{R}\left(\frac{\partial E_r}{\partial \theta} - R\frac{\partial E_\theta}{\partial r} - E_\theta \cos\phi\right) = -\mu\frac{\partial H_\phi}{\partial t} \quad . \quad (21)$$

$$\frac{1}{r}\frac{\partial E_\theta}{\partial \phi} - \frac{1}{R}\frac{\partial E_\phi}{\partial \theta} - \frac{1}{R}E_\theta \sin\phi = -\mu\frac{\partial H_r}{\partial t} \quad . \quad (22)$$

$$\frac{1}{r}\left(H_\phi + r\frac{\partial H_\phi}{\partial r} - \frac{\partial H_r}{\partial \phi}\right) = \sigma E_\theta + \epsilon\frac{\partial E_\theta}{\partial t} \quad . \quad . \quad (23)$$

$$\frac{1}{R}\left(\frac{\partial H_r}{\partial \theta} - R\frac{\partial H_\theta}{\partial r} - H_\theta \cos\phi\right) = \sigma E_\phi + \epsilon\frac{\partial E_\phi}{\partial t} \quad . \quad (24)$$

$$\frac{1}{r}\frac{\partial H_\theta}{\partial \phi} - \frac{1}{R}\frac{\partial H_\phi}{\partial \theta} - \frac{1}{R}H_\theta \sin\phi = \sigma E_r + \epsilon\frac{\partial E_r}{\partial t} \quad . \quad (25)$$

with $$R = R_a + r\cos\phi \quad . \quad . \quad . \quad . \quad . \quad (26)$$

Now if we assume that we can satisfy these equations by sinusoidal variation in time and a suitable distribution in space of the three field components H_ϕ, E_r and E_θ, normally associated with the axial cylindrical surface wave supported by this form of waveguide, we find

$$\frac{1}{R^2}\frac{\partial^2 \mathscr{H}_\phi}{\partial \theta^2} + \frac{\partial^2 \mathscr{H}_\phi}{\partial r^2} + \left(\frac{1}{r} + \frac{\cos\phi}{R}\right)\frac{\partial \mathscr{H}_\phi}{\partial r} = \left(\kappa^2 + \frac{1}{r^2} - \frac{\cos\phi}{Rr}\right)\mathscr{H}_\phi \quad (27)$$

Inside the metal core of the guide, when $r \leqslant s$ then $\sigma \gg \omega\epsilon$, and even if there is a slight change in σ with curvature over the cross-section, this could not satisfy the condition $\gamma R =$ constant. Thus, within the metal we must accept $\gamma =$ constant, and doing

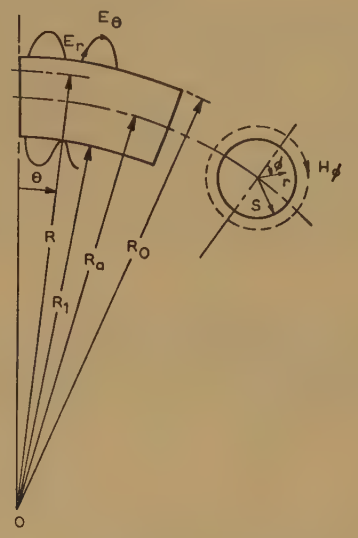

Fig. 2.—Bend in axial cylindrical surface waveguide.
Toroidal co-ordinate system and field components.

so yields the following wave equation in terms of that part of the magnetic field $\mathscr{H}_{\phi r}$ which is dependent upon r:

$$\frac{\partial^2 \mathscr{H}_{\phi r}}{\partial r^2} + \left(\frac{1}{r} + \frac{\cos\phi}{R} - 2\gamma\theta\cos\phi\right)\frac{\partial \mathscr{H}_{\phi r}}{\partial r} + \left[\gamma^2 - \kappa^2 + \left(\frac{\cos\phi}{rR} - \frac{1}{r^2}\right) - \left(\frac{1}{r} + \frac{\cos\phi}{R}\right)(\gamma\theta\cos\phi) + (\gamma\theta\cos\phi)^2\right]\mathscr{H}_{\phi r} = 0 \quad (28)$$

For waveguides in which we are interested $R \gg r$, and within the metal $|u| \simeq |\kappa| \gg |\gamma|$, so that for bends through angles θ even as much as 2π and values of $\cos\phi \leqslant 1$ we can rewrite eqn. (28) without serious error as

$$\frac{\partial^2 \mathscr{H}_{\phi r}}{\partial r^2} + \frac{1}{r}\frac{\partial \mathscr{H}_{\phi r}}{\partial r} - u^2\mathscr{H}_{\phi r} = 0 \quad . \quad . \quad . \quad (29)$$

to which we have the usual solution

$$\mathscr{H}_{\phi r} = C_1 J_0(jur)$$

with $u = a + jb$.

It therefore follows that, so far as the metal core of the waveguide is concerned, bending does not produce any serious departure from the appropriate field distribution within it.

Outside the conductor when $r \geqslant s$, we will suppose, for simplicity, that when the waveguide is straight we have a homogeneous dielectric medium surrounding it and extending to a radius sufficient to make the field at the outer surface negligible. This condition is not difficult to meet at microwave frequencies, because the decay of the field with increasing radius is very rapid.

Using eqn. (27) we now put

$$\mathscr{H}_\phi = C_2\mathscr{H}_{\phi r}\varepsilon^{-\gamma R\theta} \quad . \quad . \quad . \quad . \quad (30)$$

and with $\gamma R =$ constant we get

$$\frac{\partial^2 \mathscr{H}_{\phi r}}{\partial r^2} + \left(\frac{1}{r} + \frac{\cos\phi}{R}\right)\frac{\partial \mathscr{H}_{\phi r}}{\partial r} + \left(\gamma^2 - \kappa^2 - \frac{1}{r^2} + \frac{\cos\phi}{Rr}\right)\mathscr{H}_{\phi r} = 0 \quad . \quad . \quad . \quad (31)$$

This is precisely the same equation, although in terms of a different field component, as was obtained previously[1] for bends

in the circular H_{01} tubular metal waveguide, and we can apply the same arguments in making approximations.

Thus with $R \gg r$ eqn. (31) becomes very nearly

$$\frac{\partial^2 \mathscr{H}_{\phi r}}{\partial r^2} + \frac{1}{r}\frac{\partial \mathscr{H}_{\phi r}}{\partial r} - \left(u^2 + \frac{1}{r^2}\right)\mathscr{H}_{\phi r} = 0 \quad . \quad . \quad (32)$$

with u given as before by eqn. (10).

When u = constant the general solution to eqn. (32) is

$$\mathscr{H}_{\phi r} = C_3 H_1^{(1)}(jur) + C_4 H_1^{(2)}(jur) \quad . \quad . \quad (33)$$

To satisfy the surface wave requirements of an evanescent field structure over the wavefront with a small component of power directed towards the surface of the conductor to supply the losses in it, we have, with $u = a - jb$, to discard the second term in eqn. (33) giving

$$\mathscr{H}_{\phi r} = C_3 H_1^{(1)}(jur) \quad . \quad . \quad . \quad . \quad (34)$$

Applying the large-argument approximations to the Hankel functions it becomes evident that the second kind of function is not an appropriate part of the solution in this case (when there is no significant reflection at the outer surface of the dielectric). We have therefore arrived at the usual form of expression for the magnetic-field component of the axial cylindrical surface wave. To do so has involved the two basic assumptions, namely γR = constant and $u^2 = \kappa^2 - \gamma^2$ = constant, in the dielectric medium surrounding the conductor. These assumptions proved to be equally necessary to the solution of the corresponding problem in the case of the hollow tubular metal waveguides.

The approximations required for the circular H_{01} waveguide and the surface waveguide are identical, but there is a difference in the behaviour of these waveguides when subject to disturbances of the field pattern. The tubular waveguide is necessarily multi-mode, because the circular H_{01} wave is not the dominant one and others of a propagating variety may be set up. In the surface waveguide the equivalent penalty of any discontinuities is radiation.

(4) REQUIREMENTS TO BE MET IN PROVIDING FOR SMOOTH PROPAGATION AROUND BENDS

As already shown in a previous paper[1] dealing specifically with the circular H_{01} waveguide-bend problem, the essential conditions $\kappa^2 - \gamma^2$ = constant and γR = constant can best be established by an appropriate variation of the permittivity and/or the permeability over the cross-section of the dielectric medium through which the wave is propagated. By this means the whole of the wavefront can be kept radial with respect to the centre of curvature of the bend, and the proposition is a perfectly general one, applicable to all waveguides supporting characteristic wave modes.

Thus if $\gamma = \gamma_a$ and $\kappa = \kappa_a$ at $R = R_a$ (and additionally in the case of the surface waveguide $r = s$) then

$$\kappa^2 - \gamma^2 = \kappa_a^2 - \gamma_a^2 \quad . \quad . \quad . \quad . \quad (35)$$

and

$$\gamma R = \gamma_a R_a \quad . \quad . \quad . \quad . \quad . \quad (36)$$

or

$$\kappa^2 = \kappa_a^2 + \frac{\gamma_a^2(R_a^2 - R^2)}{R^2} \quad . \quad . \quad . \quad . \quad (37)$$

If the losses in the dielectric medium are comparatively small, $\kappa^2 = -\omega^2\mu\epsilon$ and $\kappa_a^2 = -\omega^2\mu_a\epsilon_a$

so that

$$\mu\epsilon = \mu_a\epsilon_a - \frac{\gamma_a^2(R_a^2 - R^2)}{\omega^2 R^2} \quad . \quad . \quad . \quad (38)$$

or with $\mu = \mu_a = \mu_0$, $\gamma_a = j\beta_a$ and $R \gg (R - R_a)$

$$\epsilon = \epsilon_a + \frac{2\beta_a^2(R_a - R)}{\omega^2\mu_0 R_a} = \epsilon_a - \frac{2\beta_a^2 r\cos\phi}{\omega^2\mu_0 R_a} \quad . \quad (39)$$

In a recent paper Morgan[5] gives what he calls the optical solution to the problem of bends in circular H_{01} waveguides. His result

$$\epsilon = \epsilon_a\left(1 - \frac{2r\cos\phi}{R_a}\right) \quad . \quad . \quad . \quad . \quad . \quad (40)$$

is equivalent to putting $u = 0$ in eqn. (10), and therefore represents the requirements for a plane wave. Calculations based on Morgan's expression would thus appear to lead to considerable errors in some cases.

From eqn. (39) it is easy to show that a very small change of permittivity and/or permeability of the dielectric over the cross-section of the waveguide suffices to provide the condition required. The mechanical compression which occurs naturally on the inside of the bend and the corresponding expansion on the outside can in principle be conveniently applied to this purpose. Thus from eqn. (39) we can write

$$\frac{d\epsilon}{dR} = -\frac{2\beta_a^2 R_a^2}{\omega^2\mu_0 R^3} \quad . \quad . \quad . \quad . \quad . \quad (41)$$

and the longitudinal strain of the dielectric arising from the bending is $q = (R_a - R)/R_a$

so that

$$\frac{dq}{dR} = -\frac{1}{R_a} \quad . \quad . \quad . \quad . \quad . \quad (42)$$

From eqns. (41) and (42) it appears that we require a fractional change in the permittivity of the medium of nearly double the corresponding change in the strain.

We can estimate the change of permittivity of a dielectric with density by applying the Clausius–Mossotti relation, namely

$$\frac{\epsilon_r - 1}{\epsilon_r + 2} = \frac{Np}{3\epsilon_0} = \frac{N_0 gp}{3\epsilon_0 M} \quad . \quad . \quad . \quad . \quad (43)$$

where p = Molecular polarizability.
N = Number of molecules per unit volume.
ϵ_r and ϵ_0 are the relative and free-space permittivities.
N_0 = Avogadro's number = $6{\cdot}02 \times 10^{23}$.
g = Density, kg/m^3.
and M = Molecular weight, kg.

Thus

$$\frac{d\epsilon_r}{dg} = \frac{9\epsilon_0 MN_0 p}{(3\epsilon_0 M - N_0 gp)^2} = \frac{(\epsilon_r + 2)(\epsilon_r - 1)}{3g} \quad . \quad (44)$$

Applying eqn. (44) to solid polythene, for which $\epsilon_r = 2{\cdot}5$ and $g = 1\,000$ kg/m^3, we find that for a 1% change in density the permittivity might be expected to change by 0·9%. A similar calculation for cellular polystyrene having $\epsilon_r = 1{\cdot}05$ and $g = 30$ kg/m^3 gives only 0·05% change in permittivity for a 1% change in density.

Alternatively, for a tubular metal waveguide transmitting an H-mode it might be possible to use an artificial dielectric[6] consisting of an array of small metal discs supported in the plane of the electric field by a transparent cellular material as shown in Fig. 3. In this case bending will produce a change in the dimension a, and since

$$\epsilon_r = \frac{1 + 2m/3}{1 - m/3} \quad . \quad . \quad . \quad . \quad . \quad (45)$$

where

$$m = 16\rho^3/ab^2$$

we find

$$\frac{d\epsilon_r}{da} = -\left(\frac{9m}{9 + 3m - 2m^2}\right)\frac{\epsilon_r}{a} \quad . \quad . \quad . \quad (46)$$

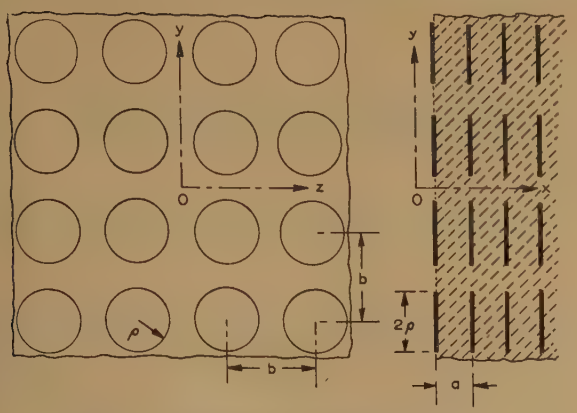

Fig. 3.—Metal-disc type of artificial dielectric.

Electric field can be in any direction in the *yz*-plane with wave propagation in the *x*-direction.

Thus for an array of discs having $b = 0{\cdot}25\,\text{cm}$, $a = 0{\cdot}1\,\text{cm}$ and $\rho = 0{\cdot}085\,\text{cm}$, $\epsilon_r = 4{\cdot}2$ and a 1% change in a gives 1·6% change in ϵ_r.

(5) CONCLUSIONS

There can be no doubt about the value of the principle embodied in the thesis that the wavefront should be kept radial with respect to the centre of curvature of the bend, and that this principle has wide application. Dielectric-coated wires acting as surface waveguides should automatically embody this principle to some extent and consequently might be expected to show some reduction of the radiation at bends. With a dielectric coating which becomes suitably inhomogeneous when the wire is bent it should be possible to banish the radiation almost completely. Similar behaviour of dielectric filling in a H_{01} tubular waveguide would also go a long way towards solving the problem of bends in this case. There is therefore an urgent need to develop dielectric materials for these applications. A degree of flexibility is necessary, in addition to change of ϵ and/or μ with density. For some purposes, e.g. surface waveguides, solid materials are suitable; for others, e.g. the hollow tubular metal waveguides, cellular structures may be more appropriate; but it seems likely that the change of permittivity with density will be roughly proportional to the original permittivity of the material, and consequently a loading material such as barium titanate, or even an artificial dielectric embodying small metal discs, may be helpful.

(6) ACKNOWLEDGMENTS

The author is indebted to Professor Cullen and to his colleagues Dr. John Brown, Mr. Wilson and Mr. Rickard for helpful discussions on this problem. He is also grateful to the Admiralty Signals Research Establishment for its support of experimental work on the subject.

(7) REFERENCES

(1) Barlow, H. E. M.: 'Propagation of the Circular H_{01} Low-Loss Wave Mode around Bends in Tubular Metal Waveguide', *Proceedings I.E.E.*, Paper No. 2369 R, July, 1957 (**104** B, p. 403).

(2) Rice, S. O.: 'Reflections from Circular Bends in Rectangular Waveguides', *Bell System Technical Journal*, 1948, **27**, p. 305.

(3) Scott, J. M. C.: Unpublished communication from Cavendish Laboratory, Cambridge.

(4) Halford, G. J.: Unpublished communication from R.R.E., Malvern.

(5) Morgan, S. P.: 'Theory of Curved Circular Waveguide Containing an Inhomogeneous Dielectric', *Bell System Technical Journal*, 1957, **36**, p. 1209.

(6) Brown, J.: 'Microwave Lenses' (Methuen Monograph, London), p. 40.

621.372.6

The Institution of Electrical Engineers
Monograph No. 312
Sept. 195

A TOPOLOGICAL INVESTIGATION OF NETWORK DETERMINANTS

By P. R. BRYANT, M.A., M.Sc.

(*The paper was first received* 1st *March, and in revised form* 20th *May*, 1958. *It was published as an* INSTITUTION MONOGRAPH *in September*, 1958)

SUMMARY

Polynomials associated with network functions are investigated by simple topological methods.

The main result is contained in Theorem 1, which states that the determinant of the nodal admittance matrix P of a connected *RLC* network without transformers is of the form:

$$\det P = \frac{\left[\begin{array}{l}\text{Polynomial in } \lambda \text{ containing a constant term and} \\ \text{of degree } (2N + 2 - S_C - S_{CR} - S_L - S_{LR})\end{array}\right]}{\lambda^{N+1-S_L-S_{LR}}}$$

Here, λ is the complex frequency variable, N is the number of nodes in the network and S_C, S_{CR}, S_L and S_{LR} are the connectivities of those sub-networks of the given network formed, respectively, of the capacitors only, the capacitors and resistors only, the inductors only and the inductors and resistors only.

This result is based upon an expression for det P as the sum of tree-products, which are defined.

A dual result is obtained for the determinant of the loop-impedance matrix, and the extension to other network functions is indicated, the driving-point admittance function being taken as an example.

LIST OF SYMBOLS

B = Number of branches of a network.
B_T = Number of branches of a tree.
c = Number of capacitors in a network.
d_1 = Number of capacitors in a tree.
d_2 = Number of inductors in a tree.
d_3 = Number of resistors in a tree.
l = Number of inductors in a network.
M = Number of independent loops in a network.
$\mathcal{N}$ = Typical *RLC* network without mutual inductance or ideal transformers.
$\mathcal{N}(C)$,etc. = Networks formed from $\mathcal{N}$ by open-circuiting those elements *not* denoted in the brackets.
$\mathcal{N}^*(C)$,etc. = Networks formed from $\mathcal{N}$ by short-circuiting those elements *not* denoted in the brackets.
$\mathcal{N}'$ = Network formed from $\mathcal{N}$ by short-circuiting together nodes 0 and 1.
N = Number of nodes of a network.
P = Nodal admittance matrix of $\mathcal{N}$ with respect to node 0.
det P = The determinant of P.
P' = Nodal admittance matrix of $\mathcal{N}'$.
Q = Loop impedance matrix of $\mathcal{N}$.
r = Number of resistors in a network.
S = Connectivity of a network.
t = Typical tree product.
λ = Complex frequency variable.

(1) INTRODUCTION

The form taken by the determinant of an electrical network matrix is well known to be a polynomial in the complex frequency variable λ, divided by some power of λ (see, for example, Section 2.5 of Reference 1).

In 1955, Reza[9] suggested an expression for what he called 'the order of complexity' of a network composed of resistors, inductors, capacitors and ideal transformers. More recently Otterman[7] gives the results of an investigation which enables one to find the order of the differential equation describing such networks. Both these numbers, i.e. the order of complexity† and the order of the differential equation, are equal to the degree of the numerator polynomial of the determinant of the network matrix.

We study here networks which consist solely of resistors, inductors and capacitors, and which do not contain any mutual inductance or ideal transformers. For such networks, which are called *RLC* networks, we obtain expressions for the degree of the numerator polynomial and for the power of λ in the denominator, for both the nodal-admittance matrix and the loop-impedance matrix. We also indicate the extension of these results to other network functions, taking as an example the driving-point admittance function.

The methods of proof used are based upon simple topological arguments. It is felt that these methods may be of as much interest as the actual results obtained.

Several topological terms are used and are duly defined. For a more general list of topological terms used in electrical network theory the reader is referred to Reference 5.

We require several lemmas which are proved elsewhere. These are included for completeness, giving references to where proofs may be found. Examples are given in the Appendix.

(2) THE NODAL ADMITTANCE MATRIX

Definition 1.—We denote a typical *RLC* network by $\mathcal{N}$, and assume that it contains N nodes [numbered 0 to $(N-1)$], B branches (i.e. l inductors, c capacitors and r resistors, where $l + c + r = B$) and M independent loops or circuits. [See Figs. 1 and 2.]

Definition 2.—We will denote by S the connectivity or number of separate parts of $\mathcal{N}$. If $S = 1$, we say that $\mathcal{N}$ is connected.

It is obvious that for any $\mathcal{N}$, $S \geqslant 1$.

Lemma 1.[13]—For any $\mathcal{N}$ we have the relation

$$M = B - N + S \quad . \quad . \quad . \quad . \quad . \quad . \quad (1)$$

From any given *RLC* network $\mathcal{N}$ we shall form other networks in certain specified ways. Thus, for example, we may assume that all of the inductors and resistors of $\mathcal{N}$ are open-circuited, leaving a capacitor-only network. Alternatively we may short-circuit all the inductors and resistors of $\mathcal{N}$, leaving another

Correspondence on Monographs is invited for consideration with a view to publication.

Mr. Bryant is at the Engineering Laboratory, University of Cambridge.

† In his introduction Reza defines the order of complexity as the number of finite natural frequencies, but in his discussion he restricts his considerations to the number of finite *non-zero* natural frequencies. It is this latter number which will be the same as the degree of the numerator polynomial of the network determinant.

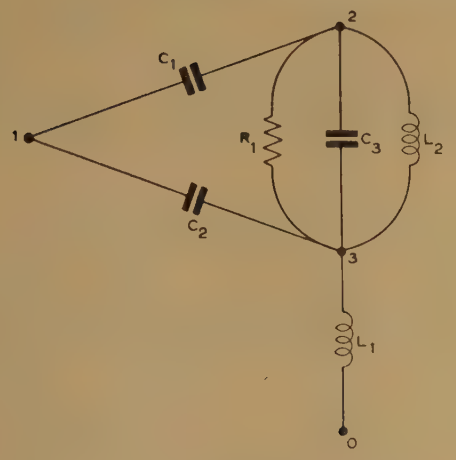

Fig. 1.—A typical connected *RLC* network, $\mathcal{N}$.

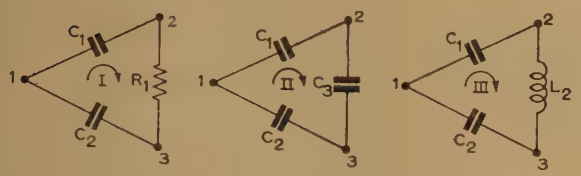

Fig. 2.—A set of three independent loops of $\mathcal{N}$.

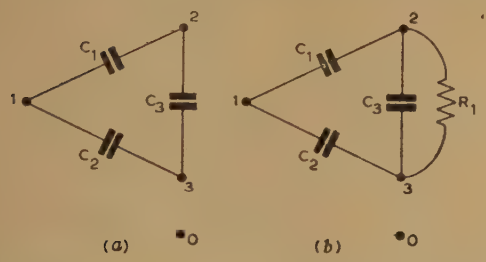

Fig. 3.—The networks $\mathcal{N}(C)$ and $\mathcal{N}(CR)$ formed from $\mathcal{N}$.
(*a*) $\mathcal{N}(C)$.
(*b*) $\mathcal{N}(CR)$.

capacitor-only network. For these various networks we use the following notations:

Definition 3.—$\mathcal{N}(C), \mathcal{N}(L), \mathcal{N}(R), \mathcal{N}(CR), \ldots$ etc., denote those networks obtained from $\mathcal{N}$ by substituting open-circuits for those elements *not* denoted in the brackets (see Fig. 3).

Definition 4.—$\mathcal{N}^*(C), \mathcal{N}^*(L), \mathcal{N}^*(R), \mathcal{N}^*(CR), \ldots$ etc., denote those networks obtained from $\mathcal{N}$ by substituting short-circuits for those elements *not* denoted in the brackets (see Fig. 4).

Lemma 2.—The number of nodes in each of the unstarred networks defined in Definition 3, is N, the number of nodes in $\mathcal{N}$.

The proof of this is really a matter of definition, for although open-circuiting sets of elements may leave certain nodes isolated, we still regard these nodes as being part of the resultant network.

As a matter of definition, in the formation of the starred networks of Definition 4, two nodes joined together by a short-circuit are considered as identified. Hence Lemma 2 is *not* true in general for these starred networks.

Lemma 3.—The connectivity of each of the starred networks of Definition 4 is S, the connectivity of $\mathcal{N}$.

The truth of this lemma is self-evident.

Fig. 4.—The network $\mathcal{N}^*(L)$ formed from $\mathcal{N}$.

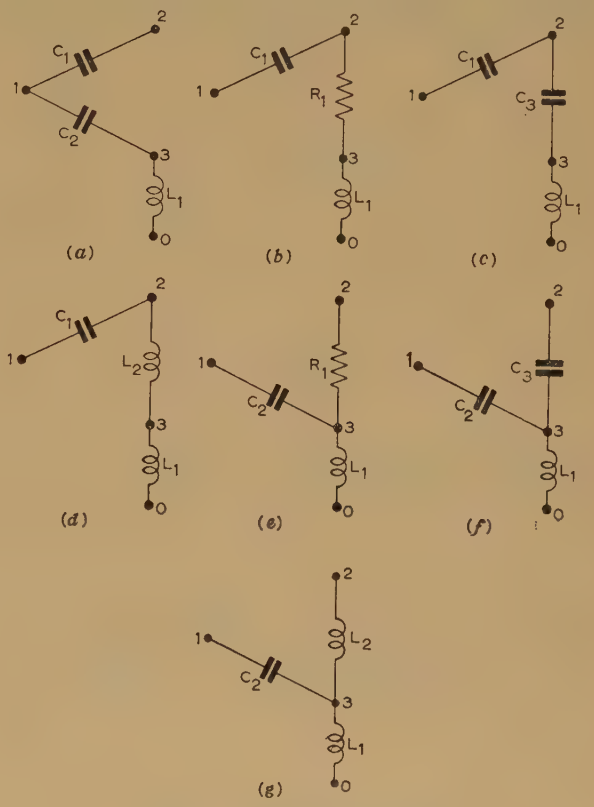

Fig. 5.—The seven trees of $\mathcal{N}$.

Lemma 3 is *not* true in general for the unstarred networks of Definition 3.

As we shall wish to refer to properties of these various starred and unstarred networks, we need a notation for the numbers of nodes and branches, etc. We use the obvious notation of Definition 5:

Definition 5.—$N_C, B_C, M_C, S_C, N_L^*, B_L^*$, etc., denote the number of nodes, branches, loops and separate parts of $\mathcal{N}(C), \mathcal{N}^*(L)$, etc.

We now introduce a concept which is of great use in the topological theory of networks.

Definition 6.—A *tree* of a network $\mathcal{N}$ is any connected sub-network of $\mathcal{N}$ containing all the nodes, but containing no loops (see Fig. 5).

It should perhaps be made clear that a tree of a network $\mathcal{N}$ only differs from $\mathcal{N}$ by at most the substitution of open-circuits for some of its branches; the definition does *not* permit the creation of new nodes by the separation of branches at a common node.

Notes: (*a*) From this definition it is obvious that $\mathcal{N}$ itself must be connected before it can contain a tree.

(*b*) Since the tree contains no loops, and since it also contains N nodes and is connected, it follows from Lemma 1 that any tree of $\mathcal{N}$ must contain B_T branches, where

$$B_T = N - 1 \quad . \quad . \quad . \quad . \quad . \quad . \quad . \quad . \quad (2)$$

Lemma 4.[4]—Any connected network contains at least one tree.

We find that the limitation of connectivity to the term tree is too severe for our needs. However, rather than widen the scope of the term itself, contrary to general usage—at least in the electrical network field—we introduce the following terms for our own use:

Definition 7.—A *wood* of any network $\mathcal{N}$, not necessarily connected, is a sub-network, not necessarily connected, which contains no loops (see Figs. 6 and 7).

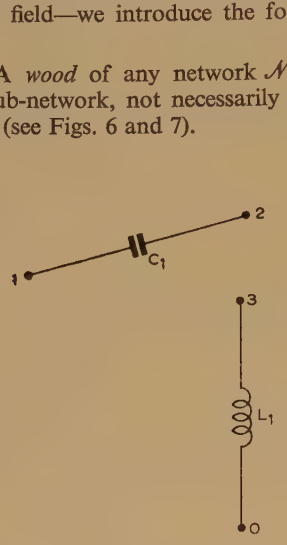

Fig. 6.—A wood of $\mathcal{N}$ of order 2.

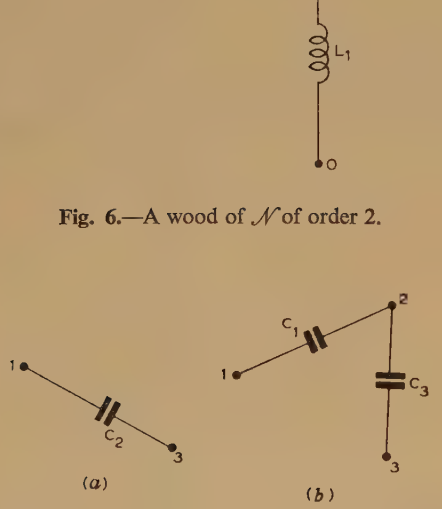

Fig. 7.—Two woods of $\mathcal{N}(C)$.

Definition 8.—The *order* of a wood is the number of branches it contains.

Lemma 5.[10]—Given any wood of a connected network $\mathcal{N}$, there exists at least one tree of $\mathcal{N}$ containing it.

Lemma 6.—The order of any wood of $\mathcal{N}$ is not greater than $N - S$.

Proof.—Consider the sub-network of $\mathcal{N}$ formed by adding to the wood all the nodes of $\mathcal{N}$ not already contained in it but adding no more branches. This sub-network of $\mathcal{N}$ contains N nodes and cannot have a connectivity of less than S. Hence, since it contains no loops, Lemma 1 shows that it can contain no more than $N - S$ branches, and so the order of the wood is not greater than $N - S$.

In view of Lemma 6, for any network $\mathcal{N}$ there is an upper limit $(N - S)$ on the order of its woods. Thus we may frame the following definition:

Definition 9.—A *forest* of a network $\mathcal{N}$, not necessarily connected, is a wood of $\mathcal{N}$ of the highest possible order (see Fig. 8).

Lemma 7.—Any network $\mathcal{N}$ whether connected or not, contains at least one forest of order $(N - S)$.

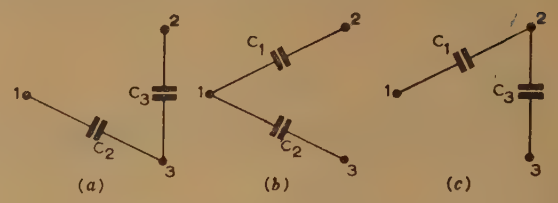

Fig. 8.—The three forests of $\mathcal{N}(C)$.

Proof.—If $\mathcal{N}$ is connected, then since $S = 1$ and $B_T = N - 1$ any tree of $\mathcal{N}$ is a forest and so the Lemma is true in this case.

If $\mathcal{N}$ is not connected, we consider each connected separate part of $\mathcal{N}$, say $\mathcal{N}_1, \mathcal{N}_2, \ldots \mathcal{N}_S$. Since each $\mathcal{N}_j$ is connected, then by Lemma 4 $\mathcal{N}_j$ contains a tree having $(N_j - 1)$ branches, where N_j is the number of nodes in $\mathcal{N}_j$. Consider the sub-network of $\mathcal{N}$ formed by the logical addition of each of the S trees. This sub-network certainly contains no loops. Further it contains

$$\sum_{j=1}^{S} (N_j - 1) \text{ branches.} \quad \text{Now } \sum_{j=1}^{S} N_j = N$$

Hence this sub-network contains $N - S$ branches, and so by Lemma 6 and Definition 9 it must be a forest.

Lemma 8.—All forests of a network $\mathcal{N}$ contain $(N - S)$ branches.

Proof.—From Definition 9, all forests of $\mathcal{N}$ must contain the same number of branches. By Lemma 7 this number is $N - S$.

As an obvious extension to Lemma 5 we have Lemma 9:

Lemma 9.—Given any wood of any network $\mathcal{N}$ (not necessarily connected), there exists at least one forest of $\mathcal{N}$ containing it.

So far, we have been purely topological in our definitions and lemmas. We now begin to pay more attention to the electrical character of our network. The essential link between the two is contained in the following two definitions and Lemma 10:

Definition 10.—A *tree-product* of a connected network $\mathcal{N}$ is the product of the branch admittances forming any tree of $\mathcal{N}$. We denote a typical tree product of $\mathcal{N}$ by t.

If we assume that t contains d_1 capacitors, d_2 inductors and d_3 resistors then Note (*b*) to Definition 6 tells us that $d_1 + d_2 + d_3 = N - 1$.

Definition 11.—We denote by P the nodal admittance matrix of a connected network $\mathcal{N}$ containing N nodes numbered from 0 to $N - 1$, node 0 being taken as the reference-node, or earth. P is of order $(N - 1)$.

Lemma 10.[2, 8, 10]—For a connected network containing no mutual inductance and no ideal transformers,

$$\det P = \sum_{\text{(all trees)}} t \quad . \quad . \quad . \quad . \quad . \quad (3)$$

Before coming to the main theorem concerning the form of $\det P$ we need three more lemmas.

Lemma 11.—If d_1, d_2 and d_3 are defined as in Definition 10 then

(*a*) $\underset{\text{(all trees)}}{\text{Maximum}}\ d_1 = N - S_C$ (and similarly for d_2, etc.).

(*b*) $\underset{\text{(all trees)}}{\text{Minimum}}\ d_2 = S_{CR} - 1$ (and similarly for d_1, etc.).

Proof.—(*a*) d_1 is a maximum for those trees of $\mathcal{N}$ which precisely contain forests of $\mathcal{N}(C)$ (possible by Lemma 5); for if any sub-network of $\mathcal{N}$ contains more capacitors than are contained in such forests of $\mathcal{N}(C)$ (i.e. more than $N - S_C$ capacitors by Lemma 2 and Lemma 8) then by Lemma 1 applied to $\mathcal{N}(C)$ these capacitors must contain a loop in $\mathcal{N}(C)$, and so also in $\mathcal{N}$. Hence such a sub-network cannot be part of a tree of $\mathcal{N}$. Thus d_1 is a maximum for those trees of $\mathcal{N}$ which contain $N - S_C$ capacitors, and so $N - S_C$ must be this maximum value.

(*b*) d_2 is a minimum for those trees which have $(d_1 + d_3)$ a maximum. Applying (*a*) above to $\mathcal{N}(CR)$, this must be when $d_1 + d_3 = N - S_{CR}$. Hence

$$\text{Minimum } d_2 = (N-1) - (N - S_{CR}) = (S_{CR} - 1)$$

Lemma 12.—There is at least one tree in any connected network $\mathcal{N}$ which has d_1 a maximum and d_2 a minimum at the same time.

Proof.—From Lemma 11, d_1 is a maximum for trees precisely containing forests of $\mathcal{N}(C)$, and d_2 is a minimum for trees precisely containing forests of $\mathcal{N}(CR)$. Now any forest of $\mathcal{N}(C)$ is part of at least one forest of $\mathcal{N}(CR)$ by Lemma 9, and this forest of $\mathcal{N}(CR)$ is part of at least one tree of $\mathcal{N}$ (by Lemma 5). Hence this tree of $\mathcal{N}$, containing forests of $\mathcal{N}(C)$ and of $\mathcal{N}(CR)$, must have both d_1 a maximum and d_2 a minimum.

Lemma 13.—

$$(a)\ \underset{\text{(all trees)}}{\text{Maximum}}\ (d_1 - d_2) = (N - S_C - S_{CR} + 1) \quad . \quad (4)$$

$$(b)\ \underset{\text{(all trees)}}{\text{Minimum}}\ (d_1 - d_2) = (S_L + S_{LR} - N - 1) \quad . \quad (5)$$

The proof follows directly from Lemma 11 and Lemma 12.

We may now give our main theorem.

Theorem 1.—For a connected RLC network, det P is of the form

$$\det P = \frac{\left[\begin{array}{c}\text{Polynomial in } \lambda \text{ containing a constant term and} \\ \text{of degree } (2N + 2 - S_C - S_{CR} - S_L - S_{LR})\end{array}\right]}{\lambda^{N+1-S_L-S_{LR}}} \quad (6)$$

where λ is the complex frequency variable.

Proof.—From Lemma 10, $\det P = \underset{\text{(all trees)}}{\Sigma}\, t$, and from Definition 10, any tree product t is of the form

$$t = k\lambda^{d_1 - d_2}$$

where k is some positive constant independent of λ.

Now by Lemma 13, the highest powered tree-product is of the form

$$k\lambda^{N+1-S_C-S_{CR}}$$

and the lowest powered tree-product is of the form

$$k\lambda^{S_L+S_{LR}-N-1}$$

Hence we may take out a factor of $\lambda^{S_L+S_{LR}-N-1}$, or $1/\lambda^{N+1-S_L-S_{LR}}$ as given in the theorem, which will leave a polynomial containing a constant term and of degree $(2N + 2 - S_C - S_{CR} - S_L - S_{LR})$. Hence the theorem.

Before showing the equivalence of Theorem 1 to the results suggested by Reza[9] and to those given by Otterman,[7] we need a further lemma.

Lemma 14.—The number of nodes in any of the starred networks defined in Definition 4 is equal to the connectivity of the complementary unstarred network, e.g. $N_L^* = S_{CR}$, etc.

Proof.—We shall prove the lemma for the particular case quoted. The proof for any other particular case is then obvious.

Each of the S_{CR} separate parts of $\mathcal{N}(CR)$ must become single nodes when the C's and R's of $\mathcal{N}$ are short-circuited to form $\mathcal{N}^*(L)$; since this statement takes in all the nodes in $\mathcal{N}(CR)$ including any isolated nodes, it also takes in all the nodes in $\mathcal{N}$ (by Lemma 2). Hence these separate parts of $\mathcal{N}(CR)$ become identified with the nodes of $\mathcal{N}^*(L)$, and the lemma follows.

We are now able to prove Reza's conjecture for the case of *RLC* networks. In our terminology this becomes Theorem 2.

Theorem 2.—The degree of the numerator polynomial in the determinant of the nodal admittance matrix of a connected *RLC* network† is $(M_L^* - M_L) + [(N_C - S_C) - (N_C^* - S_C^*)]$.

Proof.—By Theorem 1 the degree is $(2N + 2 - S_C - S_{CR} - S_L - S_{LR})$ and we show that Reza's expression is equal to this. Considering each term in Reza's expression,

$M_L^* = l - N_L^* + S_L^*$ [By Lemma 1 applied to $\mathcal{N}^*(L)$ l defined in Definition 1]
$= l - S_{CR} + 1$ (By Lemma 14 and Lemma 3)
$M_L = l - N_L + S_L$ [By Lemma 1 applied to $\mathcal{N}(L)$]
$= l - N + S_L$ (By Lemma 2)
$N_C = N$ (By Lemma 2)
$S_C = S_C$
$N_C^* = S_{LR}$ (By Lemma 14)
$S_C^* = S = 1$ (By Lemma 3)

Putting these values into Reza's expression we obtain $(2N + 2 - S_C - S_{CR} - S_L - S_{LR})$, and hence we get the theorem.

By making use of the various lemmas and some algebraic manipulation, various expressions for the degree of the polynomial and for the power of λ can be obtained. We give some of these in the following corollary to Theorem 2.

Corollary 2.1.—Other expressions we may obtain are as follows:

$$\left.\begin{array}{l}\text{Power of } \lambda \\ = (N+1-S_L-S_{LR}) = (M-M_L-M_{LR}+l-c) \\ = (N+1-N_{CR}^*-N_C^*) = (M_{CR}^*+M_C^*-M+l-c)\end{array}\right\} . \quad (7)$$

$$\left.\begin{array}{l}\text{Degree of polynomial} \\ = (2N+2-S_C-S_{CR}-S_L-S_{LR}) \\ = (2M-M_C-M_{CR}-M_L-M_{LR}) \\ = (2N-2-N_{CR}^*-N_{LR}^*-N_C^*-N_L^*) \\ = (M_{LR}^*+M_{CR}^*+M_L^*+M_C^*-2M) \\ = (M_C^*-M_C)+(M_{CR}^*-M_{CR}) \\ = (l+c+2-N_C^*-N_L^*-M_C-M_L)\end{array}\right\} . \quad (8)$$

This last expression for the degree of the polynomial is that which would be obtained by following Otterman's procedure in the case of a connected *RLC* network. Hence our result is in this case, equivalent to his.

(3) THE LOOP-IMPEDANCE MATRIX

Using the dual expression for the determinant of the loop-impedance matrix[6] in terms of co-tree impedance products,† we may obtain similar expressions for the form of this determinant.

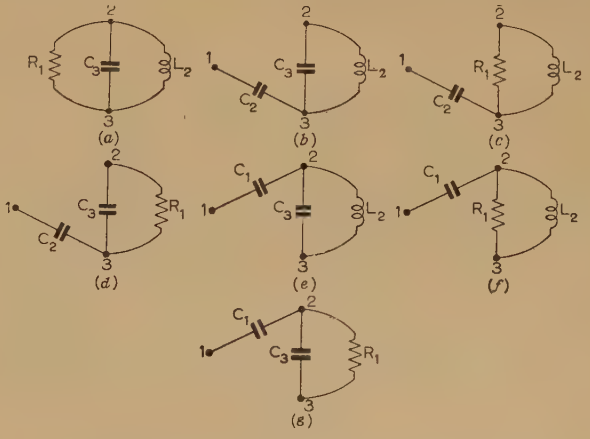

Fig. 9.—The seven co-trees of $\mathcal{N}$.

A simpler method, however, having obtained the result of Theorem 1, is to use a result obtained by both Tsang[12] and Cederbaum.[3] This is contained in the following lemma:

† It is of interest to note that Reza's[9] formula 3.7 is correct for the *RLC* case if we use the same interpretation of notation as that which he gives for the *LC* case only. Thus his new interpretation given on pp. 7–18 of Reference 9 for the *RLC* case is unnecessary.

† A co-tree is a set of M branches whose complement forms a tree of $\mathcal{N}$; see Fig. 9; a co-tree impedance product is the product of the impedances of such a set of branches.

Lemma 15.[3,12]—If Q is an $M \times M$ loop impedance matrix of a connected *RLC* network $\mathcal{N}$ containing no mutual inductance or ideal transformers, and P is the nodal admittance matrix of $\mathcal{N}$, then

$$\frac{\det Q}{\det P} = k^2 \text{ (product of all the branch impedances)} \quad . \quad (9)$$

where k is some positive or negative integer (which is unity if Q is what Cederbaum calls 'simple' or 'basic').

From this lemma, and using Corollary 2.1, we obtain Theorem 3.

Theorem 3.—For a connected *RLC* network, det Q is of the form

$$\det Q = \frac{\left[\begin{array}{l}\text{Polynomial in } \lambda \text{ containing a constant and of} \\ \text{degree } (2M - M_C - M_{CR} - M_L - M_{LR})\end{array}\right]}{\lambda^{M - M_L - M_{LR}}} \quad . \quad (10)$$

Proof.—The product of the branch impedances is of the form $k\lambda^{l-c}$, and using the expression for det P obtained from Corollary 2.1,

$$\det P = \frac{\text{polynomial of degree } (2M - M_C - M_{CR} - M_L - M_{LR})}{\lambda^{M - M_L - M_{LR} + l - c}} \quad . \quad . \quad . \quad . \quad (11)$$

the result follows immediately. Note that the degree of the numerator polynomial is the same as in the case of the nodal-admittance matrix.

(4) EXPRESSIONS FOR OTHER NETWORK FUNCTIONS

Given any connected *RLC* network, the various network functions associated with it are usually ratios of various co-factors of one or other of the network determinants. Sometimes these co-factors are themselves determinants of the corresponding matrix of the original network when modified in some way or other. By using this fact, various expressions for the form of these network functions may be obtained. As an example, we obtain an expression for a driving-point admittance function.

Definition 12.—Suppose we have a connected *RLC* network $\mathcal{N}$ containing N nodes numbered 0 to $N-1$. Denote by $\mathcal{N}'$ the network obtained from $\mathcal{N}$ by shorting node 1 to node 0, and similarly obtain $\mathcal{N}'(C), \mathcal{N}'^*(C)$, etc., as obvious extensions of Definitions 3 and 4 (see Fig. 10).

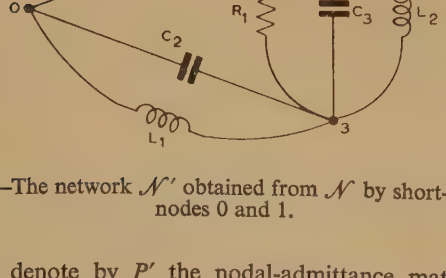

Fig. 10.—The network $\mathcal{N}'$ obtained from $\mathcal{N}$ by short-circuiting nodes 0 and 1.

Further denote by P' the nodal-admittance matrix of $\mathcal{N}'$ relative to node 0.

Lemma 16.[10]—The co-factor of P_{11} in P is det P'.

It is well known (see Reference 1, Section 1.9) that the driving-point admittance between nodes 0 and 1 is of the form

$$Y = \frac{\det P}{\text{co-factor of } P_{11} \text{ in } P} \quad . \quad . \quad . \quad . \quad (12)$$

Hence we obtain immediately:

Lemma 17.—The driving-point admittance Y between nodes and 1 is of the form $Y = \det P / \det P'$.

Using Lemma 17 and Theorem 1 applied to $\mathcal{N}'$ we obtai immediately Theorem 4.

Theorem 4.—The driving-point admittance Y between nodes and 1 of a connected *RLC* network, before the cancellation c any common factors, is of the form

$$Y = \frac{\left[\begin{array}{l}\text{Polynomial of degree} \\ (2N+2-S_C-S_{CR}-S_L-S_{LR})\end{array}\right]}{\left[\begin{array}{l}\text{Polynomial of degree} \\ (2N-S'_C-S'_{CR}-S'_L-S'_{LR})\end{array}\right]} \lambda^{[(S_L - S'_L) + (S_{LR} - S'_{LR}) -} \quad (13$$

where the dashed quantities are defined in Definition 12, an where each polynomial contains a non-zero constant term.

(5) ACKNOWLEDGMENTS

The author is indebted to The General Electric Company Limited, for the award of a G.E.C. Scholarship and for per mission to publish the paper; also to Dr. K. F. Sander of th Department of Engineering, Cambridge University, for valuabl discussions.

(6) REFERENCES

(1) BODE, H. W.: 'Network Analysis and Feedback Amplifie Design' (D. Van Nostrand, 1945).

(2) BROOKS, R. L., SMITH, C. A. B., STONE, A. H., and TUTT W. T.: 'Dissection of Rectangles into Squares', *Duk Mathematical Journal*, 1940, **7**, p. 312.

(3) CEDERBAUM, I.: 'Invariance and Mutual Relations of Elec trical Network Determinants', *Journal of Mathematic and Physics*, 1956, **34**, p. 236.

(4) INGRAM, W. H.: 'On the Foundations of Electrical Networ Theory', *ibid.*, 1944, **23**, p. 134.

(5) INSTITUTE OF RADIO ENGINEERS: 'Definitions of Terms i Network Topology', *Proceedings of the Institute of Radi Engineers*, 1951, **39**, p. 27.

(6) KIRCHOFF, G.: 'Über die Auflösung der Gliechungen a Welche man bei der Untersuchung der Linearer Vertailung Galvanischer Ströme geführt Wird', *Annale der Physik und Chemie*, 1847, **72**, p. 497.

(7) OTTERMAN, J.: 'On the Order of the Differential Equatio describing an Electrical Network', *Proceedings of t Institute of Radio Engineers*, 1957, **45**, p. 1024.

(8) PERCIVAL, W. S.: 'The Solution of Passive Electrical Ne works by means of Mathematical Trees', *Proceedin I.E.E.*, Paper No. 1492 R, May, 1953 (**100**, Part II p. 143).

(9) REZA, F. M.: 'Order of Complexity and Minimal Structur in Network Analysis' (Proceedings of the Symposiu on Circuit Analysis, University of Illinois, 1955).

(10) SESHU, S.: 'Topological Considerations in the Design Driving Point Functions', *Transactions of the Institute Radio Engineers on Circuit Theory*, 1955, **CT-2**, p. 356.

(11) TRENT, H. M.: 'A Note on the Enumeration and Listi of all Possible Trees in a Connected Linear Grap *Proceedings of the National Academy of Sciences*, U.S.A 1954, **40**(B), p. 1004.

(12) TSANG, N. F.: 'On Electrical Network Determinant *Journal of Mathematics and Physics*, 1954, **33**, p. 185.

(13) VEBLEN, O.: 'Analysis Situs' (American Mathematic Society Colloquium Publications, Vol. 5, Part II, Secon Edition, 1931).

(7) APPENDIX

(7.1) Introduction

In this Appendix we give a specific example of a connected *RLC* network, and use it to illustrate the various definitions and results of the paper. The subdivisions correspond with the main divisions of the paper.

(7.2) Nodal Admittance Matrix

In Fig. 1 we show a typical connected *RLC* network $\mathcal{N}$. It contains 4 nodes and 6 branches (i.e. 2 inductors, 3 capacitors and 1 resistor). Thus we have

$$\left.\begin{aligned} N &= 4 \\ B &= 6\ (l = 2,\ c = 3,\ r = 1) \\ S &= 1 \end{aligned}\right\} \quad . \ . \ . \quad (14)$$

Hence by Lemma 1, the number of independent loops is

$$M = B - N + S = 3 \quad . \ . \ . \ . \ . \quad (15)$$

A set of 3 independent loops is shown in Fig. 2.

In Fig. 3 we show $\mathcal{N}(C)$ and $\mathcal{N}(CR)$. From the Figure we have

$$\left.\begin{aligned} N_C &= 4 \\ B_C &= 3 \\ S_C &= 2 \\ M_C &= 1 \end{aligned}\right\} \quad . \ . \ . \ . \ . \quad (16)$$

$$\left.\begin{aligned} N_{CR} &= 4 \\ B_{CR} &= 4 \\ S_{CR} &= 2 \\ M_{CR} &= 2 \end{aligned}\right\} \quad . \ . \ . \ . \ . \quad (17)$$

We include the isolated node 0 as part of $\mathcal{N}(C)$ and $\mathcal{N}(CR)$.

Fig. 4 shows $\mathcal{N}^*(L)$. We have identified those nodes which become joined together by short-circuits. Here

$$\left.\begin{aligned} N_L^* &= 2 \\ B_L^* &= 2 \\ S_L^* &= 1 \\ M_L^* &= 1 \end{aligned}\right\} \quad . \ . \ . \ . \ . \ . \quad (18)$$

To illustrate Definition 6 we give in Fig. 5 all the trees of $\mathcal{N}$. Each tree contains N (i.e. four) nodes, $(N-1)$ (i.e. three) branches and no loops.

$\mathcal{N}(C)$ can contain no trees, since it is not connected.

Fig. 6 shows a wood of $\mathcal{N}$ of order 2. It is part of those trees of $\mathcal{N}$ shown in Figs. 5(*a*)–5(*d*). (See Lemma 5.)

By Definition 7, a network which is not connected, e.g. $\mathcal{N}(C)$, will contain woods. Two woods of $\mathcal{N}(C)$ are shown in Fig. 7; that in Fig. 7(*a*) is of the order 1, while that in Fig. 7(*b*) is of the order 2.

Lemma 6 tells us that no wood of $\mathcal{N}(C)$ can have more than two branches, while Lemma 7 tells us that at least one wood of this order will exist. Such a wood we call a forest (Definition 9). $\mathcal{N}(C)$ contains three forests, which we show in Fig. 8. Figs. 8(*a*) and 8(*b*) are the forests containing the wood of Fig. 7(*a*). (See Lemma 9.)

To illustrate Definition 10 in regard to tree products, we show in Table 1 the value of the tree product t for each of the trees of $\mathcal{N}$ as shown in Fig. 5.

Table 1

Part of Fig. 5	(*a*)	(*b*)	(*c*)	(*d*)	(*e*)	(*f*)	(*g*)
Tree-product, t	$\frac{C_1C_2}{L_1}\lambda$	$\frac{C_1}{L_1R_1}$	$\frac{C_1C_3}{L_1}\lambda$	$\frac{C_1}{L_1L_2}\frac{1}{\lambda}$	$\frac{C_2}{L_1R_1}$	$\frac{C_2C_3}{L_1}\lambda$	$\frac{C_2}{L_1L_2}\frac{1}{\lambda}$

Now the nodal admittance matrix P of $\mathcal{N}$ relative to the reference node 0 is

$$P \equiv \begin{bmatrix} (\lambda C_1 + \lambda C_2) & -\lambda C_1 & -\lambda C_2 \\ -\lambda C_1 & \left(\lambda C_1 + \lambda C_3 + \frac{1}{R_1} + \frac{1}{\lambda L_2}\right) & -\left(\lambda C_3 + \frac{1}{R_1} + \frac{1}{\lambda L_2}\right) \\ -\lambda C_2 & -\left(\lambda C_3 + \frac{1}{R_1} + \frac{1}{\lambda L_2}\right) & \left(\lambda C_2 + \lambda C_3 + \frac{1}{R_1} + \frac{1}{\lambda L_1} + \frac{1}{\lambda L_2}\right) \end{bmatrix} \quad . \ . \ . \ . \quad (19)$$

From Lemma 10, the determinant of P using Table 1 is,

$$\det P = \frac{C_1C_2}{L_1}\lambda + \frac{C_1}{L_1R_1} + \frac{C_1C_3}{L_1}\lambda + \frac{C_1}{L_1L_2}\frac{1}{\lambda} + \frac{C_2}{L_1R_1} + \frac{C_2C_3}{L_1}\lambda + \frac{C_2}{L_1L_2}\frac{1}{\lambda} \quad . \quad (20)$$

i.e. $\det P =$

$$\frac{L_2R_1(C_1C_2 + C_2C_3 + C_3C_1)\lambda^2 + L_2(C_1 + C_2)\lambda + R_1(C_1 + C_2)}{L_1L_2R_1\lambda} \quad . \ . \ . \ . \quad (21)$$

It may be noted in passing that, since for each tree of $\mathcal{N}$ we get precisely one positive term in eqn. (20), we may calculate the number of trees in $\mathcal{N}$ by evaluating $\det P$ for $\lambda = 1$ and unity element values throughout.[11]

At this stage the reader may care to verify Lemmas 11, 12 and 13 and Theorem 1 for the network of Fig. 1.

The proof of Lemma 14 will perhaps be clarified by illustration. Applied to our $\mathcal{N}$ of Fig. 1, the proof points out that since we form $\mathcal{N}^*(L)$ by substituting short-circuits for all capacitors and resistors and then identifying those nodes which have become joined by short-circuits, then each separate part of $\mathcal{N}(CR)$ in Fig. 3(*b*) must correspond with a node of $\mathcal{N}^*(L)$ in Fig. 4. This may be verified by comparing the two Figures.

The rest of Section 2 may now be applied to Fig. 1 without any difficulty.

(7.3) Loop-Impedance Matrix

We now consider Section 3. Although we made only a passing mention of co-trees, we shall illustrate here the co-trees of $\mathcal{N}$. Thus each tree of $\mathcal{N}$ defines a co-tree, and so we have seven co-trees as shown in Fig. 9, where the order of arrangement corresponds with that of Fig. 5. Note that each co-tree contains M (i.e. three) branches.

Using the loops defined in Fig. 2, the loop-impedance matrix Q is given by

$$Q \equiv \begin{bmatrix} \left(R_1 + \frac{1}{\lambda C_1} + \frac{1}{\lambda C_2}\right) & \left(\frac{1}{\lambda C_1} + \frac{1}{\lambda C_2}\right) & \left(\frac{1}{\lambda C_1} + \frac{1}{\lambda C_2}\right) \\ \left(\frac{1}{\lambda C_1} + \frac{1}{\lambda C_2}\right) & \left(\frac{1}{\lambda C_1} + \frac{1}{\lambda C_2} + \frac{1}{\lambda C_3}\right) & \left(\frac{1}{\lambda C_1} + \frac{1}{\lambda C_2}\right) \\ \left(\frac{1}{\lambda C_1} + \frac{1}{\lambda C_2}\right) & \left(\frac{1}{\lambda C_1} + \frac{1}{\lambda C_2}\right) & \left(\frac{1}{\lambda C_1} + \frac{1}{\lambda C_2} + \lambda L_2\right) \end{bmatrix} \quad . \ . \ . \ . \quad (22)$$

Lemma 15 tells us that

$$(\det Q) = k^2 (\det P) (\text{product of all branch impedances}) \quad . \quad (23)$$

for some positive or negative integer k. In this case the set of loops chosen is simple,[3] and so $k^2 = 1$. Hence

$$(\det Q) = (\det P)\left(\frac{R_1 L_1 L_2}{C_1 C_2 C_3}\ \frac{1}{\lambda}\right) \quad . \quad . \quad . \quad (24)$$

$$= \frac{R_1 L_2 (C_1 C_2 + C_2 C_3 + C_3 C_1)\lambda^2 + L_2 (C_1 + C_2)\lambda + R_1 (C_1 + C_2)}{C_1 C_2 C_3 \lambda^2}$$

$$. \quad . \quad . \quad . \quad (25)$$

Eqn. (10) of Theorem 3 may now easily be verified.

(7.4) Expressions for Other Network Functions

In Section 4 we considered the driving-point admittance between nodes 0 and 1.

We illustrate here Definition 12 by showing in Fig. 10 the network $\mathcal{N}'$ obtained from $\mathcal{N}$ by short-circuiting nodes 1 and 0. The nodal admittance matrix P' of $\mathcal{N}'$, relative to node 0, is given by

$$P' \equiv \begin{bmatrix} \left(\lambda C_1 + \lambda C_3 + \frac{1}{R_1} + \frac{1}{\lambda L_2}\right) & -\left(\lambda C_3 + \frac{1}{R_1} + \frac{1}{\lambda L_2}\right) \\ -\left(\lambda C_3 + \frac{1}{R_1} + \frac{1}{\lambda L_2}\right) & \left(\lambda C_2 + \lambda C_3 + \frac{1}{R_1} + \frac{1}{\lambda L_1} + \frac{1}{\lambda L_2}\right) \end{bmatrix}$$

. . . . (2

We notice that this matrix is obtained from P (eqn. 19) by deletir the first row and column. This gives, in fact, the proof Lemma 16.

From Fig. 10 we may obtain the various values used in eqn. (1 of Theorem 4. They are

$$\left.\begin{aligned} S'_C &= 1 \\ S'_{CR} &= 1 \\ S'_L &= 1 \\ S'_{LR} &= 1 \end{aligned}\right\} \quad . \quad . \quad . \quad . \quad . \quad . \quad . \quad (2$$

Hence from Theorem 4 we deduce that the driving-point admi tance Y between nodes 0 and 1 of $\mathcal{N}$ before the cancellation any common factors, is of the form

$$Y = \left(\frac{\text{Polynomial containing a constant and of degree 2}}{\text{Polynomial containing a constant and of degree 4}}\right)\lambda \ . \ (2$$

This may be verified by straightforward calculation.

621.317.41 : 621.314.2

The Institution of Electrical Engineers
Monograph No. 313 M
Oct. 1958

THE TIME DECREASE OF PERMEABILITY IN TRANSFORMER STEEL

By Professor A. K. SMOLINSKI, Dipl.Ing., D.Sc., Associate Member, and M. ZBIKOWSKI, Dipl.Ing.

(*The paper was first received 27th February, and in revised form 11th June, 1958. It was published as an* INSTITUTION MONOGRAPH *in October, 1958.*)

SUMMARY

The paper describes some measurements of time-decrease of permeability on three types of samples stamped out from 4%-silicon hot-rolled transformer steel. The first samples contained severe mechanical stresses. Secondly, samples annealed at 800° C were used, and the maximum time of permeability decrease of about 24 hours was reduced after annealing to about 8 hours.

Finally samples annealed at 1 250° C in hydrogen atmosphere were measured and the results showed that the time-decrease phenomenon was practically eliminated according to the theory of Snoek.[3,4]

(1) INTRODUCTION

One form of magnetic viscosity, the so-called 'time-decrease of permeability' was first described by Ewing in 1885. This phenomenon might cause difficulties in quantitative testing of the properties of soft-magnetic materials and might—in worst cases—be responsible for errors of more than 100%, if necessary precautions were not taken. The time decrease of permeability was first investigated thoroughly by Webb and Ford[1] in 1933, although it had been previously mentioned by others. In 1938 Paterson[2] added a useful contribution to this problem, and in the same year Snoek[3] advanced a formal theory and physical explanation.[4] Recently Feldtkeller and Sorger[5] indicated that there exists a connection between the time decrease of permeability and the changes in the hysteresis loop.

The present paper presents some results of tests carried out on silicon-steel in the form of laminations used in communication transformers. The influence of internal stresses on the permeability decrease is also discussed.

(2) DESCRIPTION OF THE PHENOMENON OF TIME-DECREASE OF PERMEABILITY

Many measurements of permeability at low magnetizing-fields performed on magnetic materials, and especially on transformer steels, reveal a pronounced decrease of permeability with time after demagnetization.

The process of demagnetization consists generally in inducing in the material an alternating magnetic-field of greater intensity than that corresponding to technical saturation and subsequently reducing it gradually to zero. The material is demagnetized, but this magnetic state does not remain steady. The measurements show that the low-field permeability decreases with time, Fig. 1. This decrease of permeability at low fields extends over a long period of time. As Webb and Ford have shown, it can last for two weeks and the difference of permeability can become greater than 100%. Paterson[2] stated that for electrical steels of medium silicon content the decrease of permeability at 10 gauss amounts to between 5 and 15% of its initial value during the first 24 hours after demagnetization. Practically no change occurs later.

This phenomenon, which appears at low field intensities, can introduce large errors in the results of measurements of inductances of transformers and chokes if the necessary precautions are not taken. Therefore the A.S.T.M. Standards[6] introduce the rule of 24-hour time periods between the demagnetization and the process of measurements. This is rather irksome in normal factory routine, and it is desirable to find some means of shortening the time. Measurements performed on cores cut out from one sort of 4% silicon-steel used for low-frequency transformers showed that, after an annealing process, the time between demagnetization and measurements, necessary for achieving correct results, can be shortened considerably. It will be shown later that this interval depends on the temperature, the duration and the atmosphere of the annealing process.

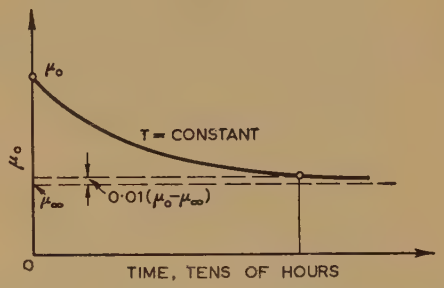

Fig. 1.—Variations of alternating-current permeability with time at low magnetizing forces.

(3) THE PREPARATION OF SAMPLES AND THE MEASURING TECHNIQUE

The samples were stamped out with a compound die from 4%-silicon hot-rolled factory-annealed transformer steel (0·35 mm thick) which has at 20 millioersteds a permeability, μ_{20}, equal to or greater than 700 gauss/oersted.[7]

They took the form of rings of 68–48 mm diameters. The measurements were performed in three stages.

First, samples containing severe mechanical stresses caused by plastic deformation on the edges of the rings were used. It was shown by X-ray photographs that the middle portions of the rings were practically free of stresses. These stresses lowered the permeability of the samples by not more than 20% of its original value of the whole sheet. This reduction in permeability can be used to estimate the magnitude of the stresses in the samples.

Secondly, the samples were used after an annealing process consisting of heating for 4 hours at 800° C without any access of air and subsequent slow cooling. The X-ray photographs showed that the external stresses practically vanished from the whole sample and the permeability increased.

In the third stage, the annealing process was carried out for 4 hours in the atmosphere of hydrogen at 1 250° C with subsequent slow cooling. The material was purified, the carbon content was reduced, thereby relieving to some extent the internal stresses and again increasing the permeability.

All measurements were made with a Maxwell bridge specially arranged for permeability measurements with a constant mag-

Correspondence on Monographs is invited for consideration with a view to publication.
Prof. Smolinski and Mr. Zbikowski are at the Institute of Basic Technical Problems, Polish Academy of Science, Poland.

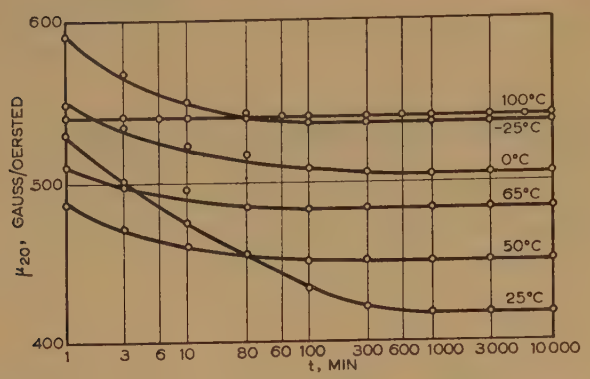

Fig. 2.—Variations of 20-millioersted permeability of unannealed samples over a long period.

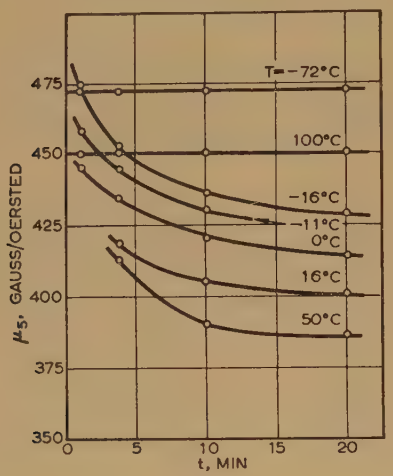

Fig. 3.—Variations of 5-millioersted permeability of unannealed samples over a short period.

netizing force. The frequency was low, 60 c/s being used to avoid the influence of stray fields from the mains supply frequency of 50 c/s. A wave analyser was used as a sensitive null indicator. Good results were obtained with samples in alternating fields of the order of a few millioersteds. In each cycle of measurements the sample was first demagnetized in a coil carrying a strong current at 50 c/s, and then measured by means of a bridge with the magnetizing current switched on during the whole time of the process of measuring. The first measurements were carried out at room temperature, but later also at temperatures from −80° to +100° C. The difficulty of maintaining a constant temperature during several days was the cause of some scatter of the results.

(4) MEASUREMENTS PERFORMED ON UNANNEALED SAMPLES

The first measurements were made at a field intensity of 20 millioersteds, which is the normal value used for the permeability measurements prescribed by standards used in Central Europe.[8] It will be shown later that this field intensity provides nearly the greatest permeability difference. This value is rather too high because it slightly obscures the observed phenomenon. Therefore later a field intensity of 5 millioersteds was used, which is about the smallest value that can safely be used to avoid effects of stray fields.

The typical time dependence of permeability at 20 millioersteds

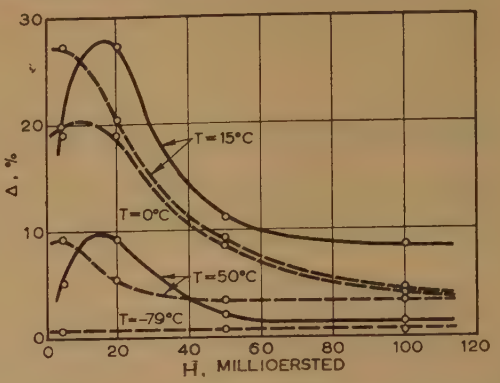

Fig. 4.—The difference of permeability measured 1 min and about 4 hours after demagnetization plotted against field intensity.
—— Samples unannealed, 15° C and 50° C.
---- Samples annealed, −79° C, 0° C and 50° C.

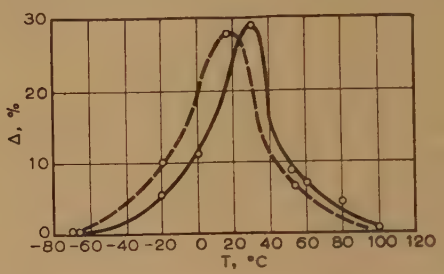

Fig. 5.—The permeability difference measured one minute and abou 48 hours after demagnetization plotted against temperature at 2 millioersteds.
—— Samples unannealed; ---- Samples annealed.
$\Delta_{20} = f(t)$

for various temperatures is shown in Fig. 2. The longest tim decrease of permeability and the greatest permeability differenc exist at about 25° C; the first is of the order of 12 hours, beyon which the permeability difference is only 1% of the greates permeability difference ($\mu_0 - \mu_\infty$) (Fig. 1). At other tem peratures the permeability difference and the time decrease c permeability are smaller. The last value is several hours onl at 0° and at 50° C and falls definitely to zero at −70° and a +100° C (Fig. 3).

It can be shown from these measurements that the Webb an Ford equation

$$\Delta = \frac{\mu - \mu_\infty}{\mu_\infty} 100\% = K \exp(-At^n)$$

is satisfied for $n = 0{\cdot}25$ with a few per cent error. The corre sponding coefficients for 15° C and field intensity $H = 5$ millioer steds are $K \simeq 30$ and $A \simeq 0{\cdot}5$. These coefficients decrease wit increase of temperature.

The greatest permeability decreases, Δ' (defined with per meability μ' measured one minute after demagnetization) appear at field intensities of approximately 20 millioersted (Fig. 4). The same result was obtained by Webb and Ford At a temperature of 25° C the permeability decrease reached maximum near 30% (Fig. 5).

Permeability variations in low field intensities versus tem perature for constant permeabilities, μ_∞, have a characteristi minimum, first shown by Snoek,[3] at a temperature of abou 25° C (Fig. 6). For the measurements made one minute afte demagnetization this minimum is shifted to about 50° C. O the ascending part of the permeability curve there is a maximu of power factor tan δ (Fig. 7), also first shown by Snoek.[3]

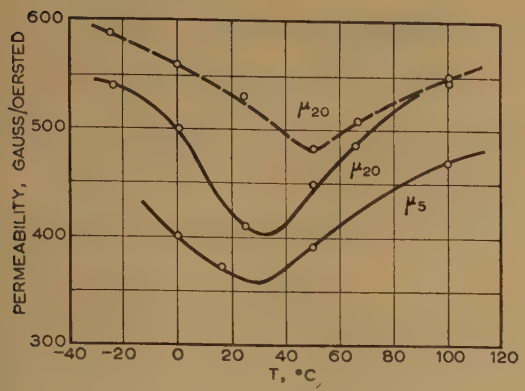

Fig. 6.—Constant (μ_∞) and 'one minute' (μ') values of permeability plotted against temperature.

—— μ_∞ ---- μ'

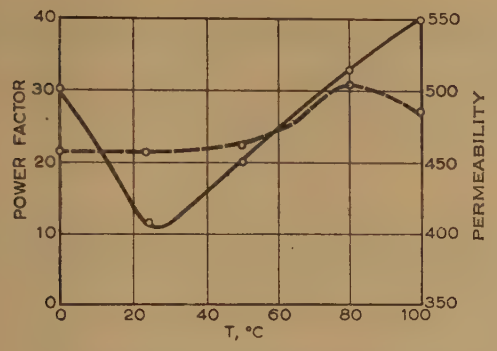

Fig. 7.—Constant values of permeability and power factor of permeability plotted against temperature.

—— Permeability. ---- Power factor.

The permeability/field-intensity curves taken at various temperatures are shown in Fig. 8 for the samples measured 24 hours after demagnetization. The nearly flat part observed at small field intensities is characteristic for the time decrease of permeability phenomenon.[5]

(5) MEASUREMENTS ON SAMPLES ANNEALED IN LOWER TEMPERATURES

In the second part of these experiments the measurements were made on samples annealed at 800° C and cooled slowly. A few examples of these measurements are shown in Figs. 9–11. Curves of permeability are plotted for 20 and 5 millioersteds in Figs. 9 and 10 for long periods of time, whereas Fig. 11 gives the corresponding curve for the permeability at 5 millioersteds during a short period. Comparison with the results of measurements on unannealed samples shows that the effect of annealing is to reduce the maximum time of permeability decrease by a factor of about three, i.e. to about 8 hours. During the first 20 min the permeability decreases in both types of samples are nearly the same. Marked differences show up later.

The effect of annealing on the position of the maxima of the permeability difference is shown in Figs. 4 and 5. The maximum position on the field-intensity axis is shifted to smaller values, and the maximum position on the temperature axis is slightly shifted to lower temperatures. The maximum heights are not affected.

The other properties of annealed samples are of the same character as those of samples not annealed and therefore are not presented here.

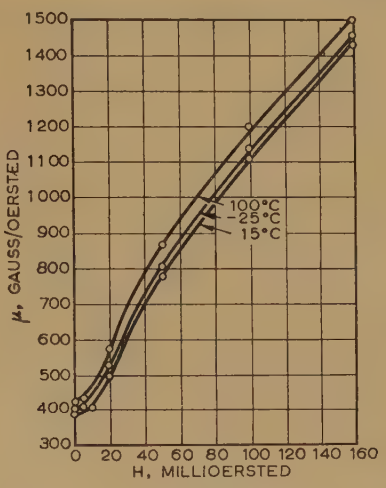

Fig. 8.—Constant values of permeability, μ_∞, plotted against field intensity, H, at different temperatures.

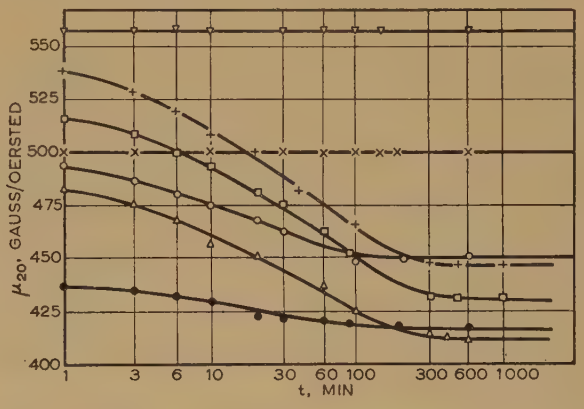

Fig. 9.—Variations of 20-millioersted permeability of annealed samples at 800° C, over a long period.

▽ −79° C.
\+ 25° C.
□ 15° C.
× 100° C.
○ −20° C.
△ 0° C.
● 50° C.

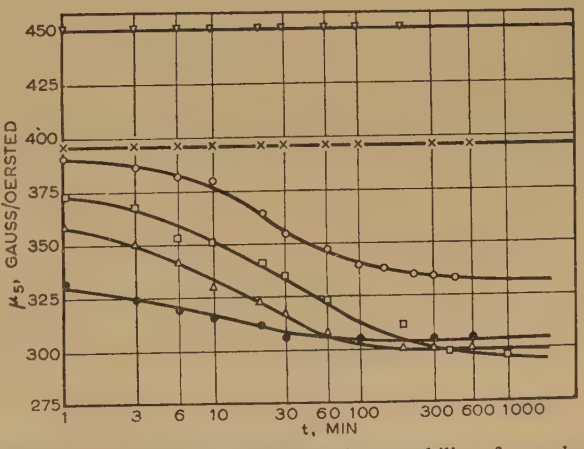

Fig. 10.—Variations of 5-millioersted permeability of annealed samples at 800° C, over a long period.

▽ −79° C.
× 100° C.
○ −20° C.
△ 0° C.
● 50° C.
□ 15° C

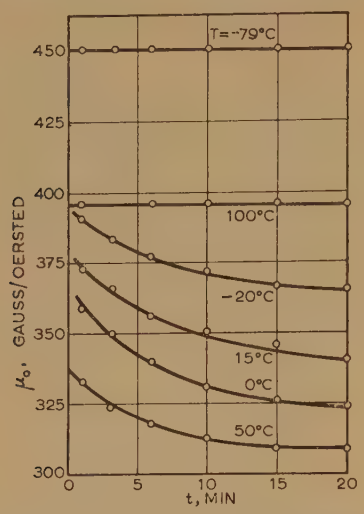

Fig. 11.—Variations of 5-millioersted permeability of annealed samples at 800° C, over a short period.

(6) MEASUREMENTS ON SAMPLES ANNEALED AT HIGHER TEMPERATURES IN AN ATMOSPHERE OF HYDROGEN

The third part of the experiments consisted of preliminary measurements on samples annealed in hydrogen atmosphere at 1 250° C. The results of measurements of permeability decrease are shown in Figs. 12 and are compared with corresponding curves for the low-temperature annealed and unannealed conditions. From this Figure we can see that the high-temperature annealing process carried out in hydrogen practically eliminates the time-decrease phenomenon in accordance with the theory of Snoek;[3,4] the time of permeability variations is reduced to a few minutes and the magnitudes of permeability variations diminish to a few per cent.

(7) DISCUSSION OF RESULTS

The time decrease of permeability appears distinctly in laminations stamped out from silicon-steels as used in telecommunication transformers and chokes. It attains its greatest values at room temperatures and in field intensities of about 20 millioersteds, i.e. in normal measuring conditions. The permeability differences are not greater than 30% and practically disappear in 24 hours. This time period is recommended in A.S.T.M. Standards for measuring magnetic materials.[6]

In laminations stamped out and annealed at lower temperatures (about 800° C) the time periods between demagnetization and measurement process are about three times shorter (7 or

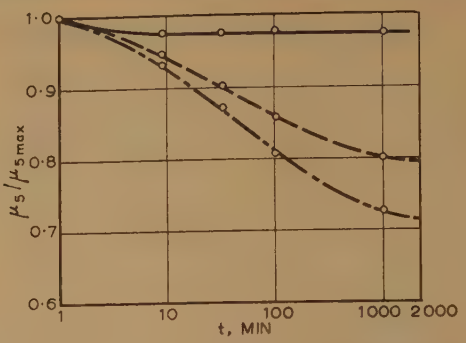

Fig. 12.—The comparison of time decrease of permeability of different samples.
—— High-temperature hydrogen annealed.
---- Low-temperature annealed.
—·— Unannealed.

8 hours). This enables us to perform the whole measurement one day, and is very convenient from the point of view of factor routine.

The high-temperature hydrogen-annealed 4% silicon-steels a practically free from the described time decrease of permeabili ten minutes after demagnetization.

(8) REFERENCES

(1) WEBB, C. E., and FORD, L. H.: 'The Time-Decrease Permeability at Low Magnetizing Forces', *Journal I.E.E* 1934, **75**, p. 787.
(2) PATERSON, G. R.: 'Drift of Magnetic Permeability at Lo Inductions after Demagnetization', *Journal of Appli Physics*, 1938, **9**, p. 646.
(3) SNOEK, J. L.: 'Time Effects in Magnetization', *Physica*, 193 **5**, No. 5, p. 663.
(4) SNOEK, J. L.: 'New Developments in Ferromagnet Materials' (Elsevier, 1949), p. 41.
(5) FELDTKELLER, R., and SORGER, G.: 'Magnetische Nac wirkungen der Anfangspermeabilität und der Bar hausensprünge', *Archiv der Elektrische Übertragung*, 195 **7**, No. 2, p. 79.
(6) ASTM A34–47: 'Standard Methods of Testing Magnet Materials'.
(7) SMOLINSKI, A.: 'Transformer Cores with Special Properti obtained from Silicon Steel', *Bulletin de l'Academ Polonaise des Sciences*, Cl.IV, 1953, **1**, No. 3, p. 109.
(8) DIN E41301: 'Weicheisen für Übertragerbleche', 1943.
(9) BOZORTH, R. M.: 'Ferromagnetism' (Van Nostrand, 1951 p. 795.

621.311.153.2

The Institution of Electrical Engineers
Monograph No. 314 S
Oct. 1958

THE RELATIONSHIP BETWEEN WEATHER AND ELECTRICITY DEMAND

By M. DAVIES, M.Sc., Ph.D.

(*The paper was first received 2nd April, and in revised form 19th June, 1958. It was published as an* INSTITUTION MONOGRAPH *in October, 1958.*)

SUMMARY

A method is described for statistically analysing the relationship between weather and electricity demand for applications to practical load estimating by electricity supply engineers. The characteristics of the specific meteorological elements to which the demand has been found to respond are discussed, particularly those affecting heating and lighting demands. The thermal-lag factor appropriate to the delay in consumer response to temperature changes and the influence of the cooling power of the wind on heating load are examined. In order to assess the lighting load, observations of the atmospheric transmission of light are used to derive a method for reducing cloud and visibility forecasts to their daylight illumination equivalents.

(1) INTRODUCTION

The purpose of the paper is to provide technical information concerning the effect of weather on electricity demand. The first part of the paper is expository and outlines a scheme for analysing weather/load relationships, and the second part is devoted to researches on the weather parameters which the scheme requires.

(2) LOAD/WEATHER ANALYSIS BY MULTIPLE REGRESSION METHODS

(2.1) Electricity Demands considered as Time Series

The area covered by this investigation is that of the supply system of England and Wales.

When the demands for a particular half-hour are plotted serially day by day, the points form a time series with a pronounced trough in the summer months and a peak in the winter months. On this seasonal trend is superimposed a large erratic variation which is attributable to weather, together with a regular rhythmic variation between the different days of each week. In these circumstances it is natural to premise that the demand for any one half-hour can be represented by a smooth basic demand curve, modified only by a regular systematic variation with day of week, plus a weather-susceptible component.

Because of the continuous variation of the composition of the demand with time of day, separate analyses of these time series are necessary for each half-hour under consideration. Attention has been concentrated on the demands at the half-hours ending 0900, 1200 and 1700 hours (clock time) because throughout the year the daily maximum demands fall closely around one of these times.

(2.2) Meteorological Data

Hourly weather reports are made at a large number of observing stations in this country by the Meteorological Office.

For each specific meteorological factor investigated it is necessary to calculate a weighted average of the simultaneous values at reporting stations selected according to the geographical distribution of load density. The weighting is proportional to the weather-sensitive component of demand in the region of which each reporting station is considered representative, the weights being in the first instance established by analysis of each Grid Control Area separately. Some 20 stations were used to calculate these weights, but in subsequent applications it was found that sufficient accuracy could be obtained using six stations.

The meteorological elements found to affect the demand are as follows:

(*a*) Temperature.
(*b*) Wind speed.
(*c*) Cloud.
(*d*) Visibility.
(*e*) Precipitation.

Elements (*a*) and (*b*) control the heating demand, the wind speed being allied to temperature in dissipating heat from buildings; (*c*), (*d*) and (*e*) are used to estimate the level of daylight illumination which determines the lighting demand. Like net-radiation and wind, (*e*) also affects the rate of heat loss from the external surfaces of buildings, but the disturbance in the thermal flow at interior surfaces is so attenuated that in practice the only other effects of precipitation are direct ones such as keeping people indoors and so increasing the demand for electricity. Thus of the three weekday peaks studied in detail the only peak for which the effect of rainfall has been detected is the evening peak where it may be assumed that the public have greater powers of choice.

For comparison with the demand series the meteorological information is reduced to a number of specific factors designated as follows:

(i) 'Effective' temperature, X_1.
(ii) Cooling power of the wind, X_2.
(iii) Daylight illumination index, X_3.
(iv) Rate of precipitation, X_4.

These factors and their genesis are discussed in Section 3 under their respective headings. For the present it is sufficient to explain that in calculating X_1 account is taken of thermal time-lag effects, that X_2 is based on an empirical formula which combines the effects of temperature and wind, and that X_3 is the estimated daylight illumination on a logarithmic scale. A logarithmic scale is used primarily because experiments which have been carried out when the heating demand was considered constant have indicated that the load varies linearly with the logarithm of the daylight illumination.[1]

(2.3) Linear Regression Method of Load Analysis

In deriving the functional relationships between the variation of demand and the specific meteorological factors to which it is sensitive the basic assumption is made that the weather-sensitive component of the demand can be expressed as a sum of functions of the respective meteorological factors.

As a first approximation, and in order to provide a basis for

Correspondence on Monographs is invited for consideration with a view to publication.
Dr. Davies is with the Central Electricity Generating Board.

a more accurate determination, the functional relationships will be assumed linear. To derive these relationships from, say, a year's data, it is necessary to eliminate the combined seasonal and long-term trend and also the day-of-week effect.

A regression equation of the form:

$$Y = a + b_1X_1 + b_2X_2 + b_3X_3 + F(t) + \delta \quad . \quad . \quad (1)$$

is therefore fitted to the data, where Y is the demand at a fixed time each day, X_1, X_2, X_3 are the corresponding specific meteorological factors, $F(t)$ is a polynomial function of the time of year t, δ is the day-of-week correction which takes on different values on different days of the week, and a, b_1, b_2, b_3 are constants.

In this expression the known quantities are the dependent variate Y and the independent variates X_1, X_2, X_3, t, and the analysis has for its object the estimation of the 'best' values of the regression coefficients b_1, b_2, b_3 and the values of δ. Prescribed meteorological variables may be added to or removed from this expression as required. Thus in the analysis of 1700 hours demand, the variable X_4 is incorporated, while in the analysis of demands in darkness X_3 is evanescent.

The two sides of eqn. (1) cannot be made to balance exactly on every occasion, and in the least-squares sense the best values of the coefficients are those which minimize the sums of squares of the residuals, i.e. the differences ϵ between the two sides of this expression.

We have therefore to minimize

$$\Sigma\epsilon^2 = \Sigma[Y - a - b_1X_1 - b_2X_2 - b_3X_3 - F(t) - \delta]^2 \, . \quad .(2)$$

where the summation sign refers to the entire N sets of data.

Since the observations are uniformly spaced, the most convenient form of the terms of $F(t)$ are the orthogonal polynomials of least squares:[2]

$$F(t) = a_1P_1 + a_2P_2 + \ldots + a_jP_j + \ldots \quad . \quad . \quad (3)$$

where P_j is an orthogonal polynomial of degree j, and a_j its associated coefficient in the regression equation.

The orthogonal polynomials P_j have been widely tabulated, but not for N as large as that corresponding to a whole year of daily observations. However, as the form of the basic demand curve may be closely approximated by a step function, where the width of the steps is one week, it is sufficient to take t to be the number of weeks reckoning from the first week of the period and to use the set of orthogonal polynomials corresponding to the number of weeks n in the period.

It was found that a good fit to a year's data could be obtained by fitting polynomials up to the sixth degree, and for purposes of illustration this degree of fitting will be assumed.

In evaluating δ it is convenient to express it in terms of (0, 1) indicators. Thus for a 5-day week from Monday to Friday we write:

$$\delta = \delta_MX_M + \delta_TX_T + \delta_WX_W + \delta_{Th}X_{Th} + \delta_FX_F \quad . \quad (4)$$

where the suffixes M, T, . . ., F refer to the different days of the week, and $X_D = 1$ on day D and zero on other days. When eqns. (3) and (4) are substituted in eqn. (2) and the expression minimized, the day-of-week corrections δ_M, δ_T, . . ., δ_F then emerge as regression coefficients in the resulting normal equations. The minimization is carried out subject to the linear constraint:

$$\delta_M + \delta_T + \ldots + \delta_F = 0 \quad . \quad . \quad . \quad . \quad (5)$$

(2.4) Computational Procedure for Linear Regression

On development, the above process is reducible to the following scheme:

Writing

$$A = \begin{bmatrix} \Sigma X_1^2 & \Sigma X_1X_2 & \Sigma X_1X_3 \\ \Sigma X_1X_2 & \Sigma X_2^2 & \Sigma X_2X_3 \\ \Sigma X_1X_3 & \Sigma X_2X_3 & \Sigma X_3^2 \end{bmatrix} \quad . \quad . \quad . \quad (6$$

$$F = \begin{bmatrix} \underset{M}{\Sigma X_1} & \underset{M}{\Sigma X_2} & \underset{M}{\Sigma X_3} \\ . & . & . \\ . & . & . \\ . & . & . \\ \underset{F}{\Sigma X_1} & \underset{F}{\Sigma X_2} & \underset{F}{\Sigma X_3} \end{bmatrix} \quad . \quad . \quad . \quad (7$$

$$G = \begin{bmatrix} \frac{\Sigma X_1P_1}{\sqrt{\Sigma P_1^2}} & \frac{\Sigma X_2P_1}{\sqrt{\Sigma P_1^2}} & \frac{\Sigma X_3P_1}{\sqrt{\Sigma P_1^2}} \\ . & . & . \\ . & . & . \\ . & . & . \\ \frac{\Sigma X_1P_6}{\sqrt{\Sigma P_6^2}} & \frac{\Sigma X_2P_6}{\sqrt{\Sigma P_6^2}} & \frac{\Sigma X_3P_6}{\sqrt{\Sigma P_6^2}} \end{bmatrix} \quad . \quad . \quad (8$$

where the symbol $\underset{D}{\Sigma}$ means summation over days of type D, we construct the elements $\Sigma' x_r x_s$ of the 'reduced' information matrix:

$$A - \frac{1}{n}F'F - G'G \quad . \quad . \quad . \quad . \quad . \quad (9$$

where primes affixed to matrix symbols denote transposed matrices. Computationally, this is done by regarding the columns of F and G as data columns for calculating sums of squares and products as in ordinary correlation analysis. The same rule gives the reduced product sums $\Sigma' x_r y$ of X_r with Y, etc.

The elements ΣX_rP_j required for constructing G are obtained by multiplying the P_j's extracted from tables[2] by the weekly sums of the respective variates, since $P_j(t)$ is held constant throughout each week, and for a 5-day week each ΣP_j^2 is 5 times its tabular value.

The covariance matrix of the b_r's:

$$C = \begin{bmatrix} c_{11} & c_{12} & c_{13} \\ c_{21} & c_{22} & c_{23} \\ c_{31} & c_{32} & c_{33} \end{bmatrix} \quad . \quad . \quad . \quad . \quad (10$$

is calculated by inverting eqn. (9):

$$C = \left(A - \frac{1}{n}F'F - G'G\right)^{-1} \quad . \quad . \quad . \quad . \quad (11$$

and the covariance matrix of the δ's is then given by

$$D = \frac{1}{n}I_5 + \frac{1}{n^2}ECE' \quad . \quad . \quad . \quad . \quad . \quad (12$$

where I_5 is a unit matrix and E is the day-of-week matrix obtained from the crude matrix (7) by subtracting $\frac{1}{5}\Sigma X_1$, $\frac{1}{5}\Sigma X_2$, $\frac{1}{5}\Sigma X$ from the elements of the first, second and third columns respectively.

The quantities of immediate interest in this analysis are the meteorological regression coefficients b_1, b_2, b_3 which measure the weather responses (i.e. the change in demand per unit change of each meteorological variable) and the day of week corrections δ_M, . . . δ_F, together with their standard errors. These and the other terms in eqn. (1) are calculated in succession by applying the formulae:

$$b_r = c_{r1}\Sigma' x_1 y + c_{r2}\Sigma' x_2 y + c_{r3}\Sigma' x_3 y \qquad (r = 1, 2, 3$$

$$a = (\Sigma Y - b_1\Sigma X_1 - b_2\Sigma X_2 - b_3\Sigma X_3)/N$$

$$\delta_D = (\underset{D}{\Sigma} Y - na - b_1\underset{D}{\Sigma} X_1 - b_2\underset{D}{\Sigma} X_2 - b_3\underset{D}{\Sigma} X_3)/n \qquad (D = M, T, \ldots, F)$$

$$a_j = (\Sigma YP_j - b_1\Sigma X_1P_j - b_2\Sigma X_2P_j - b_3\Sigma X_3P_j)/\Sigma P_j^2 \qquad (j = 1, \ldots, 6)$$

The multiple correlation coefficient R is given by

$$R^2 = [b_1\Sigma X_1Y + b_2\Sigma X_2Y + b_3\Sigma X_3Y - (\bar{Y} - a)\Sigma Y + (a_1\Sigma P_1Y + \ldots + a_6\Sigma P_6Y) + (\delta_M\underset{M}{\Sigma} Y + \ldots + \delta_F\underset{F}{\Sigma} Y)]/N\sigma_y^2$$

and the residual standard deviation of demands by

$$\sigma = \sigma_y(1 - R^2)^{1/2} \quad . \quad . \quad . \quad . \quad . \quad (13)$$

where $$\sigma_y^2 = \frac{\Sigma Y^2}{N} - \bar{Y}^2$$

As thus expressed, no cognizance is taken of the fact that, if eqn. (1) contains p disposable constants, it will give a perfect fit to p sets of data even if there is no real correlation between Y and the other variates. An unbiased estimate of the residual variance of Y is given by

$$\sigma^2 = \Sigma\epsilon^2/(N - p)$$

and therefore σ as calculated from eqn. (13) should be multiplied by the factor $[N/(N-p)]^{1/2}$ in order to allow for the effects of sampling bias. In the case discussed here $p = 14$ since there are only four independent day-of-week terms.

An estimate of the standard error of each b_r is then $\sigma\sqrt{c_{rr}}$, and of each δ_D is $\sigma\left[\frac{1}{n} + \frac{1}{n^2}(ECE')_{DD}\right]^{1/2}$, by eqn. (12). The last term of the latter expression is usually negligible compared with the first, and therefore, to the order $0(1/n^{3/2})$, the standard error of each δ_D is $\sigma/\sqrt{n}$.

The multiple correlation coefficient R between the demand and all the variables introduced into the analysis is so near to unity that of itself it conveys very little intelligence. A more informative parameter is the correlation coefficient R_W between the demand and the weather, which is given by

$$R_W^2 = 1 - \frac{\Sigma\epsilon^2}{\Sigma' y^2}$$

Having calculated the b_r's and δ_D's, the run of basic demands may be determined by adjusting the actual demands to some standard set of weather conditions and eliminating the day-of-week variation. Although the coefficients $a_1, a_2, \ldots, a_6$ are evaluated incidentally in the process of the regression computations, a smooth polynomial fit gives an inadequate description of the *detailed* structure of the basic demand curve.

(2.5) Graphical Curvilinear Regression Analysis

If the relationships between the demand and the specific meteorological factors to which it responds are non-linear, the linear functions introduced into the regression analysis will only yield average effects over the range covered by the data. For instance, a change of temperature of 1° F would not be expected to produce as great a change in demand in summer as in winter; this could be allowed for by incorporating in the regression equation squares and higher powers of X_1, and, in fact, a quadratic or cubic parabola can be made to fit the load/temperature relationship quite well over a limited range.

However, as there is no *a priori* justification for assuming a particular mathematical form for the functional relationships, it is preferable to proceed step by step, and a graphical approach has the advantage that the results are at once amenable to practical applications. Graphical methods of regression analysis have been treated by Ezekiel,[3] and in connection with the particular problem of load analysis by Vedere.[4]

Keeping the functional relationships unspecified, the regression equation (1) assumes the form

$$Y = f_1(X_1) + f_2(X_2) + f_3(X_3) + F(t) + \delta \quad . \quad . \quad (14)$$

where the additive constant has been absorbed in the basic demand curve $F(t)$. In this expression t is taken to be the days of the year numbered consecutively.

As a first approximation to the form of the functional relationships $f_1(X_1)$, $f_2(X_2)$, $f_3(X_3)$, straight lines are drawn whose slopes have the values of the corresponding linear regression coefficients. These are shown as broken lines in Figs. 1, 2 and 3, which refer to the 0900 hours analysis in 1957.

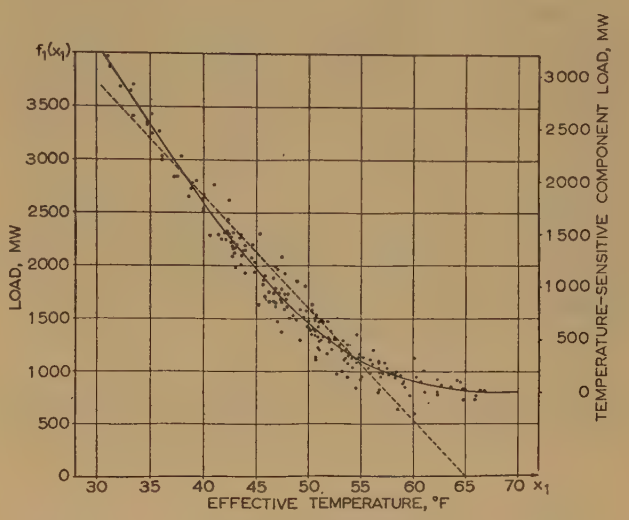

Fig. 1.—Relation between demand and effective temperature, 0900 hours, 1957.

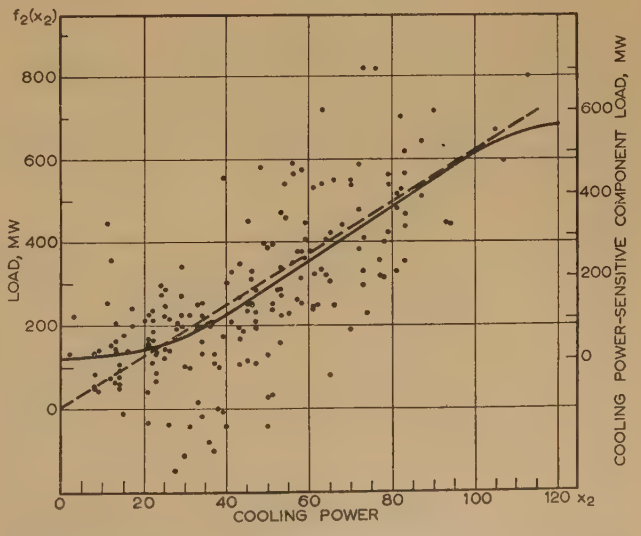

Fig. 2.—Relation between demand and cooling power, 0900 hours, 1957.

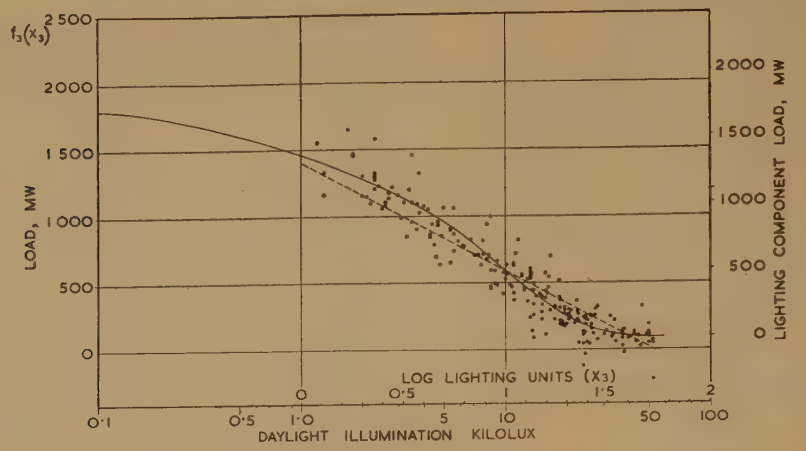

Fig. 3.—Relation between demand and daylight illumination, 0900 hours, 1957.

In general, the x-axis intercepts of these lines are arbitrary since they depend on an arbitrarily prescribed level of weather appropriate to the basic demand. It is, however, convenient to define $F(t)$ as the 'no weather' basic demand from which all the weather-sensitive component is completely removed. Since it is not certain beforehand what the associated weather conditions are, a provisional definition of them must be assumed. This can subsequently be revised from the results of the investigation. For the 0900-hours demands the definition chosen was a temperature of 65°, no wind, and daylight illumination equivalent to perfectly clear and cloudless conditions at the summer solstice, and the three lines were positioned accordingly.

Transposing eqn. (14) to the form

$$F(t) + \delta = Y - f_1(X_1) - f_2(X_2) - f_3(X_3)$$

and reading off from the graphs the first approximation values to the functions on the right, we see that on each occasion an estimate may be made of the quantity on the left. By groupin these estimates according to day of week and taking the depar tures of their respective means from the grand mean, firs approximations to the day-of-week adjustments δ are assessed The estimates obtained in this way with the estimated day-of week variation eliminated, are plotted against the day number in similar fashion to Fig. 4, and a smooth curve fitted by eye t the points to give a first estimate of the smoothed basic-deman curve $F(t)$.

The departures of the individual points from the smoot curve are the residuals ϵ, and these are read from the grap and then adjusted by the constant increments which make thei respective sums for each day of week severally vanish, thes adjustments being compensated for by making correspondin equal and opposite adjustments to the δ's. This step is neces sary in order to allow for the growth of basic demand withi each week. The adjusted residuals are then measured off o

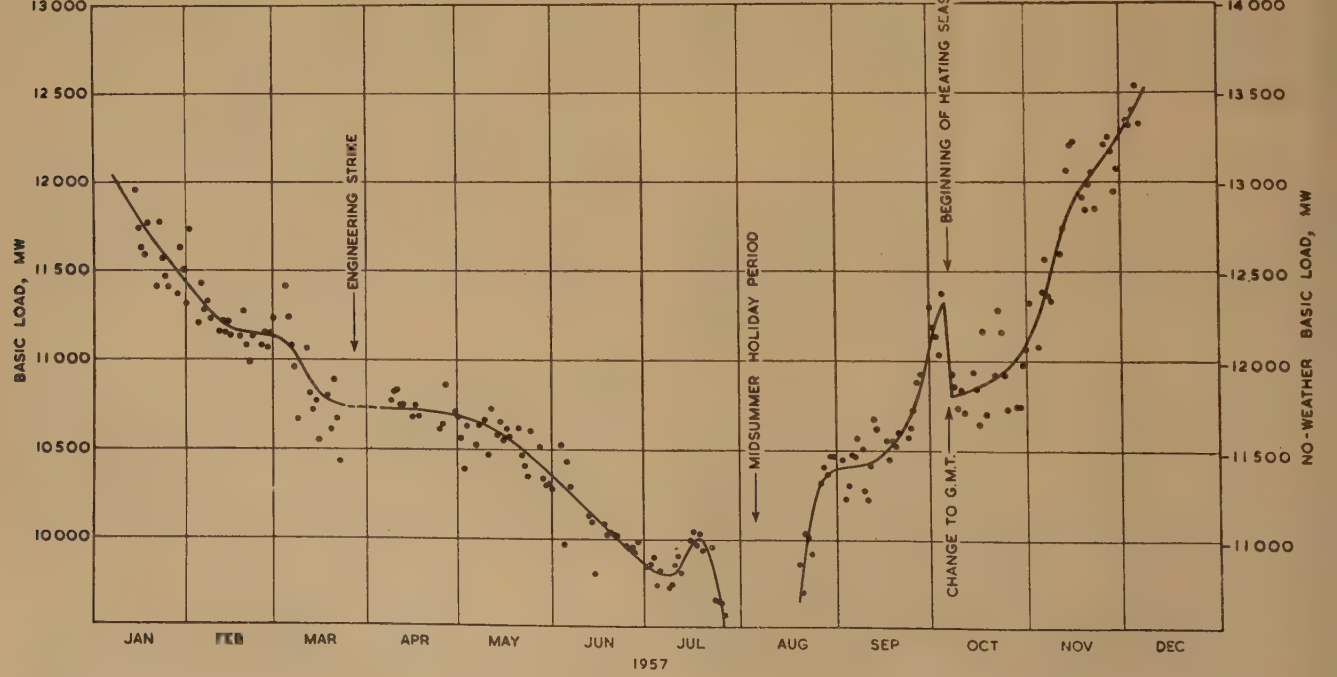

Fig. 4.—Basic load curve, 0900 hours, 1957.

the diagrams for the meteorological variables as ordinates stepped off from the provisional straight lines at the values of X_1, X_2, X_3 corresponding to t.

An inspection of the residuals, as plotted on the diagrams, will reveal whether they are scattered at random about each of the straight lines or whether there is a systematic trend of the points away from any one of them, in which case its shape is amended accordingly by drawing a smooth curve evenly through the points. The above steps are then repeated using the revised curve in place of the straight line, and a new set of residuals calculated and stepped off the graphs. Proceeding in this way the straight-line approximations are replaced by curvilinear relationships and the process is continued until no further improvement can be obtained.

Strictly speaking, only one curve can be modified at a time except where emendations are carried out for segments of different curves which do not influence common residuals. With experience, however, this iterative process can be made very rapid, and, in practice, use is made of the outlines of curves from previous investigations and any logical constraints as an aid to the fitting.

The final set of weather response curves and the basic demand curve with their associated residuals for the 0900 hours demands in 1957 are shown in Figs. 1 to 4. The temperature-response curve is first sensibly horizontal at 70° F, where it may be assumed that all the temperature-sensitive heating load has been removed from the system. The definition of the no-weather basic demand can therefore now be amended to read 70° F for the temperature. With this definition the left-hand ordinates of the temperature curve have to be decreased by 800 MW and this amount has to be added to the basic demand curve. As it is convenient to retain the assumed definitions of the other meteorological factors in the no-weather basic demand, it will be seen that the amounts required to be transferred to the basic-demand curve are 120 MW for the cooling power and 100 MW for the lighting curve, i.e. a net transfer of 1 020 MW for all three factors. The resulting scales having their zeros at the no-weather basic demand are shown on the right-hand vertical axes of the diagrams.

In application to daily load estimation, the basic-demand curve is projected forward one day and to this is added the day-of-week adjustment, and the weather adjustment is obtained by applying the final set of weather-response curves to the weather forecasts. This procedure is similar in principle to a 'cut and try' method proposed by Dryar,[5] who expressed the weather adjustments as percentages of the basic demand and called them 'weather weights'.

To indicate the accuracy of the curvilinear scheme, Fig. 5 has been prepared which is a histogram of errors in estimating demands one day ahead on a large number of occasions in 1957 using *actual* weather reports. This was done on a day-to-day basis and, of course, retrospectively, but before figures of actual demands were available. The standard deviation was 1·4%, and the maximum error in a period of one year, 5·4%, on an average demand of 12 640 MW.

(3) DERIVATION OF SPECIFIC METEOROLOGICAL FACTORS

(3.1) Temperature

Temperature has a large influence on the demand, but owing to the thermal storage in the fabric of buildings the demand does not respond immediately to temperature change.

Much theoretical and experimental work has been done on the transmission of heat through walls in connection with building research. Such studies, which are invaluable in analysing special cases, are of little use for assessing the thermal time-lag appropriate to the entire consumer population. It is therefore not possible to state in advance the precise function of temperature to use in the regression analysis, and one is obliged to proceed heuristically and use the demand record itself as a means of establishing the magnitude of the thermal lag effect.

If T_0 is the ambient temperature, the simplest empirical equation which expresses the lag of internal temperature θ is the first-order lag equation:

$$\frac{d\theta}{dt} + \lambda\theta = \lambda T_0 \quad . \quad . \quad . \quad . \quad . \quad (15)$$

where $\tau = 1/\lambda$ is the thermal time-constant. This assumes that the time-constants for cooling and heating are the same. Although novel building elements have been designed for which this last assumption is not valid,[6] it is a sufficiently close approximation for conventional building structures. θ may be considered as the temperature of an unheated room in a building, which is clearly more closely correlated with electrical heating load than is outside temperature.

Ignoring the transient term, which disappears in the limit, the solution of eqn. (15) is

$$\theta = \lambda\varepsilon^{-\lambda t}\int_0^t \varepsilon^{\lambda t}T_0(t)dt$$

If t is measured towards the past and θ is the room temperature at time $t = 0$, we may write this result:

$$\theta = \lambda\int_0^\infty \varepsilon^{-\lambda t}T_0(t)dt$$

Replacing the integral by summation over sufficiently small unit time intervals:

$$\theta = \lambda(T_0 + \varepsilon^{-\lambda}T_{-1} + \varepsilon^{-2\lambda}T_{-2} + \varepsilon^{-3\lambda}T_{-3} + \ldots)$$

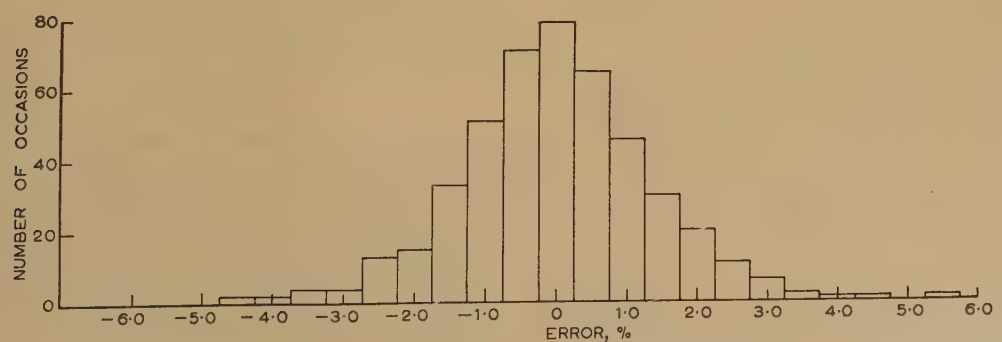

Fig. 5.—Histogram of errors in forward daily load estimation, 1957.

where T_0, T_{-1}, T_{-2}, . . . are the external air temperatures at times $t = 0, 1, 2, 3, \ldots$, and putting $\beta = \varepsilon^{-\lambda}$ and $\alpha + \beta = 1$, then, since we require $\theta \to T_0$ as all the temperatures approach equality, we must have

$$\theta = \alpha(T_0 + \beta T_{-1} + \beta^2 T_{-2} + \beta^3 T_{-3} + \ldots) \quad . \quad (16)$$

Calling θ the 'effective' temperature and writing T_E, T_{E-1}, T_{E-2}, . . . for its values at times $t = 0, 1, 2, \ldots$, we see that eqn. (16) is equivalent to the recurrence relationship:

$$T_E = \alpha T_0 + \beta T_{E-1} \quad . \quad . \quad . \quad . \quad . \quad (17)$$

In order to evaluate the thermal time-constant τ, this recurrence relationship was used to generate effective temperature series from hourly values of air temperatures (weighted as explained in Section 2.2) for the year 1956 for values of β between 0·3 and 0·99.

The outputs for 0900, 1200 and 1700 hours were then substituted as the X_1 variable in the linear regression equation (1), and in each case the partial correlation of demand on effective temperature was calculated. In this work the estimated effects of the other meteorological variables were first eliminated by applying the responses obtained from previous curvilinear analyses. For the remaining meteorological factor, the partial correlation coefficient is then given, in the notation of Section 2.4, by

$$r = \frac{\Sigma' x_1 y}{(\Sigma' x_1^2 \Sigma' y^2)^{1/2}}$$

where the prime refers to the reduced sums of squares and products.

Fig. 6 shows the correlation coefficient r plotted against β.

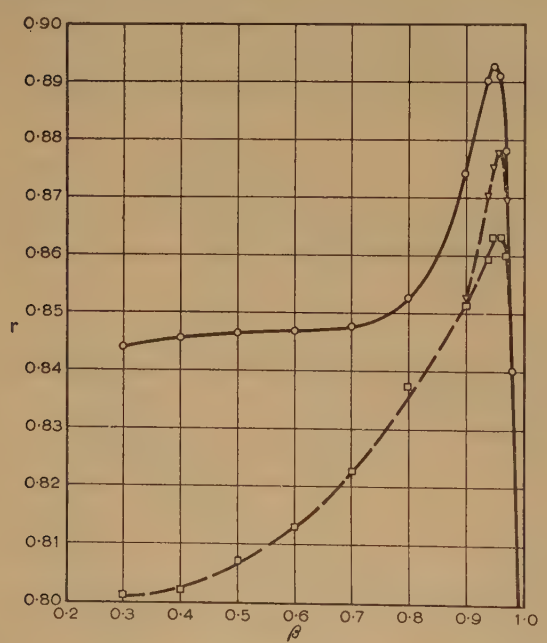

Fig. 6.—Load/effective-temperature correlation coefficient r versus thermal lag factor β.

○——○ 0900 hours.
▽- - - ▽ 1200 hours.
□----□ 1700 hours.

After the 0900 and 17000 hours data had been processed, it was evident that there was a sharp peak at around $\beta = 0{\cdot}95$ or 0·96, so the analysis for 1200 hours was confined to this region.

The three peaks occur at values of β which are so close togethe that we may take their mean, 0·955, as the estimate of its tru value. This corresponds to a value of τ of 22 hours. It interesting to note that a value of 24 hours was proposed by a official committee[7] as applying to the majority of buildings.

The final formula for effective temperature is therefore

$$T_E = 0{\cdot}045T_0 + 0{\cdot}955T_{E-1} \quad . \quad . \quad . \quad (1$$

where the T_0's are hourly air-temperatures, and this is the expre sion which has been used to define the X_1 variable in the loa analyses of Section 2. It is expeditious to apply this relation i the form

$$t_E = T_0 + 0{\cdot}955t_{E-1}$$

and convert the answer at any stage back into temperature usin

$$T_E = 0{\cdot}045t_E$$

Theoretically it is possible to improve slightly upon th concept of effective temperature by adding on the right eqn. (15) a term KL, where L is the total internal heating loa instantaneously applied against natural cooling, and K is constant which depends, *inter alia*, on the volume of the heate space. θ can then be interpreted as the internal temperatu with respect to heated rooms, and one would expect a clos relation between L and θ, say $L = L(\theta, t)$, for the whole popula tion. The exact form of this relationship is unknown, sinc other forms of heating besides electricity are used, but it suggested that there is probably a high positive correlatio between different forms of heating, so we may take $L(\theta, t)$ to b the electrical heating load alone.

Proceeding as before, the solution of the modified equatio (15) is

$$\theta = T_E + KL_E \quad . \quad . \quad . \quad . \quad . \quad (19$$

where the 'effective' heating function L_E is given by the recu rence relation

$$L_E = L_0 + \beta L_{E-1} \quad . \quad . \quad . \quad . \quad . \quad (20$$

L_0, L_{-1}, L_{-2}, . . . being the electrical heating demands at tim $t = 0$, 1 hour previously, 2 hours previously, etc. In this cas K can be interpreted physically as the rise in room temperatu per megawatt of electrical heating load contingently applied.

In application to load estimation this approach requires th construction of a demand-temperature-time surface from synthesis of curvilinear analyses, the temperature being in th first instance T_E. This surface is then modified step by ste using eqns. (19) and (20) until the T_E axis is transformed t one of θ.

Because of the involved nature of this work, it would b premature to say whether or not a definite improvement o effective temperature as a basic parameter for load estimatin can be obtained.

Fig. 1 is typical of the relationship between demand an effective temperature. Down to the lowest temperatures whic have occurred there is no evidence of demand saturation.

(3.2) Cooling Power of the Wind

It is convenient to separate the heating demand into a 'therm storage' component governed by the direct effects of temperatu and a component due to the cooling power of the wind in ass ciation with temperature. Experiments on heat transmissi through walls have shown that the effect of wind speed negligible.[8] Ventilation and infiltration of air are the essenti factors causing internal heat losses in wind conditions, rath than increased heat transfer at external surfaces. Short-peri means of 4 hours were therefore used to study the effect demand of the combined effects of temperature and wind.

Many experiments on the loss of heat from bodies exposed to wind have indicated a formula for the cooling power of the form

$$W^m(T_s - T) \quad . \quad . \quad . \quad . \quad . \quad . \quad (21)$$

where T is the ambient temperature, T_s the body temperature, W the wind speed and m a constant. The number of air changes per hour in a building is approximately a linear function of the wind speed,[9] which suggests that $m = 1$, and this value has been used in several investigations on the fuel requirements of buildings.[10–12] On the other hand, $m = \frac{1}{2}$ for convective heat losses from cylindrical wires and bulbs.[13] Heat losses from the human body[14] are also given by $m = \frac{1}{2}$, with $T_s = 98°$ F.

Because of the uncertainty regarding m, an expression of the form (21), with m and T_s undetermined constants, was substituted into a regression equation of the form of eqn. (1) and the least-squares fit found, with the following solution: $m = 0{\cdot}53$, $T_s = 66°$ F.

Since 66° F is close to the generally accepted optimum comfort temperature of 65° F indoors in this country, this result strongly suggests an analogy with the formula for the cooling of the human body, where the 'body' in this case is the building itself.

The specific meteorological factor for the cooling power of the wind was therefore taken to be

$$W^{1/2}(65 - T) \quad . \quad . \quad . \quad . \quad . \quad . \quad (22)$$

where W is the wind speed in knots and T the air temperature in deg. F.

The typical form of the relationship between demand and cooling power evaluated according to eqn. (22) has already been given in Fig. 2.

(3.3) Daylight Illumination from Sun and Sky

The lighting component of the demand is determined by the daylight illumination received at the earth's surface. The principal factors controlling the level of daylight illumination at any one time are clouds and also atmospheric turbidity and reflection at the ground.

The instrumental basis adopted for measuring daylight illumination is the photo-electric photometry of a horizontal surface exposed to luminous radiation from sun and sky, the photo-cell being fitted with a photopic filter to match its spectral response to the standard luminosity curve of the average normal human eye under light-adapted conditions.

In applications to load estimating where the demand has to be predicted from weather forecasts the reduction of meteorological information to equivalent values of daylight illumination is necessary. The flux of daylight has been continuously recorded at Kew Observatory since 1947. A sample of these data in the form of hourly averages, together with the corresponding cloud observations every three hours in the 7-year period 1947–1953, was extracted for the purpose of the present investigation. The results may be considered representative of typical urban areas in Britain.

(3.3.1) Cloudless Conditions.

The first step in the reduction of the data was to determine the daylight illumination under cloudless conditions as a function of sun's elevation so as to provide a standard of comparison. The results were in close agreement with those obtained by Blackwell[15–17] using the first five years of the Kew observations.

When carrying out this work, it was noticed that attenuation of light by airborne particles (dust, haze, etc.) was having a significant effect, the illumination tending to be higher on occasions of good visibility, and vice versa. To examine the effects of visibility more fully, the ratio of the illumination on each cloudless occasion to the corresponding value of the average illumination was plotted against the reciprocal of visibility. The results, grouped according to visibility, are shown in Fig. 7 together with the line of best fit to the points.

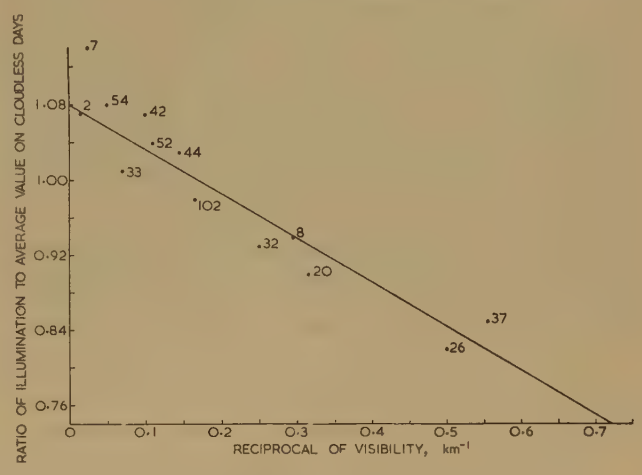

Fig. 7.—Ratio of illumination to average values on cloudless days plotted against reciprocal of visibility.
Numbers of observations are affixed to plotted points.

The reason for using the reciprocal of the visibility was to estimate the illumination under conditions of perfect visibility from the intercept of the regression line on the y-axis.

The relation expressed by Fig. 7 was then used to adjust the illumination on each cloudless occasion to the illumination under conditions of perfect visibility. The information thus derived is listed in Table 1.

Table 1

DAYLIGHT ILLUMINATION UNDER CONDITIONS OF PERFECT VISIBILITY ON CLOUDLESS DAYS

Sun's elevation	Mean illumination	Sun's elevation	Mean illumination
	kilolux		kilolux
0°	0·5	15°	22
1°	1·2	20°	31
2°	2·2	25°	40
3°	3·2	30°	48
4°	4·5	35°	57
5°	6·0	40°	66
6°	7·5	45°	74
7°	8·9	50°	82
		55°	89
10°	14	60°	93

In applications of this Table, the sun's elevation h is calculated from the following formula of spherical astronomy:

$$\sin h = \cos \delta \cos \Phi \cos H + \sin \delta \sin \Phi$$

where Φ is the latitude, H the local hour angle (L.H.A.) and

$$\text{L.H.A.} = \text{G.H.A.} + \text{east longitude},$$

the sun's declination δ and Greenwich hour angle (G.H.A.) being tabulated in the *Abridged Nautical Almanac*.

In studying the daylight illumination, I, on any specific occasion, the reference point is the illumination I_∞ which would be received on perfectly clear days with cloudless skies. The

introduction of an apparent transmission factor f permits the ratio $I : I_\infty$ to be expressed as

$$I = fI_\infty \quad . \quad . \quad . \quad . \quad . \quad . \quad . \quad (23)$$

the word 'apparent' being used to denote that it refers to observations made at the ground.

The important property of f is that in all of the many cases examined there was no statistical evidence to suggest that f was not independent of the sun's elevation. The transmission through the entire atmosphere was found to increase with the sun's elevation in both perfectly clear and cloudy atmospheres, but the form of the variation was practically the same in both cases, so that their ratio remained sensibly constant.

For the same reason the relation between the apparent transmission factor f_0 and visibility on cloudless days represented by the data of Fig. 7 was found to be independent of the sun's elevation. f_0 is extended to values of low visibilities in Table 2, as derived from a similar study of illumination in fog conditions.

Table 2

VARIATION OF APPARENT TRANSMISSION FACTOR WITH VISIBILITY ON CLOUDLESS DAYS

Visibility	Apparent transmission	Visibility	Apparent transmission	Visibility	Apparent transmission
m	f_0	km	f_0	km	f_0
20	0·17	0·9	0·56	3·0	0·86
40	0·19	1·0	0·59	3·5	0·88
60	0·21	1·1	0·62	4·0	0·89
80	0·22	1·2	0·64	4·5	0·90
100	0·23	1·3	0·67	5·0	0·91
		1·4	0·69		
200	0·29	1·5	0·71	6	0·93
300	0·34	1·6	0·73	8	0·94
400	0·39	1·7	0·74	10	0·96
500	0·43	1·8	0·76		
600	0·47			20	0·98
700	0·50	2·0	0·78	40	0·99
800	0·53	2·5	0·83	60	0·99

(3.3.2) **Cloud Layers.**

Single cloud-layer occasions manifestly afford the most tractable data for estimating the effects of cloud on daylight illumination from observations. A special study was therefore made on such occasions, and from this the effects of multiple layers were estimated by application of simple theory which was afterwards tested by reference to actual observations.

In considering single layers it was conceptually advantageous to divide the sky hemisphere into areas subtending equal solid angles at the point of observation using the okta ($\frac{1}{4}\pi$ steradians) as the unit, and to regard the total flux of illumination at the ground as deriving from the vertical flux contributed by each okta of the sky separately.

The separate contributions to the illumination at the ground by the clouded and unclouded regions would, of course, vary with the position of the cloud in the sky and with respect to the sun, but over all occasions and for all observing points at which a definite amount N oktas of a given cloud layer is observed the average total illumination I from sun and sky can be expressed as

$$I = I_\infty\left[f_0\left(1 - \frac{N}{8}\right) + b\frac{N}{8}\right] . \quad . \quad . \quad . \quad (24)$$

where the respective contributions from unclouded and clouded sky are given by the two terms of this dichotomy. b is t apparent transmission of cloud and underlying atmosphere a thus measures the relative brightness of the cloud as seen fro the ground, and we may therefore term it the apparent clo brightness; likewise f_0 is a measure of the sky brightness of t unclouded areas in terms of the flux at the ground.

According to the theory of the transmission of light throu scattering media[18, 19] the transmission T of fully diffused lig by a cloud layer is given by

$$T = \frac{1}{1+z} \quad . \quad . \quad . \quad . \quad . \quad . \quad . \quad (2$$

where z is the optical thickness of the cloud. z depends on t scattering properties of individual droplets, on the droplet si distribution and water content at each level in the cloud, on t geometrical thickness of the cloud and on the reflectance the ground.

For several cloud layers the optical thicknesses are additi and hence the transmission through n layers is given by

$$\frac{1}{T} - 1 = \sum_{r=1}^{n}\left(\frac{1}{T_r} - 1\right) \quad . \quad . \quad . \quad . \quad (2$$

where T_r is the transmission through layer r.

This formula enables the total transmission through multip layers to be expressed at once in terms of the combined tra mission of any decomposition of the system into sub-syste considered in any order. It may readily be shown that the sa result holds if transmissions are replaced by apparent transm sions as previously defined.

Regarding the underlying atmosphere as an additional lay application of this result to a single cloud layer gives

$$\frac{1}{b} = \frac{1}{b_\infty} + \frac{1}{f_0} - 1 \quad . \quad . \quad . \quad . \quad . \quad (2$$

and for two layers denoted by suffixes 1 and 2 this becomes

$$\frac{1}{b_{12}} = \frac{1}{b_{\infty 1}} + \frac{1}{b_{\infty 2}} + \frac{1}{f_0} - 2 \quad . \quad . \quad . \quad . \quad (2$$

and similarly for a greater number of layers, the b_∞'s denot apparent cloud brightness under conditions of perfect visibil at the ground.

Eqn. (25) does not yield very good results when used calculate the transmission through a cloud, except possibly a particular sun's elevation[20] of 23°, because the incident light not completely diffused. In the present context, however, t apparent transmission is independent of the sun's elevation, so may expect the formula to hold more accurately; for tenu cloud, where the inaccuracies of the formula are greatest, reduction in illumination is small anyhow, while if the cloud broken the contribution by the unclouded sky is not affected the formula in any way.

Eqns. (24) and (27) make it possible, in principle, to evalu b_∞ from each single-layer observation, but owing to the se tivity of b_∞ to small changes in the apparent transmissi $f = I/I_\infty$, it was necessary to determine the average value o on all occasions on which a single cloud layer of given type a amount occurred, and associate this with the average visibil on those occasions.

The results, in terms of f_∞, the apparent transmission fac at infinite visibility, are shown in Table 3 for the following clo types: stratus; stratocumulus; cumulus; cumulonimbus; t altostratus and altocumulus; thick altostratus; nimbostrat cirrus; cirrostratus.

Table 3

APPARENT TRANSMISSION AT PERFECT VISIBILITY ON DRY OCCASIONS. VALUES OF f_∞ FOR SINGLE CLOUD LAYERS

Amount (eighths)	St	Sc	Cu	Cb	Ac, thin As	Thick As	Ns	Ci	Cs
1	0·94	0·96	1·00		0·97			1·00	0·99
2	0·86	0·88	0·99		0·92			1·00	0·97
3	0·79	0·79	0·96		0·85			0·98	0·95
4	0·72	0·72	0·91	0·85	0·76			0·95	0·92
5	0·65	0·68	0·84	0·74	0·68			0·91	0·88
6	0·58	0·62	0·74	0·60	0·63			0·87	0·83
7	0·42	0·47	0·58	0·41	0·56			0·83	0·78
8	0·22	0·27	0·26	0·15	0·50	0·32	0·25	0·79	0·73

From these results it is possible to estimate the daylight illumination on single-layer occasions in terms of cloud and visibility. When this was done for different clouds, it was found that, owing to the association between b_∞ and N, the apparent transmission f could be expressed numerically as a function of only two parameters, namely f_0 and f_∞.

The conclusion that the apparent transmission can be expressed in terms of the visibility and the apparent transmission at infinite visibility without further regard to the state of the sky suggests that this function is also applicable to multiple-layer days if f_∞ can be determined. This was done by calculating the sky brightness of each overlapping and non-overlapping portion of the sky and then combining the contributions on the assumption that the different cloud layers are distributed randomly with respect to one another when projected on the sky background.

After carrying out many of these computations, it was found that in every case, whenever identical sets of component values of f for the different cloud layers were combined, they always gave rise to the same resultant f irrespective of the amounts or types of cloud to which they referred. On account of this property it was possible to construct numerically the function for combining the apparent transmission factors of different layers (including the underlying atmosphere regarded as an additional layer), and this is given in Section 3.3.3.

For completeness it was also necessary to consider the case of clouds from which precipitation was falling. Since most of the wet observations were restricted to large cloud amounts, the best that could be done was to determine the ratio of apparent transmissions for dry and wet clouds of the same type and amount, and in applications assume that their optical thicknesses would stand in the same ratio for smaller cloud amounts. The results are summarized in Table 4, from which it will be seen that there is a strong association between rate of precipitation and optical thickness.

Table 4

TRANSMISSION THROUGH PRECIPITATING CLOUDS. RATIO OF b_∞ ON WET/DRY OCCASIONS

Type of cloud	Rate of precipitation		
	Slight*	Moderate*	Heavy*
Layer type	0·82	0·70	0·60
Convection type ..	0·74	0·57	0·31

* Average precipitation over hour preceding observation: Slight < 0·4 mm; moderate = 0·4–0·7 mm; heavy > 0·7 mm.

The standard deviations of error obtained in applying the above methods to predict the daylight illumination on a large number of clear, cloudy but dry, and wet days were 6, 8 and 5 kilolux for average received illuminations of 42, 22 and 9 kilolux respectively. In all three cases the mean error was not significantly different from zero.

The most important factor which has been explicitly omitted in the analysis is cloud thickness, but as this is not quoted in surface reports, to have attempted to estimate it retrospectively would have been impracticable. Other factors which have been omitted are the effects of a freshly fallen snow cover and of heavy smoke pollution. Owing to the paucity of observations, only rough estimates of the latter effects can be made, and reference should be made to papers by Kalitin[21] and by Helliwell and Blackwell.[22]

(3.3.3) **Estimation of the Lighting Demand.**

In application to load estimation the daylight illumination is expressed on a logarithmic scale defined by

$$\text{Illumination index} = \log_{10} I$$

where I is the illumination in kilolux. As will be seen from Fig. 3, which has been tentatively extrapolated towards an asymptotic limit in complete darkness, the relation between lighting demand and daylight illumination is only approximately logarithmic, but it was found convenient to retain this index as a working unit.

Following the nomenclature of photographic densitometry, the apparent transmission factor f in eqn. (23) can be expressed in terms of

$$D = \log_{10}(1/f)$$

which we may call the daylight illumination deficit. The process of calculating the illumination index on any occasion then consists in estimating D from the reports of cloud and visibility using Tables 2, 3 and 4 and subtracting it from the illumination index on perfectly clear days.

From a study of the geometry of the surface representing the empirical function for combining transmission factors of several layers, referred to in Section 3.3.2, it was found that for D_1 and D_2 both $<0{\cdot}65$ the illumination deficit for two layers could be expressed to within 0·01 as a sum of functions of the respective sums and differences of the illumination deficits D_1, D_2 of the component layers:

$$D = \phi(D_1 + D_2) + \psi(D_1 - D_2) \qquad (D_1 \geqslant D_2)$$

where ϕ and ψ are given in Table 5.

For more than two layers, D is obtained by successive applications of this Table. In all other cases, repeated application of the formula:

$$\frac{1}{f} = \frac{1}{f_1} + \frac{1}{f_2} - 1$$

where the suffixes 1 and 2 refer to the two layers being combined, was found to give close agreement with the empirical surface.

(3.4) Precipitation

As mentioned earlier, the direct effects of precipitation are only evident at 1700 hours. The increase in total system demand is at present approximately 350 MW/(mm of rainfall per hour).

Table 5

COMBINATION TABLE FOR COMBINING ILLUMINATION DEFICITS $< 0{\cdot}65$

Values of $\phi(D_1 + D_2)$

$D_1 + D_2$	0·00	0·01	0·02	0·03	0·04	0·05	0·06	0·07	0·08	0·09
0·0	0·00	0·01	0·02	0·03	0·04	0·05	0·06	0·07	0·08	0·09
0·1	0·09	0·10	0·11	0·12	0·13	0·14	0·15	0·16	0·17	0·18
0·2	0·19	0·20	0·21	0·22	0·22	0·23	0·24	0·25	0·26	0·27
0·3	0·28	0·29	0·30	0·30	0·31	0·32	0·33	0·33	0·34	0·35
0·4	0·36	0·36	0·37	0·38	0·39	0·39	0·40	0·41	0·41	0·42
0·5	0·43	0·44	0·44	0·45	0·46	0·46	0·47	0·48	0·49	0·49
0·6	0·50	0·51	0·51	0·52	0·53	0·54	0·54	0·55	0·56	0·57
0·7	0·57	0·58	0·59	0·60	0·60	0·61	0·62	0·62	0·63	0·64
0·8	0·64	0·65	0·65	0·66	0·67	0·67	0·68	0·68	0·68	0·69
0·9	0·69	0·70	0·70	0·71	0·71	0·72	0·72	0·73	0·73	0·73
1·0	0·74	0·74	0·75	0·75	0·76	0·76	0·77	0·77	0·78	0·79
1·1	0·79	0·80	0·81	0·81	0·82	0·82	0·83	0·83	0·84	0·84
1·2	0·84	0·85	0·86	0·87	0·87	0·88	0·88	0·89	0·89	0·90

Values of $\psi(D_1 - D_2)$

$D_1 - D_2$	0·00	0·01	0·02	0·03	0·04	0·05	0·06	0·07	0·08	0·09
0·0	0·00	0·00	0·00	0·00	0·00	0·00	0·00	0·00	0·00	0·00
0·1	0·00	0·00	0·00	0·00	0·01	0·01	0·01	0·01	0·01	0·01
0·2	0·01	0·01	0·01	0·01	0·01	0·02	0·02	0·02	0·02	0·02
0·3	0·02	0·02	0·03	0·03	0·03	0·03	0·03	0·03	0·04	0·04
0·4	0·04	0·04	0·05	0·05	0·05	0·05	0·05	0·06	0·06	0·06
0·5	0·06	0·07	0·07	0·07	0·07	0·08	0·08	0·08	0·09	0·09
0·6	0·09	0·09	0·10	0·10	0·11					

The top row is the second decimal place of the argument.

(4) CONCLUSIONS

A comprehensive scheme of practical load estimation is provided by the foregoing results of researches on the relationship between weather and electricity demand. Within this framework, meteorological data can be transformed into a form to which demands may be directly related for numerical processing by statistical techniques. In particular, the time-constant of the lag in consumer response to temperature change has been shown to be of the order of one day, and basic information is given for translating complex skies coded according to standard meteorological practice into equivalent values of daylight illumination.

In general, the relationships between the demand and the several meteorological factors to which it is sensitive are non-linear in character. The suggested method of deriving these relationships consists of a multiple linear regression analysis followed by a graphical curvilinear regression analysis. Empirical curves are thereby obtained, typical forms of which are illustrated in Figs. 1–3, and which can be used as a basis for adjusting demands to standard weather conditions.

In spite of the appreciable arithmetical labour involved in such analyses, it is considered that an objective approach on the lines given in the paper represents an important step in accurate load estimation.

(5) ACKNOWLEDGMENT

The paper is published by permission of the Central Electricity Generating Board.

(6) REFERENCES

(1) SCHILLER, P.: 'Relation between Daylight Illumination and System Load', E.R.A. Report Ref. K/T115; 1945.

(2) VAN DER REYDEN, D.: 'Curve Fitting by the Orthogon Polynomials of Least Squares', *Onderstepoort Journal Veterinary Science and Animal Husbandry*, 1943, 1 p. 355.

(3) EZEKIEL, M.: 'Methods of Correlation Analysis' (Joh Wiley, 1941).

(4) VEDERE, E.: 'Further Work in Connection with the Influen of Weather Conditions on the Paris and Paris Regio Networks', U.N.I.P.E.D.E. Proceedings, London Co gress, 1955, Paper No. VII.2.

(5) DRYAR, H. A.: 'The Effect of Weather on the System Loa *Transactions of the American I.E.E.*, 1944, **63**, p. 1006.

(6) PRATT, A. W., and WESTON, J. C.: 'The Thermal Capaci of Buildings', *Building Research Congress*, 1951, Div. Part 2, p. 88.

(7) 'Basic Design Temperatures for Space Heating', Post-W Building Studies No. 33, 1955 (H.M. Stationery Offic

(8) PARSONS, J. J.: 'Heat Transmission through Extern Walls', *Journal of the Institution of Heating and Ventilati Engineers*, 1949, **17**, p. 339.

(9) DICK, J. B.: 'Experimental Studies in Natural Ventilati of Houses', *ibid.*, 1949, **17**, p. 420.

(10) WESTON, J. C.: 'Heating Research in Houses', *ibid.*, 194 **17**, p. 235.

(11) WESTON, J. C.: 'Heating Research in Occupied House *ibid.*, 1951, **19**, p. 47.

(12) LACY, R. E.: 'Variations of the Winter Means of Te perature, Wind Speed and Sunshine, and their Effect the Heating Requirements of a House', *Meteorologi Magazine*, 1951, **80**, p. 161.

(13) HILL, SIR L.: 'The Katathermometer', Studies of Bo Heat and Efficiency, Medical Research Council, 19 (H.M. Stationery Office).

(14) BRUNT, SIR D.: 'Some Physical Aspects of the Heat Balance of the Human Body', *Proceedings of the Physical Society*, 1947, **59**, p. 713.

(15) BLACKWELL, M. J.: 'Five Years' Continuous Recording of Daylight Illumination at Kew Observatory', Meteorological Research Committee, Air Ministry, London, Paper No. 831, 1953.

(16) BLACKWELL, M. J., *et al.*: 'Estimation of the Reflection and Absorption of Solar Radiation by a Cloudless Atmosphere from Recordings at the Ground, with Results from Kew Observatory', *ibid.*, Paper No. 894, 1954.

(17) BLACKWELL, M. J., and POWELL, D. B. B.: 'On the Development of an Improved Daylight Illumination Recorder', *ibid.*, Paper No. 988, 1956.

(18) SCHUSTER, SIR A.: 'Radiation through a Foggy Atmosphere', *Astrophysical Journal*, 1905, **21**, p. 1.

(19) CHANNON, H. J., *et al.*: 'The Behaviour of Scattering Media in Fully Diffused Light', *Proceedings of the Royal Society*, A, 1918, **94**, p. 222.

(20) NEIBURGER, M.: 'Reflection, Absorption and Transmission of Insolation by Stratus Cloud', *Journal of Meteorology*, 1949, **6**, p. 98.

(21) KALITIN, N. N.: 'Einfluss der Bewölkung auf die Helligkeit der Erdoberfläche durch diffuses Licht der Atmosphäre', *Strahlentherapie*, 1931, **39**, p. 717.

(22) HELLIWELL, N. C., and BLACKWELL, M. J.: 'Day Time Darkness over London on January 16, 1955', *Meteorological Magazine*, 1955, **84**, p. 342.

621.317.33:621.318.42

The Institution of Electrical Engine
Monograph No. 315
Oct. 19

THE CALIBRATION OF INDUCTORS AT POWER AND AUDIO FREQUENCIES

By G. H. RAYNER, B.A., Associate Member.

(*The paper was first received* 18*th March and in revised form* 24*th June*, 1958. *It was published as an* INSTITUTION MONOGRAPH *in October*, 195

SUMMARY

A brief description of the standard inductors at the National Physical Laboratory is given. The principal characteristics of self- and mutual inductors are then considered in relation to their measurement. The methods of inductance measurement at the N.P.L. are described; these include the calibration of mutual and self-inductors, the measurement of their variation with frequency, the a.c. resistance of inductors, and the components of self-capacitance. Emphasis is given to the precautions necessary to ensure precision.

(1) INTRODUCTION

All measurements of inductance are ultimately dependent upon inductors of calculated value. An inductor rather than a capacitor is used as a primary reactance standard, since, up to the present time, a simple geometric shape that is amenable to calculation is realizable with more precision in an inductor. At the N.P.L. the primary standard of mutual inductance, designed and constructed by A. Campbell, provides the basis for the measurement of inductance, resistance and capacitance. This paper provides an account of the methods employed at the N.P.L. in deriving the values of various standard inductors from the primary standard, as well as descriptions of circuits that are suitable for measuring or comparing the various characteristics of inductors. Some of the methods have been in use for a number of years and have been described previously, or are well known in principle; these are treated briefly, particular consideration being given to the elimination of errors.

The working standards of inductance comprises a number of continuously variable mutual inductors, or inductometers, and a set of self-inductors, with values of 1, 2, 5, 10 μH . . . etc., up to 1 henry, which can be used at frequencies up to the radio range; in addition there are self and mutual inductors designed for more specialized applications.

(2) INDUCTANCE STANDARDS

(2.1) Standards of Mutual Inductance

The Campbell primary standard of mutual inductance[1] has a primary winding consisting of two single-layer coaxial helical coils and a secondary winding consisting of many closely wound turns placed in the mid-plane between the primary coils. The value of the primary standard is 10 mH; this is found in practice to be a convenient magnitude, as it is large enough to allow sufficient sensitivity in the most precise measurements, and to reduce to insignificant proportions the uncertainties introduced by any stray mutual inductances that are likely to be present. On the other hand the value is not so large that the effects of capacitance in a normal working standard of mutual inductance are unduly great. The large self-inductance and self-capacitance of the secondary winding of the primary standard render it necessary to use a frequency as low as 10 c/s if the effective mutual inductance is not to differ by more than 1 part in 10^6 from the value for direct current, for which the value of t standard is calculated.

It is estimated that the calculated value of mutual inductan may be in error by an amount not exceeding 10 parts in 1(the largest contribution to this uncertainty arises from t possible errors in the dimensions of the primary coils, while smaller, but not insignificant, error may be introduced by unc tainties in the precise position of the secondary turns.

Secular changes in the dimensions of the primary winding ha occurred. For example, between 1936 and 1952 the calculat value decreased by 17 parts in 10^6 on this account; but it probable that this was in part a reversion to the dimensions pr to 1936, as changes in dimensions were observed in 1936 duri a determination of the temperature coefficient for which t primary winding was subjected to rather large and rapid te perature changes.

In addition to the main secondary winding there are auxilia windings[2] that provide a continuous variation of mutual indu tance up to 100 μH with an accuracy of 0·005 μH or 1 part 10^4; these windings may be used in conjunction with or in pendently of the main winding.

Instruments more flexible in their use than the primary sta dard are necessary to cater for a range of mutual inductan values and to extend the frequency range; for these purpo continuously variable mutual inductors are used. The m stable of these is the one constructed in 1938 by Astbury a Ford;[3, 4] it has a range of 11·1 mH, which is covered by th decade dials and a continuous scale, and readings to 0·01 μ may easily be made. This instrument has shown no tende to drift in value at the maximum setting, and during the l ten years there have been random variations within an extre range of 0·15 μH (15 parts in 10^6). Thus it will be seen t the stability at this setting is not greatly inferior to the prim standard. The temperature coefficient is $+12 \times 10^{-6}$/deg C the 10mH setting. At intermediate settings of the larg decade there has been a small, steady drift in their relative valu this is a maximum at the 5 mH setting and amounts to ab 0·03 μH per year. This instrument may be used at frequenc up to a few kilocycles per second provided that a correctio applied; the correction is approximately proportional to (f quency)^2 and it depends to some extent upon the setting: 1 kc/s and a setting of 10 mH it is about +3·2 parts in 10^4.

Other variable mutual inductors are also available, one wit maximum of 111 mH and another of 1·1 mH; however, these less stable instruments, and they have larger temperature coe cients and larger frequency corrections.

All these instruments have closely wound coils which have consequence large self-capacitances, and because some of capacitances are associated with tapped coils their effect on mutual inductance is complex. Therefore, for the measurem of mutual inductance above power frequencies it is necess to have a set of auxiliary standards of mutual inductance w simple coils having small capacitances; from a knowledge the capacitances it is possible to calculate the change of effec inductance produced by them. The auxiliary standards con of a number of fixed mutual inductors, up to 10 mH in va for use in the audio-frequency range. They have air-spa

Correspondence on Monographs is invited for consideration with a view to publication.

The paper is an official communication from the National Physical Laboratory.

urns of finely stranded wire, so that both the capacitances nd eddy currents are minimized; the various component capaci- ances have been measured and the corresponding frequency oefficients and impurities calculated.[5] In addition, the effect f eddy currents in the terminals has been determined (no other netal parts are used in the construction). In the case of the 0 mH inductor, the capacitive frequency correction at 1 kc/s or a negative mutual inductance (i.e. the mutual inductance educes the self-inductance) is about +1 part in 10^5 and that lue to eddy currents in the terminals is −1 part in 10^5; the sum f these gives the effective coefficient, which is zero for this articular condition.

(2.2) Standards of Self-Inductance

The set of working standards of self-inductance, ranging from μH to 1 henry, are of commercial manufacture;[6] they have paced stranded windings on formers designed to give compensa- ion for temperature changes. These inductors exhibit small hanges of value with changes in temperature or atmospheric elative humidity, but if both the humidity and temperature are naintained constant an excellent stability is obtained.

The terminals of the inductors are 1 in apart and are mounted n brass blocks; these carry a second pair of terminals which may e connected together by a link to short-circuit the winding in definite and reproducible manner. The inductance is the ncrease of inductance introduced into a circuit when the link s completely removed; it is assumed that there is no coupling etween the inductor and the rest of the circuit, or if coupling is resent that it is allowed for by reversal. The provision of the ink greatly reduces the uncertainty that arises from the incom- leteness of the circuit of the inductor due to the small gap etween the terminals, and it is particularly advantageous with he low-value inductors. In the case of the inductors of 10 μH r less the resistance of the link is not negligible in comparison vith that of the winding, and a significant fraction of the current vill pass through the winding when the link is in position. This raction depends upon the ratio of resistance of the link to that f the winding (provided that the frequency is not so high that he reactances determine the current distribution), and if the hort-circuit inductance is to be definite the current ratio—and herefore the resistance ratio—must be kept constant. In the ase of the 1 μH inductor a tarnish film on the link may increase he link resistance by 0·1 milliohm and this will produce an ncrease of the inductance with the link in position by a few housandths of a microhenry, thereby giving a smaller than ormal inductance change on removing the link.

The eddy currents in the stranded winding have an effect on he inductance that only becomes appreciable towards the upper nd of the audio-frequency range. However, eddy currents in he rather large terminal blocks and the screws produce detect- ble effects on both the inductance and resistance even at low udio-frequencies.

The fixed mutual inductors may be used in addition as self- nductors with values up to 100 mH. The low-frequency roperties of these are slightly superior to those of the inductors entioned above, as there are no screws in their construction nd their terminals are smaller.

(3) INDUCTOR CHARACTERISTICS

(3.1) Self-Inductance

Before proceeding to describe the methods of measurement it vill be convenient to outline the characteristic parameters of nductors. Considering self-inductors first, the simplest equiva- nt circuit comprises a self-inductance, L, a resistance, R, and a elf-capacitance, C, as shown in Fig. 1(a). This circuit of lumped

(a) (b)

Fig. 1.—Equivalent circuits of self-inductor.

impedances is found to be applicable for frequencies up to self-resonance,[7] provided that the parameters R and, to a small limited extent, L are considered to be dependent upon frequency on account of eddy currents; C is independent of frequency, except in so far as it is a capacitance associated with solid dielectric of which the permittivity changes with frequency. Fig. 1(b) gives the circuit of an inductor which has earth capacitances and no direct earth connection, as, for example, in a bridge with Wagner earthing arms. The capacitances of Fig. 1(b) are independent of one another, and if the terminal A or B is connected to earth, the self-capacitance of the coil is obtained by adding C_{BE} or C_{AE}, as the case may be, to C_{AB}; if the inductor is isolated and free of any earth connection, C_{AE} and C_{BE} will be in series.

The effective series resistance, R_S, and inductance, L_S, of the inductor shown in Fig. 1(a) are given by

$$R_S = \frac{R}{(1-\omega^2LC)^2 + (\omega CR)^2} \quad . \quad . \quad . \quad . \quad (1)$$

$$L_S = \frac{L(1-\omega^2LC) - CR^2}{(1-\omega^2LC)^2 + (\omega CR)^2} \quad . \quad . \quad . \quad . \quad (2)$$

At frequencies well below that of self-resonance, i.e. $\omega^2LC \ll 1$, the following approximations may be used,

$$R_S \simeq R(1 + 2\omega^2LC)$$

$$L_S \simeq L(1 + \omega^2LC)$$

In any circuit, whether a bridge or a resonant one, the effective values are the only quantities which can be directly determined, and where no statement is made below, this is to be understood. If the parameters R and L are required, they must be derived from measurements made at two or more frequencies by application of the above formulae; for this the parameters must either be constant over the frequency range or vary in a known manner. It is usually possible, by extending sufficiently the frequency of measurement, to find a range over which L is sensibly constant so that C can be determined by fitting eqn. (2) to the observations in this range. This value of C may then be applied at lower frequencies and also in eqn. (1) for the determination of R.

(3.2) Mutual Inductance

In the case of mutual inductors consisting of two coils, each coil will in general have the capacitances of a self-inductor as in Fig. 1(b), and in addition there will be four capacitances between the ends of coils as shown in Fig. 2(a). Since in most networks involving mutual inductors the two coils can be connected directly together, thereby short-circuiting some of the capacitances, the equivalent network can usually be reduced to the system given in Fig. 2(b).

The effect of the capacitances C_1, C_2 and C_{12} can be regarded as modifying the mutual inductance to give an effective value, M_e, and, in combination with the resistance of the windings,

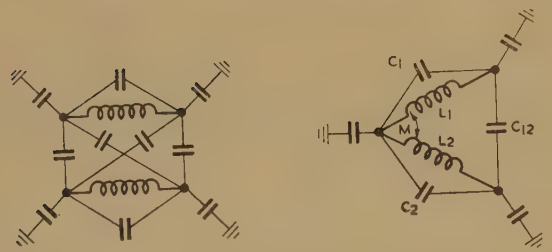

Fig. 2.—Equivalent circuit of mutual inductor.

introducing a resistive component or impurity, σ, into the mutual impedance; these quantities are given approximately by[5]

$$M_e = M - R_1R_2C_{12} + \omega^2[C_1L_1M + C_2L_2M + C_{12}(L_1 + M)(L_2 + M)] \quad . \quad (3)$$

$$\sigma = \omega^2\{C_1R_1M + C_2R_2M + C_{12}[R_2(L_1 + M) + R_1(L_2 + M)]\} \quad . \quad (4)$$

The component capacitances in Fig. 2(*a*) between the two coils will be different, and therefore the capacitances C_1, C_2 and C_{12} in Fig. 2(*b*) will vary for the different connections of the coils.

The effect of the earth capacitances shown in Fig. 2(*b*) can only be analysed by considering the whole of the network of which the mutual inductor is a part. When the analysis is attempted it will be found that the expressions are usually too complex for direct application; the better solution to the problem is to eliminate their effect from a measurement, as far as possible, by employing Wagner earthing arms. In most networks two of the earth capacitances can be eliminated in this way, while the effect of the third can often be estimated experimentally if its value is approximately known.

(3.3) Resistance of Self-Inductors

The resistance, R, of a self-inductor will normally increase as the frequency is raised, on account of eddy currents, both in the conductor of the winding and in any metal in the neighbourhood of the inductor, and also on account of dielectric loss in the insulating material in the electric field of the inductor. The increase in resistance due to eddy currents in a straight cylindrical conductor[8] is given by $R = R_0(1 + F)$, where R_0 is the d.c. resistance and F is a function of a parameter depending upon the diameter, conductivity, permeability, and frequency, f. At low frequencies $F \propto f^2$, and at high frequencies $F \propto f^{1/2}$, with a range of transition in between. For a stranded conductor consisting of a number of separate, insulated wires the general characteristic is similar to that of a single wire, except that the transition range is somewhat lower than for a similar wire in isolation. The eddy currents induced in the terminals and other large metallic parts will be developed at a much lower frequency because of the large cross-section, and the increase in resistance which they produce at low frequencies will be relatively greater than the increase due to eddy currents in the conductor.

Fig. 3 shows in a general way the increase in resistance, δR, from the d.c. value, with variation of frequency. At low frequencies, *a*–*b*–*c* on the curve, δR is almost entirely due to losses arising from eddy currents in the terminals, etc.; these losses are initially proportional to f^2 and they still predominate up to *c*. Above *c* skin effect in the conductor of the winding makes a greater contribution; at first this is proportional to f^2 and then, above *d*, to $f^{1/2}$. At *e* the resistance contribution due to dielectric

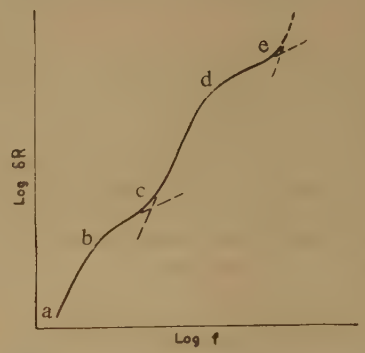

Fig. 3.—Increase of inductor resistance with frequency.

loss becomes significant; this produces an increment proportio to f^3 if the loss angle of the dielectric is independent of frequen The effect of dielectric loss is only likely to be significant frequencies approaching that of self-resonance, and in a w designed coil having a small amount of insulating material good quality it may still be small at the self-resonant frequen

It is unlikely that all the portions on the curve of Fig. 3 v be apparent in a single inductor. The point *b* may be at a f tens or hundreds of cycles per second, while *e* or even *d* m be above the self-resonant frequency; in many cases *d* will above the point at which dielectric loss will become appreci and the upper inflection of the curve will be absent. On acco of the complex nature of the characteristic, caution should exercised in any extrapolations of an observed resistance cha with frequency.

A conductor having insulated strands with one or more the strands broken will show an anomalous decrease in resista from direct to alternating current, since with direct current broken strands do not carry current but with alternating curr the inter-strand capacitances allow them to carry their proportion of the current.

(4) INDUCTANCE MEASUREMENTS

(4.1) Comparison of Mutual Inductors

The comparison of two mutual inductors, one of which m be adjustable, is readily made using the circuit due to Hartsho shown in Fig. 4. The conditions at balance are

$$M_1 + M_2 + l = 0 \quad . \quad . \quad . \quad . \quad . \quad .$$

$$\sigma_1 + \sigma_2 + r = 0 \quad . \quad . \quad . \quad . \quad . \quad .$$

Their mutual inductances must be of opposite signs, a since l is normally negligible, equal in magnitude; if it is desi to compare two instruments with mutual inductances of

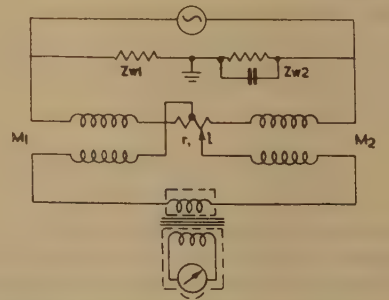

Fig. 4.—Comparison of mutual inductances.

ame sign, a substitution of one for the other may be made vith a third inductor of the opposite sign on the other side of he bridge.

At power frequencies the effects of capacitance are usually nsignificant and it is only necessary to take precautions to ıvoid stray mutual inductance. Coupling between the two nutual inductors can be minimized by placing them well apart vith their axes perpendicular and one inductor on the axis of he other; the error due to coupling is eliminated if the mean esult is taken of observations made with a reversal of both the oils of one of the inductors. Stray mutual inductance between he coils and the leads connecting them can be eliminated if the eads are twisted flex or coaxial cable. If the latter is used vith the outer conductor of each lead connected to the potentio- neter, r, there is no contribution to the capacitance between the nds of the coils, that is, to the capacitance C_{12} in Fig. 2(b). At igher frequencies it may be necessary to allow for the extra apacitance across the two coils which the leads introduce; these apacitances are added to C_1 and C_2 of Fig. 2(b) and their effect nay be calculated by means of formulae (3) and (4).

In addition to the capacitances across the coils of the mutual nductors there will be capacitances from them to earth. The arthing arms are adjusted to bring the resistor r to earth potential and earth capacitances from this point do not affect the balance; earth capacitances from the supply points of the bridge are effectively included in the earthing arms. The only earth capacitances that require further consideration are those from he points connected to the detector. Astbury has shown that hese cause no error at low frequencies provided that the earthing rms are correctly balanced.[2] However, at audio frequencies hey may cause appreciable errors which are related in a complex way with the various resistances and inductances of the circuit, but which are directly proportional to the earth capacitances. If these are known it is simpler to determine their effect by experiment rather than by calculation. Since the errors are proportional to the capacitances, if to each side of the detector a capacitance to earth is added equal to that already present an equal additional error which may be measured is introduced, and allowance can be made for the original earth capacitance error.

At power frequencies the simplest form of detector is the vibration galvanometer: it has adequate sensitivity and does not introduce large earth capacitances. An amplifier is usually necessary to provide high sensitivity at audio frequencies, and his will normally be connected to the bridge through a trans- former. It is desirable that the transformer should have an arthed screen between its windings and that the capacitances between the screen and the ends of the input winding should be small and approximately equal. Since these screen capacitances constitute the largest components of the detector to earth capaci- tances, a knowledge of them alone usually suffices; they may be measured in the same manner as the earth capacitances of self-inductors as described later.

An alternative way of dealing with the detector earth capaci- tances is to maintain the screen of the transformer at the same potential as the detector points. A cathode-follower with an nput capacitance of less than 1 pF and a gain of 0·99 has been lesigned for this purpose;[10] its input is connected to one of the detector points and the screen to the cathode. This device reduces the effect of the earth capacitance by a factor of 50. t is desirable to have an independent earthed screen around the ransformer output winding so that there is no capacitive coupling between this winding and the screen maintained at the bridge detector potential.

When determining the change in effective mutual inductance vith frequency it is not permissible to reverse the coils of a nutual inductor, since doing this may alter the capacitances upon which the change with frequency depends. Therefore, the frequency change must be measured without any alteration in the circuit.

It was mentioned above that auxiliary air-spaced mutual inductors, which constitute the standards for frequency changes, are affected slightly in the audio-frequency range by their terminals. The magnitude of this effect has been measured by observing the changes in mutual inductance and impurity which occur when an identical set of terminals is placed in a similar position near the inductor. The magnitude of the eddy-current effects is not dependent upon the sign of the mutual inductance or the sense in which the coils are connected.

(4.2) Derivation of Self-Inductance from Mutual Inductance

At the N.P.L. the Campbell–Heaviside bridge provides the link between mutual inductance and self-inductance. This net- work is incorporated as part of the Astbury bridge for the calibra- tion of capacitors,[11, 12] and provision is made for the insertion of a self-inductor into the circuit.

For the most precise measurements a bridge with equal ratio arms is preferred, since any small inequality may be allowed for by reversing them and no measurement of the ratio is necessary.

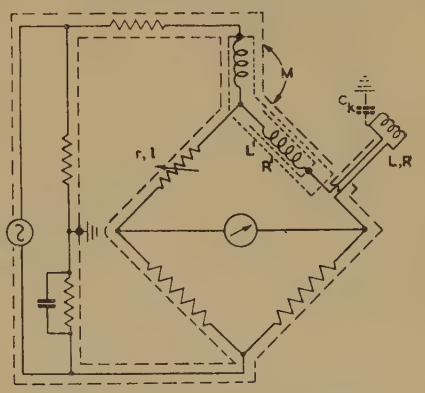

Fig. 5.—Measurement of self-inductance.

The bridge with its screening is shown in Fig. 5. With equal ratios the inductance, L, is given by

$$L = 2(M_1 - M_2) + l_1 - l_2 \quad . \quad . \quad . \quad . \quad (7)$$

where the suffixes 1 and 2 refer to the values with the self- inductor in and out of the circuit respectively. The resistance, R, of the inductor is balanced by an equal increase in the resis- tance, r, which is the value of a resistor with decade dials and a continuously variable slide-wire. The residual inductance of these has been measured[13] and is known to $\pm 0{\cdot}01\,\mu$H. For measurements at audio frequency it is necessary to apply a correction for the change in mutual inductance with frequency. The most accurate procedure is to determine the overall correc- tions to be applied to the bridge from measurements on self- inductors having negligible or known frequency coefficients.

The Wagner arms eliminate the effects of earth capacitances from the detector points of the bridge, and screening within the bridge eliminates internal earth capacitances from points other than the detector and supply terminals. A coaxial lead con- nects the inductor to the bridge, and the only earth capacitance which needs consideration is that from the end of the inductor which is not at the detector potential. The error due to an earth capacitance, C_K, at this point is $C_K R' R$; $R' = 1{\cdot}5$ ohms in this bridge, and for the 10 mH sub-standard inductor $R = 4{\cdot}4$ ohms and $C_K = 5\,\mu\mu$F, so that in this case the error is 30×10^{-12}H, which is negligible.

In the Astbury bridge the greatest value of self-inductance which can be measured with equal ratio arms is about 10 mH, because the maximum value of M is about 11 mH and the value of M_2 which is required to balance L' is about 5·7 mH. While self-inductances less than 10 mH may be measured, the accuracy, expressed as a fraction of the value, becomes progressively less, and it is more satisfactory to compare other self-inductors with the 10 mH inductor. Inductors of value greater than 10 mH can be measured using unequal ratios of 10 : 1 or 100 : 1 which are incorporated in the bridge, but it is more accurate and usually more convenient to make a comparison of self-inductors as described in the next Section.

(4.3) Comparison of Self-Inductors

The bridge shown in Fig. 6 is used to compare self-inductors in the range 1 μH to 1 henry at power and audio frequencies.

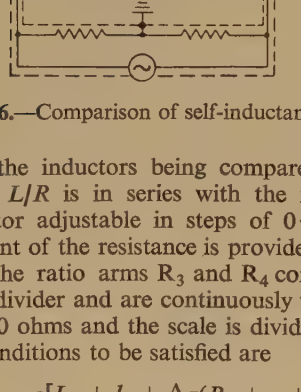

Fig. 6.—Comparison of self-inductances.

L_1 and L_2 are the inductors being compared; the one with the higher ratio L/R is in series with the resistance r of a five-decade resistor adjustable in steps of 0·1 ohm. A continuous adjustment of the resistance is provided by the 0·1-ohm slide wire pq. The ratio arms R_3 and R_4 consist of a Kelvin–Varley potential divider and are continuously variable; the total resistance is 1 000 ohms and the scale is divided to 0·001 ohm. At balance the conditions to be satisfied are

$$L_1 + l_1 = \rho[L_2 + l_2 + \Delta\tau(R_2 + r + r_2 + p)] \quad . \quad (8)$$

and

$$R_1 + r_1 + q = \rho[R_2 + r + r_2 + p - \omega^2\Delta\tau L_2] \quad . \quad (9)$$

where $\rho = R_4/R_3$; $\Delta\tau = \tau_4 - \tau_3 = l_4/R_4 - l_3/R_3$; r_1 and r_2 represent the resistances of the leads in arms 1 and 2, and l_1 and l_2 their inductances; $\Delta\tau$, the difference of time-constant of arms 3 and 4, has been measured by methods already described and is known with an accuracy of 1×10^{-9} H/ohm for all except the extreme ratios.[13] The resistance calibration of the potential divider is determined for about thirty settings which are commonly used; the accuracy with which the ratio is known is 1 part in 10^5 or better for any ratio ρ, between 1/10 and 10/1.

The inductances of the leads in arms 1 and 2 must be known and their measurement is described below. The variations with setting of the residual inductance of the slide-wire pq and the resistor r have been measured and are known to 0·001 μH or 0·002 μH/ohm, whichever is the greater.

In order to achieve high precision the wiring should be disposed so that any loops are made as small as possible; the inductors should be well separated and arranged to minimize the coupling between them; the other components and the connections should be in earthed screens. Therefore, to each of the inductors there is a pair of individually screened leads about 60 cm (24 in) long, and the supply and detector points are screened and close together, the leads to them also being screened and twisted. The Wagner arms eliminate the effects of all the earth capacitances except for C_K in Fig. 6 from th junction of L_2 and r; this increases the equivalent inductance arm 2 by rR_2C_K, which, however, is usually negligible compar with L_2.

The error due to any residual mutual inductance between th inductors is eliminated by taking the mean of measuremen made before and after reversing the connections to one of th inductors, care being taken not to move the inductors. Whe measuring small inductors the changes in inductance incident to reversing the connections are usually greater than the stra mutual inductances with the inductors positioned carefully, ar no reversal is made.

Unscreened inductors may have stray capacitances betwee them. These can be considered as four capacitances betwee their terminals; two of the four have little effect, one being acro the supply and the other at the ends adjacent to the detecto the other two will augment the self-capacitances of the inductor one being added to each. Since the capacitances are likely t be unequal, at high frequencies large inductors should be co nected when possible so that the larger capacitances have th smallest effect on the bridge, and it is advisable to eliminate determine the stray inductive coupling between the inductors b a measurement at a frequency which is low enough for the effec of capacitance to be negligible.

The procedure adopted for the calibration of the sub-standar inductors is as follows. First, the 10 mH inductor is measure on the Campbell–Heaviside bridge; then the other inducto between 1 and 100 mH are compared with it and with on another in all the cases for which the ratio of the values does n exceed 10 : 1. By similar inter-comparisons, within a 10 : ratio, the range is extended down to 20 μH and up to 1 henr Thus the value of each inductor less than 10 mH is derive from comparisons with the three next larger inductors, an similarly each of the inductors greater than 10 mH is derive from the three next smaller ones. In general, over the rang 100 μH to 1 henry, it is found that the individual comparison give results which are within 1 part in 10^5 of the mean value an inductor, and that in no case does an individual result diff by more than 2 parts in 10^5 from the mean. It is estimated th the value of any inductor in the range is known to 5 parts in 10 The uncertainty in the inductance of the bridge leads becom increasingly important as the inductor value is reduced an inductors of 10 μH and below are compared only with th 100 μH or 50 μH inductors. For inductors of about 1 μH agre ment with other methods to 0·000 5 μH is obtained, and for 10 μH inductor the accuracy is about $\pm$0·002 μH. When a accuracy of $\pm$0·01 μH or better is required it is essential measure the inductance of the bridge leads without disturbin them. Except for one or two of the larger values, the ratio L/R of the standard inductors steadily decreases with the valu and the smaller of any pair being compared must be placed arm 1; therefore it is only necessary to measure l_1 with th highest accuracy. The value of l_1, which is about 1 μH with short-circuited coil in arm 1, is measured with the 50 or 100 μ inductor in arm 2, so that no great accuracy is required for th residual inductance in this arm. Although under these condition the convergence of the bridge at 1 kc/s is poor, it is possible measure l_1 to within 0·000 5 μH. The residual inductance arm 2, with the dials of the resistor r set at zero, is about 2 μH having obtained the value of l_1, that of l_2 can be obtained comparison with it when the short-circuiting link on the induct in arm 2 is inserted. Again the convergence is poor, but accuracy of 0·005 μH is readily obtained. The variation of th inductance over the range of the slide wire pq has been dete mined from measurements of the residual inductances at vario settings; the inductance variation is 0·20 μH/ohm over th

range of the slide wire (0·1 ohm) and for small resistance changes of up to 0·01 ohm it may be estimated to 0·000 1 μH.

(5) MEASUREMENT OF SMALL INDUCTORS

(5.1) Self-Inductors

Some of the methods for measuring the residual inductance of resistors may be adapted and are convenient for the measurement of small values of self-inductance, four-terminal inductors and mutual inductors of low or medium value.

The bridge shown in Fig. 7 may be used to measure self-inductors up to some tens of microhenrys at audio frequencies and up to a few millihenrys at power frequency. It is essentially a bridge with four resistive arms, and in one of these the inductance, L, being determined is counter-balanced by a capacitance, C_1, across a resistance, R_1. The ratio arms R_3 and R_4 consist of a Kelvin–Varley potential divider and are variable; the resistor R_2 is fixed in value and is conveniently about the same value as R_1. The experimental procedure is as follows: first with the inductor out of circuit or short-circuited the bridge is balanced by adjusting C_1 and the ratio R_4/R_3; it is sometimes necessary to place a small, fixed capacitor across R_2 in order to achieve this balance. The inductor is then connected in the circuit and the bridge rebalanced by adjusting C_1 and the ratio. Let the suffixes a and b denote the values of these after and before inserting the inductor. The inductance is then given by

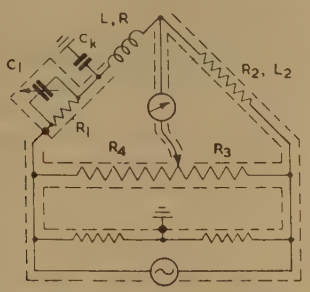

Fig. 7.—Measurement of small self-inductances.

$$L = R_1^2\left[\frac{C_{1a}}{1+\omega^2R_1^2C_{1a}^2} - \frac{C_{1b}}{1+\omega^2R_1^2C_{1b}^2}\right] + (\Delta\tau_a - \Delta\tau_b)R_1 + \Delta\tau_a R + L_2(\rho_a - \rho_b) \quad . \quad (10)$$

where $\rho = R_4/R_3$, $\Delta\tau = \tau_4 - \tau_3$ and L_2 is the equivalent inductance of arm 2. The last three terms in eqn. (10) are small quantities: $(\Delta\tau_a - \Delta\tau_b)$ may be kept small by altering only the lower dials of the potential divider between the a and b balances, and therefore R_2 should be selected so that a change in the first dial is avoided. It is also desirable to arrange the settings of the divider so that $\Delta\tau$ is small to minimize the next term in the equation. In the last term, $(\rho_a - \rho_b)$ is approximately proportional to R for given values of R_1 and R_2, and it is usually found that L_2 can be estimated with sufficient accuracy. With regard to the terms in the square brackets, C_{1b} is usually small and the expression $\omega^2R_1^2C_{1b}^2$ in the denominator negligible; the expression $\omega^2R_1^2C_{1a}^2$ in the denominator of the first term is approximately equal to ω^2L^2/R_1^2, and if the correction it introduces is not to exceed a fraction α, R_1 must be not less than $\omega L/\sqrt{\alpha}$. That is to say, R_1 should be increased as the frequency or the inductance being measured is increased, and C_{1a} should be reduced.

The presence of an earth capacitance C_K at the junction of R_1 and L makes the measured inductance too large by an amount RR_1C_K; because of this, the value of R_1 should be low for small inductances, and since for these it is permissible to make C_{1a} large, stray capacitances are not important in this case. When R_1 must be large and C_1 small, it is advisable to screen the various components and connections; it is better in this case to connect the screens of R_1, C_1, and the lead between them and L, not to earth but to the supply point, as shown in Fig. 7.

(5.2) Mutual Inductors

Mutual inductors can be measured by a method which is a development of those described by Astbury[14] and Ford.[15] The circuit is shown in Fig. 8; arm 1 comprises a parallel combination of a known resistor R_1 and an adjustable capacitor C in series with one coil of the mutual inductor; R_2 is fixed and of about the same value as R_1, and the Kelvin–Varley potential divider is again used for the ratio arms. The bridge is balanced by varying C and the ratio $\rho = R_4/R_3$ with the detector connected first to the point a and then to b; using these as suffixes to denote the values at the two balances, with the notation above, we have

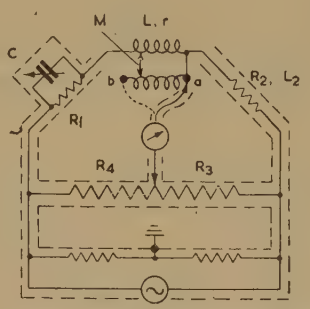

Fig. 8.—Measurement of small mutual inductances.

$$M(1+\rho_b) = R_1^2\left[\frac{C_b}{1+\omega^2R_1^2C_b^2} - \frac{C_a}{1+\omega^2R_1^2C_a^2}\right] + (\Delta\tau_a - \Delta\tau_b)(R_1 + r) + L_2(\rho_b - \rho_a) \quad . \quad (11)$$

As the ratio only requires a slight adjustment between the two balances, to allow for the alteration in the effective series resistance of R_1 and C, the second and third terms are nearly always negligible. The effects of earth capacitances from the points in arms 1 and 2 which are at neither supply nor detector potential are the same for the two balances and no error is introduced.

(6) FREQUENCY VARIATION OF SELF-INDUCTORS

Measurements of the variation of inductance with frequency are ultimately dependent upon the constancy of capacitance of an air capacitor with frequency, the effects of series inductance being allowed for if necessary.

An air capacitor can be used direct at radio frequencies by forming a simple resonant circuit, and the technique required to achieve high precision by this method has been fully described.[7] The frequency may be extended downwards to some extent by using mica capacitors, but at audio frequencies, bridges are more accurate and convenient.

The Maxwell inductance-capacitance bridge shown in Fig. 9 can be used over a wide frequency range as the balance is independent of frequency to a first order. The conditions for balance are

$$L_1 = R_2R_4C_3[1 - \omega^2\tau_2\tau_4 + (\tau_2 + \tau_4)/C_3R_3] \quad . \quad (12)$$

and

$$R_1R_3 = R_2R_4\{1 - \omega^2[\tau_2\tau_4 + (\tau_2 + \tau_4)C_3R_3]\} \quad . \quad (13)$$

$$\simeq R_2R_4[1 - \omega^2(\tau_2 + \tau_4)C_3R_3] \quad . \quad . \quad . \quad . \quad (14)$$

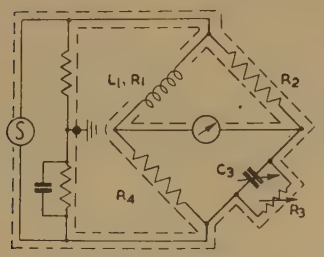

Fig. 9.—Measurement of variation of inductance with frequency.

where τ_2 and τ_4 are the time-constants of arms 2 and 4. At high frequencies the effects of these time-constants require consideration; when each of them is small compared with C_3R_3, as will normally be the case, $\tau_2\tau_4$ will be small compared with $(\tau_2 + \tau_4)C_3R_3$ and the approximate equation (14) may be used. If they are approximately equal in value and if their sum is such that the resistive balance is independent of frequency to a first order, their effect on the inductance will be negligible to a second order. The required time-constants may be obtained experimentally without difficulty; the time-constants of R_2 and R_4 may be compared and adjusted to equality without a knowledge of their absolute values. They can be further adjusted to be approximately zero by satisfying the condition that there is no change of resistive balance with frequency. These adjustments are facilitated if the resistors are initially slightly inductive and small trimmer capacitors can be connected across them. The condition used as the criterion for the adjustment to zero assumes that the resistance of the inductor does not change appreciably with frequency, and this has been true of the inductors which have been measured with the circuit. However, if a small error should arise from this cause it will usually be proportional to ω^2, and will appear as an alteration to the self-capacitance rather than to the inductance as calculated from eqn. (2).

A screened variable air-capacitor is used for C_3 and a value of 1 000 pF is convenient. The variable resistor R_3 will be of high value, between 0·1 and 1 megohm probably, and its shunt capacitance must be independent of frequency and setting; a resistor satisfying these requirements has been constructed by mounting a carbon track of the appropriate value from a commercial potentiometer on a former of good dielectric material and enclosing it in an earthed screen. The resistors R_2 and R_4 may be comprised of a few fixed values, from which the ones appropriate to the inductor under test can be selected; they should be wound with fine wire to minimize skin effect, and their terminals should be close together; the resistors and terminals should be in individual screens. The inductor should be placed at some distance from the other components—about 15 in is suitable—and the leads to it should be separately screened and twisted; the change of inductance of the leads may be significant when measuring small inductances; it can be measured in the same way an an inductor and an allowance made.

Measurements on the smaller-value inductors have been carried out on this bridge at frequencies between 1 and 100 kc/s; for the larger values the approach to self-resonance sets the upper limit. A few of the larger inductors have been measured at frequencies down to 60 c/s, but here the method is limited by the difficulty of obtaining a sufficiently fine adjustment of R_3 so that C_3 may be set with the requisite accuracy. At low frequencies it is permissible to use larger, mica capacitors, thereby enabling the value of R_3 to be reduced so that a decade resistance box may be used; as only small changes in the resistance are required the time-constant will not be altered and need not be known. It is necessary to know the variation of the capacitance C_3 wit frequency.

At high frequencies it may be necessary to allow for the indu tance in series with C_3, to determine the effective capacitance the arm; the inductance is best obtained from a measurement the self-resonant frequency of the capacitor and its leads wit these short-circuited at the bridge terminals.

(7) MEASUREMENT OF THE A.C. RESISTANCE OF INDUCTORS

At high frequencies the resistance of an inductor is most readi measured by forming a resonant circuit with an air capacito the resonant technique may be extended to lower frequencies fo the larger values of inductance by using mica capacitors, and this case it is advantageous to use the resonant circuit in a bridg network. The resonant circuit may be either of the series o parallel type; with the latter, the effective parallel resistance high and very dependent upon frequency, being given approx mately by ω^2L^2/R. In the former type the resistance is lo and varies only slightly with frequency, but it has the disad vantage that errors may be introduced by stray capacitance from the junction of the capacitor and inductor. In practic it is found that the series-arm bridge is to be preferred, provide that the earth capacitance C_K in Fig. 10 can be estimated an

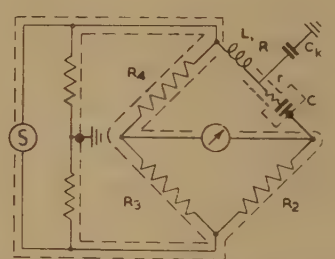

Fig. 10.—Series-arm bridge for measuring the a.c. resistance of inductors.

allowed for. All the bridge components except the inducto should be screened; the screen of the capacitor and of the lea between it and the inductor should be connected to a termin of the capacitor and not to earth, in order to avoid any additio to the earth capacitance C_K. The capacitance C_K will then on consist of the capacitance to earth from this end of the inducto The effect of the earth capacitance is to modify the dire impedance of the arm, which becomes

$$Z_1 = r + R(1 + C_K/C) + j[\omega L(1 + C_K/C) - 1/\omega C] \quad . \quad (1$$

where R and L are the effective series resistance and indu tance. It will be observed that the earth capacitance intro duces an error in the resistance proportional to C_K/C; sinc $C \simeq 1/\omega^2 L$ this term is approximately proportional to th square of the frequency, and the error is small at low frequencie for which the greatest accuracy in resistance measurement likely to be required. The equivalent series resistance, r, of th capacitor is obtained from the power factor, γ, according to th usual expression $r = \gamma/\omega C \simeq \gamma\omega L$; it is therefore proportion to the frequency if the power factor is independent of frequenc While the power factor is likely to vary with frequency to a sma degree, the expression serves to indicate that at lower frequencie the loss in the capacitor may be of relatively greater importan when measuring resistance changes which vary as the square the frequency.

The bridge is balanced by adjusting the capacitor and one the three resistors; the total effective resistance in arm 1 is give

by $R_1 = R_2R_4/R_3$. If it is desired to obtain a precise measurement of the increase in the a.c. resistance over the d.c. value, a d.c. measurement should be made immediately following the a.c. one. This can be done using the same bridge circuit with the capacitor short-circuited and a d.c. supply and detector substituted for the a.c. ones; if provision is made for a rapid changeover, by means of convenient switches or plugs, any change in the resistance of the inductor due to temperature variations is minimized.

The Maxwell bridge, Fig. 9, described above, may be used for measuring the resistance of large inductances at frequencies up to a few tens of kilocycles per second. A mica capacitor rather larger than for the inductance measurements is required in order that the value of R_3 may be reduced so that its value may be known accurately. It is necessary to know the power factor, γ_3, of the capacitor, and, at the higher frequencies, the time-constants of R_2 and R_4. The expression for the resistance in arm 1 is

$$R_1 = R_2R_4\{1 - \omega^2[\tau_2\tau_4 + (\tau_2 + \tau_4)C_3R_3]\}(1/R_3 + \omega C_3\gamma_3) \quad . \quad . \quad . \quad . \quad (16)$$

If τ_2 and τ_4 are small their product may be neglected as before.

This bridge is convenient for measurements at low frequencies, and it is particularly appropriate for determining the d.c to a.c. resistance change, since both balances can be made on the bridge without any alteration to it.

Having determined the resistance of an inductor over a range of frequencies, the inductor may then be used as a standard from which the resistances of other inductors of different values may be obtained for the same frequency range. The bridge shown in Fig. 6 may be used for this comparison. For high precision it is desirable to reduce the errors due to uncertainties in the temperatures of the inductors and to follow the a.c. balance by a d.c. balance, thereby obtaining a comparison of d.c. to a.c. changes of resistance of the two inductors. The procedure is first to balance the a.c. bridge in the normal manner, by adjusting the ratio, and r and pq, and then quickly to substitute a d.c. supply and detector and to rebalance the bridge by means of r and pq. The resistances of the inductors are related by the following equation, in which each of the terms with δ is the excess of the a.c. value over the d.c. value; for example, δR_1 is the increase in the effective resistance of the inductor in arm 1 from d.c. to a.c., and δr is the difference of reading of r between the d.c. and a.c. balances.

$$\delta R_1 + \delta r_1 = \rho(\delta R_2 + \delta r_2 + \delta r - \omega^2 L_2\Delta\tau) + (\rho + 1)\delta p \quad . \quad (17)$$

The changes in the resistances of the leads, δr_1 and δr_2, are usually negligible compared with the other terms.

When using this bridge for the resistance comparison the effect of an earth capacitance C_K requires further consideration. In addition to the increase of inductance in arm 2, mentioned above, such a capacitance modifies the effective series resistance of the arm and this becomes $R_2 + r(1 - \omega^2L_2C_K)$; the error introduced may be significant if r is of the same order as R_2. To reduce the earth capacitance the screen of r, and of the lead between it and L_2, should be connected to the adjacent detector point for resistance measurements; this alteration introduces a capacitance across r, and, although it produces an error in the inductance, the series resistance is not affected.

(8) SELF-CAPACITANCE OF INDUCTORS

It was pointed out above that, to obtain the values of L and R of an inductor from the measured effective values, a knowledge of the self-capacitance, C, is necessary. The self-capacitance will be definite and fixed in value for an inductor with a screen which is connected to one of its terminals; for an unscreened inductor, or one with an isolated screen, the capacitance depends upon the manner in which the inductor is connected relative to the earth or the screen. Furthermore, with an unscreened inductor the external capacitances will depend to some extent upon the closeness of other metallic objects. In circuits where the earth capacitances are eliminated, the self-capacitance only comprises the distributed winding capacitances and is less subject to the influence of nearby metal.

The self-capacitance can often be obtained most readily by determining the self-resonant frequency of the inductor in the appropriate conditions. For example, self-resonance in an inductor with one terminal earthed may be observed by means of a high-impedance voltmeter connected through a small capacitor of known value; for this the inductor is energized from a variable-frequency high-impedance source. An alternative method is to find the frequency at which the inductor has zero reactance or susceptance when it is connected to a suitable bridge or other circuit.

The component capacitances of an inductor can be measured with a Schering bridge having Wagner earthing arms.[12] When the bridge supply frequency is near to that of self-resonance of the inductor, its impedance will appear as a high resistance in parallel with a small capacitance, C', which will be positive or negative depending upon whether the frequency is above or below self-resonance. Thus the capacitance C_{AB} [Fig. 1(*b*)] of the inductor is given by $1/\omega^2L + C'$; in this expression the low-frequency value of L may be used.

The capacitances C_{AE} and C_{BE} are eliminated from the above measurement; one of these is between a bridge detector point and earth and the other is between a supply point and earth.* The latter is thus across a Wagner arm and, on connecting the inductor to the bridge, necessitates a reduction in the Wagner arm capacitor. This reduction will give the earth capacitance from one end of the inductor winding; the capacitance from the other end is obtained with the inductor reversed.

The screen-to-winding capacitances of a transformer or a screened inductor can be measured by this method, the screen being connected to earth. They may also be measured by connecting the winding between one of the bridge detector points and earth, and connecting the screen to the junction of the two capacitance arms; one of the winding-to-screen capacitances is thrown across a bridge arm, enabling it to be measured. In this method the frequency is not restricted to that near self-resonance and any convenient frequency may be used.

(9) ACKNOWLEDGMENT

The work described above has been carried out as part of the research programme of the National Physical Laboratory, and the paper is published by permission of the Director of the Laboratory.

(10) REFERENCES

(1) CAMPBELL, A.: 'On a Standard of Mutual Inductance', *Proceedings of the Royal Society*, 1907, **79** A, p. 428.

(2) ASTBURY, N. F.: 'The Primary Standard of Mutual Inductance at the National Physical Laboratory', *Philosophical Magazine*, 1938, **25**, p. 290.

(3) ASTBURY, N. F., and FORD, L. H.: 'Screened Sub-Standard Inductometer', *ibid.*, 1938, **25**, p. 1009.

(4) RAYNER, G. H., and FORD, L. H.: 'The Stability of Inductance Standards', *Journal of Scientific Instruments*, 1950, **27**, p. 19.

* The high-voltage bridge connection is the more convenient for this measurement and it is assumed here, but the conjugate form may be used.

(5) HARTSHORN, L.: 'The Properties of Mutual Inductance Standards at Telephonic Frequencies', *Proceedings of the Physical Society*, 1926, **38**, p. 302.

(6) GRIFFITHS, W. H. F.: 'Recent Improvements in Air Cored Inductances', *Wireless Engineer*, 1942, **19**, p. 8.

(7) HARTSHORN, L., and DENTON, J. J.: 'The Calibration of Inductance Standards at Radio Frequencies', *Proceedings I.E.E.*, Paper No. 2080 M, July, 1956 (**103** B, p. 429).

(8) HARTSHORN, L.: 'Radio-Frequency Measurements' (Chapman and Hall, 1940).

(9) HARTSHORN, L.: 'A Precision Method for the Comparison of Unequal Mutual Inductances at Telephonic Frequencies', *Journal of Scientific Instruments*, 1925, **5**, p. 145.

(10) RAYNER, G. H., and WILMER, R. W.: 'A Method of Decreasing the Effect of Earth Admittances in A.C. Bridges', *ibid.*, 1950, **27**, p. 103.

(11) ASTBURY, N. F., and FORD, L. H.: 'The Precision Measurement of Capacitance', *Proceedings of the Physical Society*, 1939, **51**, p. 37.

(12) RAYNER, G. H., and FORD, L. H.: 'The Calibration of Capacitors at the National Physical Laboratory, 1947', *Journal I.E.E.*, 1948, **95**, Part II, p. 312.

(13) RAYNER, G. H., and FORD, L. H.: 'The A.C. Properties of Resistors and Potential Dividers at Power and Audio Frequencies, and their Measurement', *Journal of Scientific Instruments*, 1957, **34**, p. 190.

(14) ASTBURY, N. F.: 'A Simple Method for Measurements of Residual Inductance on Potentiometers and Four Terminal Resistance Coils', *ibid.*, 1931, **8**, p. 221.

(15) FORD, L. H.: 'A Note on the Measurement of Four Terminal Inductances by Astbury's Method', *ibid.*, 1949, **26**, p. 108.

621.372.54 : 621.391

The Institution of Electrical Engineers
Monograph No. 316 R
Oct. 1958

ON THE INTERPOLATION AND PREDICTION OF SIGNALS PLUS NOISE FOR INFINITE AND FINITE SMOOTHING TIMES

By D. McDONNELL and R. W. PERKINS.

(*The paper was first received* 24*th February, in revised form* 20*th May, and in final form* 26*th July*, 1958. *It was published as an* INSTITUTION MONOGRAPH *in October*, 1958.)

SUMMARY

The first part of the paper is concerned with the choice of the optimum filter for the extrapolation or interpolation of a signal which is contaminated by noise. The problem has been completely solved by Wiener in his book on the subject. The method used here for solving the integral equations is different and leads to the solution for the lagging case without having to approximate $\varepsilon^{-p\tau}$ by the ratio of polynominals in p. Laplace transformations are used and lead directly to the solution. The second part of the paper deals with the solution of the optimum filter when the error is minimized at a particular time after switching on, the averaging being taken over an ensemble. Examples of each problem are given.

(1) INTRODUCTION

The problem of filtering and prediction has been the subject of much study during the last few years. Many papers have been written on the subject; there are some in the form of heuristic expositions and others concerned with generalizations of the problem first solved by Wiener.* This is yet another; it is the outcome of much effort in trying to solve the optimization problems with engineering mathematics, in particular by the use of Laplace-transformation techniques. The variational part of the problem is repeated along the lines proposed by Wiener. It is repeated here because the arguments used depend upon the fact that the formal variational procedure does not include a variation of the impulse part. Section 2 deals with the case in which the error has to be minimized when averaged over an infinite time. Section 3 contains the solution to a more practical problem in which the error has to be minimized at a particular time when averaged over an infinite ensemble. This case includes the first as a special case.

(2) THE MINIMIZATION OF THE MEAN SQUARE ERROR BY USE OF A CONSTANT-PARAMETER LINEAR NETWORK WHEN AVERAGED OVER ALL TIME

(2.1) The Permitted Operator

The linear operator which represents the operation of the network is

$$\int_0^t (\quad) h_1(t-\tau)d\tau \quad . \quad . \quad . \quad . \quad . \quad (1)$$

where $h_1(t)$ is permitted to be any function with a finite number of discontinuities for positive time and equal to zero for negative time. The function may contain any finite number of impulses of any finite order either at the origin or elsewhere.

The problem is to find the weighting function $h_1(t)$ which, when used in the operator (1) to operate on the signal plus noise, will minimize the mean square deviation between the resultant and the signal either at the current time or future or past time.

The first mathematical process to find $h_1(t)$ involves a minimization procedure; this is more straightforward if $h_1(t)$ is separated into two parts, $h(t)$ and $h_2(t)$, which are respectively the part of $h_1(t)$ which is free from impulses and the impulses.

If $h_2(t)$ contains impulses at the origin, the resultant due to this part of $h_2(t)$ will be the signal plus noise and the derivatives thereof with appropriate constant multipliers. Impulses other than at the origin produce terms in the resultant due to the signal plus noise being delayed and the derivatives thereof.

(2.2) Mathematical Statement of the Problem

Let the signal plus noise be represented by $g(t)$ and the signal by $s(t)$; then the problem is to minimize E_2, where

$$E_2 = \frac{1}{T}\int_0^T \left[\int_0^\infty g(t-\tau)h_1(\tau)d\tau - s(t)\right]^2 dt \quad . \quad . \quad (2)$$
$$T\to\infty$$

In eqn. (2) the limit of the integration has been extended to infinity; this has to be done since the signal and noise are supposed to have started indefinitely far in the past. Expanding eqn. (2) and including with E_2 the mean square of the signal, which is independent of $h_1(t)$, to form E_1 gives

$$E_1 = \frac{1}{T}\int_0^T \left[\int_0^\infty g(t-\tau)h(\tau)d\tau\right]^2 dt - \frac{2}{T}\int_0^T \left[s(t)\int_0^\infty g(t-\tau)h_1(\tau)d\tau\right]dt$$
$$T\to\infty$$

Changing the order of the last two integrals and substituting

$$x(\tau) = \frac{1}{T}\int_0^T g(t-\tau)s(t)dt$$

gives

$$E_1 = \frac{1}{T}\int_0^T \left[\int_0^\infty g(t-\tau)h_1(\tau)d\tau\right]^2 dt - 2\int_0^\infty h_1(\tau)x(\tau)d\tau \quad (3)$$
$$T\to\infty$$

(2.3) Variation of $h_1(\tau)$

As mentioned in Section 2.1, the impulse response $h_1(\tau)$ will be written as the sum of two terms, $h(\tau)$ which is finite and $h_2(\tau)$ which has no continuous parts and contains impulses only. (The impulses can be of any finite order.) The reason for this is that the variational procedure which will be used does not include a variation of the impulse part. As a result of applying the variation technique to $h(\tau)$ only we obtain the Wiener–Hopf equation

$$\int_0^\infty h_1(\tau)\phi(\tau-s)d\tau = x(s) \quad . \quad . \quad . \quad . \quad (4)$$

as being a necessary but not necessarily a sufficient condition on $h_1(\tau)$. It is obvious that the solution to the Wiener–Hopf equation is not unique, since the solution, $h_3(\tau)$, not necessarily

* WIENER, N.: 'The Interpolation, Extrapolation and Smoothing of Stationary Time Series' (Wiley, 1950).

Correspondence on Monographs is invited for consideration with a view to publication.
Mr. McDonnell is, and Mr. Perkins was, at the Vickers Group Research Establishment.

zero if impulsive, can be multiplied by an arbitrary function of s and added to a particular solution of eqn. (4):

$$\int_0^\infty h_3(\tau)\phi(\tau - s)d\tau = 0$$

However, by a variation of the impulse part of $h_1(\tau)$ the unique solution can be found. The procedure then will be to arrive at eqn. (4) as being a necessary condition on $h_1(\tau)$ but still having to vary the impulse part to give a sufficient condition. The general solution to eqn. (4) will be obtained, and then, by varying those parts containing impulses, the arbitrary constants will be determined.

Substitution of $h(\tau) + h_2(\tau)$ for $h_1(\tau)$ in eqn. (3) gives

$$E_1 = \frac{1}{T}\int_0^T\left[\int_0^\infty g(t-\tau)h(\tau)d\tau\right]^2 dt + \frac{1}{T}\int_0^T\left[\int_0^\infty g(t-\tau)h_2(\tau)d\tau\right]^2 dt + \frac{2}{T}\int_0^T\left[\int_0^\infty g(t-\tau)h(\tau)d\tau\int_0^\infty g(t-\tau)h_2(\tau)d\tau\right]dt - 2\int_0^\infty h(\tau)x(\tau)d\tau - 2\int_0^\infty h_2(\tau)x(\tau)d\tau \quad (5)$$

$T\to\infty$

In eqn. (5) the terms containing $h_2(\tau)$ can be written in terms of the delayed derivatives of the appropriate functions if

$$\int_0^\infty g(t-\tau)h_2(\tau)d\tau = \sum^n a_n\frac{d^{\beta_n}g(t-s_n)}{dt^{\beta_n}} = g_1(t) \quad . \quad (6)$$

Then

$$\int_0^\infty h_2(\tau)x(\tau)d\tau = \sum^n a_n\frac{d^{\beta_n}x(t-s_n)}{dt^{\beta_n}} = K \quad . \quad . \quad (7)$$

$t=0$

Substitution of eqns. (6) and (7) in eqn. (3) to make it look simpler gives

$$E_1 = \frac{1}{T}\int_0^T\left[\int_0^\infty g(t-\tau)h(\tau)d\tau\right]^2 dt + \frac{1}{T}\int_0^T[g_1(t)]^2 dt + \frac{2}{T}\int_0^T\int_0^\infty g(t-\tau)h(\tau)d\tau g_1(t)dt - 2\int_0^\infty h(\tau)x(\tau)d\tau - 2K \quad (8)$$

Now since the impulse part $h_2(t)$ is not going to be varied, $g_1(t)$ will remain constant together with K, and these may be included in E_1 to give E in eqn. (9):

$$E = \frac{1}{T}\int_0^T\left[\int_0^\infty g(t-\tau)h(\tau)d\tau\right]^2 dt + \frac{2}{T}\int_0^T\int_0^\infty g(t-\tau)h(\tau)d\tau g_1(t)dt - 2\int_0^\infty h(\tau)x(\tau)d\tau \quad (9)$$

$T\to\infty$

In eqn. (9), for a chosen impulse part $h_2(t)$, the finite part $h(\tau)$ can be varied to make E a minimum; then replacing $h(\tau)$ by $h(\tau) + ek(\tau)$ will produce a new error which will be greater than E for either sign of e. Using this fact leads in the usual way to

$$\int_0^\infty h(s)\phi(s-\tau)ds + \int_0^\infty h_2(s)\phi(s-\tau)ds = x(\tau) \quad . \quad (10)$$

for $\tau\geqslant 0$

as a necessary condition on $h(s)$ and $h_2(s)$, where $\phi(s-\tau)$ is given by

$$\phi(s-\tau) = \frac{1}{T}\int_0^T g(t-\tau)g(t-s)dt \quad . \quad . \quad . \quad (11)$$

Eqn. (10) is the usual Wiener–Hopf equation, which has here been shown to be a necessary condition. There is, in fact, only one solution to eqn. (10) which leads to a finite r.m.s. value for the value of the output of the filter; this will be seen when we obtain the general solution.

The particular solution giving this finite output will be obtained by varying the arbitrary constants occurring in the impulse part.

(2.4) General Solution of the Wiener–Hopf Equation

The statement of the problem [eqn. (2)] was the filtering case with zero prediction. If instead of the filtering case the filtering and prediction case had been considered, then instead of eqn. (2) we should have had

$$E_2 = \frac{1}{T}\int_0^T\left[\int_0^\infty g(t-\tau)h_1(\tau)d\tau - s(t+v)\right]^2 dt \quad . \quad (12)$$

which would have led to

$$\int_0^\infty h_1(s)\phi(s-\tau)ds = x(\tau+v) \text{ for } r\geqslant 0 \quad . \quad . \quad (13)$$

instead of eqn. (10), where v is positive for prediction and negative for the lagging case.

To solve eqn. (13) we multiply by $\varepsilon^{-p\tau}$ and integrate over all positive τ; i.e. taking Laplace transformations of both sides gives

$$X(p,v) = \int_0^\infty \varepsilon^{-p\tau}\int_0^\infty h_1(s)\phi(s-\tau)dsd\tau \quad . \quad . \quad (14)$$

where

$$X(p,v) = \int_0^\infty \varepsilon^{-p\tau}x(v+\tau)d\tau \quad . \quad . \quad . \quad (15)$$

In eqn. (14), if the order of integration is changed and the substitution $\tau = s + t$ is made, we have, since ϕ is even,

$$X(p,v) = \int_0^\infty h_1(s)\varepsilon^{-ps}\int_{-s}^\infty \varepsilon^{-pt}\phi(t)dtds \quad . \quad . \quad (16)$$

In eqn. (16) $\int_{-s}^\infty \varepsilon^{-pt}\phi(t)dt$ is a known function of s and p. Writing this as

$$\int_{-s}^\infty \varepsilon^{-pt}\phi(t)dt = \Phi(p,s) \quad . \quad . \quad . \quad . \quad (17)$$

eqn. (16) becomes

$$X(p,v) = \int_0^\infty \varepsilon^{-ps}h_1(s)\Phi(p,s)ds \quad . \quad . \quad . \quad (18)$$

Now, for most cases of practical importance $\phi(t)$ can be expressed as

$$\phi(t) = \sum^n A_n\varepsilon^{-\alpha_n|t|} \quad . \quad . \quad . \quad . \quad (19)$$

where α_n may be complex. If $\phi(t)$ contains terms like $|t^n|\varepsilon^{-\alpha|t|}$ these can be considered as limiting cases of exponentials; for example if

$$\phi(t) = |t|\varepsilon^{-\alpha|t|} + \text{other terms}$$

this can be considered as being

$$\phi(t) = \frac{\varepsilon^{-\alpha|t|}}{e} - \frac{\varepsilon^{-(\epsilon+\alpha)|t|}}{e} + \text{other terms}$$

$e\to 0$

which is covered by eqn. (19), the limiting process being left until the optimum filter is found in terms of e. Multiple poles in $\Phi(p)$ can be included in the same way. If $\phi(t)$ is expressed as a sum of Laguerre polynominals, a similar process can be used

Substitution of eqn. (19) in eqn. (17) and then eqn. (17) in eqn. (18) gives

$$X(p, v) = \sum^{n} A_n \int_0^{\infty} h_1(s)\left[\varepsilon^{-ps}\left(\frac{1}{p+\alpha_n} - \frac{1}{p-\alpha_n}\right) + \frac{\varepsilon^{-\alpha_n s}}{p-\alpha_n}\right] ds$$

or
$$X(p, v) = \sum^{n} A_n \left[\frac{H_1(p)}{p+\alpha_n} + \frac{H_1(\alpha_n)}{p-\alpha_n} - \frac{H_1(p)}{p-\alpha_n}\right] \quad (20)$$

where
$$H_1(p) = \int_0^{\infty} \varepsilon^{-ps} h_1(s) ds \quad . \quad . \quad . \quad . \quad (21)$$

Transposition of eqn. (20) gives

$$H_1(p) = \frac{X(p, v) - \sum^{n} A_n \frac{H(\alpha_n)}{p-\alpha_n}}{\sum^{n} A_n \frac{2\alpha_n}{p^2-\alpha_n^2}} \quad . \quad . \quad . \quad (22)$$

where the $H(\alpha_n)$ are as yet arbitrary constants to be determined by variation of the impulse part of $h_1(t)$.

Before giving examples it is necessary to consider the form in which $X(p, v)$ appears. $x(t)$ will again be represented by sums of exponential terms, but since $x(t)$ is not necessarily an even function it will be more general to define it separately for positive and negative time; thus let

$$\underset{t \geqslant 0}{x(t)} = \sum^{m} C_m \varepsilon^{-\gamma_m t} \quad . \quad . \quad . \quad . \quad . \quad (23)$$

$$\underset{t \leqslant 0}{x(t)} = \sum^{n} C_n' \varepsilon^{-\gamma_n' t} \quad . \quad . \quad . \quad . \quad . \quad (24)$$

$$\sum^{m} C_m = \sum^{n} C_n \quad . \quad . \quad . \quad . \quad . \quad . \quad (25)$$

The last condition of eqn. (25) must hold for real physical variables, otherwise there would be a discontinuity in the cross-correlation between the signal and the noise at the origin.

By inspection of eqn. (13) it is clear that if $x(\tau)$ can be split into separate additive parts the $h_1(\tau)$ can be found for each part separately and then added to give the complete $h_1(\tau)$. Thus it is sufficiently general to solve eqn. (22) for the $X(p, v)$ corresponding to $x(t)$ with one exponential term for t greater than zero and another exponential term for t less than zero.

By using eqn. (15) together with eqns. (23) and (24) the general case of $X(p, v)$ is

$$X(p, v) = \sum^{m} C_m \frac{\varepsilon^{pv}}{p+\gamma_m} + \sum^{n} C_n' \left(\frac{\varepsilon^{\gamma_n' v}}{p-\gamma_n'} - \frac{\varepsilon^{pv}}{p-\gamma_n'}\right) \quad (26)$$

for $v \leqslant 0$.

$$X(p, v) = \sum^{m} C_m \frac{\varepsilon^{-\gamma_m v}}{p+\gamma_m} \quad . \quad . \quad . \quad (27)$$

for $v \geqslant 0$.

(2.5) Examples of the Method

Example 1. $x(t) = C\varepsilon^{-\gamma|t|} \quad v = 0$ (filtering case)
$\phi(t) = A\varepsilon^{-\alpha|t|}$

From eqn. (27), $X(p, 0) = \dfrac{C}{p+\gamma}$

From eqn. (20),

$$\frac{C}{p+\gamma} = A\left[\frac{H_1(p)}{p+\alpha} + \frac{H_1(\alpha)}{p-\alpha} - \frac{H_1(p)}{p-\alpha}\right]$$

or
$$H_1(p) = H_1(\alpha)(p+\alpha) - \frac{C}{2\alpha A}\frac{(p+\alpha)(p-\alpha)}{p+\gamma} \quad . \quad (28)$$

The inverse Laplace transformation of eqn. (28) gives the time-function which satisfies eqn. (13), i.e.

$$h_1(t) = \left[H(\alpha) - \frac{C}{2\alpha A}\right]\delta'(t) + \left[H(\alpha)\alpha + \frac{\gamma C}{2\alpha A}\right]\delta(t) + \frac{C(\alpha^2-\gamma^2)}{2\alpha A}\varepsilon^{-\gamma t} \quad (29)$$

where $\delta(t)$ and $\delta'(t)$ are respectively a Dirac delta function at the origin and its derivative, and $H(\alpha)$ is an arbitrary constant.

The impulse response given by eqn. (29) would in the example taken lead to an infinite output mean power unless $H(\alpha)$ were chosen to make the derivative of the impulse vanish. This is the necessary variation of the impulse part of $h_1(t)$ mentioned earlier.

Choosing $H_1(\alpha)$ to give the finite output power means that

$$H(\alpha) = \frac{C}{2\alpha A}$$

and $h_1(t)$ becomes

$$h_1(t) = \frac{C}{2\alpha A}[(\alpha+\gamma)\delta(t) + (\alpha^2-\gamma^2)\varepsilon^{-\gamma t}] \quad . \quad (30)$$

Example 2. Let $\underset{t \geqslant 0}{x(t)} = \sum^{m} C_m \varepsilon^{-\gamma_m t}$, $v < 0$ (Lagging case)

$$x(t) = \sum^{n} C_n' \varepsilon^{-\gamma_n' t}, \; t \leqslant 0$$

$$\phi(t) = A\varepsilon^{-\alpha|t|}$$

Again from eqns. (26) and (22),

$$H_1(p) = -\left[\sum^{m} \frac{C_m \varepsilon^{pv}}{p+\gamma_m} + \sum^{n}\left(\frac{C_n' \varepsilon^{\gamma_n' v}}{p-\gamma_n'} - \frac{C_n' \varepsilon^{pv}}{p-\gamma_n'}\right)\right] \frac{p^2-\alpha^2}{2\alpha A} + H_1(\alpha)(p+\alpha) \quad (31)$$

Again the arbitrary constant $H_1(\alpha)$ must be chosen to give a finite mean square output power from the filter. Thus, if $H_1(p)$ is expanded in partial fractions, the value of $H_1(\alpha)$ must be chosen to make the coefficient of p vanish, otherwise again an infinite output power will be obtained.

It is worth noting that eqn. (25) must hold, otherwise there would be a term $p\varepsilon^{pv}$ in $H_1(p)$ which would again lead to an infinite output power.

Choosing $H_1(\alpha)$ to eliminate the term in p due to

$$\sum^{n} \frac{C'\varepsilon^{-\gamma_n' v}}{p-\gamma_n'}\frac{(p^2-\alpha^2)}{2\alpha A} \text{ gives } H(\alpha) = \frac{1}{2\alpha A}\sum C_n' \varepsilon^{-\gamma_n' v} \quad (32)$$

And substitution of this in eqn. (31) together with eqn. (25) gives

$$H_1(p) = \frac{1}{2\alpha A}\left(\varepsilon^{pv}\left\{\sum^{n} C_n'\left[-\frac{\gamma_n'+\alpha}{p-\gamma_n'} + \gamma_n'\right] - \sum^{m} C_m\left(\frac{\gamma_m-\alpha}{p+\gamma_m} - \gamma_m\right)\right\} + \sum^{n} C_n' \varepsilon^{-\gamma_n' v}\frac{(\alpha-\gamma_n')(p+\alpha)}{p-\gamma_n'}\right) \quad (33)$$

It will be noted that this transfer function will give rise to exponentials with positive exponents in the impulse response. The exponentials however will cancel for times greater than $t = v$.

Example 3.

$v > 0$ Prediction case

Let $x(t) = C\varepsilon^{-\gamma|t|}$

$\phi(t) = A\varepsilon^{-\alpha|t|} + C\varepsilon^{-\gamma|t|}$

Again from eqn. (22), we have

$$H_1(p) = \frac{\frac{C\varepsilon^{-\gamma v}}{(p+\gamma)} - \frac{AH_1(\alpha)}{(p-\alpha)} - \frac{CH_1(\gamma)}{(p-\gamma)}}{-\left(\frac{2A\alpha}{p^2-\alpha^2} + \frac{2C\gamma}{p^2-\gamma^2}\right)} \quad . \quad . \quad (34)$$

or

$$H_1(p) = \frac{[C\varepsilon^{-\gamma v} - AH_1(\alpha) - CH_1(\gamma)]p^3 - [C\gamma\varepsilon^{-\alpha_2 v} + A\alpha H_1(\alpha) + C\gamma H_1(\gamma)]p^2 - [C\alpha^2\varepsilon^{-\gamma v} - A\gamma^2 H_2(\alpha) - C\alpha^2 H_1(\gamma)]p + [C\gamma\alpha^2\varepsilon^{-\gamma v} + A\alpha\gamma^2 H_1(\alpha) + C\gamma\alpha^2 H(\gamma)]}{-p^2(2A\alpha + 2C\gamma) - (2A\alpha\gamma^2 + 2C\gamma\alpha_1^2)} \quad (35$$

Now $H_1(p)$ must have no p term, otherwise this will give an infinite power out of the network; therefore

$$AH_1(\alpha) = C\varepsilon^{-\gamma v} - CH(\gamma) \quad . \quad . \quad (36)$$

Using eqn. (36), eqn. (35) becomes

$$H(p) = \frac{ap^2 + bp + C}{dp^2 + e} \quad . \quad . \quad . \quad . \quad (37)$$

where

$a = C\gamma\varepsilon^{-\gamma v} + C\alpha\varepsilon^{-\gamma v} - C\alpha H_1(\gamma) + C\gamma H_1(\gamma)$

$b = C\alpha^2\varepsilon^{-\gamma v} - C\gamma^2\varepsilon^{-\gamma v} + C\gamma^2 H_1(\gamma) - C\alpha^2 H(\gamma)$

$c = C\gamma\alpha^2\varepsilon^{-\gamma v} + C\alpha\gamma^2\varepsilon^{-\gamma v} - C\alpha\gamma^2 H_1(\gamma) + C\gamma\alpha^2 H_1(\gamma)$

$d = 2A\alpha + 2C\gamma$

$e = 2A\alpha\gamma^2 + 2C\gamma\alpha^2$

Dividing out, eqn. (37) gives

$$H_1(p) = \frac{1}{d}\left[a + \frac{X}{p - \left(\frac{d}{e}\right)^{1/2}} + \frac{Y}{p + \left(\frac{d}{e}\right)^{1/2}}\right] \quad . \quad (38)$$

where

$$X = \tfrac{1}{2}\left[b - \frac{c - \frac{ad}{e}}{\left(\frac{d}{e}\right)^{1/2}}\right], \quad Y = \tfrac{1}{2}\left[b + \frac{c - \frac{ad}{e}}{\left(\frac{d}{e}\right)^{1/2}}\right]$$

Now $H_1(p)$ must not contain divergent exponentials which do not cancel after a finite time; therefore $H_1(\gamma)$ must be chosen by variation of the impulse part to make X equal zero. Putting X equal to zero and substituting the value of $H_1(\gamma)$ so obtained gives

$$H_1(p) - \frac{2\gamma C(\alpha+\gamma)\varepsilon^{-\gamma v}(p+\alpha)}{d\left[\left(\frac{d}{e}\right)^{1/2} + \gamma\right]\left[p + \left(\frac{d}{e}\right)^{1/2}\right]} \quad . \quad (39)$$

and

$$h(t) = \frac{2\gamma c(\alpha+\gamma)\varepsilon^{-\gamma v}\delta t}{d\left[\left(\frac{d}{e}\right)^{1/2} + \gamma\right]} + \frac{2\gamma C(\alpha+\gamma)\varepsilon^{-\gamma v}[\alpha - (d/e)^{1/2}]\varepsilon^{-(d/e)^{1/2}t}}{d\left[\left(\frac{d}{e}\right)^{1/2} + \gamma\right]} \quad . \quad . \quad . \quad . \quad (40)$$

The advantage if any in the method is in the lagging case where it was not necessary to factorize ε^{-pv}, i.e. in cases like Example 2.

(3) OPTIMUM FILTER FOR MINIMUM ERROR AT A PAR TICULAR TIME WHEN AVERAGED OVER AN INFINIT ENSEMBLE

(3.1) Statement of the Problem

The problem is to find the transfer function of the similar net works which when connected at time zero to separate signal contaminated by noise will produce outputs at time t_1 whic have the minimum mean square deviation from their signals a the time $t_1 + h$ when averaged over the infinite ensemble c networks. (h may be either positive for the prediction cas or negative for the lagging case.) The signals and the nois are ergodic. By the ergodic property the infinite ensemble c networks can be replaced by a single network which is use an infinite number of times. Fig. 1 shows the system unde investigation.

The switch S_1 is closed at time $t = 0$ and the output at th time $t = t_1$ is measured. The measured output is subtracte from the signal at time $t = t_1 + h$ and the error is noted. Th

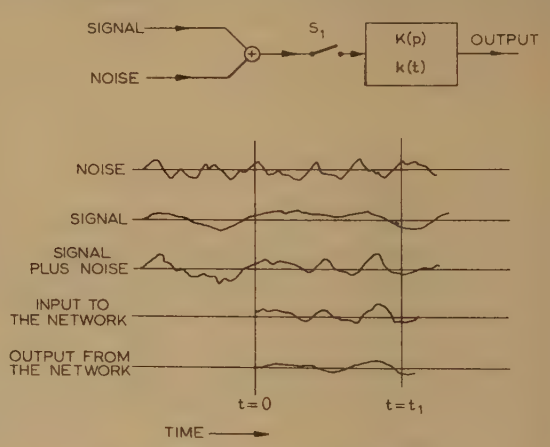

Fig. 1.—System under consideration.

switch is again opened; all the currents and charges in the net work are reduced to zero; the experiment is repeated, and nev errors are obtained. We seek that network which will give minimum mean square error over an infinity of experiments Stating the problem in mathematical form, we have for th filtering case, $v = 0$,

$$E = \frac{1}{M}\sum_{n=1}^{n=M}\left\{S_n(t) - \int_0^{t_1}[S_n(t-\tau) + N_n(t-\tau)]k(t_1,\tau)d\tau\right\}^2 \quad (41$$

where $k(t_1, \tau)$ (the impulse response of the network with t_1 as parameter) must be chosen to minimize the mean square error E The number M is the number of experiments. $S_n(t)$ is the signa as a function of time during the nth experiment. $N_n(t)$ is th noise as a function of time during the nth experiment.

(3.2) Variation of the Operator

Multiplying out the square in eqn. (41) and changing the orde of integration where necessary, we have, on making the followin substitutions,

$$\gamma_1(\tau) = \lim_{M\to\infty}\frac{1}{M}\sum_{n=1}^{n=M} N_n(t)N_n(t-\tau)$$

$$\phi_1(\tau) = \frac{1}{M}\sum_{n=1}^{n=M} S_n(t)S_n(t-\tau)$$

$$x_1(\tau) = \frac{1}{M}\sum_{n=1}^{n=M} S_n(t)N_n(t-\tau)$$

$$E = \phi_1(0) - 2\int_0^{t_1}\phi_1(\tau)k(t_1,\tau)d\tau - 2\int_0^{t_1}x_1(\tau)k(t_1,\tau)d\tau + \int_0^{t_1}\int_0^{t_1}\phi(\tau-s)k(t_1,\tau)k(t_1,s)d\tau ds + \int_0^{t_1}\int_0^{t_1}[x_1(\tau-s)+x_1(s-\tau)k(t_1,\tau)k(t_1,s)d\tau ds + \int_0^{t_1}\int_0^{t_1}\gamma_1(\tau-s)k(t_1,\tau)k(t_1,s)d\tau ds \quad . \quad . \quad (42)$$

If the operator $k(t_1,\tau)$ in eqn. (42) is chosen to minimize E, any other operation will produce a greater mean square error. A variation of the impulse response from $k(t_1,\tau)$ to $k(t_1,\tau)+eh(\tau)$ will produce an error greater than E independently of the sign of e.

Substitution of the variation in eqn. (42), letting e tend to zero and making use of the fact that the new error must be greater than E leads to the condition

$$\int_0^{t_1}h(\tau)\left\{\int_0^{t_1}[\phi_1(\tau-s)+\gamma_1(\tau-s)+x_1(\tau-s)+x_1(s-\tau)]k(t_1,\tau)d\tau-\phi_1(s)-x_1(s)=0\right\}$$

Writing

$$\phi_1(\tau-s)+\gamma_1(\tau-s)+x_1(\tau-s)+x_1(s-\tau)=\phi(\tau-s)$$

and

$$\phi_1(s)+x_1(s)=x(s)$$

gives

$$\int_0^{t_1}h(\tau)\int_0^{t_1}\phi(\tau-s)k(t_1,\tau)d\tau - x(s)ds = 0$$

And, for this to be satisfied for arbitrary $h(s)$ (not containing impulse derivatives), we have

$$\int_0^{t_1}\phi(\tau-s)k(t_1,\tau)d\tau = x(s) \text{ for } 0\leqslant s\leqslant t \quad . \quad (43)$$

If, instead of the filtering case, the filtering and prediction or filtering and lagging case had been taken, we should have instead of eqn. (43)

$$\int_0^{t_1}\phi(\tau-s)k(t_1,\tau)d\tau = x(s+v) \text{ for } 0\leqslant s\leqslant t_1 \quad (44)$$

(It is seen that the Wiener–Hopf equation is obtained when $t_1\to\infty$. This means that the problems solved in Section 2, i.e. Wiener's case, could have been stated differently, i.e. to minimize the error at infinity when averaged over an ensemble.) We seek here a solution to this equation for any positive value of t_1. The minimization procedure which led to eqn. (44) did not include a variation of the impulse part of $k(t_1,\tau)$ should it contain them. The impulse response $k(t_1,\tau)$ should have been split into two parts as in Section 2, but the variation follows along exactly similar lines, and this procedure has therefore been omitted here. It is important to note, however, that eqn. (44) is only a necessary condition on $k(t_1,\tau)$, and the impulse part $k(t_1,\tau)$ will have to be varied later to give the optimum filter. The solution to eqn. (44) will contain an arbitrary constant multiplied by the solution of

$$\int_0^{t_1}\phi(\tau-s)k(t_1,\tau)d\tau = 0 \quad . \quad . \quad . \quad . \quad (45)$$

The extra conditions required to eliminate the arbitrary constants due to the solution of eqn. (45) are obtained by a variation of the impulse part of $k(t_1,\tau)$ contained in the solution of eqn. (44). This, in some cases, only amounts to making the mean square value of the output from the network finite in the steady state.

Eqn. (44) is solved by developing from it an algebraic equation, solving that, and then reversing the transforms to obtain $k(t_1,\tau)$. The algebraic equation is eqn. (64).

(3.3) Solution of the Integral Equation

By inspection of eqn. (44) it is clear that there is no requirement on the desired optimum filter response $k(t_1,\tau)$ for values of $\tau > t_1$ and is thus arbitrary there.

The network need not in fact be stable (if rendered inoperative before $t=0$), unless a condition of steady-state ultimate output is imposed.

In eqn. (44) let $s = t_1 - u$, thus

$$\int_0^{t_1}\phi(t_1-u-\tau)k(t_1,\tau)d\tau = x(t_1-u+v) \quad 0\leqslant u\leqslant t_1$$

Multiplying by ε^{-pu} and integrating with respect to u from $u=0$ to $u=t_1$ we have

$$\int_0^{t_1}k(t_1,\tau)\int_0^{t_1}\phi(t_1-u-\tau)\varepsilon^{-pu}du d\tau = \int_0^{t_1}\varepsilon^{-pu}x(t_1-u+v)du \quad . \quad . \quad . \quad . \quad (46)$$

In eqn. (46) the function $\int_0^{t_1}\varepsilon^{-pu}\phi(t_1-\tau-u)du$ is a known function of t_1, p and τ. Also, using the fact that ϕ is even, it can be split into two parts, one a function of $t_1-\tau$ and p, and the other a function of τ and p. Thus

$$\int_0^{t_1}\varepsilon^{-pu}\phi(t_1-\tau-u)du = \varepsilon^{-p(t_1-\tau)}[\Phi(p,t_1-\tau)+\Phi(-p,\tau)] \quad . \quad . \quad . \quad . \quad (47)$$

where

$$\Phi_1(p,t) = \int_0^{t}\varepsilon^{ps}\phi(s)ds \quad . \quad . \quad . \quad . \quad (48)$$

Substitution of eqn. (47) in eqn. (46) gives

$$\int_0^{t_1}k(t_1,\tau)\varepsilon^{-p(t_1-\tau)}[\Phi_1(p,t_1-\tau)+\Phi_1(-p,\tau)]d\tau = \int_0^{t_1}\varepsilon^{-pu}x(t_1-u+v)du$$

and the ε^{-pt_1} cancels to give

$$\int_0^{t_1}k(t_1,\tau)\varepsilon^{p\tau}[\Phi_1(p,t-\tau)+\Phi_1(-p,\tau)]d\tau = \int_0^{t_1}\varepsilon^{ps}x(s+v)ds \quad . \quad (49)$$

Multiplying both sides of eqn. (49) by ε^{-qt_1} and integrating over all positive t_1 gives

$$\int_0^{\infty}\varepsilon^{-qt_1}\int_0^{t_1}\varepsilon^{p\tau}k(t_1,\tau)\Phi_1(p,t_1-\tau)+\Phi_1(-p,\tau)d\tau dt_1 = \int_0^{\infty}\varepsilon^{-qt_1}\int_0^{t_1}\varepsilon^{ps}x(s+v)ds dt_1 \quad . \quad (50)$$

The right-hand side of eqn. (50) is a known function of p, q and v and may be written as $X(p,q,v)$. The first part of the left-hand side of eqn. (50) is

$$\int_0^{\infty}\varepsilon^{-qt_1}\int_0^{t_1}\varepsilon^{p\tau}k(t_1,\tau)\Phi_1(p,t_1-\tau)d\tau dt$$

which is equal to

$$\int_0^\infty \varepsilon^{-qt_1}\Phi_1(p,t_1)\int_0^\infty \varepsilon^{-(q-p)\tau}\mathrm{k}(t_1+\tau,\tau)d\tau dt$$

Writing $$\int_0^\infty \varepsilon^{-(q-p)\tau}\mathrm{k}(t_1+\tau,\tau)d\tau = \mathrm{K}(q-p,t_1) \quad . \quad . \quad (51)$$

and noting that if we subsequently solve for $\mathrm{K}(q, t_1)$ we can obtain $\mathrm{k}(t_1+\tau,\tau)$ and hence $\mathrm{k}(t_1, \tau)$ by use of the inversion theorem,

$$\mathrm{k}(t_1+\tau,\tau) = \frac{1}{2\pi i}\int_c \varepsilon^{q\tau}\mathrm{K}(q,t_1)dq \quad . \quad . \quad . \quad (52)$$

We thus have, on substitution in eqn. (50),

$$\int_0^\infty \varepsilon^{-qt_1}\left[\Phi_1(p,t_1)\mathrm{K}(q-p,t_1) + \int_0^{t_1}\mathrm{k}(t_1,\tau)\varepsilon^{p\tau}\Phi_1(-p,\tau)d\tau\right]dt_1 = \mathrm{X}(p,q,v) \quad . \quad (53)$$

Using eqn. (52), we have

$$\mathrm{k}(t_1,\tau) = \frac{1}{2\pi i}\int_c \varepsilon^{q_1\tau}\mathrm{K}(q_1,t_1-\tau)dq_1 \quad . \quad . \quad (54)$$

where C_1 encloses the poles of $\mathrm{K}(q_1, t_1-\tau)$ (meanwhile q has been changed to a new dummy variable q_1). Now $\mathrm{k}(t_1,\tau)$ as given by eqn. (54) may be substituted in eqn. (53) giving

$$\int_0^\infty \varepsilon^{-qt_1}\left[\Phi_1(p,t_1)\mathrm{K}(q-p,t_1) + \frac{1}{2\pi i}\int_{C_1}\int_0^{t_1}\varepsilon^{(q_1+p)\tau}\mathrm{K}(q_1,t_1-\tau)\Phi_1(-p,\tau)d\tau dq_1\right]dt_1 = \mathrm{X}(p,q,v) \quad . \quad . \quad . \quad . \quad (55)$$

If we define $$\int_0^\infty \varepsilon^{-q_1t_1}\mathrm{K}(q,t_1)dt_1 = \mathrm{K}_1(q,q_1) \quad . \quad . \quad . \quad (56)$$

and solve for $\mathrm{K}_1(q, q_1)$ we can obtain $\mathrm{K}(q_1, t_1)$ by the use of the inversion integral

$$\mathrm{K}(q,t_1) = \frac{1}{2\pi i}\int_{C_2}\varepsilon^{q_1t_1}\mathrm{K}_1(q,q_1)dq_1 \quad . \quad . \quad . \quad (57)$$

where C_2 encloses the poles of $\mathrm{K}_1(q, q_1)$.

Subsitution of eqn. (57) in the first part of eqn. (55) and of eqn. (56) in the second part, after inverting the t_1, τ order of integration, gives

$$\frac{1}{2\pi i}\left[\int_{C_2}\mathrm{K}_1(q-p,q_1)\int_0^\infty \varepsilon^{-(q-q_1)t_1}\Phi_1(p,t_1)dt_1dq_1 + \int_{C_1}\mathrm{K}_1(q_1,q)\int_0^\infty \varepsilon^{-(q-q_1-p)t_1}\Phi_1(-p,t_1)dt_1dq_1\right] = \mathrm{X}(p,q,v) \quad . \quad . \quad . \quad . \quad (58)$$

Note that $$\int_0^\infty \varepsilon^{-(q-q_1)t_1}\Phi_1(p,t_1)dt_1 = \frac{\Phi(q-q_1-p)}{(q-q_1)}$$

and $$\int_0^\infty \varepsilon^{-(q-q_1-p)t_1}\Phi_1(-p,t_1)dt_1 = \frac{\Phi(q-q_1)}{q-q_1-p}$$

where $$\Phi(p) = \int_0^\infty \varepsilon^{-pt}\phi(t)dt \quad . \quad . \quad . \quad . \quad . \quad (59)$$

Making the substitutions we have

$$\frac{1}{2\pi i}\left[\int_{C_2}\mathrm{K}_1(q-p,q_1)\frac{\Phi(q-q_1-p)}{q-q_1}dq_1 + \int_{C_1}\mathrm{K}_1(q_1,q)\frac{\Phi(q-q_1)}{(q-q_1-p)}dq_1\right] = \mathrm{X}(p,q,v) \quad . \quad (60$$

for $\phi(t)$ given by

$$\phi(t) = \sum^n A_n\varepsilon^{-\alpha_n|t|} \quad . \quad . \quad . \quad . \quad . \quad (61$$

where α_n may be complex eqn. (60) can be reduced to an algebrai equation since the contour integrations can be evaluated withou knowing $\mathrm{K}_1(q_1, q)$. The contours C_2 and C_1 enclose the pole of $\mathrm{K}_1(q-p, q_1)$ and $\mathrm{K}_1(q_1, q)$.

[We note that if

$$\int_c \frac{1}{(p_1+\alpha)}\,\frac{1}{(p-p_1+\beta)}dp_1 = \mathrm{I}(p)$$

where C encloses only the pole at $p_1 = \alpha$, we get the same valu for the contour integral as if we consider the contour to enclos the pole at $p_1 = p+\beta$ and not the pole at α. This metho can be extended with suitable conditions on the integrand to a equation of the form

$$\int_c \mathrm{H}(p_1)\mathrm{G}(p-p_1)dp_1 = \mathrm{I}_1(p)$$

If the contour includes only the poles in H we can evaluat the integral by taking instead the residues, with a change c sign, at the poles of $\mathrm{G}(p-p_1)$.]

Thus, continuing, from eqn. (61) $\Phi(p)$ is given by

$$\Phi(p) = \sum^n \frac{A_n}{p+\alpha_n} \quad . \quad . \quad . \quad . \quad . \quad (62$$

and substitution of this in eqn. (60) gives

$$\frac{1}{2\pi i}\sum^n A_n\left[\int_{C_2}\frac{\mathrm{K}_1(q-p,q_1)}{(q-q_1)(q-q_1-p+\alpha_n)}dq_1 + \int_{C_2}\frac{\mathrm{K}_1(q_1,q)}{(q-q_1-p)(q-q_1+\alpha_n)}dq_1\right] = \mathrm{X}(p,q,v) \quad . \quad (63$$

Evaluating the contour integrations we have

$$\sum^n A_n\left[\frac{\mathrm{K}_1(q-p,q-p+\alpha_n)}{p-\alpha_n} - \frac{\mathrm{K}_1(q-p,q)}{p-\alpha_n} + \frac{\mathrm{K}_1(q-p,q)}{p+\alpha_n} - \frac{\mathrm{K}_1(q+\alpha_n,q)}{p+\alpha_n}\right] = \mathrm{X}(p,q,v) \quad . \quad (64$$

Thus by transposition

$$\mathrm{K}_1(q-p,q) = \frac{\sum^n A_n\left[\frac{\mathrm{K}_1(q+\alpha_n,q)}{p+\alpha_n} - \frac{\mathrm{K}_1(q-p,q-p+\alpha_n)}{p-\alpha_n}\right] + \mathrm{X}(p,q,$$

$$\sum^n A_n\left(\frac{1}{p+\alpha_n} - \frac{1}{p-\alpha_n}\right)$$

By substitution of $p = \alpha_n$ and $p = -\alpha_n$ we find that the fun tions $\mathrm{K}_1(q+\alpha_n, q)$ and $\mathrm{K}_1(q-p, q-p+\alpha_n)$ are not define and therefore they may be replaced by arbitrary functions; th

$$\mathrm{K}_1(q-p,q) = \frac{\sum^n A_n\left[\frac{\mathrm{F}_1(q)}{p+\alpha_n} - \frac{\mathrm{F}_2(q-p)}{p-\alpha_n}\right] + \mathrm{X}(p,q,v)}{\sum^n A_n\left(\frac{1}{p+\alpha_n} - \frac{1}{p-\alpha_n}\right)} \quad . \quad (6$$

The arbitrary functions arise because the solution of eqn. (44) contains the solution of eqn. (45), which is given by eqn. (65) when $X(p, q, v) = 0$. In our problem $F_1(q)$ and $F_2(q - p)$ will be defined by a variation of the impulse parts of $k(t_1, \tau)$.

(3.4) Example of the Method

The following simple example will show the method of inversion from $K_1(q, q_1)$ to $k(t_1, \tau)$. We will take the simplest case, i.e.

$$\phi(\tau) = A\varepsilon^{-\alpha|\tau|} \qquad x(\tau) = B\varepsilon^{-\beta|\tau|}$$

and take $v = 0$.

From eqn. (50) it follows that $X(p, q, v)$ is given by

$$X(p, q, 0) = -\frac{B}{(p - q - \beta)(p - \beta)} - \frac{B}{(p - \beta)q}$$

From eqn. (65),

$$K_1(q, q_1) = \frac{\sum^n A_n\left[\frac{F_1(q_1)}{q_1 - q + \alpha_n} - \frac{F_2(q)}{q_1 - q - \alpha_n}\right] + X(q - q_1, q, v)}{\sum^n A_n\left(\frac{1}{q_1 - q + \alpha_n} - \frac{1}{q_1 - q - \alpha_n}\right)} \quad . \quad . \quad . \quad . \quad (66)$$

And, for the simple example taken, eqn. (66) becomes

$$K_1(q, q_1) = \frac{A\left[\frac{F_1(q_1)}{q_1 - q + \alpha} - \frac{F_2(q)}{q_1 - q - \alpha}\right] + B\left[\frac{1}{(q_1 - q - \beta)(q + \beta)} - \frac{1}{(q_1 - q - \beta)q_1}\right]}{A\left[\frac{-2\alpha}{(q_1 - q)^2 - \alpha^2}\right]}$$

or
$$K_1(q, q_1) = \frac{1}{2\alpha}\left\{(q_1 - q + \alpha)F_2(q) - (q_1 - q - \alpha)F_1(q_1) - \frac{B}{A(q + \beta)}\left(q_1 - 2q + \frac{q^2 - \alpha^2}{q_1}\right)\right\} \quad . \quad . \quad . \quad . \quad (67)$$

Inverting eqn. (67) according to eqn. (57) gives

$$K(q, t_1) = \frac{1}{2\alpha}\left\{[\delta'(t_1) - (q - \alpha)\delta(t_1)]F_2(q) - \frac{df_1(t_1)}{dt_1} + (q + \alpha)f_1(t_1) - \frac{B}{A(q + \beta)}[\delta'(t_1) - 2q\delta(t) + q^2 - \alpha^2)]\right\} . \quad (68)$$

where $\delta'(t_1)$ and $\delta(t_1)$ are the derivatives of a Dirac delta function and the function respectively, and $f_1(t_1)$ is an arbitrary function of t_1.

The next step is to invert according to eqn. (54); we must therefore change the variable to give

$$K(q, t_1 - \tau) = \frac{1}{2\alpha}\left\{[\delta'(t_1 - \tau) - (q - \alpha)\delta(t_1 - \tau)]F_2(q) - \frac{df_1(t_1 - \tau)}{d(t_1 - \tau)} + (q + \alpha)f_1(t_1 - \tau) - \frac{B}{A(q + \beta)}[\delta(t_1 - \tau) - 2q\delta(t_1 - \tau) + q^2 - \alpha^2]\right.$$

Putting the second term in partial fractions in q gives

$$K(q, t_1 - \tau) = \frac{1}{2\alpha}[(\delta'(t_1 - \tau) - (q - \alpha)\delta(t_1 - \tau)]F_2(q)$$

$$- \frac{df_1(t_1 - \tau)}{d(t_1 - \tau)} + (q + \alpha)f_1(t_1 - \tau) - \frac{B}{A}\left[\frac{\delta'(t_1 - \tau)}{q + \beta} - 2\delta(t_1 - \tau) + \frac{2\beta}{(q + \beta)}\delta(t_1 - \tau) + q - \beta + \frac{\beta^2 - \alpha^2}{(q + \beta)}\right.$$

Using eqn. (54) gives

$$k(t_1, \tau) = \frac{1}{2\alpha}\left\{\delta'(t_1 - \tau)f_2(\tau) - \delta(t_1 - \tau)\frac{df_2(\tau)}{d\tau} + \alpha\delta(t_1 - \tau)f_2(\tau) - \delta(\tau)\frac{df_1(t_1 - \tau)}{d(t_1 - \tau)} + \delta'(\tau)f_1(t_1 - \tau) + \alpha\delta(\tau)f_1(t_1 - \tau) - \frac{B}{A}[\delta'(t_1 - \tau)e^{-\beta\tau} - 2\delta(t_1 - \tau)\delta\tau + 2\beta\delta(t_1 - \tau)e^{-\beta\tau} - \beta\delta\tau + (\beta^2 - \alpha^2)e^{-\beta\tau}]\right\} \quad . \quad . \quad (69)$$

The whole of eqn. (69) satisfies eqn. (70):

$$A\int_0^{t_1} \varepsilon^{-\alpha|\tau - s|}k(t_1, \tau)d\tau = B\varepsilon^{-\beta s} \qquad 0 \leqslant s \leqslant t_1 \quad . \quad (70)$$

The terms containing arbitrary functions satisfy eqn. (71):

$$\int_0^{t_1} \varepsilon^{-\alpha|\tau - s|}k_1(t_1, \tau)d\tau = 0 \quad . \quad . \quad . \quad . \quad (71)$$

If the solution which we seek is the one with a finite output spectrum (i.e. having an output which builds up to a steady state of finite fluctuation after a long time), then since the input spectrum taken is given by

$$S_1(\omega) = \frac{A}{\omega^2 + \alpha^2}$$

the filter must not contain differentiators without smoothing between the input and output, and therefore the functions $f_1(t_1 + \tau)$ and $f_2(\tau)$ must be chosen to eliminate the derivative terms, i.e.

$$f_2(\tau) = \frac{B}{A}\varepsilon^{-\beta\tau}$$

and
$$f_1(\tau) = \frac{B}{A}$$

With these choices of $f_2(\tau)$ and $f_1(\tau)$ the solution becomes

$$k(t_1, \tau) = \frac{B}{2\alpha A}[(\alpha - \beta)\delta(t_1 - \tau)\varepsilon^{-\beta\tau} + (\alpha + \beta)\delta(\tau) + (\alpha^2 - \beta^2)\varepsilon^{-\beta\tau}] \quad . \quad . \quad . \quad . \quad (72)$$

Eqn. (72) gives the required solution uniquely determined in the range $0 \leqslant \tau \leqslant t_1$ which satisfies eqn. (70). (It is so simple that it should have been possible to guess it.)

As $t_1 \to \infty$ the result is

$$k(\infty, \tau) = \frac{B}{2\alpha A}\{(\alpha + \beta)[\delta(\tau) + (\alpha - \beta)\varepsilon^{-\beta\tau}]\}$$

which is the correct result for the Wiener–Hopf equation.

For more complicated values of $x(\tau)$ or for the lagging and prediction cases, the values of $x(\tau)$ may be expressed as the sum of terms like

$$x(t + v) = B\varepsilon^{-\beta|t+v|}$$

In the lagging case, i.e. for v negative, $X(p, q, v)$ will contain delay functions ε^{pv}; these will shift the positions of the impulses when inverting the transforms. The individual terms o $X(p, q, v)$ may be taken separately and the resultant values o $k(t, \tau)$ added to give the complete impulse response. In the cas when $\phi(\tau)$ consists of several terms, a little more algebra will b required to give the answer, but the working is straightforwar

(4) ACKNOWLEDGMENT

The authors wish to thank the Directors of Vickers Ltd. fo permission to publish the paper.

621.385.032.213 : 621.315.59

The Institution of Electrical Engineers
Monograph No. 317 R
Nov. 1958

THE CONDUCTIVITY OF OXIDE CATHODES

Part 6. Conductivity in a Magnetic Field

By G. H. METSON, M.C., D.Sc., Ph.D., M.Sc., B.Sc.(Eng.), Member.

(*The paper was first received* 28*th February, and in revised form* 30*th July*, 1958. *It was published as an* INSTITUTION MONOGRAPH *in November*, 1958.)

SUMMARY

In this Part the conductivity of the oxide-cathode matrix in an S-type valve in the presence of a magnetic field is examined, and it is shown that the matrix exhibits a powerful magnetic-resistance effect. However, the effect occurs only when the electron transfer is by free flight through the hollow pores of the matrix and when the magnetic field is in a transverse direction, and the solid-particle phase of the conduction mechanism shows no measurable magneto-resistance effect.

LIST OF PRINCIPAL SYMBOLS

V_A = Potential across matrix, volts.
I_A = Electron current through matrix, in absence of magnetic field, mA.
I'_A = Electron current through matrix in presence of magnetic field, mA.
H = Magnetic field, oersteds.
θ = Angle defining direction of magnetic field with respect to the S-type assembly (see Fig. 1).
T_M = Matrix temperature, deg K.
R_d = Matrix resistance in absence of magnetic field, ohms.
R'_d = Matrix resistance in presence of magnetic field, ohms.
ρ = Resistivity of a conductor, ohm-cm.
$\Delta\rho$ = Change in ρ due to application of magnetic field.
σ = Conductivity of matrix, millimhos.
σ_v = Pore conductivity of matrix, millimhos.
σ_s = Solid (particle) conductivity of matrix, millimhos.
T_{max} = Temperature of maximum value of f(R), deg K.
T_{int} = Temperature of intercept of conductivity phases, deg K.
T_c = Critical temperature for f(R) = 0, deg K.
I_V = Vacuum element of matrix current, mA.
I_S = Solid conduction element of matrix current, mA.

(1) EXPERIMENTAL PHENOMENA

(1.1) Experimental Arrangements

The experimental observations discussed in the present Part result from a straightforward application of a magnetic field to a standard S-type assembly.* A schematic of the assembly in relation to the direction of application of the field is shown in Fig. 1, from which it will be seen that the field of strength H is applied parallel to the shorter working edges of the rectangular metal box cores. Arrangements are available, however, for rotating the assembly about a central axis AB, so that H can be inclined at any angle θ to the normal to the direction of flow of electrons between the two core faces. With $\theta = 0°$ or 180° the electrons cross the lines of magnetic force normally and experience their greatest lateral force; with $\theta = 90°$ or 270° the electrons move parallel to the magnetic field and the lateral force is zero.

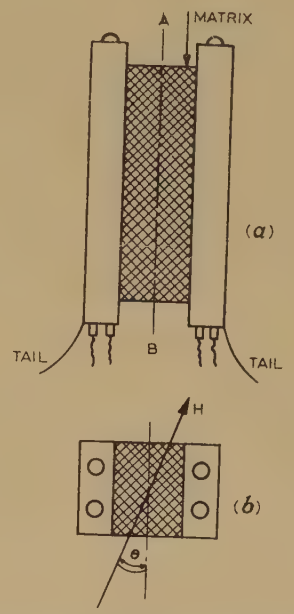

Fig. 1.—Arrangement of S-type assembly in the magnetic field.
(*a*) Elevation: H is normal to the plane of the paper.
(*b*) Plan.

The magnetic field used in the measurements has been derived from a large electromagnet calibrated over a range of 0–2 500 oersteds. For work at fixed field strengths a permanent magnet of 2 700 oersteds has been employed.

(1.2) Method of Measurement

The method of measurement is shown in Fig. 2. A current, I_A, is driven through the matrix at a potential V_A. The magnetic

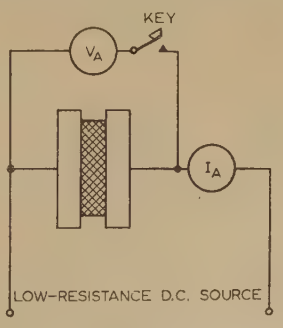

Fig. 2.—Test circuit.

* Specification of standard S-type assembly:
Cores: Active nickel or pure platinum.
Matrix: Co-precipitated equimolar barium-strontium oxide.
Matrix density: About 1·0.
Matrix thickness: 150 μ.
Matrix area: 0·45 cm².
The assemblies are vacuum-processed to the standard schedule detailed in Table 1 of Part 1.

This paper is a continuation of Monographs Nos. 221 R and 243 R, published in February and June, 1957 (see 104 C, pp. 316 and 496), and Nos. 268 R, 269 R and 289 R, published in December, 1957, and February, 1958 (see 105 C, pp. 183, 189 and 374).
Correspondence on Monographs is invited for consideration with a view to publication.
Dr. Metson is at the Post Office Research Station.

field strength, H, is now raised from zero to some convenient level and the new value of current, I'_A, is noted with V_A maintained across the core faces. Then the resistance increment function, f(R), is defined by

$$f(R) = \frac{R'_d - R_d}{R_d} \times 100$$

where $R_d = V_A/I_A$ and $R'_d = V_A/I'_A$. The function f(R) is therefore a measure of the relative increase in resistance on application of the field.

Two minor practical points in the experimental arrangement are perhaps worthy of mention. The d.c. power source is arranged to have a resistance which is negligible in relation to that of the S-type assembly. This useful arrangement leaves the potential across the device unchanged following a current decrement ΔI_A, consequent on application of the magnetic field. The second point concerns the current carried by the voltmeter, which may be greater than the current through the matrix under certain conditions. To avoid the computation necessary to exclude this current it is convenient to set the voltmeter to the required reading and then eliminate the instrument from the circuit by means of the key shown in Fig. 2.

(1.3) Field Direction

In this first experiment a standard S-type assembly with platinum cores is activated in the usual manner and is mounted on a turntable between the pole-pieces of the electromagnet. The initial orientation of the assembly with respect to the direction of the magnetic field is that defined in Fig. 1 with angle $\theta = 0°$. With zero magnetic field strength the oxide matrix is raised to some convenient temperature and a current I_A is driven through it by a voltage V_A. After the initial current I_A has been noted, H is increased from zero to 2000 oersteds and the depressed level of current, I'_A, is recorded. With H and V_A held constant the assembly is now rotated and the variation of I'_A with θ is measured over a full cycle of four quadrants.

The derived characteristic of f(R)/θ is shown in Fig. 3 and leads to the following conclusions:

(*a*) When the magnetic field is parallel to the normal electron run the resistance of the matrix is undisturbed by the field.
(*b*) When the magnetic field is at right angles to the normal electron run the resistance of the matrix is increased by the presence of the field.

The direction of normal electron run is assumed to coincide with the shortest distance between the two core faces.

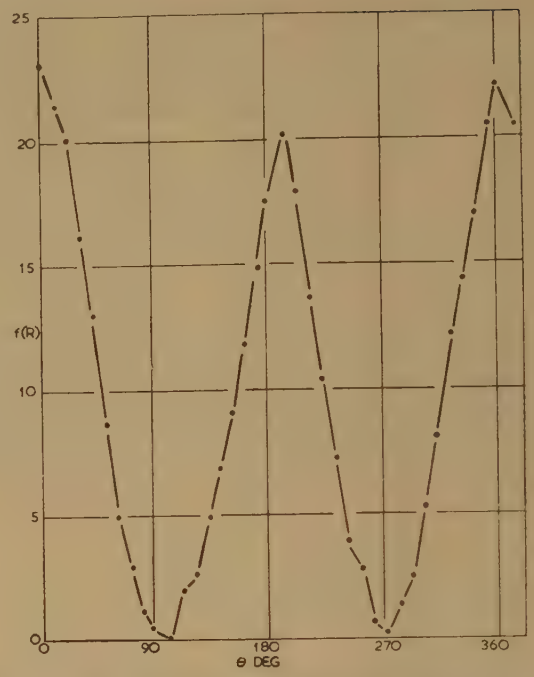

Fig. 3.—f(R) as a function of the direction of the magnetic field.

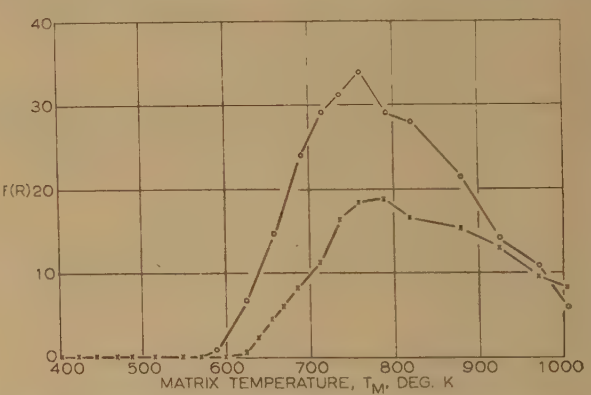

Fig. 4.—Variation of f(R) with temperature of the matrix.
○○○ Tube No. S–164.
×××Tube No. S–170.

(1.4) Influence of Matrix Temperature

In this second experiment a standard S-type assembly with platinum cores is set up between the pole-pieces of the electromagnet in the manner of Fig. 1. The angle θ is arranged to be zero, so that the normal electron run in the matrix is at right angles to the direction of the magnetic field, i.e. the maximum conductance decrement is achieved. The matrix temperature is controlled by variation of the common heater voltage applied to the insulated core heaters, and is measured by a thermocouple welded to the back of one of the cores. The experimental sequence is as follows. The heater voltage is set to give some convenient matrix temperature, T_M, the magnetic field strength being left at zero, and a current, I_A, is driven through the matrix by a voltage V_A. With V_A constant the field strength is now raised from zero to 2000 oersteds and the new debased level of current, I'_A, is recorded. The two currents give the value of f(R) for this particular temperature setting. The experiment is now repeated for a new temperature setting, and so on until the range 400–1000° K has been covered. The resulting variation of f(R) with T_M at constant V_A is shown in Fig. 4 for two typical samples.

From experiments such as the above the following conclusions may be drawn:

(*a*) A critical temperature (approximately 570 ± 30° K) exists below which the value of f(R) is always zero. (The zero value is taken as one too small to detect on the moving-coil instrument employed, i.e. less than 0·2%.)
(*b*) Above the critical temperature, f(R) increases up to a maximum in the range 750–800° K.
(*c*) Above 800° K, f(R) falls at first rapidly and then more slowly to make an asymptotic approach to zero as the temperature is progressively increased above 1000° K.

There seem then to be three bands of temperature in which f(R) behaves in significantly different fashion. These bands vary with individual valves, but the figures set out in Table 1 cover all cases examined.

The object of the present Part is to examine these temperature trends of f(R) and to interpret them in terms of the conductivity state of the matrix.

Table 1

TEMPERATURE CHARACTERISTICS OF f(*R*)

Temperature range	Characteristic behaviour of f(*R*)
Below 500° K	Always zero
500°–800° K	Increases with increasing temperature
Above 800° K	Decreases with increasing temperature

(1.5) Influence of Current Density

Since the previous experiment is carried out at constant applied voltage, the current I_A increases as the matrix temperature is increased. There is therefore an obvious possibility that the relationship between f(*R*) and the matrix temperature is dependent upon I_A at that matrix temperature. This possibility is examined in the following way. A standard S-type assembly is fixed between the pole-pieces of the electromagnet with $\theta = 0$ for maximum current decrement. With zero magnetic field the temperature is first set at some value below the critical temperature—the particular value chosen for the sequence set out in Fig. 5 is 515° K. With $H = 2\,700$ oersteds the value of f(*R*) is now explored over a range of currents by varying V_A. The

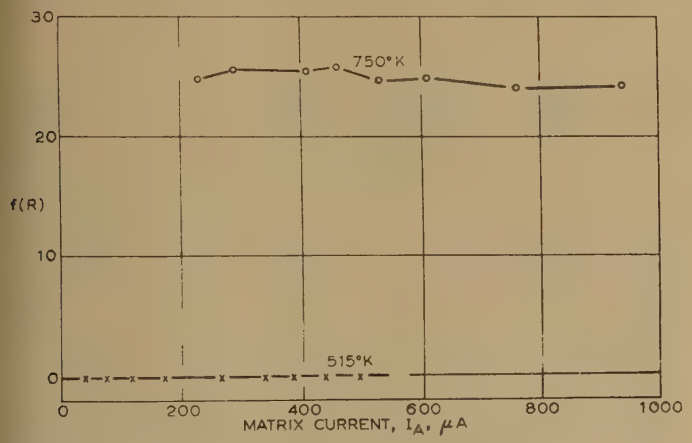

Fig. 5.—Variation of f(*R*) with current at temperatures above and below the critical temperature.

resulting characteristic (Fig. 5) shows that, below the critical temperature, f(*R*) remains zero for all values of I_A.

The temperature is next raised to 750° K, where maximum current decrement occurs, and the experimental sequence is repeated. Fig. 5 shows that here, too, the magnitude of f(*R*) is invariant with I_A. It clearly follows that the characteristics shown in Fig. 4 would be unchanged by arranging the experimental sequence at constant current instead of constant voltage—in short, f(*R*) is determined primarily by matrix temperature or some parameter dependent on temperature.

(1.6) Influence of Matrix Resistance

The parameter of the S-type assembly most obviously dependent on temperature is its resistance, R_d, and the magnitude of R_d is determined by the density of the electron cloud within the vacuum pores of the matrix. The density of this cloud will, of course, increase with temperature at a rate determined by Richardson's law, with a magnitude at any one temperature depending on the concentration of electron-emitting centres on the pore walls. If at any one temperature the concentration of pore-wall emitting centres is decreased by an oxygen attack, the electron-cloud density falls and the resistance rises. A pertinent question now arises: at a given temperature and under an oxygen attack, does f(*R*) change in sympathy with R_d? If such a correlation is observed, there will be reason to suppose that f(*R*) and electron-cloud density are interdependent.

The idea has been put to experimental test, and some typical results are given in Fig. 6 as the variation of f(*R*) with the

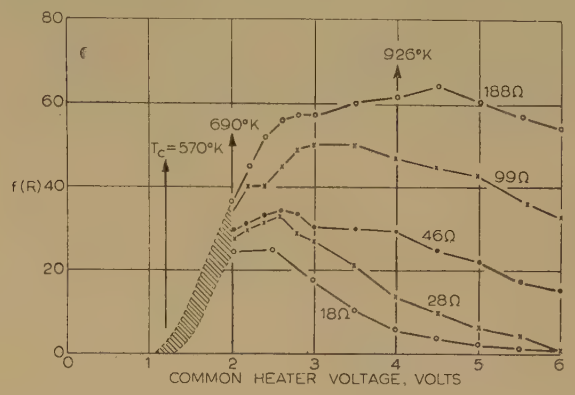

Fig. 6.—f(*R*) as a function of heater voltage for several values of R_d.

common heater voltage at constant V_A and an applied field of 2 700 oersteds. The resistance indicated on each characteristic represents the R_d of the tube measured with a heater voltage of 6·0 volts (i.e. at a nominal 1 020° K) in the absence of magnetic field. The higher resistances are obtained by subjecting the matrix to a controlled oxygen attack from a heated barium-peroxide spiral. From such experimental results the following conclusions are drawn:

(*a*) Above 700° K, and in conditions affecting the electron-cloud density in the vacuum pores of the matrix, f(*R*) and R_d move in apparent sympathy. A characteristic of f(*R*)/R_d at constant temperature, $T_M = 926°$ K, is extracted from Fig. 6 and shown in Fig. 7.

(*b*) Below 700° K R_d has little effect on f(*R*), and for this reason all characteristics in Fig. 6 have been included in a common envelope.

(*c*) The position of the critical temperature, T_c, is hardly affected by R_d.

Since 600° K is the temperature at which the matrix begins to give appreciable thermionic emission, it seems reasonable to

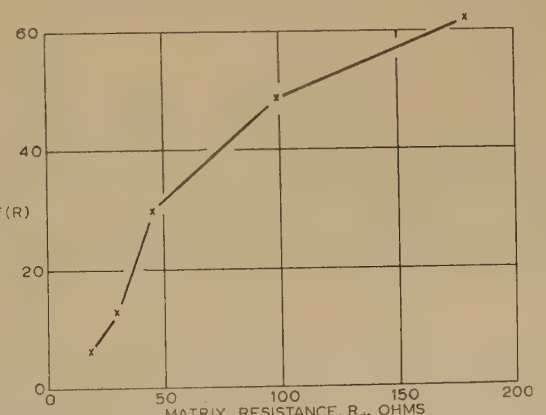

Fig. 7.—f(*R*) as a function of matrix resistance at constant temperature. $T_M = 926°$ K.

suppose that f(*R*) is associated only with the movement of free electrons in the vacuum pores, and furthermore that f(*R*) decreases as the density of the electron-cloud increases.

(1.7) Influence of Magnetic Field

Measurements of the variation of f(R) with H is a simple matter. A platinum-cored S-type assembly is arranged with $\theta = 0$ between the pole-pieces of the electromagnet. The matrix temperature is set at 750° K, where maximum current decrement can be expected, and a constant potential $V_A = 1{\cdot}0$ volt is applied between the core faces. The field strength is now raised from zero to some convenient value and the measure of f(R) is taken: this sequence is repeated until the range of field strength covered is 0–2 300 oersteds. The resulting variation of f(R) with H is given in Fig. 8 and shows that the relation is linear

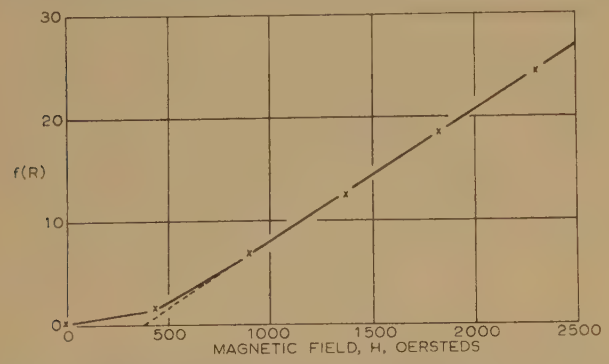

Fig. 8.—f(R) as a function of magnetic field.

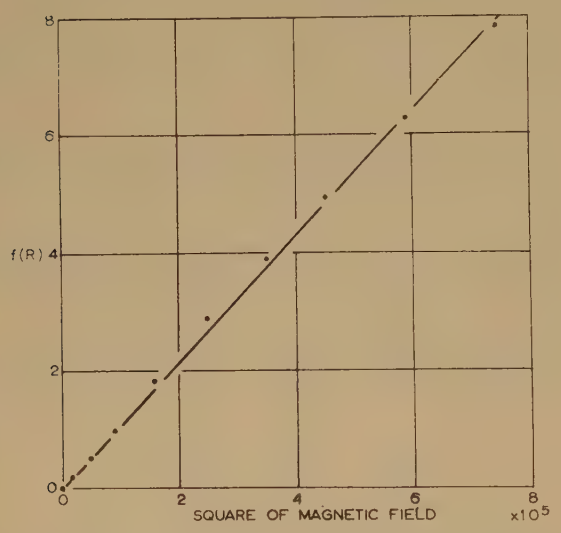

Fig. 9.—f(R) as a function of the square of the magnetic field.

above about 900 oersteds. Fig. 9 shows f(R) as a function of the square of the field strength over the range 0–900 oersteds. The relation between f(R) and H is thus seen to follow a square law at low field strengths and a linear law at higher field strengths.

(1.8) Correlation of f(R) with Conductivity State

It was shown in Table 1 that f(R) has three distinctive forms of behaviour linked to specific temperature ranges, and an attempt will now be made to correlate these forms with the two conducting states of the matrix. The inquiry is carried out on a standard S-type assembly with platinum cores fitted with thermocouples. The tube is first measured for conductivity over the temperature range 400–1 100° K, and then for f(R) over the same range using an 'on-off' field strength of 0–2 700 oersteds. Both characteristics are plotted in Fig. 10 against the reciprocal

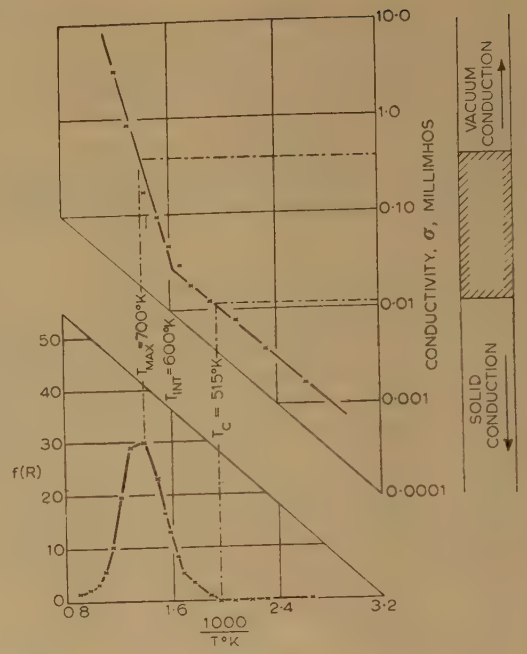

Fig. 10.—Correlation of f(R) with conductivity state.

of the absolute temperature, using a logarithmic scale for conductivity and a linear one for f(R).

The conductivity characteristic, which is quite typical for a platinum-cored assembly, consists of two straight-line phases intercepting at 600° K. The f(R) characteristic has its critical temperature at 515° and its 'maximum' temperature at 700° K, and these two significant points are marked on Fig. 10 to emphasize the conjugate points on the conductivity characteristic. It now becomes reasonable to extend the subdivision of the conductivity characteristic from two to three phases, in which the upper and lower are concerned with simple vacuum and solid conductions respectively, while the intermediate phase of 515°–700° K is identified with mixed vacuum and solid conductivities in comparable magnitudes. The three phases are indicated on the right of Fig. 10, the shaded area representing the mixed conductivity phase. Examination of the characteristic shows that the two conductivity phases intersect at 600° K and that this is approximately equal to the mean of the two temperatures limiting the phase of f(R) which increases with increasing temperature. Then

$$T_{int} = T_c + 100°$$
$$= T_{max} - 100°$$

in round figures. We now have a tentative numerical relationship between the conductivity characteristic and the reaction of the matrix to an applied magnetic field. Table 1 can thus be generalized into the form of Table 2.

Table 2

f(R) IN RELATION TO CONDUCTIVITY STATE, AS A FUNCTION OF TEMPERATURE

Temperature range	Behaviour of f(R)	Conductivity state
$<(T_{int} - 100°)$	Always zero	Solid
$(T_{int} - 100°)$ to $(T_{int} + 100°)$	Increases with temperature	Mixed
$>(T_{int} + 100°)$	Decreased with temperature	Vacuum

It is on the basis of Table 2 that the experimental results will be discussed in Section 2.

(1.9) Influence of Core-Metal Variation

It will have been noticed that all experiments so far described in the present Part have employed S-type assemblies with platinum cores. This deliberate choice of a diamagnetic core material avoids the appearance of disturbing mechanical forces which might be set up across the oxide matrix when ferromagnetic core pieces are inserted in a magnetic field.

The behaviour of the active-nickel core assembly is broadly similar to the platinum case, as will appear from the characteristics set out in Fig. 11. Above 620° K, f(R) rises swiftly to

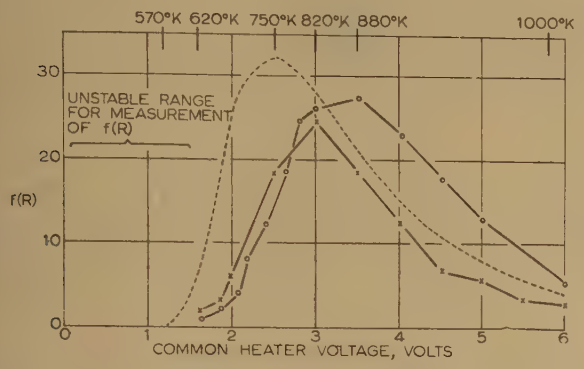

Fig. 11.—f(R) as a function of heater voltage for S-type assemblies with active-nickel cores.
Magnetic field = 2 700 oersteds.
× × × Tube No. S–147.
○ ○ ○ Tube No. S–100.
Broken line represents the behaviour of a typical platinum-core assembly.

a maximum near 850° K, and then falls asymptotically towards zero with rising temperature. The one significant difference here is that the temperature for maximum f(R) is about 100° higher than it is for the platinum assembly. The characteristics between 620°–1 050° K are essentially stable, but below 620° K this stability is lost, with f(R) assuming large positive and negative values in apparently random fashion. The shift of T_{max} and the low-temperature instability will now be considered separately.

It was suggested in Section 1.8 that the temperature for peak values of f(R) was related to that at which the two conductivity phases intersect. If this relationship ($T_{int} = T_{max} - 100°$) holds for the S-type assembly with active-nickel cores, then any shift of T_{max} relative to the platinum case should be accompanied by an equal shift in respect of T_{int}. Fig. 12 shows that such is the case and that movement of the peaks of the two f(R) characteristics is closely correlated to movement of the intercept points of the conductivity characteristics. The reason for the higher value of T_{max} for the active-nickel cores is thus due to the higher level of solid conductivity of the matrix obtained with these cores. The two conductivity characteristics can be regarded as typical.*

The instability of f(R) below 620° K for the active-nickel case is explained in the following terms. Conductivity below 620° K becomes progressively more dependent on solid-state conduction, where f(R) is always seen to be zero for the platinum case. In the nickel-core case, however, the conducting matrix is subjected to mechanical force when the field H is applied. These forces affect the packing of the 3-dimensional web of particles which make up the solid-state conductor, causing its resistance to change in random fashion. Changes in I_A, result, therefore,

* Some of the factors controlling the level of solid conductivity in the S-type assembly will be described in a later Part of the paper.

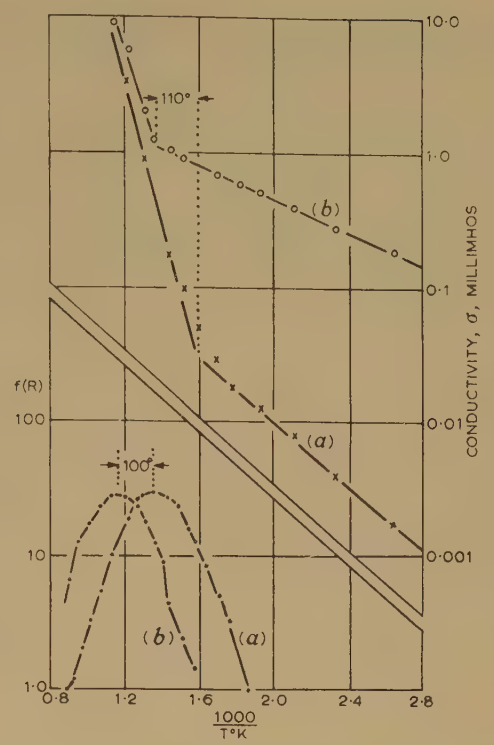

Fig. 12.—Comparison of temperature characteristics of conductivity and f(R) for S-type assemblies with (*a*) platinum, and (*b*) active-nickel cores.

from mechanical rather than electromagnetic causes and measurements of f(R) cease to have meaning. The change from stable to unstable state is surprisingly sharp and may depend on the passing of the Curie point of nickel at 633° K.

(1.10) Summary of Experimental Results

It has been shown that the resistance of the matrix increases in a transverse magnetic field and that the magnitude of the change is represented by f(R). The observed properties of f(R) may be summarized as follows:

(*a*) f(R) is always zero (or less than 0·2%) when the electron transfer mechanism is a solid-state one.
(*b*) f(R) increases with increasing temperature when the transfer mechanism is a mixed one of solid-state and vacuum in comparable magnitudes.
(*c*) f(R) decreases with increasing temperature when the transfer mechanism is preponderantly vacuum-wise.
(*d*) The temperature at which the two conductivity phases intersect determines the temperature at which f(R) is a maximum.
(*e*) The magnitude of f(R) at any one temperature is an inverse function of the electron density in the vacuum pores at that temperature. The matrix resistance and f(R) are therefore determined by the same basic phenomenon and must themselves be directly related.
(*f*) f(R) is independent of current.
(*g*) f(R) is a quadratic function of H at low values of H and a linear function at high values.

In addition to the above it will be recalled that turning the transverse magnetic field through 90° to bring it parallel with the line of current flow results in f(R) falling to zero (or less than 0·2%).

(2) DISCUSSION OF RESULTS

(2.1) Magnetoresistance

The results of the previous Section will be discussed in terms of the phenomenon known as *magnetoresistance*, defined as the

resistance change experienced by a conductor when placed in a magnetic field. Magnetoresistance is closely allied to the Hall effect, but its underlying mechanism is much more obscure. Suppose that a current is passed through a conductor which is situated in a transverse magnetic field. Electrons will tend, under the Lorentz force, to build up a space charge on one side of the conductor, and this will give rise to a transverse electric potential known as the Hall voltage. In equilibrium the result of the Hall voltage is to balance the Lorentz force, so that the electrons pass through the conductor without deviation. Such a picture is, of course, valid only if all electrons have the same drift velocity, and such a mechanism will give rise to no magnetoresistance effect. If, however, the electrons possess a velocity distribution, the transverse Hall potential will balance the electrons only under an average Lorentz force—electrons faster than the average will suffer deviation in one direction and slower electrons in the other direction. Deviated electrons will thus experience more collisions in completing their passage than will undeviated electrons, and the effect will be that of shortening their mean free paths. The overall result of a velocity distribution is thus to introduce a distribution of mean-free-path lengths and a corresponding increase in longitudinal resistance. With a longitudinal magnetic field replacing the transverse one, the magnetoresistance should be zero on the velocity-distribution model. If the resistivity without magnetic field is ρ, it is usual to write magnetoresistance as $\Delta\rho/\rho$, where $\Delta\rho$ is the increase on application of the field. Thus, in the terminology of the previous Section, we have

$$f(R) = \frac{\Delta\rho}{\rho} \times 100$$

Work on magnetoresistance can be digested on the following lines. For metallic conduction in a transverse magnetic field Kapitza[1] finds that $\Delta\rho/\rho \propto H^2$ for weak fields and $\Delta\rho/\rho \propto H$ for strong fields, and that $\Delta\rho/\rho$ is about $0{\cdot}1 \times 10^{-6}$ for the better-conducting metals at 1 000 oersteds. For semi-metals the value may be much higher. When the magnetic field is turned into a direction parallel to that of current flow, Kapitza shows that magnetoresistance is still present although on a somewhat reduced scale.

Harding[2] has studied magnetoresistance in semiconductors and finds the same general reactions as Kapitza. The magnitudes of $\Delta\rho/\rho$ are, however, very much greater for semiconductors, and there may be little difference between the cases of transverse and longitudinal magnetic fields. Information on temperature dependence is very limited, but, assuming a similarity to behaviour of the Hall coefficient, it might reasonably be expected that $\Delta\rho/\rho$ will fall with increase of temperature or charge density. Dunlap[3] shows, for example, that the logarithm of the Hall coefficient varies linearly with $1/T$ for p-type germanium.

An obvious weakness of the simple velocity-distribution theory is its failure to account for magnetoresistance in metals and semiconductors in a longitudinal magnetic field.

(2.2) Three Cases of f(*R*)

The three observed phases of f(R) will now be discussed. The solid-conductivity phase for temperatures less than $(T_{int} - 100)°$K needs little comment. Under the strongest available field ($H = 2\,700$ oersteds) the experimental method employed is insufficiently sensitive to detect any magnetoresistance effect. In the solid state f(R) is less than $0{\cdot}2$, i.e. $\Delta\rho/\rho < 0{\cdot}002$.

The mixed-conduction temperature range $(T_{int} \pm 100)°$K shows f(R) increasing with increasing temperature. This rather surprising phenomenon proves on examination to be based on a false premiss—the method of calculation of f(R) set out in Section 1.2 assumes that a single phenomenon is involved, whereas in the present temperature range we have contributions from two quite independent phenomena. Suppose that the current with constant voltage is composed of a vacuum-conduction element, I_V, and a solid-conduction element, I_S. On application of the magnetic field the current falls to I'_A, and the decrement $(I_A - I'_A)$ occurs only in respect of I_V, since f(R) = 0 for I_S. The true value of f(R) in the mixed range must then be derived from I_V and ΔI_A, where

$$\Delta I_A = I_A - I'_A$$

and this value will be much greater than the apparent value of f(R) which has been used so far.

An attempt has been made to derive the true value of f(R) on the grounds that

$$I_V = I_A \frac{\sigma_v}{\sigma_v + \sigma_s}$$

where $\sigma_v/(\sigma_v + \sigma_s)$ is the ratio of vacuum to total conductivity. This ratio can be extracted from the two straight-line conductivity characteristics shown in Fig. 10; the result is shown in Fig. 13, together with a characteristic for f(R). The derivation of the true value of f(R) in the range 500–700° K is now simple, but unfortunately the numerical result is useless, since it depends largely on small differences in the already small temperature displacement of the two characteristics over the interesting temperature range. All that can be said, then, is that the true value of f(R) over the mixed-conductivity range is much larger than its apparent value and that it may indeed fall rather than rise with increasing temperature.

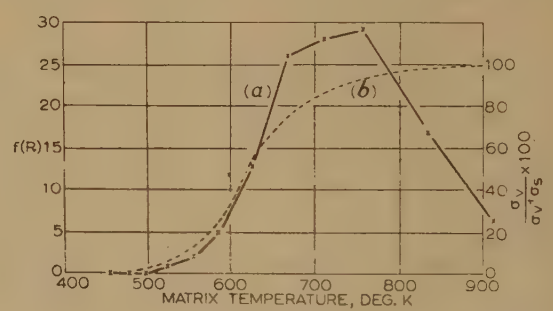

Fig. 13.—Temperature characteristic of (*a*) f(R) and (*b*) $\sigma_V/(\sigma_V + \sigma_S)$

We come now to the last temperature range, above $(T_{int} + 100)°$K, wherein f(R) falls continuously with increase of temperature. The bulk of experimental evidence lies here and is clearly consistent with the usual properties of magnetoresistance. The magnitude of the effect is a quadratic function of magnetic field in weak fields and a linear function in stronger fields. The decline of f(R) with increasing temperature and its growth on suppression of pore electron-cloud density are likewise to be expected. The one point in which the oxide matrix differs significantly from metals and semiconductors is its reaction to a longitudinal magnetic field. In this respect the matrix behaves in the manner predicted by the simple velocity-distribution model.

(2.3) Conclusions

The oxide-cathode matrix is capable of showing a powerful magnetoresistance effect in a magnetic field, but the effect occurs

only when the electron transfer mechanism is by free flight through the hollow pores and when the magnetic field is arranged in a transverse direction. The magnitude of the effect is determined by the magnetic field strength and the electron-cloud density.

If a magnetoresistance effect occurs in the solid-state conduction phase, it is very small, with $\Delta\rho/\rho < 0{\cdot}002$.

(3) ACKNOWLEDGMENTS

Acknowledgment is made to the Engineer-in-Chief of the Post Office for permission to make use of the information contained in the paper. The author also wishes to thank Mr. H. Batey for skilled assistance throughout the work.

(4) REFERENCES

(1) KAPITZA, P.: 'Electric Conductivity in Strong Magnetic Fields', *Proceedings of the Royal Society*, A, 1929, **123**, p. 292.

(2) HARDING, J. W.: 'Change of Resistance of a Semi-Conductor in a Magnetic Field', *ibid.*, 1933, **140**, p. 205.

(3) DUNLAP, W. C.: 'Introduction to Semiconductors' (Wiley, 1957).

621.396.8

The Institution of Electrical Engineers
Monograph No. 318
Dec. 195

A COMPARISON OF MILLINGTON'S METHOD AND THE EQUIVALENT NUMERICAL DISTANCE METHOD WITH THE THEORY OF GROUND-WAVE PROPAGATION OVER AN INHOMOGENEOUS EARTH

By Z. GODZIŃSKI.

(*The paper was first received* 20*th February*, 1957, *and in revised form* 4*th September*, 1958. *It was published as an* INSTITUTION MONOGRAPH *in December*, 1958.)

SUMMARY

The paper presents a comparison of Millington's method and the equivalent numerical distance method with theory. It is shown that Millington's method may be used in most practical problems of ground-wave propagation. For overland paths the errors of this method are very small; for land–sea paths they may be larger, up to about 2·7 dB for 2-section paths, up to about 5·5 dB for 3-section paths, and up to about 2·5 dB for each land–sea boundary for very long paths. In most cases the equivalent numerical distance method shows considerable errors. This method may be used for paths representing small numerical distances, especially for overland paths. It may also be applied to longer paths when the differences between the electrical parameters of the sections are insignificant.

LIST OF PRINCIPAL SYMBOLS

E = Effective value of normal component of electric field strength, volts/m.
D = Length of path, m.
x_{j-1}, x_j = Distances from the transmitter to the ends of the jth section ($x_0 = 0$), m.
l_j = Length of the jth section of the path, m.
l_l, l_s = Lengths of land and sea sections, respectively.
a = Earth's radius, m.
λ = Wavelength, m.
$k = 2\pi/\lambda$ = Propagation coefficient in free space, m^{-1}.
σ = Conductivity of the ground, mhos/m.
ϵ' = Complex relative permittivity of the ground.
ρ = Sommerfeld's numerical distance.
$y(\rho)$ = Sommerfeld's attenuation function for plane earth.
s = Factor transforming geometrical distance into numerical distance.
Subscripts of s denote:
1, 2, . . . = Number of respective sections.
l, s = Land and sea, respectively.
w = Attenuation function.
Subscripts of w denote the method of calculation:
t = Theoretical (correct) value.
M = Value according to Millington's method.
ρ = Value according to equivalent numerical distance method.
$\tau_0 = \alpha_0 - i\beta_0$, δ = Parameters in residue series [see eqns. (20)–(24)].

(1) INTRODUCTION

The theoretical analysis of the problem of ground-wave propagation over an inhomogeneous earth may be carried out in several ways. In an earlier paper[1] (referred to hereafter as Part 1) an analysis based on approximate boundary conditions for the field vectors led to an integral equation for the attenuation function over an inhomogeneous spherical earth. It was shown in Part 1 that the integral equation obtained may be solved in every case when the path is composed of a number of homogeneous sections; the calculations are, however, generally very laborious. A simplified method of calculation was proposed based on the concept of equivalent secondary sources. It makes possible an easy and rapid computation of the attenuation function in such mixed-path problems when only a few equivalent secondary sources need to be introduced. In complicated cases, however, this method also becomes laborious. This is a direct consequence of the process of multiple scattering which constitutes the physical background of mixed-path propagation: when the number of interacting path elements grows, the complexity of the calculations increases rapidly.

The laboriousness of existing theoretical methods is a great disadvantage in practical applications. In this respect the so-called semi-empirical methods are very convenient. Many investigations have been devoted to their experimental verification. However, in order to compare any method with experiment, an exact knowledge of the earth constants over the path is necessary. While some methods have been developed which make possible the measurement of the earth constants for homogeneous or stratified soil, their applicability to the general case of horizontally and vertically inhomogeneous ground has not yet been investigated theoretically. In many cases, the changes of the earth constants are so rapid that it is necessary to introduce suitable average values; how to compute them is, however, not yet sufficiently clear. Serious complications are also caused by irregularities of the earth's surface. These circumstances make an exact comparison with experiment of any mixed-path methods of calculation, including semi-empirical ones, extremely difficult. In most of the existing experimental investigations, the conductivity of the soil has, in fact, only been estimated. The errors which have been thus introduced are unknown, and under such circumstances it is very difficult to decide whether the approximate method of calculation under examination may be used in practice.

Another possibility of determining the errors and limits of application of semi-empirical methods is to compare them with theory. This paper presents such a comparison, based on the theory in Part 1.

(2) COMPARISON OF MILLINGTON'S METHOD WITH THEORY

(2.1) Preliminary Considerations

The so-called Millington method has been proposed by Millington[2] for the amplitude of the wave, and later by Pressey, Ashwell and Fowler[3] for the phase of the wave. If, however, we introduce complex quantities, the initial formula of Millington comprises both cases.

Correspondence on Monographs is invited for consideration with a view to publication.
Mr. Godziński is at the Instytut Łączności, Wrocław, Poland.

Millington's method consists in applying Eckersley's method[4] twice, first with the transmitter and receiver at their proper places [electric field strength $E'(D)$ and attenuation function $w'(D)$], and secondly with the transmitter and receiver interchanged [electric field strength $E''(D)$ and attenuation function $w''(D)$]. The field $E(D)_M$ and the attenuation function $w(D)_M$ are then calculated as the geometrical mean from both results; the subscript M denotes values calculated according to Millington's method. For a path composed of n homogeneous sections characterized by parameters $s = s_1, s_2, \ldots s_n$ the electric field strengths and attenuation functions are

$$E'(D) = \frac{E_{s1}(x_1)}{E_{s2}(x_1)} \frac{E_{s2}(x_2)}{E_{s3}(x_2)} \cdots \frac{E_{s(n-1)}(x_{n-1})}{E_{sn}(x_{n-1})} E_{sn}(D) \quad . \quad (1)$$

$$E''(D) = \frac{E_{sn}(D - x_{n-1})}{E_{s(n-1)}(D - x_{n-1})} \frac{E_{s(n-1)}(D - x_{n-2})}{E_{s(n-2)}(D - x_{n-2})} \cdots \frac{E_{s2}(D - x_1)}{E_{s1}(D - x_1)} E_{s1}(D) \quad . \quad (2)$$

$$E(D)_M = \sqrt{[E'(D) \, . \, E''(D)]} \quad . \quad . \quad . \quad . \quad (3)$$

$$w'(D) = \frac{w_{s1}(x_1)}{w_{s2}(x_1)} \frac{w_{s2}(x_2)}{w_{s3}(x_2)} \cdots \frac{w_{s(n-1)}(x_{n-1})}{w_{sn}(x_{n-1})} w_{sn}(D) \quad . \quad (4)$$

$$w''(D) = \frac{w_{sn}(D - x_{n-1})}{w_{s(n-1)}(D - x_{n-1})} \frac{w_{s(n-1)}(D - x_{n-2})}{w_{s(n-2)}(D - x_{n-2})} \cdots \frac{w_{s2}(D - x_1)}{w_{s1}(D - x_1)} w_{s1}(D) \quad . \quad (5)$$

$$w(D)_M = \sqrt{[w'(D)w''(D)]} \quad . \quad . \quad . \quad . \quad (6)$$

with

$$\rho = sd; \quad s = -i\frac{k}{2(\epsilon' + 1)} \quad . \quad . \quad . \quad . \quad (7)$$

The arguments in parentheses are the distances. The subscript s denotes that the field strength or attenuation function should be calculated as for homogeneous earth characterized by a given parameter s. The time factor has been assumed to be of the form $\varepsilon^{i\omega t}$.

For a plane earth and small real numerical distances, Millington's method is equivalent to Eckersley's,[5] at least as regards the amplitude of the field. In fact, for small real numerical distances the Sommerfeld attenuation function $y(\rho)$ may be described by the following empirical formulae:

According to Norton.[6]

For $\rho \leqslant 4{\cdot}5$ $\quad |y(\rho)| \simeq \exp(-0{\cdot}43\rho + 0{\cdot}01\rho^2) \quad . \quad . \quad (8)$

According to Sacco.[7]

For $\rho < 3$ $\quad |y(\rho)| \simeq \exp(-0{\cdot}43\rho) \quad . \quad . \quad . \quad (9)$

For $\rho < 5$ $\quad |y(\rho)| \simeq \exp(-0{\cdot}4\rho) \quad . \quad . \quad . \quad (10)$

i.e. for small numerical distances

$$|y(\rho)| \simeq \exp(-\kappa\rho) \quad . \quad . \quad . \quad . \quad . \quad (11)$$

where κ is a certain coefficient. The substitution of formula (11) in eqns. (4) and (5) gives

$$|w'(D)| = |w''(D)| = \exp\{-\kappa[s_1x_1 + s_2(x_2 - x_1) + \ldots + s_n(D - x_{n-1})]\} \quad . \quad . \quad . \quad . \quad (12)$$

and thus

$$|E'(D)| = |E''(D)| = |E(D)_M|$$
$$|w'(D)| = |w''(D)| = |w(D)_M| \quad . \quad . \quad . \quad (13)$$

As Millington's method is twice as laborious as Eckersley's, the resulting technique may be of value for practical computations. It must be stressed at this point that the limits for the equivalence of Millington's and Eckersley's methods are set, not by the magnitudes of the numerical distances of particular sections of the path, by the overall numerical distance of the path or by the geometrical length of the whole path, but only by the condition that all numerical distances appearing in Millington's formula must be sufficiently small.

(2.2) General Discussion

As the first problem, we will discuss the changes of the attenuation function on passing the boundary between two different sections of the path.

First we will consider a 2-section plane path of overall length D, with the second section of length δ. According to eqn. (56) in Part 1, the attenuation function at short distances from the boundary is equal to

$$w(D)_t = y(s_1D)\left[1 + \frac{\sqrt{s_2} - \sqrt{s_1}}{\sqrt{s_2}} v(s_2\delta)\right] \quad . \quad . \quad (14)$$

The subscript t denotes the theoretical (correct) value. For very short distances, $v(s_2\delta)$ may be replaced by the first term of the corresponding expansion (see eqn. 34 in Part 1), which gives

$$w(D)_t = y(s_1D)\left[1 - i\frac{2}{\sqrt{\pi}}(\sqrt{s_2} - \sqrt{s_1})\sqrt{\delta}\right] \quad . \quad (15)$$

According to Millington's method [see eqns. (4), (5) and (6)]

$$w(D)_M = \left\{y[s_1(D - \delta)]\frac{y(s_2D)}{y[s_2(D - \delta)]} y(s_2\delta)\frac{y(s_1D)}{y(s_1\delta)}\right\}^{1/2} \quad . \quad (16)$$

For small numerical distances ρ, Sommerfeld's attenuation function may be expanded in a well-known series:

$$y(\rho) = 1 - i\sqrt{(\pi\rho)} - 2\rho + \ldots \quad . \quad . \quad . \quad (17)$$

Similarly the functions $y[s_1(D - \delta)]$ and $y[s_2(D - \delta)]$ may be expanded in Taylor series about the point D. We thus obtain for $w(D)_M$ an expression containing terms in $\delta^{1/2}$, δ, $\delta^{3/2}$, ... Neglecting all terms with higher powers of δ we finally derive for small distances from the boundary:

$$w(D)_M \simeq y(s_1D)\left[1 - i\frac{\sqrt{\pi}}{2}(\sqrt{s_2} - \sqrt{s_1})\sqrt{\delta}\right] \quad . \quad (18)$$

Comparison of eqns. (18) and (15) shows that, for points near the boundary, Millington's method gives a correct trend of the changes of amplitude and phase of the field, but the changes are too small[8] by about 21·5%. It follows from the discussion in Part 1 (see eqns. 74 and 85 and the remarks in Section 6.3) that this result is independent of the number of sections in the path and is always valid when the distance from the end of the preceding section is comparatively very short, not only for short paths but also for longer ones when the curvature of the earth's surface must be taken into account.

According to the reciprocity theorem the transmitter and the receiver may be interchanged. Consequently the results of the above discussion will also apply to a path with a very short first section. Thus the influence of a very short first section when calculated according to Millington's method is correct as regards its character but too small in magnitude by about 21·5%.

As the second problem, we will discuss plane paths for which all numerical distances in Millington's formula (6) are very great. Accordingly, the first and the last sections of such paths must represent very great numerical distances, and for no section

can the parameter s be very small. For great numerical distances $y(\rho) = -1/(2\rho)$, and thus

$$w(D)_M = -\frac{1}{2\sqrt{(s_1 s_n)D}} \quad . \quad . \quad . \quad . \quad (19)$$

This result is in agreement with eqns. (61), (72) and (73) from Part 1.[8] It must be stressed, however, that those formulae are only approximate; with regard to their errors we refer to the discussion in Part 1.

As the third general problem, we will consider paths composed of n very long sections. We assume the lengths of the sections to be so great that, when a transmitter is placed at one end of a section, the other end is within the diffraction region. The calculation of the attenuation function for distances reaching into the diffraction zone is very simple, since only the first term of the residue series needs to be taken into account. The attenuation function over the homogeneous earth is then of the form

$$w(D) = (\sqrt{D})C \exp(tD) \quad . \quad . \quad . \quad . \quad (20)$$

with

$$C = \frac{\left(-\frac{2\pi i}{a}\right)^{1/2}(ka)^{1/6}}{2\tau_0 - 1/\delta^2} \quad . \quad . \quad . \quad . \quad (21)$$

$$\tau_0 = \alpha_0 - i\beta_0 \quad . \quad . \quad . \quad . \quad . \quad . \quad (22)$$

$$t = -ik(ka)^{-2/3}\tau_0 = k(ka)^{-2/3}(-i\alpha_0 - \beta_0) \quad . \quad (23)$$

$$\delta = -i\frac{\epsilon'}{(ka)^{1/3}(\epsilon' - 1)^{1/2}} = \frac{(ka)^{1/6}}{(2as)^{1/2}}\varepsilon^{-i\frac{1}{4}\pi} \quad . \quad . \quad (24)$$

Values of α_0 and β_0 have been given by Norton[9]; a is the earth's radius.

According to eqn. (105) in Part 1 the attenuation function for such a path is

$$w(D)_t = (\sqrt{D})C_n\frac{-i}{\sqrt{\pi}}C_1\frac{\sqrt{s_1} - \sqrt{s_2}}{t_1 - t_2}\frac{-i}{\sqrt{\pi}}C_2\frac{\sqrt{s_2} - \sqrt{s_3}}{t_2 - t_3}\cdots$$
$$\cdots\frac{-i}{\sqrt{\pi}}C_{n-1}\frac{\sqrt{s_{n-1}} - \sqrt{s_n}}{t_{n-1} - t_n}$$
$$\exp[t_1x_1 + t_2(x_2 - x_1) + \ldots + t_n(D - x_{n-1})] \quad . \quad (25)$$

The subscripts 1, 2, . . . denote the parameters of the first, second, etc., sections of the path.

According to Millington's method,

$$w(D)_M = \sqrt{D}\sqrt{(C_1C_n)}$$
$$\exp[t_1x_1 + t_2(x_2 - x_1) + \ldots + t_n(D - x_{n-1})] \quad . \quad (26)$$

Using the notations of the homogeneous earth theory we obtain for the ratio $w(D)_M/w(D)_t$

$$\frac{w(D)_M}{w(D)_t} = \frac{(2\tau_{01} - 1/\delta_1^2)^{1/2}(\tau_{02} - \tau_{01})(2\tau_{02} - 1/\delta_2^2)^{1/2}}{1/\delta_1 - 1/\delta_2}$$
$$\frac{(2\tau_{02} - 1/\delta_2^2)^{1/2}(\tau_{03} - \tau_{02})(2\tau_{03} - 1/\delta_3^2)^{1/2}}{1/\delta_2 - 1/\delta_3}\cdots$$
$$\frac{[2\tau_{0(n-1)} - 1/\delta_{n-1}^2]^{1/2}[\tau_{0n} - \tau_{0(n-1)}](2\tau_{0n} - 1/\delta_n^2)^{1/2}}{1/\delta_{n-1} - 1/\delta_n}$$
$$. \quad . \quad . \quad . \quad (27)$$

The ratio $w(D)_M/w(D)_t$ depends on the product of $n - 1$ factors $B_{i,k}$ of the form

$$B_{i,k} = \frac{(2\tau_{0i} - 1/\delta_i^2)^{1/2}(\tau_{0k} - \tau_{0i})(2\tau_{0k} - 1/\delta_k^2)^{1/2}}{1/\delta_i - 1/\delta_k} \quad . \quad (28)$$

According to Bremmer,[10] when discussing the magnitude of t factors $B_{i,k}$ we may put

for $|\delta| \ll 1$

$$\tau_0 \simeq \tau_{0,0} - \delta - \tfrac{2}{3}\tau_{0,0}\delta^3, \quad \tau_{0,0} = 1{\cdot}856\varepsilon^{-i\pi/3} \quad . \quad (2$$

for $|\delta| \gg 1$

$$\tau_0 \simeq \tau_{0,\infty} - \frac{1}{2\tau_{0,\infty}\delta} - \frac{1}{8\tau_{0,\infty}^3\delta^2} - \frac{1 + 3/(4\tau_{0,\infty}^3)}{12\tau_{0,\infty}^2}\frac{1}{\delta^3}$$
$$\tau_{0,\infty} = 0{\cdot}808\varepsilon^{-i\pi/3} \quad . \quad . \quad . \quad . \quad . \quad (3$$

We then obtain

for $|\delta_i|, |\delta_k| \ll 1 \quad B_{i,k} \simeq 1 - \frac{1}{3}\tau_{0,0}(\delta_i - \delta_k)^2 \quad . \quad . \quad . \quad . \quad (3$

for $|\delta_i|, |\delta_k| \gg 1 \quad B_{i,k} \simeq 1 - \frac{3 + 8\tau_{0,\infty}^3}{96\tau_{0,\infty}^4}\left(\frac{1}{\delta_i} - \frac{1}{\delta_k}\right)^2 \quad . \quad . \quad (3$

When one of the parameters δ_i, δ_k is very large and the oth very small,

$$B_{i,k} \simeq i\sqrt{(2\tau_{0,\infty})}(\tau_{0,0} - \tau_{0,\infty}) = 1{\cdot}33\angle 0° \quad . \quad (3$$

According to eqn. (28) $B_{i,k} = B_{k,i}$. Consequently, in the ca considered, the errors of Millington's method do not depe on the relative positions of the sections but only on the fact th there is a boundary between two different media. Eqns. (3 and (32) show that, when the differences of electrical paramet of sections are small, the errors of Millington's method, bo as regards the amplitude and the phase of the wave, are ve small. In the case of large differences of δ, e.g. for land–s boundaries, the phase of the wave is correct but considera amplitude errors appear; they may amount to about 2·5 dB f each boundary. Consequently, for very long 2-section land-s paths the errors of Millington's method may be as high as abo 2·5 dB, for land–sea–land paths about 5 dB, and so on.

As the last general problem, we will consider the changes the attenuation function very far from the last boundary, i.e. f large distances $D - x_{n-1}$. As shown in Part 1, it is th possible to reduce the path to a homogeneous ground by suitable modification of the magnitude of the primary source radiation. The attenuation of the wave with distance is th the same as over a homogeneous earth with the parameter This conclusion is valid: (*a*) for a plane earth when $x_{n-1} \ll$ (*b*) for very long paths when the nth section is also very long (more precisely, when, after interchanging the transmitter a the receiver, the first, second, . . . and $(n - 1)$th sections lie the diffraction zone).

It may be easily shown that the same is true for Millingto method, except for the magnitude of the modified prima source, which is different from the theoretical value. Thus large distances from the boundary, Millington's method correct describes the attenuation of the wave with distance. Cons quently, at large distances from the boundary, the errors Millington's method cease to change and reach some limiti value depending on the parameters of the preceding sections.

(2.3) Discussion of Numerical Examples

In the preceding Section, Millington's method has been co pared analytically with theory in some simple cases; furth discussion must be based on suitable examples. Using Milli ton's method, especially large errors may be expected where difference between electrical parameters of the sections are ve great, e.g. for land–sea paths. This follows from the fact t Millington's method gives correct results for homogeneous pat and from formula (13) in Part 1 for the magnitude of second sources; subsequent discussion will confirm this conclusi

We may assume, therefore, that the errors of Millington's method may be regarded as greatest in the case of land–sea paths.

The errors of Millington's method for paths composed of very long sections have been discussed in the preceding Section. We should now consider very long paths composed of some long and some short sections, and then short paths. However, as shown in Section 4 in Part 1, the influence of a short section of the path depends very much on its location. It is smallest for sections located in the middle of the path, and largest for those lying close to the transmitting or receiving antenna, i.e. when such a section is the first or the last one. In the case of a very long path with a short first or last section the influence of such a short section is, however, approximately the same as for the plane earth (see Sections 6.2 and 6.3 in Part 1 and the remarks at the end of Section 2.2 of the present paper). Therefore, when discussing numerical examples it seems sufficient to consider only comparatively short paths, i.e. to assume the earth to be plane. This assumption has been made in all examples in the present Section.

For 2-section paths representing real numerical distances not greater than 5, an interesting comparison of Millington's method with theory has been made by Wait.[11] In the cases he considers, the errors of Millington's method for land–sea paths do not generally exceed a few per cent in amplitude and about 3° in phase; only in two cases, for land–sea paths with comparatively short sea sections, are the errors larger, amounting to 10–15%. In overland paths with small differences between the electrical parameters of the sections the errors of Millington's method are small or even practically negligible.

Wait has compared Millington's method with theory only for paths representing comparatively small numerical distances. In order to extend the range of parameters, Millington's method has been compared with theory for a number of 2-section land–sea paths representing different numerical distances; the results are summarized in Fig. 1. Where the land section represents large numerical distances, the theoretical attenuation function $w(D)_t$ has been computed according to a formula derived by Feinberg[12, 13]:

$$w(D)_t = -\frac{1}{2s_lD} - \frac{i}{\sqrt{\pi}}\sqrt{\left(\frac{l_s}{s_lDl_l}\right)} \quad . \quad . \quad . \quad (34)$$

where l_l, l_s, s_l, s_s = Lengths and parameters of land and sea sections, respectively; $s_s \neq 0$.

In the remaining cases $|w(D)_t|$ has been calculated by means of graphs given by Furutsu[14, 15] or according to eqn. (55) in Part 1. As follows from Fig. 1(*a*), large amplitude errors appear when $|s_ls_s|$ is very large and $|s_ll_l|$ is greater than about 2. Assuming a very unfavourable condition, $l_s/l_l = \infty$, the amplitude errors of Millington's method have been computed for different values of s_ll_l, Fig. 1(*c*). The largest errors, amounting to about 2·7 dB, have been found for $s_ll_l \simeq 5$ and s_l real.

When $|s_ll_l|$ and $|s_ls_s|$ are very large, the first term in formula (34) for $w(D)_t$ may be omitted with reasonable approximation. According to Millington's method in such cases

$$w(D)_M = -\frac{i}{\sqrt{2}}\sqrt{\left(\frac{l_s}{s_lDl_l}\right)} \quad . \quad . \quad . \quad . \quad (35)$$

and consequently $w(D)_M/w(D)_t \simeq \sqrt{(\pi/2)}$. The phase of the wave when calculated according to Millington's method is then correct, but the amplitude is too great by about 2 dB;[8, 13] this result is in agreement with Fig. 1(*a*).

According to Fig. 1(*a*) large errors amounting to about −2 dB also appear in cases of land–sea paths with s_ll_l real and very large and $s_ls_s \simeq 2$.

In Fig. 1(*b*) are shown the phase errors of Millington's method

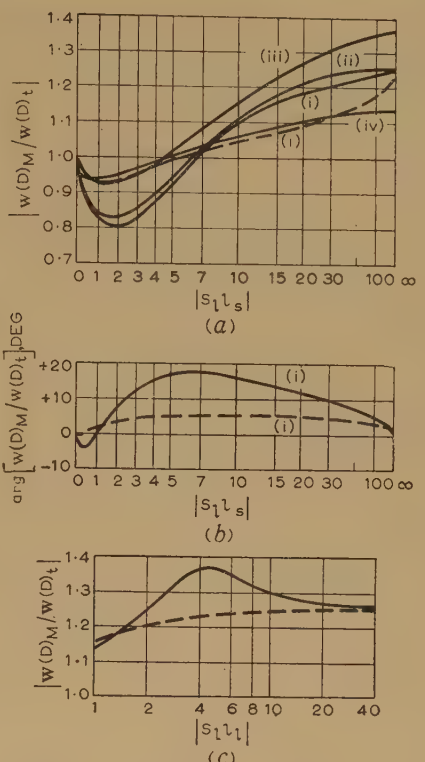

Fig. 1.—Comparison of Millington's method with theory for two-section land–sea paths.

ψ_l is the phase angle of $s_l[s_l' = |s_l| \exp(-i\psi_l)]$; $s_s = 0$

(*a*), (*b*) $w(D)_M/w(D)_t = f(s_ls_s)$.
(i) $|s_ll_l| = \infty$; (ii) $s_ll_l = 40$; (iii) $s_ll_l = 5$; (iv) $s_ll_l = 1$.

(*c*) $|w(D)_M/w(D)_t| = f(s_ll_l)$ for $l_s/l_l = \infty$.
——— $\psi_l = 0°$; ---- $\psi_l = 90°$.

for land–sea paths with land sections representing very large numerical distances and various lengths of sea sections. In agreement with the previous discussion, the phase errors at large distances from the shore (i.e. for large s_ls_s) are small, but at shorter distances may be as big as about 18°.

In order to obtain some indication of the errors of Millington's method for small and moderate imaginary numerical distances, the attenuation function $w(D)_t$ has been calculated by numerical integration of eqn. (7) in Part 1 for a number of 2-section land–sea paths. The values of the attenuation function according to Millington's method $[w(D)_M]$ have then been compared with $w(D)_t$; the results are summarized in Table 1. The Table also shows the results of the calculation of the attenuation function $w(D)_\rho$ according to the equivalent numerical distance method; this method will be discussed in the next Section.

In the preceding examples the discussion has been limited mainly to land–sea paths; overland paths have been considered only for small numerical distances. In order to obtain some indication of the dependence of errors of Millington's method on the degree of inhomogeneity in the case of longer paths, the attenuation function $w(D)_t$ has been computed for a number of paths of varying inhomogeneity and compared with $w(D)_M$ and $w(D)_\rho$; the results are summarized in Table 2. This Table and the graphs of Wait indicate that the errors of Millington's method diminish rapidly with decreasing inhomogeneity of the path. According to Table 2 the agreement of Millington's method with theory becomes very good when the numerical distances of the sections are very large. This is a direct consequence of the fact, discussed in Section 2.2, that for paths

Table 1

COMPARISON OF MILLINGTON'S METHOD AND EQUIVALENT NUMERICAL DISTANCE METHOD WITH THEORY FOR TWO-SECTION LAND-SEA PATHS

$\lvert s_1 l_1\rvert$	ψ_1	$\frac{l_1}{D}$	$w(D)_t$	$\frac{w(D)_M}{w(D)_t}$	$\frac{w(D)_P}{w(D)_t}$
1·5	0°	1/3	0·59 $\angle -73°$	0·97 $\angle +7°$	0·91 $\angle -41°$
		1/2	0·58 $\angle -77°$	0·95 $\angle +3°$	0·93 $\angle -38°$
		2/3	0·57 $\angle -82°$	0·95 $\angle -1°$	0·94 $\angle -33°$
	90°	1/3	0·39 $\angle -34°$	1·05 $\angle +3°$	0·60 $\angle -23°$
		1/2	0·37 $\angle -36°$	1·02 $\angle +3°$	0·63 $\angle -21°$
		2/3	0·35 $\angle -39°$	0·98 $\angle +1°$	0·67 $\angle -19°$
10	0°	1/3	0·16 $\angle -95°$	1·21 $\angle +5°$	0·37 $\angle -85°$
		1/2	0·15 $\angle -101°$	1·12 $\angle +11°$	0·41 $\angle -79°$
		2/3	0·12 $\angle -108°$	0·96 $\angle +13°$	0·49 $\angle -72°$
	90°	1/3	0·16 $\angle -45°$	1·13 $\angle +4°$	0·30 $\angle -36°$
		1/2	0·145 $\angle -47°$	1·10 $\angle +4°$	0·34 $\angle -34°$
		2/3	0·125 $\angle -49°$	1·05 $\angle +4°$	0·39 $\angle -32°$

$s_s = 0$; ψ_l is the phase angle of s_l [$s_l = |s_l| \exp(-i\psi_l)$].

Table 2

COMPARISON OF MILLINGTON'S METHOD AND EQUIVALENT NUMERICAL DISTANCE METHOD WITH THEORY FOR TWO-SECTION PATHS OF VARYING DEGREES OF INHOMOGENEITY

$s_1 l_1 + s_2 l_2$	$\frac{s_2}{s_1}$	$w(D)_t$	$\frac{w(D)_M}{w(D)_t}$	$\frac{w(D)_P}{w(D)_t}$
10	0·5	0·065 $\angle -178°$	1·02 $\angle 0°$	0·91 $\angle -2°$
	0·2	0·091 $\angle -168°$	1·04 $\angle 0°$	0·66 $\angle -12°$
	0·1	0·115 $\angle -152°$	1·04 $\angle 0°$	0·52 $\angle -28°$
	0	0·15 $\angle -101°$	1·12 $\angle +11°$	0·41 $\angle -79°$
20	0·5	0·029 $\angle -181°$	1·0 $\angle +1°$	0·92 $\angle +1°$
	0·2	0·040 $\angle -179°$	1·02 $\angle +1°$	0·67 $\angle -1°$
	0·1	0·058 $\angle -172°$	1·02 $\angle +3°$	0·46 $\angle -8°$
	0	0·095 $\angle -98°$	1·20 $\angle +8°$	0·28 $\angle -82°$
40	0·5	0·014 $\angle -181°$	1·0 $\angle +1°$	0·93 $\angle +1°$
	0·2	0·018 $\angle -182°$	1·0 $\angle +2°$	0·71 $\angle +2°$
	0·1	0·025 $\angle -181°$	1·02 $\angle +2°$	0·52 $\angle +1°$
	0	0·064 $\angle -96°$	1·24 $\angle +6°$	0·20 $\angle -84°$

$l_1 = l_2$; both s_1 and s_2 real.

composed of sections representing very great numerical distances Millington's method gives correct results.

The results of the discussion of 2-section plane paths also make possible the estimation of the errors of Millington's method in the general case of multi-section plane paths. As shown in Sections 4, 5.3 and 5.4 of Part 1, the influence of a section of a path depends very much on its position and is largest for sections lying close to the transmitting or receiving antenna. The same is true according to Millington's method. In fact, when computing the field according to Millington's method we apply Eckersley's method twice. In each case the first section has the largest influence because the greatest differences in the rate of change of attenuation function occur at small distances from the transmitter. Consequently the influence on the field of a short section lying close to the beginning or the end of the pa is, for a 3-section path, approximately the same as for a cor sponding 2-section path. Consequently, for a 3-section pa with first and third sections relatively short, the amplitude err of Millington's method expressed in decibels are approximat equal to the sum of the errors for the two corresponding 2-secti paths, whereas the phase errors add together arithmetically. follows from the discussion of 2-section paths, the largest err are those for land–sea paths. Thus the maximum errors Millington's method for 3-section paths with relatively short fi and third sections may be estimated from the curves in Figs. 1 and 1(*c*). The results may be summarized as follows:

(*a*) For land–sea–land paths with a long sea section and co paratively short land sections the largest errors, amounting to abo 5·5 dB, will be found for paths with land sections representing r numerical distances equal to about 5. When the numerical distan of land sections decrease toward zero the errors do the sam when they increase to infinity the errors decrease asymptotica to about 4 dB.

(*b*) For sea–land–sea paths with a long land section ($|s_l l_l|$ lar and short sea sections ($|s_l l_s|$ small) the largest errors, amounting about −4 dB, appear for $s_l l_l$ large and real and $s_l l_s$ equal to abou

(*c*) For sea–land–sea paths with a very long land section ($|s$ very large) and much shorter sea sections, for which, howev $|s_l l_s|$ is also large, the errors may be as high as about 4 dB.

Conclusions in (*c*) and in (*a*) for $|s_l l_l| \gg 1$ are in essent agreement with the results of Feinberg's discussion.[13]

When considering 3-section land–sea paths with first and l sections not very much shorter than the second one, we may two formulae derived by Feinberg:[12]

(i) *Sea–land–sea paths.* $s_1 = s_3 = 0$; $s_2 = s_l$; $|s_l(x_2 - x_1)| \gg$

$$w(D)_t = -\frac{1}{2s_l D} - \frac{i}{\sqrt{(\pi s_l D)}}\left[\sqrt{\left(\frac{x_1}{D - x_1}\right)} + \sqrt{\left(\frac{D - x_2}{x_2}\right)}\right] + \frac{1}{2}\left[1 - \frac{2}{\pi}\arcsin\frac{(x_2 - x_1)D - x_1(D - x_2)}{x_2(D - x_1)}\right] \quad (1$$

(ii) *Land–sea–land paths.* $s_1 = s_3 = s_l$; $s_2 = 0$; $|s_l x_1| \gg$ $|s_l(D - x_2)| \gg 1$;

$$w(D)_t = \frac{i}{\sqrt{\pi}}\frac{1}{2(s_l D)^{3/2}}\left\{\frac{D - 2x_1}{\sqrt{[x_1(D - x_1)]}} - \frac{D - 2x_2}{\sqrt{[x_2(D - x_2)]}}\right\} - \frac{1}{\pi s_l D}\left\{\sqrt{\left[\frac{D(x_2 - x_1)}{x_1(D - x_2)}\right]} + \arcsin\sqrt{\left[\frac{x_1(D - x_2)}{x_2(D - x_1)}\right]}\right\} \quad (1$$

For the present purpose of comparison of Millington's meth with theory we will assume for simplicity that the first and th sections are of equal lengths with $|s_l D|$ very large ($|s_l D| \to \infty$ the results of the calculations are shown in Fig. 2. As th

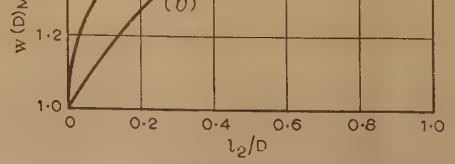

Fig. 2.—Comparison of Millington's method with theory for three-section land–sea paths.

$l_1 = l_3$

(*a*) Sea–land–sea paths; $s_1 = s_3 = 0$; $s_2 = s_l$; $|s_l l_2| \gg 1$; $|s_l l_1| = |s_l l_3| \gg 1$; $|s$ very large.
(*b*) Land–sea–land paths; $s_1 = s_3 = s_l$; $s_2 = 0$; $|s_l l_1| = |s_l l_3| \gg 1$; $|s_l D|$ very lar

hould be, the results for short first and third sections are in greement with the previous discussion.

So far we have discussed only 2- and 3-section paths. In view of the small influence which the middle parts of the path have on the field, it seems, however, that the results obtained may also be used as an estimate of the errors of Millington's method in the general case of multi-section paths.

(3) COMPARISON OF THE EQUIVALENT NUMERICAL DISTANCE METHOD WITH THEORY

(3.1) General

The equivalent numerical distance method, some modification of which represents the so-called equivalent conductivity method, has been proposed and discussed by a number of authors.[16–24, 7, 5] The method is limited to comparatively short distances over which the earth may be regarded as plane. According to this method the attenuation function [for which we will use the notation $w(D)_\rho$] for a path composed of n homogeneous sections is

$$w(D)_\rho = y(\rho_{eq}) \quad . \quad . \quad . \quad . \quad . \quad (38)$$

with

$$\rho_{eq} = \sum_{k=1}^{n} \rho_k \quad . \quad . \quad . \quad . \quad . \quad . \quad (39)$$

where ρ_k = Sommerfeld's numerical distance for the kth section.
$y(\rho_{eq})$ = Sommerfeld's attenuation function for the equivalent numerical distance ρ_{eq}.

For well-conducting soil and low and middle frequencies the displacement current may be disregarded as an approximation and thus

$$\rho_k = s_k l_k \simeq \frac{\pi}{60\lambda^2 \sigma_k} l_k \quad . \quad . \quad . \quad . \quad . \quad (40)$$

where l_k = Length of the kth section.
σ_k = Conductivity of the ground for the kth section.
λ = Wavelength.

We may then introduce the so-called equivalent conductivity (σ_{eq}) of the ground:

$$\rho_{eq} = \frac{\pi}{60\lambda^2} \frac{D}{\sigma_{eq}} = \frac{\pi}{60\lambda^2} \sum_{k=1}^{n} \frac{l_k}{\sigma_k} \quad . \quad . \quad . \quad (41)$$

and thus

$$\sigma_{eq} = \frac{D}{\sum_{k=1}^{n} l_k/\sigma_k} \quad . \quad . \quad . \quad . \quad . \quad . \quad (42)$$

(3.2) Comparison with Theory

According to eqn. (39) the attenuation function $w(D)_\rho$ depends only on the equivalent numerical distance of the path; this has three consequences. First, the influence of a section on the field does not depend on its position along the path. Secondly, the sections with a very small parameter s (e.g. sea sections) have negligible influence on the attenuation function, however long they may be. Thirdly, with increasing distance the equivalent numerical distance must always increase, and consequently the attenuation function must always diminish: thus the method does not admit the possibility of the so-called recovery effect. As follows from the discussion in Part 1, all these conclusions are in sharp contradiction to theory. We may thus conclude that the general picture which the equivalent numerical distance method gives of the process of mixed-path propagation is essentially wrong. However, in certain cases the simplicity of the method may offset its errors. It is the purpose of this Section to show under what circumstances the method may be used for engineering practice.

According to eqn. (11), for small real numerical distances $|y(\rho)| \simeq \exp(-\kappa\rho)$. After substitution in eqns. (38) and (39) we obtain

$$|w(D)_\rho| \simeq \exp[-\kappa(\rho_1 + \rho_2 + \ldots + \rho_n)] \quad . \quad . \quad (43)$$

It follows from comparison with eqns. (12) and (13) that the equivalent numerical distance method is equivalent to Millington's[7] for small real numerical distances. As Millington's method is in such cases approximately correct, so also will be the equivalent numerical distance method. The limits for the equivalence of the two methods are set, not by the magnitude of the numerical distances of particular sections of the path, but by the overall numerical distance of the path and by the condition that all numerical distances appearing in Millington's formula must be sufficiently small; it is a similar condition to that given in Section 2.1.

As for Millington's method (see remarks at the beginning of Section 2.3), so for the equivalent numerical distance method, the errors will be small when the differences of electrical parameters of sections are not great, and they will be especially large when these differences are very great, as for instance with land–sea paths.

The results of calculations for a number of land–sea paths with land sections representing small and moderate numerical distances are summarized in Fig. 3; the theoretical values have

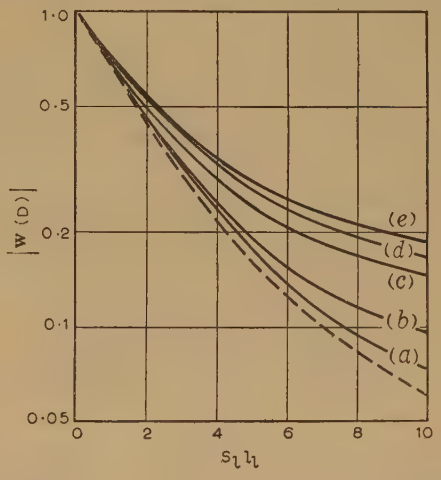

Fig. 3.—Comparison of equivalent numerical distance method with theory for two-section land–sea paths with land sections representing small and moderate numerical distances.

s_l real; $s_s = 0$.
—— $|w(D)_t|$: (*a*) $l_l/l_s = 20$; (*b*) $l_l/l_s = 5$; (*c*) $l_l/l_s = 1$; (*d*) $l_l/l_s = 0{\cdot}5$; (*e*) $l_l/l_s = 0{\cdot}1$.
---- $|w(D)_\rho|$ (independent of the ratio l_l/l_s).

been taken from graphs given by Furutsu.[14, 15] The results of computations for some land–sea paths with land sections representing real and imaginary numerical distances may also be found in Table 1. In Fig. 4 are shown the results of calculations for land–sea paths with land sections representing large and real numerical distances. The theoretical values have been computed according to eqn. (34).

Figs. 3 and 4 and Table 1 show that, even in the case of land–sea paths with land sections representing small numerical distances, the errors of the equivalent numerical distance method may be appreciable; when the numerical distances of land sections are great the errors are generally very large. In order

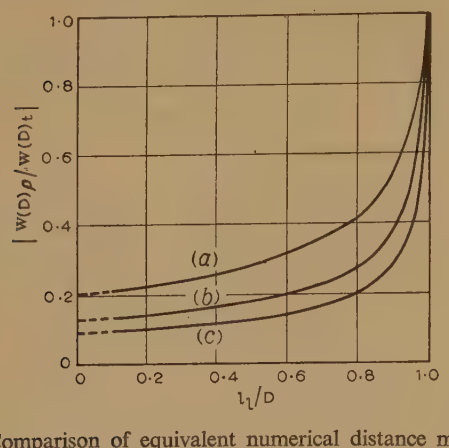

Fig. 4.—Comparison of equivalent numerical distance method with theory for two-section land–sea paths with land sections representing large numerical distances.

s_l real; $s_s = 0$.
(a) $s_1 l_1 = 20$; (b) $s_1 l_1 = 50$; (c) $s_1 l_1 = 100$.

to examine the influence of the degree of inhomogeneity of the path upon the errors, the attenuation functions for a number of 2-section paths of varying degrees of inhomogeneity have been calculated; the results are summarized in Table 2. Simple discussion is also possible for overland paths with both sections representing very large numerical distances ($|s_1 l_1| \gg 1$; $|s_2 l_2| \gg 1$). In such cases

$$w(D)_t = -\frac{1}{2\sqrt{(s_1 s_2)}D}; \quad w(D)_\rho = -\frac{1}{2(s_1 l_1 + s_2 l_2)} \quad . \quad (44)$$

Fig. 5 shows plots of $w(D)_t/w(D)_\rho$ for various ratios of s_2/s_1.

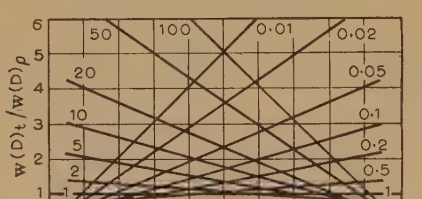

Fig. 5.—Comparison of equivalent numerical distance method with theory for two-section overland paths with sections representing large numerical distances.

$|s_1 l_1| \gg 1$; $|s_2 l_2| \gg 1$; s_2/s_1 real. The numbers denote the value of the ratio s_2/s_1.

According to theory, for 3-section paths the attenuation function depends strongly on the location of any particular section along the path. According to the equivalent numerical distance method, the position of the section has no influence on the field; thus the errors of the method may be very great. Very large errors may be expected, for example, where, in the middle of a well-conducting path, there is a section of considerably smaller conductivity. The attenuation function is then of the order of unity [see, for instance, eqn. (36)], while according to the equivalent numerical distance method the attenuation function will be very small.

It seems that the above discussion will also hold in the general case of a multi-section path. Consequently the equivalent numerical distance method may be used for practical computations only when the inhomogeneity of a multi-section path is very small.

(4) CONCLUSIONS

It follows from the discussion in Section 2 that the errors o Millington's method diminish rapidly when the inhomogeneit of the path becomes small. Thus his method may be used wit success for practical computations in cases of overlan propagation.

Millington's method may give considerable errors in th presence of great differences between the electrical paramete of particular sections, e.g. in the presence of land–sea bou daries. Making final estimations, we may disregard the sub division of land into parts with somewhat different conductivitie and will take into account only the division of the path int land and sea sections. For 2-section land–sea paths the erro of Millington's method may be as high as about 2·7 dB. Fo practical purposes such errors may be regarded as general acceptable. For 3-section land–sea paths the errors may amou to about 5·5 dB; in most cases they will, however, be somewh smaller. Such errors must be regarded as considerable, althoug for routine computations they will as a rule still be tolerabl For very long paths with a number of land–sea boundaries th errors may be about 2·5 dB times the number of boundari and Millington's method can be used only to estimate th order of the ground-wave field strength. However, the receiv lies far in the diffraction zone, the attenuation of the groun wave is very large, and consequently a simple although not ve exact method of calculation may be of practical importance.

We may thus conclude that Millington's method, because its simplicity and comparatively small errors, may be used most practical problems of ground-wave propagation.

The main advantage of the equivalent numerical distan method is its simplicity. It is approximately equivalent Millington's method only for paths representing small numeric distances; in other cases it is distinctly inferior to Millingto method. For longer paths it may be used only when th differences between electrical parameters of the sections a insignificant. The method fails completely for most land–s paths with land sections representing large numerical distanc The use of the method is limited to comparatively short pat for which the earth may be regarded as plane.

Because of its simplicity, the equivalent numerical distan method is frequently used for routine calculations when a gre number of field strength computations have to be made. such cases the practical engineer may be advised to make cont calculations from time to time, e.g. by means of some theoreti curves or by Millington's method, in order to find out if he using the equivalent numerical distance method well within t limits of its application.

It must be stressed that the discussion in this paper has be based on an assumption of a regular, i.e. a plane or spheric earth surface. The irregularities of the earth's surface may ha a profound influence on the field; this must be taken into accou when considering the possible use of any method of computati

(5) ACKNOWLEDGMENTS

The author wishes to thank Mr. G. Millington very much his valuable remarks and for his great and very kind help preparing the manuscript for publication. The author indebted to the Director of Wrocław Research Centre, Dr. Tomankiewicz, for his friendly support during the course of work, and to the Director of the Institute of Telecommunicati Docent T. Rzymkowski, for his kind permission to publish paper.

(6) REFERENCES

(1) GODZIŃSKI, Z.: 'The Use of Equivalent Secondary Sources in the Theory of Ground-Wave Propagation over an Inhomogeneous Earth', *Proceedings I.E.E.*, Monograph No. 299 R, April, 1958 (**105** C, p. 448).

(2) MILLINGTON, G.: 'Ground-Wave Propagation over an Inhomogeneous Smooth Earth', *ibid.*, Paper No. 794 R, January, 1949 (**96**, Part III, p. 53).

(3) PRESSEY, B. G., ASHWELL, G. E., and FOWLER, C. S.: 'The Measurement of the Phase Velocity of Ground-Wave Propagation at Low Frequencies over a Land Path', *ibid.*, Paper No. 1438 R, March, 1953 (**100**, Part III, p. 73).

(4) ECKERSLEY, P. P.: 'The Calculation of the Service Area of Broadcast Stations', *Proceedings of the Institute of Radio Engineers*, 1930, **18**, p. 1160.

(5) 'Ground-Wave Propagation over Mixed Paths. Review of Recent Progress', C.C.I.R., Warsaw, 1956, Document 25.

(6) NORTON, K. A.: 'The Propagation of Radio Waves over the Surface of the Earth and in the Upper Atmosphere, Part I', *Proceedings of the Institute of Radio Engineers*, 1936, **24**, p. 1367.

(7) SACCO, L.: 'Report by the Chairman of Study Group IV. Ground Wave Propagation', C.C.I.R., London, 1953, Document 104, Annex 1, p. 15.

(8) GODZIŃSKI, Z.: 'Extension of Feinberg's Theory to the Case of Electromagnetic Wave Propagation over an Inhomogeneous Spherical Earth and Introduction of an Approximate Method of Computation Based on Equivalent Secondary Sources', C.C.I.R., Warsaw, 1956, Document 454.

(9) NORTON, K. A.: 'The Calculation of Ground-Wave Field Intensity over a Finitely Conducting Spherical Earth', *Proceedings of the Institute of Radio Engineers*, 1941, **29**, p. 623.

(10) BREMMER, H.: 'Terrestrial Radio Waves' (Elsevier Publishing Co., New York, 1949), p. 44.

(11) WAIT, J. R.: 'Mixed Path Ground Wave Propagation: 1. Short Distances', *Journal of Research of the National Bureau of Standards*, 1956, **57**, p. 1.

(12) ALPERT, J. L., GINZBURG, V. L., and FEINBERG, E. L.: 'Propagation of Radio Waves' (GITTL, Moscow, 1953), Chapter IX, p. 184 (in Russian).

(13) FEINBERG, E. L.: 'Theory of Mixed Path Propagation of Radio-Waves and Engineering Methods of Calculation', C.C.I.R., Warsaw, 1956, Document 563.

(14) FURUTSU, K.: 'Propagation of Electro-Magnetic Waves over a Flat Earth across a Boundary Separating Different Media and Coastal Refraction', *Journal of the Radio Research Laboratories* (Tokyo), 1955, **2**, p. 1.

(15) FURUTSU, K.: 'Ground-Wave Propagation over Mixed Paths—Calculation of Ground-Wave Field Strengths and Phases in Propagation over Mixed Paths', C.C.I.R., Warsaw, 1956, Document 322.

(16) GROSSKOPF, J., and VOGT, K.: 'Der Zusammenhang zwischen der effektiven Bodenleitfähigkeit und der Ausbreitungsdämpfung', *Hochfrequenztechnik und Elektroakustik*, 1943, **62**, p. 14.

(17) GROSSKOPF, J.: 'Die Ausbreitung elektromagnetischer Wellen über inhomogenem Boden', *ibid.*, 1943, **62**, p. 103.

(18) GROSSKOPF, J.: 'Zur Ausbreitung von Mittelwellen über inhomogenes Gelände', *Fernmeldetechnische Zeitschrift*, 1950, **3**, p. 118.

(19) ARGIROVIĆ, M.: 'Propagation of Electromagnetic Waves over an Inhomogeneous Earth', *Elektrotechnicki Vesnik*, 1951, p. 225.

(20) ARGIROVIĆ, M.: 'Méthode générale de calcul des conductivités du sol hétérogène', *Annales des Télécommunications*, 1953, **8**, p. 212.

(21) ARGIROVIĆ, M.: 'Variations de la constante de phase de l'onde de sol', *L'Onde Électrique*, 1955, **35**, p. 687.

(22) ARGIROVIĆ, M.: 'Ground-Wave Propagation over Mixed Paths', C.C.I.R., Warsaw, 1956, Document 221.

(23) SUDA, K.: 'Estimation of Medium-Wave Field Strength over Mixed Paths', C.C.I.R., London, 1953, Documents 140 and 232.

(24) SUDA, K.: 'Field-Strength Calculation', *Wireless Engineer*, 1954, **31**, p. 249.

621.3.011

The Institution of Electrical Engineers
Monograph No. 31[illegible]
Jan. 195[illegible]

THE HEAVISIDE PAPERS FOUND AT PAIGNTON IN 1957

By H. J. JOSEPHS, Member.

(*The paper was received 2nd May*, 1958. *It was published as an* INSTITUTION MONOGRAPH *in January*, 1959.)

SUMMARY

The papers unearthed dealt mainly with problems connected with the flow of electromagnetic energy, and showed that Heaviside had extended Maxwell's theory so that gravitation could be fitted in with electromagnetism.

It was also found that Heaviside had evolved a rigorous justification for his 'operation' of extracting the square root of the process of partial differentiation; for he had discovered the conditions under which his differential time operator p lost its original significance and became the transform parameter of an infinite integral of the Stieltjes type which obeys all the laws of algebra and analysis.

(1) INTRODUCTION

Oliver Heaviside lived in Paignton from 1889 to 1897, and towards the end of 1957 a collection of his papers was found under the floorboards of his room in the house where he lived. This collection consisted of a large number of loose sheets of paper containing his formulae and notes; it also contained many annotated galley proofs, marked page proofs, scraps of old letters, envelopes, postcards, technical publications, etc. Altogether the collection filled three sacks. In spite of the decayed state of some of the papers, it was a simple matter to sort them and connect them with the corresponding parts of Heaviside's published work. This showed that most of the collection could be associated with the publication of Volumes 1 and 2 of his 'Electromagnetic Theory'.[1]

Early in 1891 the publishers of the *Electrician* proposed to Heaviside that his series of articles[2] on 'Electromagnetic Theory' just begun in that journal should be brought out later in book form. The publishers allowed Heaviside great freedom as to what he wrote in his serial articles, but they insisted that, after the first publication in their journal, not a word could be changed for the later publication as a book. This restriction was imposed in order to keep the costs of production down (for Heaviside's books were not expected to pay), and also because the type set up for the original articles had to be carefully stored (sometimes for years) until the corresponding sections of the book were printed.

Since this restriction thus prevented Heaviside from revising the text, it follows that the annotated galley proofs and manuscripts found at Paignton are of great interest; for they represent Heaviside's second thoughts and show the way he could have revised his text had he had the power to do so. He could have described his new additions to the mathematical theory of the transfer of energy; also he could have shown how Maxwell's theory can be extended to include both electromagnetic and gravitational phenomena within a single mathematical framework.

To give, within the space of a few thousand words, a complete and satisfactory report of the significance of the mathematical work on the scattered sheets in the sacks of paper Heaviside left behind at Paignton is well nigh impossible. The most that can be done in this Monograph is to outline the features which became significant during a careful examination of his calculations.

Correspondence on Monographs is invited for consideration with a view to publication.

Mr. Josephs is at the Post Office Research Station.

(2) HEAVISIDE'S DUPLEX EQUATIONS

The pencil annotations on the galley proofs, together with the analysis on the backs of the page proofs, gave a clear indication of the progress Heaviside made during the years between the first publication of his serial articles in the *Electrician* and their later publication in book form. This progress lay in the development of new and improved methods of applying his duplex circuital equations to electromagnetic problems and the consequent extension of Maxwell's theory. But before details of these new developments are given, something should be said about Heaviside's two circuital equations by way of preface.

While Heaviside was living in Camden Town he wrote a series of articles[3] for the *Electrician* entitled 'Electromagnetic Induction and its Propagation' which he concluded in 1887, two years before he moved to Paignton. Heaviside stated that his object in writing this series was to present Maxwell's theory in practical form and to give an adequate discussion of the flow of energy in the electromagnetic field.

A few years before Heaviside started this series, Maxwell, expounding Faraday's ideas, had clearly stated that the flow of energy depended on the association of two vectors, namely the electric force E and the magnetic force H. But in 'A Treatise on Electricity and Magnetism', Maxwell[4] did not develop the analytical consequences of this energy concept; his pages are filled with descriptions of early Victorian ideas about the nature of electrical energy; moreover, these ideas were expressed in a maze of symbols representing quaternionic formulations of scalar and vector potential functions, etc. The result was that engineers found Maxwell's chapter on the general equations of the electromagnetic field practically unreadable.

In his Camden Town series[3] Heaviside showed engineers that the descriptive equations of the electromagnetic field can easily be based upon the vectorial formulation of two circuital laws. The first states that the electric current J is the curl of the magnetic force H, while the second states that the magnetic current M is the negative curl of the electric force E; in symbols

$$J = \text{curl}\, H \quad . \quad . \quad . \quad . \quad . \quad . \quad . \quad (1$$

and

$$M = -\text{curl}\, E \quad . \quad . \quad . \quad . \quad . \quad . \quad . \quad (2$$

Eqns. (1) and (2) are what electrical engineers call 'Maxwell's equations'. These equations, however, are not to be found in any of Maxwell's books or papers: they were introduced by Heaviside to act as the basis of a mathematical model of Maxwell's theory; they have therefore been called 'Heaviside's equations' in this Monograph, and the technical reasons for this change are given in the Appendix.

Heaviside's eqn. (1) is the vectorial representation of the well known equation defining electric current in terms of magnetic force; eqn. (2) was introduced as the proper companion of the first in order to make a complete duplex system suitable for engineers to apply to practical problems. Heaviside showed that this system, based upon the two measurable variables E and H, readily expresses Maxwell's concept of the flow of energy in the electromagnetic field. He also pointed out that the system has the advantage of being quite independent of the unmeasurable

quaternionic formulations of scalar and vector potential functions introduced by Maxwell.[4]

Many of the pencil calculations on the loose sheets found at Paignton arose from Heaviside's applications of his two equations to engineering problems. These calculations showed that he always kept the duplex features of electromagnetism in mind: in the first place his analysis was naturally symmetrical, since it was based upon postulated electric charges and magnetic poles and because the inverse-square law was used to define and calculate the relevant quantities; furthermore, he manipulated his equations in a balanced manner, for he always wrote the electric and magnetic currents in eqns. (1) and (2) as

$$\boldsymbol{J} = \dot{\boldsymbol{D}} + \boldsymbol{J}_c \text{ and } \boldsymbol{M} = \dot{\boldsymbol{B}} + \boldsymbol{M}_c$$

Here the electric force $\boldsymbol{E}$ and the magnetic force $\boldsymbol{H}$ are related to the two fluxes $\boldsymbol{D}$ and $\boldsymbol{B}$ by

$$\boldsymbol{D} = k\boldsymbol{E} \text{ and } \boldsymbol{B} = \mu\boldsymbol{H}$$

where k and μ represent permittivity and permeability respectively. Also $\boldsymbol{J}_c$ and $\boldsymbol{M}_c$ represent electric and magnetic conduction-current densities and are related to the two forces by

$$\boldsymbol{J}_c = \sigma\boldsymbol{E} \text{ and } \boldsymbol{M}_c = \sigma_m\boldsymbol{H}$$

where σ and σ_m represent electric and magnetic conductivities respectively. It was only in the final computing stage that Heaviside took account of the zero value of the magnetic conduction-current density; in all his algebraic manipulative work he maintained the symmetry of the electrostatic and magnetostatic systems.

In these pencil calculations Heaviside wrote the scalar and vector products of his two vectors $\boldsymbol{E}$ and $\boldsymbol{H}$ as $\boldsymbol{EH}$ and $\mathrm{V}\boldsymbol{EH}$ respectively; but this notation is now obsolete, and in this Monograph these two products are written in the usual way as $\boldsymbol{E}\,.\,\boldsymbol{H}$ and $\boldsymbol{E} \times \boldsymbol{H}$. The vectors $\boldsymbol{E}$ and $\boldsymbol{H}$ are reckoned per unit length and $\boldsymbol{D}$ and $\boldsymbol{B}$ per unit area. The electric energy, U, per unit volume and the magnetic energy, T, per unit volume are given by the scalar products

$$U = \tfrac{1}{2}\boldsymbol{E}\,.\,\boldsymbol{D} \text{ and } T = \tfrac{1}{2}\boldsymbol{H}\,.\,\boldsymbol{B}$$

while the power-flow vector, $\boldsymbol{P}$, per unit area is given by the vector product

$$\boldsymbol{P} = \boldsymbol{E} \times \boldsymbol{H}$$

An examination of his calculations showed that some of them were connected with the solution of transient problems in cable telegraphy or telephony: it also became clear that, no matter what problem Heaviside was working on, the question of the mechanism of energy transfer was touched upon from one angle or another. In these applications he took the space integrals of U and T to be $\frac{1}{2}CV^2$ and $\frac{1}{2}LI^2$ respectively: for he treated the electric-energy density $\frac{1}{2}\boldsymbol{E}\,.\,\boldsymbol{D}$ as the elemental part of the total electric energy $\frac{1}{2}V\,.\,CV$, where V is the potential between the plates of a condenser whose charge is CV, while he treated the magnetic-energy density $\frac{1}{2}\boldsymbol{H}\,.\,\boldsymbol{B}$ as the elemental part of the total magnetic energy $\frac{1}{2}I\,.\,LI$, where I is the current in a coil of total induction LI. V and I were taken as the line integrals of $\boldsymbol{E}$ and $\boldsymbol{H}$ respectively.

One piece of work was connected with Heaviside's effort to make the electric and magnetic energies of a telegraph circuit equal (as they must be for distortionless transmission). In such a circuit the electric energy tends to be excessive, and his remedy was to increase the magnetic energy by increasing the inductance or to diminish the electric energy by leakance.

For dealing with the transmission of plane waves in a telegraph circuit Heaviside wrote his circuital equations as

$$-\frac{\partial H}{\partial x} = \sigma E + k\frac{\partial E}{\partial t} \text{ and } -\frac{\partial E}{\partial x} = \mu\frac{\partial H}{\partial t}$$

from which he obtained the partial differential equation known as the 'equation of telegraphy'. Various solutions of this differential equation were found among the scattered papers in the Paignton collection; many of these solutions had been published by Heaviside, but one unpublished note of particular interest was found. This showed that he regarded the parameters in his duplex equations (1) and (2), not as constant quantities, but as statistical distribution functions; to him the problem of measuring such a parameter was that of determining its law of distribution and finding its most probable value. Moreover, he regarded his duplex equations as the basis of a tractable model of Maxwell's theory which can be used by engineers to predict the results of electrical experiments yet to be made.

(3) HEAVISIDE'S UNIFIED FIELD THEORY

Between 1883 and 1885, both Heaviside and Poynting[5] did much to establish the mathematical laws describing the flow of energy. During this period they independently covered much the same ground, and discovered that the rate of energy transfer in an electromagnetic field is given by the vector product of $\boldsymbol{E}$ and $\boldsymbol{H}$. In 1884, Poynting's paper containing this theorem was published a few months before Heaviside's paper; consequently the theorem bears Poynting's name.

Poynting's method of establishing the theorem called for the modification and manipulation of Maxwell's original equations, and some heavy mathematical work was involved. Heaviside's method, however, was relatively simple and did not call for quaternionic manipulation; after writing the rate of energy loss per unit volume of the field as

$$\operatorname{div} \boldsymbol{P} = -\frac{\partial}{\partial t}(\tfrac{1}{2}\boldsymbol{E}\,.\,\boldsymbol{D} + \tfrac{1}{2}\boldsymbol{H}\,.\,\boldsymbol{B})$$

he used his equations (1) and (2) to obtain

$$\operatorname{div} \boldsymbol{P} = \boldsymbol{H}\,.\,\operatorname{curl} \boldsymbol{E} - \boldsymbol{E}\,.\,\operatorname{curl} \boldsymbol{H}$$

Recognizing the right-hand side as the expansion of div $(\boldsymbol{E} \times \boldsymbol{H})$, he saw at once that the rate-of-energy-flow vector is

$$\boldsymbol{P} = \boldsymbol{E} \times \boldsymbol{H} + \boldsymbol{G} \quad . \quad . \quad . \quad . \quad . \quad (3)$$

where $\boldsymbol{G}$ is an arbitrary vector representing a circuital energy flux. In 1884, when he established his theorem, Poynting overlooked the existence of the energy flux $\boldsymbol{G}$; Heaviside, however, while recognizing it, assumed that it represented useless energy which could be neglected.

The calculations found at Paignton showed that, within ten years, Heaviside had altered his views about the uselessness of $\boldsymbol{G}$ in eqn. (3); for he had found that it could be made to satisfy the mathematical requirements of a flux of gravitational energy and that all the energy absorbed by matter in a unified field founded on eqn. (3) could be supplied by the Poynting flux $(\boldsymbol{E} \times \boldsymbol{H})$ alone. Thus, Heaviside appears to have postulated a unified field [based on eqn. (3) and consistent with his views about the electrical constitution of matter] as a means of extending Maxwell's theory to include gravitational phenomena.

Heaviside's expression for the energy density of his unified field consisted of the sum of a number of distinct terms. One term denoted the rate of increase of an electromagnetic energy density at a point (in the empty or materially occupied space he

was considering); other terms represented the rates of increase of various localized energy densities, such as heat, chemical energy, etc. (which he regarded as being due to the electromagnetic field). His expression also contained terms representing the rate of doing work of certain ponderomotive forces acting on moving matter per unit volume at the point in question. In these terms, ρ was taken to represent the density of matter and e to denote the intensity of a gravitational force which satisfies Newton's law; Heaviside treated e as the space variation of a potential which depended upon the distribution of matter in his unified field. The product ρe expressed the moving force on ρ and has its equivalent in the increase of momentum.

Since the law of inverse squares was involved throughout, Heaviside found that the circuital flux of gravitational energy can be expressed as $(\rho u - c\dot{e})$, where u represents the velocity of ρ and c is a constant. Expressing this energy flux as the curl of a vector h, Heaviside wrote

$$\text{curl } h = \rho u - c\dot{e} \quad . \quad . \quad . \quad . \quad . \quad (4)$$

where the divergence of the vector h is arbitrary and may be made zero. Heaviside took eqn. (4) as a valid gravitational law based upon eqn. (3).

The unpublished notes found at Paignton showed that Heaviside made considerable use of his vector algebra in the development of eqns. (3) and (4). A good idea of this vectorial treatment can be obtained from Appendix B of the first volume of 'Electromagnetic Theory'.[1] This Appendix, however, was written before Heaviside had obtained his generalized energy formulations from eqn. (3), upon which he based his unified field.

Many of Heaviside's energy calculations were rather involved and difficult to interpret, and some of his elemental energy-flow vectors were such that only their total quantity (obtained by integrating over all space) was observable. It was interesting to note that Heaviside occasionally manipulated his energy-flow vectors as operational determinants. For example, he wrote the divergence of his gravitational energy-density vector as

$$h \,.\, (\nabla \times e) - e \,.\, (\nabla \times h)$$

and then expressed this in its determinantal form as

$$\begin{vmatrix} h_1 & h_2 & h_3 \\ \nabla_1 & \nabla_2 & \nabla_3 \\ e_1 & e_2 & e_3 \end{vmatrix} - \begin{vmatrix} e_1 & e_2 & e_3 \\ \nabla_1 & \nabla_2 & \nabla_3 \\ h_1 & h_2 & h_3 \end{vmatrix}$$

where ∇_1, ∇_2 and ∇_3 are the components of the Hamiltonian differentiator ∇. After replacing the right-hand determinant by its transformed equivalent

$$\begin{vmatrix} h_1 & h_2 & h_3 \\ \nabla_1 & \nabla_2 & \nabla_3 \\ e_1 & e_2 & e_3 \end{vmatrix} - \begin{vmatrix} \nabla_1 & \nabla_2 & \nabla_3 \\ e_1 & e_2 & e_3 \\ h_1 & h_2 & h_3 \end{vmatrix}$$

he obtained the determinantal form of $\nabla \,.\, (e \times h)$. From this result he obtained the energy-density vector $(e \times h)$ expressing his flux of gravitational energy to which other circuital energy fluxes may be added (see Section 9.3).

Other examples illustrating Heaviside's gravitational calculations could be given. In this connection it is interesting to see the plate facing p. 13 of 'The Heaviside Centenary Volume',[6] which is a reproduction of a photograph of an unpublished gravitational analysis involving his unified field theory; the analysis was probably made in 1896 and appeared in one of Heaviside's notebooks which was acquired by The Institution in 1927.

Heaviside's unified theory discernible in the papers unearthed at Paignton appears to be a straightforward extension of Maxwell's theory. It is based upon a dichotomy of a generalized energy law he obtained from eqn. (3), one part producing equations describing the electromagnetic field, and the other those describing the gravitational field. It is interesting to compare Heaviside's ideas with those embodied in Einstein's theory[7] of the unification of electromagnetism and gravitation published more than half a century later. Einstein's theory shows that in a Euclidean field the quantities concerned separate into a symmetrical and an antisymmetrical tensor, one set satisfying equations of the electromagnetic type and the other those of the gravitational type. Furthermore, Einstein's analysis shows clearly that the ideas of curved space are unnecessary for the development of a unified field theory. Thus it appears that Heaviside's attempt to correlate gravitation with electromagnetism in 1895 has a lot in common with Einstein's attempt in 1950.

(4) HEAVISIDE'S EXPANSION THEOREM

Some of the rough calculations found at Paignton indicated that Heaviside was trying to extend his expansion theorem to include cases containing fractional powers of his time operator p. Notes were found in which he had written his operational equation as

$$\frac{f(q)}{\Delta(q)} = \frac{f(0)}{\Delta(0)} + \sum_1^n \frac{f(q_r)}{q_r \Delta'(q_r)} \mathrm{F}(t, q_r) \quad . \quad . \quad . \quad (5)$$

where q is a function of p and $\mathrm{F}(t, q_r)$ is the equivalent of the operational expression $q/(q - q_r)$. Here $q_1, q_2, q_3, \ldots$ represent the roots of $\Delta(q) = 0$, while $\Delta'(q_r)$ is the result of substituting q_r for q in $d\Delta(q)/dq$.

If q is replaced by the differential operator p $(\equiv \partial/\partial t)$ the function $\mathrm{F}(t, p_r)$ becomes equivalent to $\exp(p_r t)$ and the interpretation of eqn. (5) is a simple matter. But when Heaviside replaced q by $\sqrt{p}$ his function $\mathrm{F}(t, p_r)$ became equivalent to

$$[1 + \mathrm{erf}(p_r\sqrt{t})] \exp(p_r\sqrt{t})^2$$

and the interpretation of eqn. (5) bristles with mathematical difficulties.

The Paignton papers gave no evidence for supposing that Heaviside overcame the difficulties embodied in the application of eqn. (5) to fractional operators. It is highly probable, however, that he abandoned the idea of using it, because in one of his notes he wrote '. . . I don't care much about the expansion theorem now, it is so tame . . .'.

Heaviside's original expansion theorem [obtained from eqn. (5) by putting $q = p$] has had a peculiar history. It was forgotten and unused for many years; then it was rediscovered and many engineers regarded it as the subject of the whole of the operational calculus. Heaviside himself, however, regarded it simply as one useful theorem in the general subject of electric-circuit theory; for it was the first formula to give easily and directly both the transient and steady-state responses of a network without calling for the determination of arbitrary integration constants from initial conditions.

In order to trace Heaviside's method of obtaining solutions directly in terms of initial conditions, the unpublished analysis on some of the loose sheets found at Paignton was examined in detail. These sheets were carefully selected, for it was the study of energy subsidence in an n-mesh electromagnetic system which led Heaviside to his expansion theorem. In these cases the solutions were based upon the set of n differential equations

$$\sum_s E_{rs} X_s = 0$$

where

$$E_{rs} = a_{rs}\frac{\partial^2}{\partial t^2} + b_{rs}\frac{\partial}{\partial t} + c_{rs}$$

In this set X_s represents the dependent variables and the coefficients a_{rs}, b_{rs} and c_{rs} are mesh parameters.

The classical method of solution available to Heaviside was to substitute for X_s the form $a_s \exp(yt)$, where a_s and y are constants. He required n equations for the a_s with a consistency condition which determines the $2n$ possible values of y. Heaviside soon found, however, that it was impossible for him to formulate the n equations from the knowledge that, at reference time $t = 0$, all the currents in the inductors and all the charges on the condensers are zero. He also found that in the general case it was impossible for him to determine the $2n$ possible values of y. It was at this point that Heaviside parted with classical methods and invented his own calculus.

Heaviside's method was to use p instead of $\partial/\partial t$ and then to consider the equations

$$\sum_s E_{rs}X_s = \sum [(a_{rs}p^2 + b_{rs}p)u_s + a_{rs}pV_s]$$

where u_s and V_s are the values of X_s and dX_s/dt when $t = 0$. He then solved for the X_s by algebra as if p were a number, and obtained a quasi-algebraic solution in the form

$$X_s = \frac{f_{rs}(p)}{\Delta(p)} = H(p)$$

where $f_{rs}(p)$ is a known polynomial in p. He now had to convert $H(p)$ into an explicit time function $C(t)$, and this he did by expanding $H(p)$ into partial fractions and using his previously established results such as

$$p^{-n} = \frac{t^n}{n!}$$

and

$$\frac{p}{(p-\alpha)^n} = \frac{t^{n-1}}{(n-1)!}\varepsilon^{\alpha t}$$

from which he obtained the desired result

$$H(p) = C(t), \quad t \geqslant 0 \quad . \quad . \quad . \quad . \quad . \quad (6)$$

(5) HEAVISIDE'S FRACTIONAL DIFFERENTIATION

In eqn. (6) $H(p)$ represents the operator Heaviside obtained from his 'algebrized' differential equations, and its conversion into the explicit time function $C(t)$ constituted his principal problem.

In the original differential equations from which $H(p)$ was derived, p^n represents $\partial^n/\partial t^n$, and its reciprocal p^{-n} denotes corresponding multiple integrations, while the index n is always integral. But it sometimes happens, as the result of formal algebraic manipulation, that non-integral or fractional powers of p arise in the operator $H(p)$. This led Heaviside to seek a meaning to $\partial^n C/\partial t^n$ when n is fractional. 'There is a universe of mathematics', he wrote, 'lying in between the complete differentiations and integrations.'

Apparently nobody told Heaviside that 'fractional differentiation' was an old subject which had been introduced by Leibniz in 1695 and developed by great mathematicians like Euler, Liouville, Gregory, Kelland and others. But Heaviside did not have access to these authorities, for the reference facilities available to a poor man working alone in Paignton over 60 years ago were practically nil. Nevertheless, he developed the subject of fractional differentiation much further in some directions than any of his illustrious predecessors.

Heaviside started his attack on the problem by trying to generalize the equation

$$p^n(t^k) = \frac{k!}{(k-n)!}t^{k-n}$$

to fractional values of n. After putting $k = 0$ in this equation he invented his inverse factorial function $g(-n)$ and established the theorem

$$n\pi g(n)g(-n) = \sin n\pi$$

for all values of n. Putting $n = 1/2$ in these equations he obtained the result

$$\sqrt{p}1 = 1/\sqrt{(\pi t)}$$

where 1 represents his unit function (zero before, unity after, time $t = 0$). All the algebraic details are given in the second volume of 'Electromagnetic Theory'.[1] Here Heaviside states that he first discovered the value of $\sqrt{p}$ experimentally; he illustrated this by showing how its value can be deduced from the known solution of a heat-flow problem obtained by classical methods. This discussion, however, did not appeal to mathematicians, since Heaviside's argument did not conform to the standards of rigour fashionable at the time.

Some of the calculations found at Paignton showed that Heaviside also arrived at the value of $\sqrt{p}$ by another process: this showed him the conditions under which his time operator p lost its original significance and became the transform parameter of a function which obeys all the ordinary mathematical rules. Consequently it follows that Heaviside could have constructed rigorous mathematical proofs of his 'fractional differentiation' theorems had he cared. But to Heaviside the construction of such proofs was merely a way of meeting the whims and fancies of certain pure mathematicians.

These unpublished calculations started with Heaviside using the Bessel expansion theorem to write

$$C(t) = \sqrt{p}1 = \int_0^\infty \int_0^\infty f(x)J_0[2\sqrt{(xy)}]J_0[2\sqrt{(yt)}]dxdy$$

where x and t are two positive real variables with differentiators σ ($\equiv\partial/\partial x$) and p ($\equiv\partial/\partial t$). After replacing the Bessel functions by their operational equivalents $\varepsilon^{-y/\sigma}$ and $\varepsilon^{-y/p}$, Heaviside integrated with respect to y and obtained

$$C(t) = \int_0^\infty f(x)\left(\frac{\sigma p}{\sigma + p}\right)1dx$$

By expanding his operator in inverse powers of p and then replacing p^{-n} by $t^n/n!$, Heaviside obtained the function $\varepsilon^{-\sigma t}\sigma 1$, which represents his unit impulse placed at the point $x = t$. Likewise, by expanding the operator in inverse powers of σ and then replacing σ^{-n} by $x^n/n!$, he obtained the function $\varepsilon^{-px}p1$, which represents his unit impulse placed at the point $t = x$. Thus the two spotting functions are identical, and since they have the same symmetrical generator, Heaviside wrote

$$C(t) = H(p) = \int_0^\infty f(t)(\varepsilon^{-pt}p)1dt \quad . \quad . \quad . \quad (7)$$

In establishing eqn. (7) Heaviside was really arguing in terms of what are now known as Stieltjes integrals; his work, however, was quite independent of that of Stieltjes.[8] In eqn. (7) the integration is against t and consequently the p which occurs must be treated as a parameter and not as an operator.

Replacing $H(p)$ by $\sqrt{p}1$, the 1 which occurs on both sides of the equation can be dropped, and Heaviside wrote

$$\sqrt{p} = \int_0^\infty f(t)\varepsilon^{-pt}pdt$$

where $f(t)$ can be determined in the ordinary way. Heaviside saw at once that $f(t) = 1/\sqrt{(\pi t)}$, because on replacing t by x^2 he obtained a probability integral whose value is $\sqrt{\pi}/2\sqrt{p}$.

These calculations must have shown Heaviside that it is meaningless to talk about 'fractional differentiation', and $\sqrt{p}$ should not be interpreted as the 'operation' of extracting the square root of the process of partial differentiation, for it is the transform parameter of an infinite integral which obeys all the laws of algebra and analysis.

It must be remembered that Heaviside made these calculations when the galley proofs of the second volume of his 'Electromagnetic Theory' were in his hands; consequently, it was then too late for him to make changes. It is possible, however, that he may have thought these changes too trivial to bother about. For Heaviside, like Newton and Laplace, had the faculty of being able to discover difficult theorems by some sort of intuition which dispensed with the usual processes of proof, and it may have been the possession of this gift that made him so contemptuous of formal logic.

(6) HEAVISIDE'S INFINITE INTEGRAL

If the integrand of the infinite integral (7) is divided by Heaviside's unit impulse function $p1$ it reduces to the integrand of the famous integral introduced by Laplace in 1812. No calculations or notes were found at Paignton to suggest that Heaviside had ever transformed eqn. (7) into a Laplace integral. This was to be expected, because Heaviside would have realized immediately that such a transformation would be a retrograde step, for it would have destroyed his integration symmetry, since his two fundamental functions

$$C(t) = \frac{t^n}{n!} \text{ and } H(p) = \frac{1}{p^n}, \qquad (n > -1)$$

would no longer belong together. Moreover, the operational form of a constant K would no longer be itself but K/p. Consequently, all his normal integration processes would have been disrupted, and his operator $H(p)$ would have differed from $f(t)$ in dimensions and serious confusion would result.

In dealing with eqn. (7) by the ordinary method it can be seen that the dimensions of p and t must be made reciprocal, in order to ensure that both the index pt and pdt are dimensionless. To make a dimensional check Heaviside would equate $f(t)$ to $H(p)$; then he would expand $f(t)$ in a convergent series of ascending (positive) powers of t, while $H(p)$ would be expanded in a convergent series of inverse (negative) powers of p. Since $f(t)$ and $H(p)$ are expansible, there is term-by-term correspondence, and the dimensions of such terms must be identical, e.g.

$$\sum_{r=0}^{\infty} (-1)^r \frac{t^{2r+1}}{(2r+1)!} = \sum_{r=0}^{\infty} \frac{(-1)^r}{p^{2r+1}}$$

The dimensional test was one which Heaviside always applied to results he obtained by direct integration of eqn. (7); and the transformation of eqn. (7) into the Laplacian form would have destroyed the dimensional equivalence of $f(t)$ and $H(p)$.

Another result of the Laplacian transformation is that the spotting features of the impulse function in eqn. (7) are eliminated, and this would have prevented Heaviside making his usual topological survey of the problem. For Heaviside was a born topologist; and he used his invention of operational spotting functions to help him to visualize intricate relations between abstract 'objects' in his postulated fields. Consequently, Heaviside's method of dealing with eqn. (7) was completely self-contained and did not call for access to a library of books containing details of mathematical transforms. This self-contained feature was important to Heaviside, for he worked in isolation and his mathematical library at Paignton was very small.

(7) CONCLUSION

The papers found at Paignton showed that Heaviside was in line with the British nineteenth-century mathematical tradition of formal algebraic manipulation; he was not an analyst in the modern sense. He was, however, a topologist, and a great one, in his visual thinking about electromagnetism; his ideas, when properly interpreted, form a firm foundation upon which engineering calculations can be based.

(8) REFERENCES

(1) HEAVISIDE, O.: 'Electromagnetic Theory' (The Electrician Printing and Publishing Co., Ltd.), Vol. 1, 1893; Vol. 2, 1899; Vol. 3, 1912.

(2) HEAVISIDE, O.: 'Electromagnetic Theory', *Electrician*, 1890–1899, **26–42**.

(3) HEAVISIDE, O.: 'Electromagnetic Induction and its Propagation', *ibid.*, 1884–1887, **14–20**.

(4) MAXWELL, J. C.: 'Treatise on Electricity and Magnetism' (Clarendon Press, 1873).

(5) POYNTING, J. H.: 'On the Transfer of Energy in the Electromagnetic Field', *Philosophical Transactions of the Royal Society*, 1884, **175**, p. 343.

(6) 'The Heaviside Centenary Volume' (The Institution of Electrical Engineers, 1950).

(7) EINSTEIN, A.: 'The Meaning of Relativity' (Methuen, 1950), Fourth Edition (with an Appendix on a unified field theory).

(8) STIELTJES, T. J.: 'Oeuvres Completes de Thomas Jan Stieltjes' (Noordhoff, Groningen, 1918), Vol. 2.

(9) HAMILTON, W. R.: 'Elements of Quarternions' (Longmans, London, 1866).

(10) MURPHY, R.: 'The Theories of Electricity' (Pitt Press, London, 1833).

(11) WHITTAKER, E.: 'Oliver Heaviside', *Bulletin of the Calcutta Mathematical Society*, 1928–29, **20**, p. 202.

(12) GRASSMAN, H. G.: 'Die Lineale Ausdehungslehre, ein neuer Zweig der Mathematik' (Reimer, Berlin, 1844).

(13) MAXWELL, J. C.: 'On the Mathematical Classification of Physical Quantities', *Proceedings of the London Mathematical Society*, 1871, **3**, p. 224.

(9) APPENDICES

(9.1) Heaviside's Equations

In his epoch-making 'Treatise on Electricity and Magnetism'[4] Maxwell's form of presentation was in harmony with the general principles of quaternions as enunciated by Hamilton.[9] The power of quaternions appealed to Maxwell, for near the beginning of his 'Treatise' (Article 10, Vol. 1, p. 9) he wrote, 'In electrodynamics we have to deal with a number of physical quantities, the relations of which to each other can be expressed far more simply by a few expressions of Hamilton's than by the ordinary equations'.

Maxwell's compact and powerful quaternionic expression of the general equations of the electromagnetic field are given in Article 619, Vol. 2, p. 258, of his 'Treatise'. This formulation appears to have little in common with the vector equations (1) and (2) discussed in this Monograph. Nevertheless, they have common features: for both the quaternionic and vector formulations describe the experimental discoveries of Oersted, Ampère, Ohm and Faraday; and both formulations can be used to predict the results of electromagnetic experiments yet to be made.

Hamilton's algebra of quaternions, unlike Heaviside's algebra of vectors, is not a mere abbreviated mode of expressing Cartesian analysis, but is an independent branch of mathe

matics with its own rules of operation and its own special theorems. A quaternion is, in fact, a generalized or hypercomplex number: thus a quaternion

$$w + ix + jy + kz$$

is formed from four real numbers, w, x, y and z, and four number units, 1, i, j and k, in the same way that the ordinary complex number $w + ix$ might be regarded as being formed from two real numbers, w and x, and two number units, 1 and i. The number units 1, i, j and k do for rotations and stretches of a line-element in space what 1 and i do for the line-element in a plane. But whereas the multiplication of complex numbers is commutative, that of quaternions is not; consequently the manipulation of quaternions calls for the application of certain special theorems.

Heaviside also studied quaternions in Hamilton's 'Elements', but had been repelled by the non-commutative property and the special theorems. He felt that Hamilton's calculus was really too hard for busy engineers to learn; it would take them too long to master the tricks. So with these ideas in mind he built his own system of vector algebra. This system was a very simple one; it was not a new branch of mathematics, like quaternions, but merely a shorthand form of ordinary Cartesian analysis. The only mathematical equipment required to apply this system was the definition of scalar and vector products, the Hamiltonian operator ∇, a few transformation formula and the integral theorems of Green and Stokes. Engineers welcomed Heaviside's vector algebra, but pure mathematicians were not enthusiastic. Prof. P. G. Tait described it as 'a sort of hermaphrodite monster, compounded of the notations of Hamilton and Grassman'. Heaviside, however, was not interested in problems of abnormal physiology, for he was busy forging a mathematical tool which would enable engineers to apply Maxwell's electromagnetic theory to their problems.

It was a simple matter for Heaviside to apply his vector algebra to the two great experimental laws of electromagnetism. These laws concern the two circuits, the electric circuit and the magnetic circuit which are always linked through a common field. By taking the line integral of the magnetic force round an elemental closed curve in this field, Heaviside obtained his eqn. (1). This vector equation does not appear explicitly in Maxwell's 'Treatise'; it is possible, however, to find its equivalent in the form of three Cartesian equations in the second volume. This is only to be expected, since these equations describe Ampère's rule for deriving the magnetic force from the electric current and had been discussed in detail by many writers before Maxwell (Murphy).[10] Considered alone, Heaviside's eqn. (1) is merely a concise vectorial description of Ampère's results.

By taking the line integral of the electric force round the closed curve in the field Heaviside obtained his eqn. (2). Again this vector equation does not appear explicitly in Maxwell's 'Treatise'; but since it describes the experimental law of electromagnetic induction, it is possible to find its equivalent in the form of sets of Cartesian equations in volume 2. These equations may be written in Heaviside's vector notation as

$$\left.\begin{aligned} E &= -\dot{A} + \nabla\psi \\ \operatorname{curl} A &= H \end{aligned}\right\}$$

where A represents Maxwell's electromagnetic momentum at a point and ψ denotes his scalar electric potential. Thus Heaviside's eqn. (2) replaces the above set of equations and eliminates Maxwell's A and ψ. Considered alone, however, Heaviside's eqn. (2) is merely a concise description of Faraday's results.

Thus, considered individually eqns. (1) and (2) may be directly related to the experimental discoveries upon which electrical science is based. However, in this Monograph eqns. (1) and (2) are not considered individually but as a correlated or 'duplex' pair of vector equations. These equations have been discussed by Sir Edmund Whittaker,[11] who stated:

> Maxwell, following Faraday's ideas, had clearly pointed out that the electric field at each point depended on two vectors, namely the electric and magnetic forces at the point, and upon the electric and magnetic displacements they produced. But in Maxwell's 'Treatise' the analytical consequences of these principles had not been developed in a straightforward and natural manner: his pages are cumbered with the debris of the older theories, with a maze of symbols representing electric and magnetic potentials, vector potentials, and so forth. I well remember, in 1893, buying for myself a second-hand copy of Maxwell which had been the property of a College lecturer on mathematical physics. When I came to the famous chapter on the 'General Equations of the Electromagnetic Field', I found scribbled in his handwriting 'from here on this book is absolutely unreadable'. The great service which Heaviside now rendered to science was to clear away this accumulation of rubbish, and base the theory on what he called the 'duplex' equations
>
> $$\left.\begin{aligned} \operatorname{curl} H &= 4\pi\Gamma \\ \operatorname{curl} E &= -\dot{B} \\ \operatorname{div}\Gamma &= 0 \\ \operatorname{div} B &= 0 \end{aligned}\right\}$$
>
> (where H is the magnetic force, Γ is the electric current, etc.), which modern writers generally call 'Maxwell's equations'—though they are not to be found in Maxwell's 'Treatise', and the modern writers have in fact copied them from Heaviside.

It will be observed that the Heaviside equations quoted by Sir Edmund are unsymmetrical, whereas eqns (1) and (2) discussed in this Monograph are perfectly symmetrical. Most modern textbooks discuss electromagnetic theory from the viewpoint of the unsymmetrical equations; they say that the lack of symmetry in the system is due to the absence of free magnetism and magnetic conduction. From the Paignton papers, however, it became clear that Heaviside always maintained the electromagnetic symmetry of eqns. (1) and (2) in his calculations; he retained the magnetic conductivity, σ_m, not merely for the sake of computing convenience, but also on account of the singular engineering application in which the electric conductivity is made to perform the functions of both the real σ and the unreal σ_m. Thus eqns. (1) and (2) are a pair of correlated vector equations upon which Heaviside built a mathematical model; this model, however, does not add anything fundamentally new to Maxwell's theory or contain anything new mathematically. It is an algorithm designed by Heaviside to enable engineers to apply Maxwell's theory to their problems.

Heaviside's Paignton calculations showed how he used his model: he would write eqns. (1) and (2) in the form

$$\operatorname{curl} H = \left(\frac{\Gamma}{Z_0}\right)E$$

$$-\operatorname{curl} E = (\Gamma Z_0)H$$

where Γ = Propagation parameter

$$= \sqrt{[(\sigma_m + i\omega\mu)(\sigma + i\omega\kappa)]}$$

and Z_0 = Characteristic impedance

$$= \sqrt{\frac{\sigma_m + i\omega\mu}{\sigma + i\omega\kappa}}$$

where σ, κ, σ_m and μ are the electric conductivity, permittivity, magnetic conductivity and permeability respectively. Thus he made his discussion of any medium formally uniform with that of any network; σ, κ, σ_m and μ for the medium corresponding to G, C, R and L for the network. This mathematical model

made Maxwell's theory workable from the engineer's point of view. For the model has the properties of an automatic machine; an engineer can feed one end with his parametric facts (or fancies) and on turning the mathematical handle, he can get results from the other end—as many as he wants.

(9.2) Maxwell's Equations

In connection with Sir Edmund Whittaker's comments on Heaviside's eqns. (1) and (2) it should be noted that the quaternionic methods used by Maxwell in Article 619 of his 'Treatise' enable these equations to be reduced to the very simple form

$$\mathrm{D}F = C$$

where D denotes the quaternionic differentiator and F and C represent Maxwell's electromagnetic bivector and current quaternion respectively. This simple Maxwellian expression embodies within itself all the fundamental electromagnetic laws and is an incomparably more powerful mathematical formulation than Heaviside's eqns. (1) and (2).

This formulation indicates that Maxwell's mathematical outlook was broader than Heaviside's. To appreciate how much broader it was, we must remember that, before Maxwell had published his 'Treatise', he had mastered Grassman's algebra[12] and could think in terms of a space of n dimensions, whereas Heaviside, some 25 years later, was still imprisoned in Euclid's three dimensions. Thus Maxwell was in possession of an algebra capable of development by specialization in various directions: this theory (which included Hamilton's quaternions as a special case) showed him how to transform his quaternions into matrices. The Grassman matrix interpretative scheme would have enabled Maxwell to determine eigenfunctions and use analytical techniques which are now common in the tensor calculus.

There can be but little doubt that Maxwell preferred to use quaternionic rather than vector analysis for dealing with really difficult electromagnetic problems. For in 1867 he outlined his own vector analysis;[13] his 'convergence' is the negative of the 'divergence' in use to-day, and he introduced what is now called the 'curl' of a vector. But in his 'Treatise' (published in 1873) he did not use his vector algebra. It appears clear, therefore, that he knew of vector methods before he wrote his 'Treatise' and quite deliberately adopted the quaternionic form of analysis as an improvement. Nobody has yet explained why the Maxwell hypercomplex scheme should not be considered an improvement.

(9.3) Maxwell's Electromagnetic Theory

Although the ideas embodied in Heaviside's eqns. (1) and (2) did not constitute an addition to Maxwell's electromagnetic theory or contain anything new mathematically, the same statement cannot be made about the ideas embodied in his development of eqns. (3) and (4). These ideas may be readily examined from the viewpoint of Maxwell's hypercomplex analysis. Expressing Maxwell's fundamental quaternionic equation

$$\mathrm{D}F = C$$

in its tensor form, we have

$$\left.\begin{aligned} \dot{E}_r &= \epsilon_{rmn}H_{n,m} & E_{n,n} &= 0 \\ \dot{H}_r &= -\epsilon_{rmn}E_{n,m} & H_{n,n} &= 0 \end{aligned}\right\}$$

where the dots indicate differentiation with respect to time; ϵ_{rmn} is the permutation symbol, and the commas denote partial differentiation with respect to the second subscripts. Maxwell showed that the electric and magnetic forces, E_r and H_r, in these equations are satisfied by

$$\left.\begin{aligned} E_r &= -\dot{\phi}_r - \psi_{,r} \\ H_r &= \epsilon_{rpq}\phi_{q,p} \end{aligned}\right\}$$

where ϕ_r (the vector potential) and ψ (the scalar potential) are both functions of position and time. Heaviside found by his own methods that these functions can be correlated with G in his eqn. (3) for both E_r and H_r are unchanged if ϕ_r and ψ are replaced by

$$\left.\begin{aligned} \phi'_r &= \phi_r + v_{,r} \\ \psi' &= \psi - \dot{v} \end{aligned}\right\}$$

where v is an arbitrary function of space and time which can be used to satisfy imposed conditions. If Heaviside could have published these Paignton developments (and shown that he could satisfy the mathematical requirements of a flux of gravitational energy), it is probable that his unified field theory would have been accepted as a valid extension of Maxwell's theory.

The above example illustrates the ease with which hypercomplex algebra can be applied to the development of Heaviside's unified-field ideas. These ideas call for the description of movements in curved Riemannian 4-space, and it is here that Maxwell's quaternionic formulations are particularly convenient; for movements in such a space can easily be effected by means of a pair of quaternions, one of which is used as a prefactor and the other as a postfactor. Again Maxwell's quaternionic equation $\mathrm{D}F = C$ describing the electromagnetic system $\mathrm{S}(x, y, z, t)$ passes readily into the form $\mathrm{D}'F' = C'$ for the system $\mathrm{S}'(x', y', z', t')$, and shows that the invariants of the field are characterized by $F^2 = 0$. Since the electric and magnetic fields can be interchanged in Maxwell's quaternion by a change of axes, it follows that the topological characteristics of the two fields can be determined.

The metric form for Heaviside's space is

$$(ds)^2 = a_{\alpha\beta}dx^\alpha dx^\beta - (dx^4)^2,\ x^4 = ct$$

For operating in this space it is best to transform Heaviside's eqns. (1) and (2) into the form

$$\left.\begin{aligned} T_{rm,n} + T_{mn,r} + T_{nr,m} &= 0; \quad g^{mn}T_{rm|n} = 0 \\ H_{\alpha\beta} = T_{\alpha\beta};\ E_\alpha = T_{\alpha 4} &= -T_{4\alpha}; \quad T_{44} = 0 \end{aligned}\right\}$$

where the comma in the suffix indicates partial differentiation, and the vertical stroke denotes covariant differentiation with respect to n. In this formulation only the fusion of the electric and magnetic fields in the tensor has physical significance. It would have been an extremely difficult matter for Heaviside to manoeuvre in this field without the aid of hypercomplex algebra.

621.385.832.032.366

The Institution of Electrical Engineers
Monograph No. 320 R
Dec. 1958

THE EFFECT OF TEMPERATURE ON THE PERSISTENCE OF LONG-PERSISTENCE CATHODE-RAY-TUBE SCREENS

By R. FEINBERG, Dr.Ing., M.Sc., Associate Member.

(*The paper was first received 2nd April, and in revised form 9th September*, 1958. *It was published as an* INSTITUTION MONOGRAPH *in December*, 1958.)

SUMMARY

The persistence characteristics of several types of long-persistence cathode-ray-tube screens were measured with the ambient temperature of the tube faces varying from about 20° C to about 50° C. It was found that increasing temperature reduced the persistence time, the temperature coefficient of persistence-time reduction being higher for some types and lower for others. In some cases temperature coefficient also decreased with increase of excitation luminance.

(1) INTRODUCTION

The qualitative theory of luminescence of solid materials is sufficiently well established for it to be possible to describe in broad outlines the mechanism of luminescence. However, only a tentative beginning has so far been made in respect of the quantitative aspect.

The luminescence of a phosphor of the type normally used in a cathode-ray tube is initiated when the phosphor is excited by bombardment with electrons. With a double-layer screen the layer adjacent to the face of the tube is excited by irradiation with ultra-violet rays produced in the layer nearer to the electron gun.

The mechanism of the luminescence process is commonly explained in terms of a single-stage cycle of events when the phosphor is of the short-persistence type, and of a two-stage cycle when it is of the long-persistence type.

The atomic structure of a crystal of a long-persistence phosphor is conceived as a matrix lattice containing so-called 'electron traps' and 'luminescence centres', which are believed to be localized electron energy states facilitating the process of long-persistence luminescence. On bombarding the phosphor with electrons, or irradiating it with ultra-violet rays, electrons of the atoms in the crystal lattice absorb energy and either become excited or leave their parent atoms if sufficient energy is absorbed. A released electron can move around in the crystal lattice and may be caught in an electron trap, where it is held captive until it escapes as a consequence of thermal agitation. Subsequently it may be retrapped, but it eventually arrives at a luminescence centre, where its energy of excitation is released and the electron returns to the so-called 'ground state'. The energy released is converted either to a photon and hence to luminescent radiation, or to lattice energy and hence dissipated in a non-radiative form.

The persistence characteristic of a long-persistence phosphor depends on the mean time of electron captivity in a trap, or a succession of traps, and the probability of radiative energy conversion in a luminescence centre. The decay is the slower the longer the mean time of electron captivity and the higher the probability of radiative energy conversion, and vice versa. An increase of temperature reduces the mean time of electron captivity in a trap, and vice versa. Hence an increase of temperature tends to accelerate the decay of phosphorescence, and a reduction tends to slow it down. In addition, temperature may in some range influence the probability of radiative energy conversion in a luminescence centre and hence affect the decay time, an increase of temperature sometimes reducing the probability and thus the decay time.

Garlick, Henderson, and Puleston* point out the dependence of the persistence behaviour of long-persistence phosphors on the conditions of phosphor excitation, and they describe the results of measurements made under conditions simulating the pulsed excitation in a p.p.i. radar display. Also, their measurements were made at constant ambient temperature.

In the following experimental investigations the effect of varying the ambient temperature is observed under conditions of a steady phosphor excitation which was made in each case to last two minutes to ensure a steady-state condition of excitation. The measurements were made with a number of different screens of types used in practice, for example in radar applications.

(2) TYPES OF LONG-PERSISTENCE CATHODE-RAY-TUBE SCREENS INVESTIGATED

A variety of screens were investigated; they were either single-layer or double-layer, and all were aluminium backed. According to their persistence behaviour, they were divided in four groups, and a typical example of each group was selected for presentation of the results of measurement. These examples are enumerated in Table 1.

Table 1

EXAMPLES OF LONG-PERSISTENCE SCREENS

A Magnesium fluoride I;	single-layer screen
B Magnesium fluoride II;	single-layer screen
C Fluor silicate;	single-layer screen
D Zinc sulphide and zinc-cadmium sulphide;	double-layer screen

(3) EXPERIMENTAL METHODS USED IN THE INVESTIGATION

(3.1) Screen Excitation

All cathode-ray tubes were operated with the same conditions of screen excitation. Each screen was excited for two minutes to ensure that the luminance had reached a steady-state condition at the end of excitation when persistence began.

The excitation pattern consisted of a television-type linear-sweep raster measuring 130 mm × 130 mm. Each field had 200 lines produced with a defocused electron beam to give as nearly as possible uniformity of excitation. The scanning frequency was 50 fields per second.

(3.2) Varying the Ambient Temperature

The cathode-ray tube under investigation was placed inside an electrically heated and thermostatically controlled chamber enabling the temperature to be varied. A motor-driven fan was

Correspondence on Monographs is invited for consideration with a view to publication.
Dr. Feinberg is with Ferranti Ltd. (seconded to the Electrical Engineering Department, Manchester College of Science and Technology).

* GARLICK, G. F. J., HENDERSON, S. T., and PULESTON, R.: 'Cathode-Ray-Tube Screens for Radar', *Journal I.E.E.*, 1946, 95, Part IIIA, p. 815.

placed in the chamber to stir the air in order to achieve uniformity of temperature.

The temperature of the air around the face of the cathode-ray tube was measured as the mean reading obtained from the resistances of four thermistors placed in different positions near the face of the tube. When changing the temperature in the chamber, about half an hour was allowed for the new condition to settle before any persistence characteristics were determined.

The ambient temperature was varied in the range from about 18° C to about 52° C.

(3.3) Measurement of the Screen Luminance

Luminance was measured with two selenium-type photovoltaic cells, one of which was used inside the heat chamber and close to the cathode-ray-tube face in order to achieve sufficient sensitivity for measuring the luminance during the time of persistence. The second cell was used to set the excitation luminance of the screen and was arranged at the end of a tube of 20 cm length outside the heat chamber so that it remained unaffected by the temperature changes inside. Its performance was that of its calibration at normal ambient temperature. The two cells were provided with suitable filters to correct the spectral response characteristic of each to that of the standard eye.

The galvanometer for measuring the photocell currents was connected to a shunt and series resistance arrangement to change its sensitivity by a factor of 10 so that a correspondingly wide range of photocell current, and hence of luminance, could be measured.

In the measurements, luminance is expressed in terms of the M.K.S. unit, the candela per square metre (1 cd/m^2 = 1/3·426 ft-lambert = 1/3·426 e.f.c.).

In their investigation of persistence behaviour, Garlick, Henderson and Puleston (*loc. cit.*) used an electron-multiplier photovalve with a correcting filter, connected to a d.c. amplifier, the output of which was displayed on the long-persistence screen of a monitor cathode-ray tube which had a flat face with a mesh scale. Their equipment was somewhat more elaborate and was specifically designed for pulse excitation of the screen under investigation.

(3.4) Measurement of a Persistence Characteristic

Each persistence characteristic was obtained by plotting seven points. To facilitate the measurement of the seven time intervals during each run of decay of phosphorescence, a manually operated electronic 'multiple-indication stop-watch' was constructed. It consisted of a 1c/s-multivibrator which produced the time pulses, one per second, an 8-bank uniselector, and seven sets of 3-stage Dekatron counters. The contacts of the uniselector banks were so connected to the inputs of the seven counters that at the first step of the wipers all seven counters received time pulses from the multivibrator simultaneously; at the second step one of the counters was stopped; at the third step, a second counter; and so on. Each step of the uniselector was initiated by manual operation of a microswitch. The first step was at the beginning of persistence, i.e. when screen excitation was switched off; and each successive step was made when the galvanometer indication passed through the predetermined measuring-point.

The contacts of the eighth bank were utilized for automatically homing the uniselector to its starting position, after the last measuring point was obtained.

The multivibrator operation was accurate for time measurement to at least one part in a thousand. Each counter was capable of measuring time to a maximum of 1 000 seconds, and it indicated directly in seconds.

(4) EFFECT OF TEMPERATURE ON THE SCREEN EFFICIENCY

The curves of Fig. 1 depict the excitation luminance, L_e, c each screen as a function of the electron beam current, I_a, wit the accelerator voltage, V_a, as parameter. It was found that th

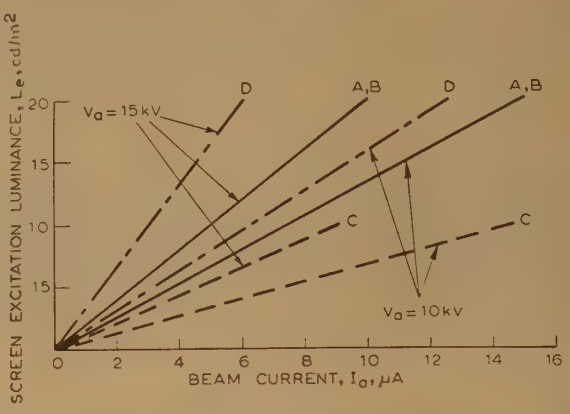

Fig. 1.—Screen excitation characteristics.
A, B, C, and D indicate the type of screens (see Table 1).

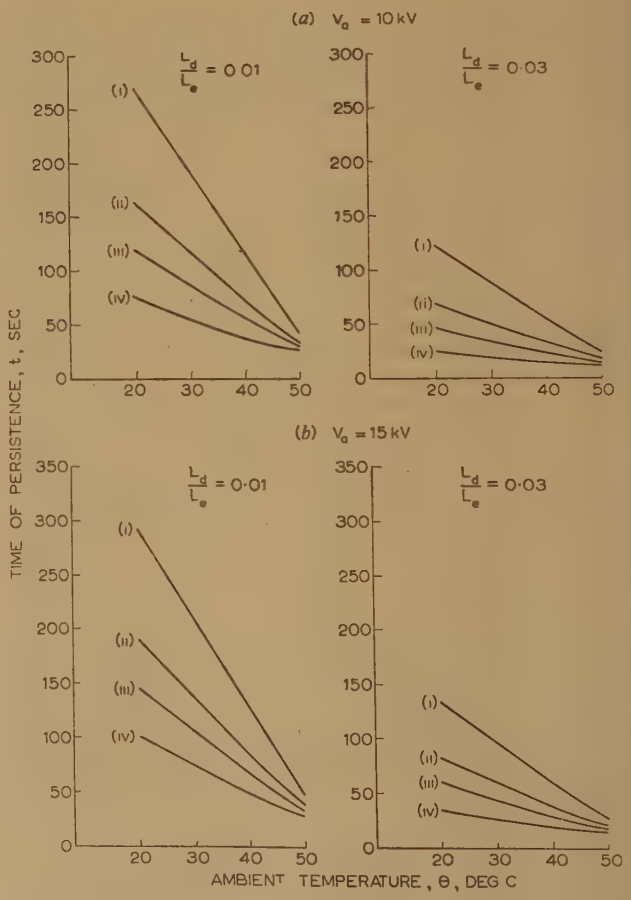

Fig. 2.—Effect of the ambient temperature on the persistence characteristics of screen A.
(i) L_e = 1 cd/m^2
(ii) L_e = 5 cd/m^2
(iii) L_e = 10 cd/m^2
(iv) L_e = 20 cd/m^2

curves, and hence the screen efficiencies, are independent of the ambient temperature in the range investigated, namely 20–50° C.

The relation between screen efficiency and ambient temperature is of interest in connection with the mechanism of the luminescence process (Section 1). Any effect which a change of ambient temperature has on the probability of radiative energy conversion in the luminescence centres manifests itself as a corresponding change in screen efficiency. Since, in the phosphors investigated and in the temperature range covered, there is no change of screen efficiency, it can be deduced that the probability of radiative energy conversion remains constant.

(5) EFFECT OF TEMPERATURE ON PERSISTENCE

The persistence characteristics of the screens enumerated in Table 1 are represented in Figs. 2 and 3 for screen A, Figs. 4 and 5 for screen B, Figs. 6 and 7 for screen C, and Figs. 8 and 9 for screen D.

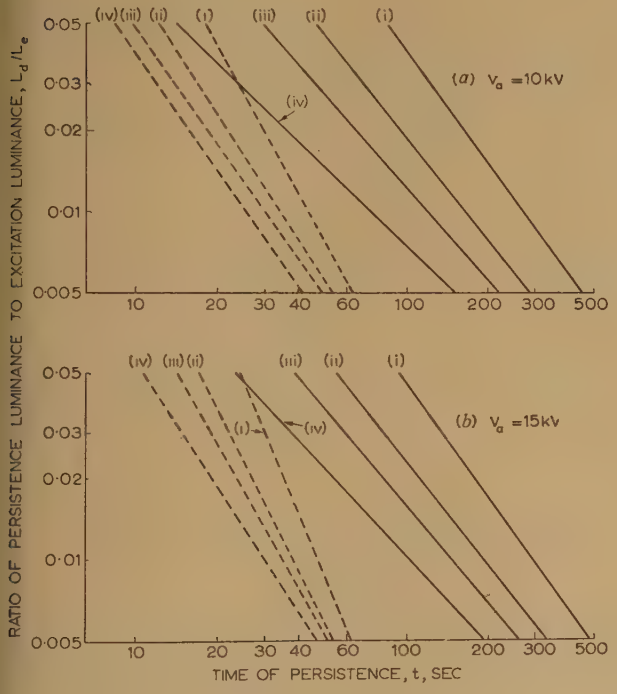

Fig. 3.—Persistence characteristics of screen A.

(i) L_e = 1 cd/m²
(ii) L_e = 5 cd/m²
(iii) L_e = 10 cd/m²
(iv) L_e = 20 cd/m²
—— θ = 20° C
---- θ = 50° C

In determining the time, t, in which phosphorescence of a screen decays from the excitation luminance, L_e, to a given value of persistence luminance, L_d, account had to be taken of the value of L_e, the ratio L_d/L_e, the accelerator voltage V_a, and the ambient temperature θ. In order to accommodate in the presentation of results the variables and parameters in such a manner that the characteristics are convenient for practical purposes, Fig. 2 depicts t as a function of θ from 20° C to 50° C, for $L_d/L_e = 0{\cdot}01$ and $0{\cdot}03$, $L_e = 1$, 5, 10 and 20 cd/m², and $V_a = 10$ kV in Fig. 2(a) and 15 kV in Fig. 2(b). Fig. 3 gives L_d/L_e, from 0·005 to 0·05, as a function of t for $\theta = 20°$ C and 50° C, $L_e = 1$, 5, 10 and 20 cd/m², and $V_a = 10$ kV in Fig. 3(a) and 15 kV in Fig. 3(b).

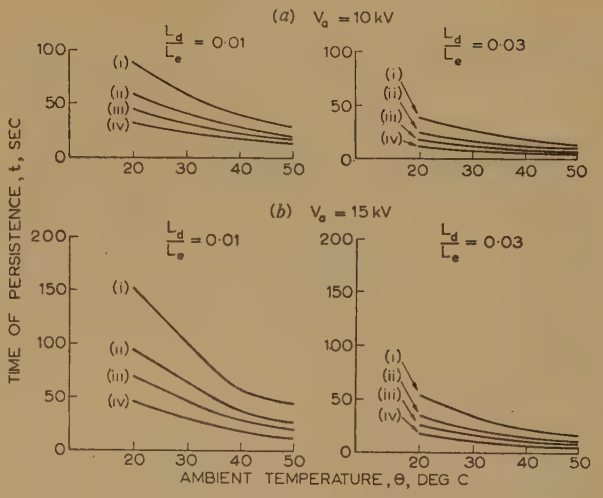

Fig. 4.—Effect of the ambient temperature on the persistence characteristics of screen B.

(i) L_e = 1 cd/m²
(ii) L_e = 5 cd/m²
(iii) L_e = 10 cd/m²
(iv) L_e = 20 cd/m²

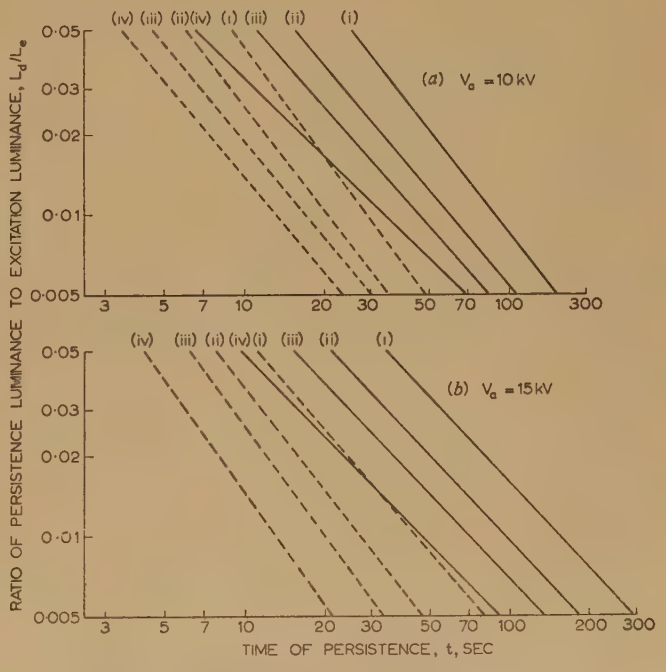

Fig. 5.—Persistence characteristics of screen B.

(i) L_e = 1 cd/m²
(ii) L_e = 5 cd/m²
(iii) L_e = 10 cd/m²
(iv) L_e = 20 cd/m²
—— θ = 20° C
---- θ = 50° C

Figs. 4, 6 and 8 correspond to Fig. 2; and Figs. 5, 7 and 9 to Fig. 3.

Analysing the persistence characteristics of the single-layer screens, Figs. 2–7, it is found that, within the range of the variables and parameters investigated, t is in fact independent of V_a and L_e, and depends only on the current density of the

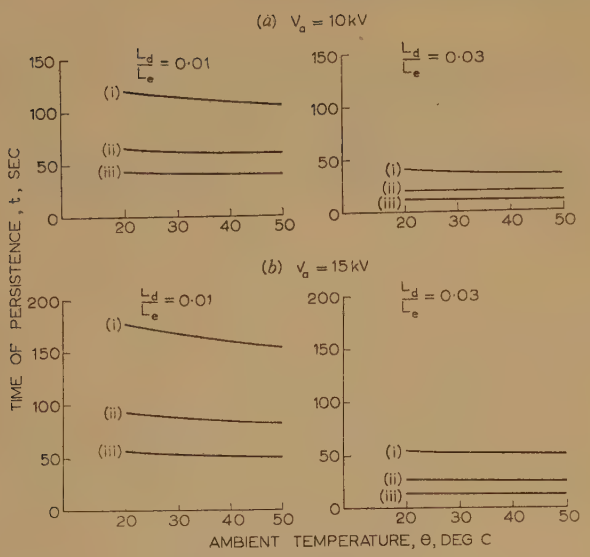

Fig. 6.—Effect of ambient temperature on the persistence characteristics of screen C.

(i) L_e = 1 cd/m²
(ii) L_e = 5 cd/m²
(iii) L_e = 10 cd/m²

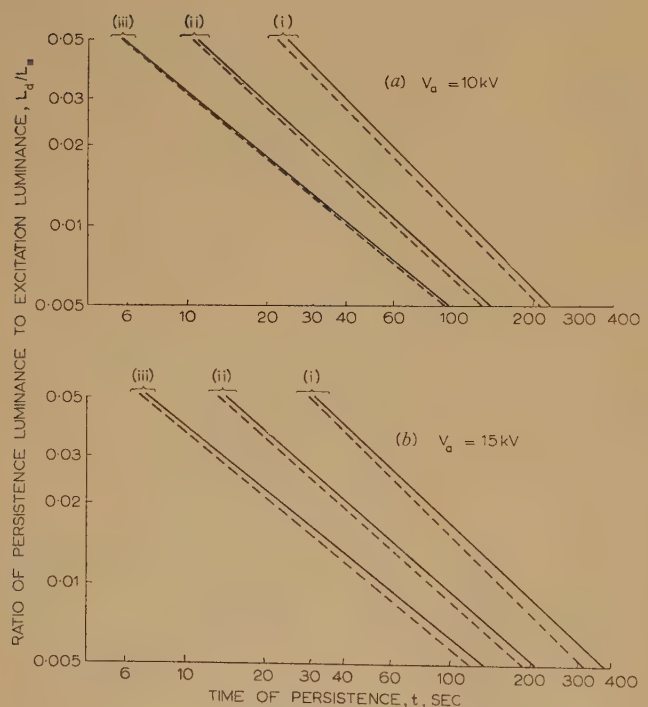

Fig. 7.—Persistence characteristics of screen C.

(i) L_e = 1 cd/m²
(ii) L_e = 5 cd/m²
(iii) L_e = 10 cd/m²
—— θ = 20° C
---- θ = 50° C

electron beam exciting the screen. Thus an increase of the beam current density causes a faster decay of phosphorescence, and a lower beam current density results in a slower decay, independent of V_a.

For the double-layer screen, Figs. 8 and 9, the persistence

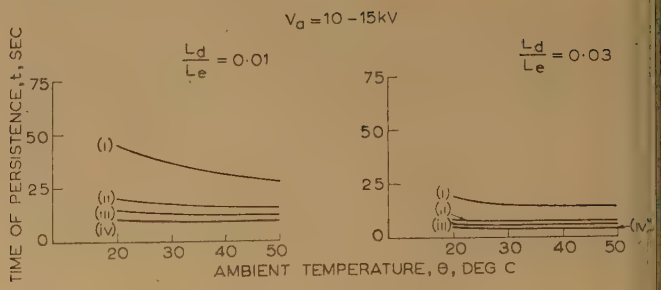

Fig. 8.—Effect of ambient temperature on the persistence characteristics of screen D.

(i) L_e = 1 cd/m²
(ii) L_e = 5 cd/m²
(iii) L_e = 10 cd/m²
(iv) L_e = 20 cd/m²

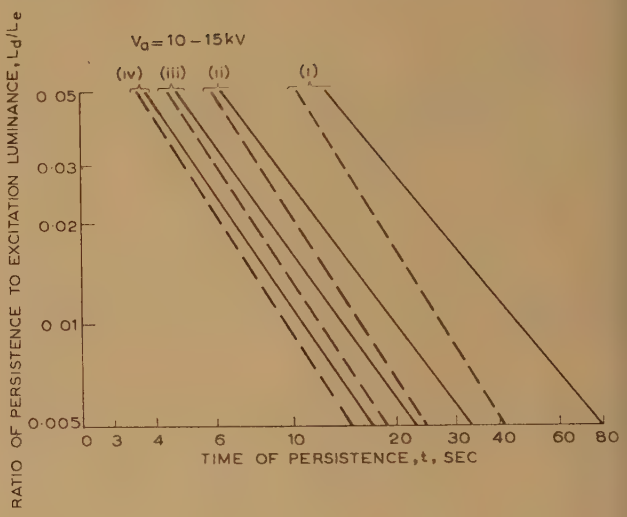

Fig. 9.—Persistence characteristics of screen D.

(i) L_e = 1 cd/m²
(ii) L_e = 5 cd/m²
(iii) L_e = 10 cd/m²
(iv) L_e = 20 cd/m²

characteristic is dependent on L_e but independent of V_a in the range investigated. This is a consequence of the cascade action of screen excitation where the long-persistence phosphor layer is excited by irradiation with ultra-violet rays and is hence free from any influence of the current density.

As was to be expected from the theory of luminescence (Section 1), t is reduced as θ is increased. The manner in which t is reduced varies from phosphor to phosphor and depends to some extent on the values of L_e and L_d/L_e. In one phosphor, screen C, t is almost independent of θ.

(6) THE TEMPERATURE COEFFICIENT OF PERSISTENCE-TIME REDUCTION

By inspection of Figs. 2, 4, 6 and 8 it can be seen that the linear sections of the t/θ curves, say in the regions around $\theta = 20°\,C$, may be represented by the relation

$$t = t_{20}[1 - \delta_{20}(\theta - 20)]$$

where t_{20} denotes the persistence time at 20° C, t that at a temperature θ, and

$$\delta_{20} = \frac{1}{t_{20}}\left(\frac{dt}{d\theta}\right)_{\theta=20°\,C}$$

the temperature coefficient of persistence-time reduction at 20° C.

The values of δ_{20} for screens A, B, and D are independent of L_e for $L_d/L_e \leqslant 0{\cdot}01$, but for $L_d/L_e > 0{\cdot}01$, δ_{20} tends to become smaller with increase of L_e. Table 2 gives the values of δ_{20}

Table 2

VALUES OF δ_{20} FOR THE SCREENS A, B AND D

Screen	$L_d/L_e \leqslant 0{\cdot}01$	$L_d/L_e = 0{\cdot}03$	
		$L_e = 1\,\text{cd/m}^2$	$L_e = 20\,\text{cd/m}^2$
A	0·03	0·03	0·025
B	0·03	0·03	0·025
D	0·02	0·02	0·001

for $L_d/L_e \leqslant 0{\cdot}01$ and for $L_d/L_e = 0{\cdot}03$ with $L_e = 1$ and $20\,\text{cd/m}^2$. For screen C, $\delta_{20} \leqslant 0{\cdot}005$.

In general terms the temperature coefficient of persistence time is defined as

$$\delta_a = \frac{1}{t_a}\left(\frac{dt}{d\theta}\right)_{\theta=a}$$

where t_a is the persistence time at $\theta = a$. Hence

$$t = t_a[1 - \delta_a(\theta - a)]$$

For all screens investigated the tendency is $\delta \to 0$ for $\theta > 50°\,\text{C}$.

(7) CONCLUSIONS

The persistence characteristic of a long-persistence screen is a property peculiar to the particular type of phosphor employed. No general rule about its behaviour at increasing ambient temperature can be formulated, except that the degree of persistence-time reduction may be higher for some phosphors and lower for others. For example, screens A and B are similar in their basic chemical structure, luminescence efficiency and temperature coefficient of persistence-time reduction, but they are different in respect of persistence times. Screen C is an example where temperature has almost no effect on the persistence characteristic.

A phosphor excited with an electron beam has a persistence characteristic which depends on the current density of the electron beam, and a phosphor excited by ultra-violet irradiation has a persistence characteristic dependent on the intensity of the ultra-violet irradiation. In the first case the persistence characteristic is independent of the velocity of the exciting electrons.

621.387: 621.316.722

The Institution of Electrical Engineers
Monograph No. 321
Dec. 195

EFFECTS OF ARGON CONTENT ON THE CHARACTERISTICS OF NEON-ARGON GLOW-DISCHARGE REFERENCE TUBES

By F. A. BENSON, D.Eng., Ph.D., Associate Member, and P. M. CHALMERS, B.Eng., Graduate.

(*The paper was first received* 24*th June, and in revised form* 15*th October*, 1958. *It was published as an* INSTITUTION MONOGRAPH *in December*, 1958, *and was read before the* RADIO AND TELECOMMUNICATION SECTION 23*rd March*, 1959.)

SUMMARY

Measurements have been made on certain glow-discharge stabilizer tubes to determine the influence of varying the argon content on the running-voltage/current curves, the running-voltage/temperature curves, the initial drifts, and the impedance/frequency and noise characteristics. Neon-filled tubes, with argon contents varying over the relatively wide range of 0·001–10%, having molybdenum anodes and cathodes, and employing high-stability reference-tube manufacturing techniques, have been specially constructed for the investigations. The results of the studies are presented and discussed.

LIST OF PRINCIPAL SYMBOLS

v = Total volume of glow-discharge tube, divided into two regions v_1 (near cathode) and v_2 (remainder).
T_1 = Temperature of glass envelope.
T_2 = Temperature of volume v_2.
W = Heat flow from cathode to tube envelope.
K = Thermal conductivity of gas.
a = Cross-sectional area of heat flow.
h = Height of cathode cylinder.
r_1 = Radius of cylindrical glass envelope.
r_2 = Radius of cathode.
A, N = Heat-conduction gas constants.
T_0 = Room temperature.
P_0 = Pressure of gas-filling at temperature T_0.
I = Tube current.
V = Tube running voltage.
ρ_0 = Gas density corresponding to P_0 and T_0.
ρ = Gas density at any temperature T in a volume dv.
ρ_2 = Gas density in volume v_2.
d_1 = Anode-envelope distance in plane-electrode tube.
d_2 = Anode-cathode distance in plane-electrode tube.

(1) INTRODUCTION

The cold-cathode glow-discharge tube has many applications in electronic circuits, but is particularly valuable as a simple voltage regulator, as a source of reference voltage in thermionic-valve stabilizers, and for switching purposes in automatic telephony.[1] The desirable characteristics of such tubes vary with the application; e.g. when used as a voltage stabilizer the tube should have a low impedance and good regulation over a large current range. With a reference tube, however, the temperature coefficient of running voltage and the initial voltage drift should be small, and, in addition, the running-voltage/current characteristic should be reproducible and free from steps and hysteresis. For automatic-telephone switching applications, the stability and impedance/frequency characteristics of the tubes and the noise produced are very important.

A great deal of work has been carried out in recent years on glow-discharge tubes. Many of the earlier investigations consisted of comparing performances of commercial stabilizer and reference tubes,[2] and the following characteristics have been studied: running-voltage/current curves, initial drift, change of running voltage with temperature, impedance/frequency curves and noise.[4] Later, tests were carried out on a number of special tubes with different cathode materials, gas fillings, gas pressures and constructions,[5, 6] to determine the effect of these tube parameters on the various characteristics. The results obtained suggested that another important tube parameter was the argon content of the gas filling, which had not been constant in the various batches of special tubes produced.

More recent investigations were therefore carried out on similar special tubes in which only the argon content was varied.[7] The tubes examined had cerium cathodes and helium and neon as the main gas fillings, the argon content being varied in steps of 0·5% from zero to 3·5%. Only fairly general conclusions could be drawn, however, as to the effect of argon on the voltage/temperature and running-voltage/current curves because in some cases the results showed a large spread for tubes of the same batch. An important feature of the running voltage/current curves was the presence of voltage steps or jumps which increased in magnitude with increasing argon content. The steps were probably largely due to non-uniformity of the cerium-cathode surface.

Complete impedance measurements were only obtained for the helium-filled tubes during the above investigations, and the results indicated that there is a rapid rise in impedance with decreasing argon content below 1%. With neon-argon tubes containing more than 2·5% argon, internal high-frequency oscillations occurred at all tube currents and no impedance results could be recorded. For tubes with argon contents between 1·0 and 2·5%, oscillations occurred when the tubes were run above the mean operating current of 20 mA. Oscillations were also observed in some helium-argon tubes having argon content greater than 3·0% when operated above 30 mA, and pure-helium and pure-neon tubes oscillated at all tube currents. It is now thought that the oscillations, although influenced by the amount of argon present, may be peculiar to cerium-cathode tubes, since nickel tubes of a similar construction do not appear to exhibit this phenomenon; further work is, however, necessary to confirm this.

In this earlier work on tubes with differing argon contents initial drifts were measured only for helium-filled tubes, and, as with impedance measurements, internal oscillations seriously limited the number of noise readings obtainable. In order to make a fuller study of the effect of varying the argon content in neon-argon filled tubes, it was decided to vary the argon content in steps over the relatively wide range of 0·001–10%, and so as to obtain more reliable characteristics, to use tubes with molybdenum anodes and cathodes and to employ high-stability reference-tube manufacturing techniques. The following percentage argon contents were chosen: 0, 0·001, 0·01, 0·1, 0·25, 0·5, 0·75, 1·0, 3·0, and 10·0, smaller increments being taken

Correspondence on Monographs is invited for consideration with a view to publication.
Dr. Benson and Mr. Chalmers are in the Department of Electrical Engineering, University of Sheffield

between 0·1 and 1·0% since this is the region of minimum running voltage.[8, 9]

Four tubes were constructed for each argon content, all the tubes being identical in every other respect. Each tube had a rod anode 1 mm in diameter and a cylindrical cathode 7·5 mm in diameter and 10 mm long. The electrode structure was mounted in a glass tube having a volume of about 8 cm^3, and the envelope was filled to a total pressure of 40 mm Hg. The tubes were sputtered until a layer of molybdenum completely covered the walls of the glass envelope. Thus, impurities from the glass were prevented from contaminating the discharge and the molybdenum layer also acted as a getter for certain impurities.[9] The tubes were operated at mean current for several days after construction, until the running voltages were sensibly constant.

Measurements were then made on all the tubes to determine the influence of the argon content on the running-voltage/current curves, running-voltage/temperature curves, initial drifts, impedance/frequency curves and noise characteristics. The results of this work are presented and discussed.

(2) MEASUREMENTS

The running-voltage/current characteristics, the changes in running voltages with temperature and the initial drifts of the tubes were obtained using measuring techniques previously described.[10, 11] Each tube was operated in turn from a stabilized d.c. supply through a suitable series resistor, a meter in the anode lead measuring the current. The running voltage was stepped down with standard decade resistance boxes, so that it could be measured with a vernier potentiometer (accurate to 1 mV), and was recorded to within 10 mV for increasing and decreasing currents over the normal operating range (i.e. in the normal-glow region). This range was found to vary with the amount of argon in the tube, being considerably greater in the case of the 10% argon content than in the others, as discussed in Section 4. In view of this, the tubes were operated at a current of 4 mA during the running-voltage/temperature and initial drift measurements, so that the discharge was normal in most cases. Throughout the measurements of running-voltage/current characteristics, the tubes were operated in air at an ambient temperature of about 20° C and the glass envelopes were shielded from draughts.

The ambient temperature was altered by immersing the tubes in an electrically-heated oil-bath. The temperature was increased in steps of about 10° C in the range 20–90° C, and the running voltage was recorded to within 1 mV. Smith[12] has pointed out that a disadvantage of this method is that high temperatures may cause voltage drifts in certain tubes, so that observed changes of voltage depend, not only on the temperature, but also on the length of time the tube is held at that temperature. In his measurements, to avoid cumulative drifts, he held tubes in a reference oil-bath at 35° C and then plunged them into one of six constant-temperature baths, covering the range 20–110° C. He recorded running-voltage changes continuously, and after five minutes the tubes were returned to the reference bath, where they were left to reach a steady state. Since the oil-bath used in the present work had a large heat capacity, and the running voltage was allowed to settle down after each temperature change for at least five minutes, the method adopted during the present investigations was thought to be sufficiently reliable.

The effective a.c. resistance and inductance of the tubes were measured over the audio-frequency range, using the modified form of Owen bridge network shown in Fig. 1. This method[13, 14] was considerably more accurate, particularly at low frequencies, than an earlier method which relied on alternating current and voltage measurements with phase-angle determination using an

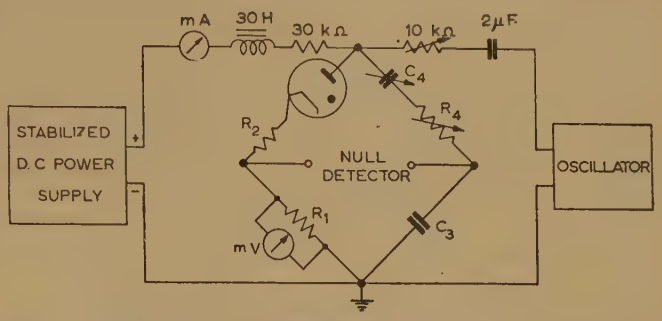

Fig. 1.—Bridge circuit for measuring the effective inductance and resistance of glow-discharge tubes.

oscillograph.[5, 7] Since the tube is a non-linear circuit-element, harmonics are present in the current waveform, but with an oscillograph as the bridge detector, the effective inductance and resistance could be measured at the fundamental frequency only. The superimposed alternating current through the tube was monitored by measuring the voltage drop across the standard resistor R_1 with a valve voltmeter. This current was held constant at 0·33 mA throughout the measurements, the value being chosen as a compromise to give an easily detectable null point with minimum distortion.

With this bridge circuit, impedance measurements could be made over the frequency range 300 c/s–30 kc/s and the arrangement gave a maximum error of 2% when calibrated against standard resistors and inductors. Measurements were limited at high frequencies by the sensitivity of the detector and the effect of stray capacitances, and at low frequencies by increased distorton and inaccuracies due to the bridge arms having widely differing impedances.

The effective resistances and inductances of all the tubes were measured for a mean tube current of 3 mA. The impedances of the tubes were also determined at frequencies of 300 c/s, 3 kc/s and 10 kc/s for various mean currents between 2 and 20 mA.

Noise measurements were made with a calibrated amplifier-detector unit having an equivalent noise bandwidth of 87 kc/s. Values of noise voltage were recorded for tube currents in the range 0·5–5 mA, for a fixed value of noise load resistor of 37·5 kilohms. A tube may be regarded as a noise-voltage generator of e.m.f. e_n in series with an equivalent noise impedance z_n. For each tube, the noise voltage was measured for a fixed tube current of 3 mA and two different values of noise load resistor, thus enabling e_n and z_n to be calculated.

(3) RESULTS

The variation of striking voltage with argon content has not been recorded because of the large spread in the results for tubes of a given type, due to the construction employed. A small pre-breakdown gap was present in each tube, and no attempt was made to keep the gap length constant from sample to sample. Even so, it was observed that there is a tendency for striking voltages to be higher at low argon contents.

The minimum running voltage, deduced from the running-voltage/current curves, is plotted against argon content in Fig. 2. The variation of full-glow current, which is a measure of the current density, is also indicated. Running-voltage/current characteristics for various argon contents are shown in Fig. 3. The curves are for a typical tube chosen from a batch of four, and although there is a spread in the tube running voltages, the form of the running-voltage/current curve does not differ appreciably for tubes of the same batch. Each curve has been

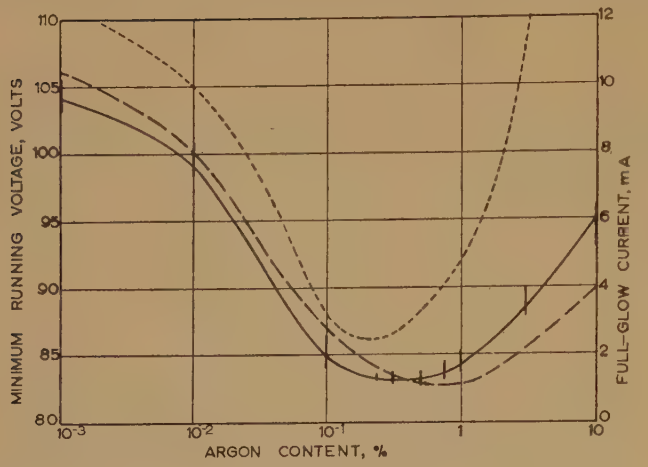

Fig. 2.—Minimum running voltage and full-glow current as a function of argon content.

——— Minimum running voltage.
— — — Minimum running voltage according to Jurriaanse, Penning and Moubis (reproduced from Reference 9 by permission of Philips Electrical Ltd.).
- - - - - - Full-glow current.

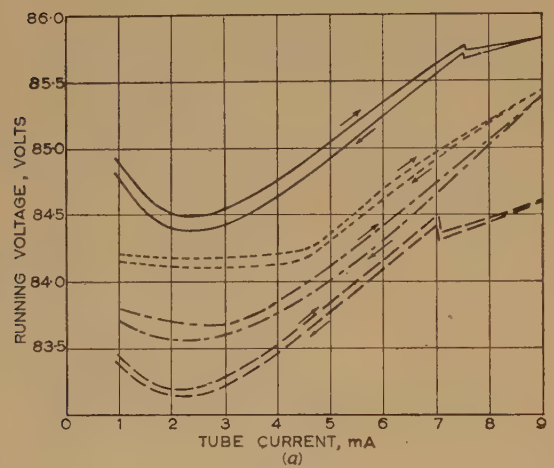

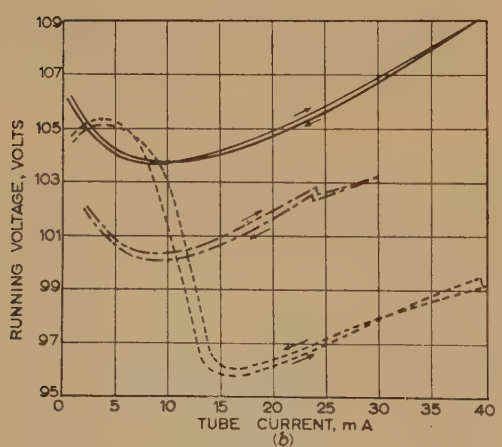

Fig. 3.—Running-voltage/current characteristics.

(*a*) ——— 0·1% argon.
— — — 0·25% argon.
— - — - 0·5% argon.
- - - - - 1·0% argon.
(*b*) ——— 10^{-3}% argon.
— - — - 10^{-2}% argon.
- - - - - 10% argon.

drawn through all the experimental points, and during t measurement the current was varied gradually, so that a voltage step or discontinuity could be observed on the vernie potentiometer null detector. The running-voltage/curre characteristics were reproducible from day to day to with 0·05 volt for tubes having up to 1·0% argon, and to with 0·1 volt for tubes with higher argon contents.

Fig. 4 illustrates the variation of running voltage with tem

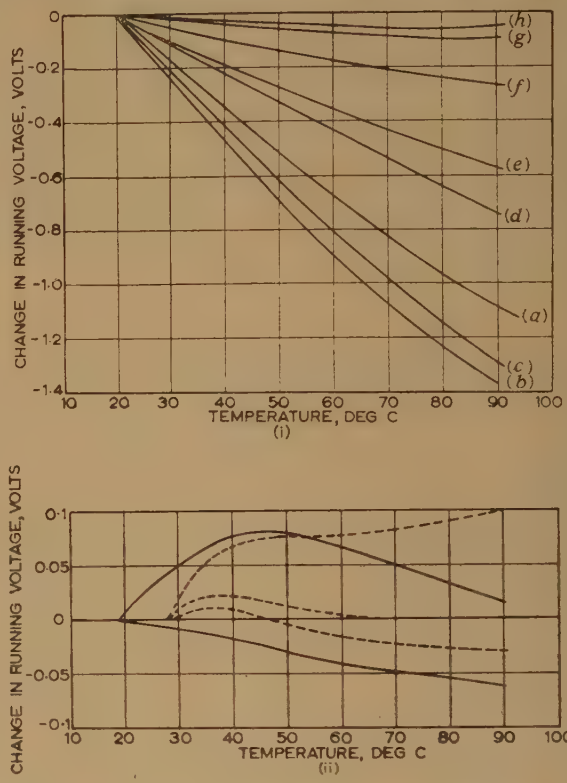

Fig. 4.—Running-voltage/temperature characteristics.

(i) *Argon contents up to* 1·0%.
(*a*) pure neon.
(*b*) 10^{-3}%.
(*c*) 10^{-2}%.
(*d*) 10^{-1}%.
(*e*) 0·25%.
(*f*) 0·5%.
(*g*) 0·75%.
(*h*) 1·0%.

(ii) *Argon contents greater than* 1·0%.
——— 3·0%.
- - - - - 10%.

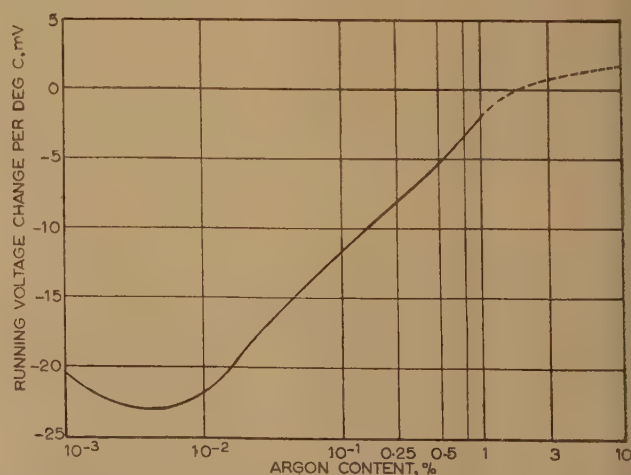

Fig. 5.—Average voltage/temperature coefficient as a function argon content.

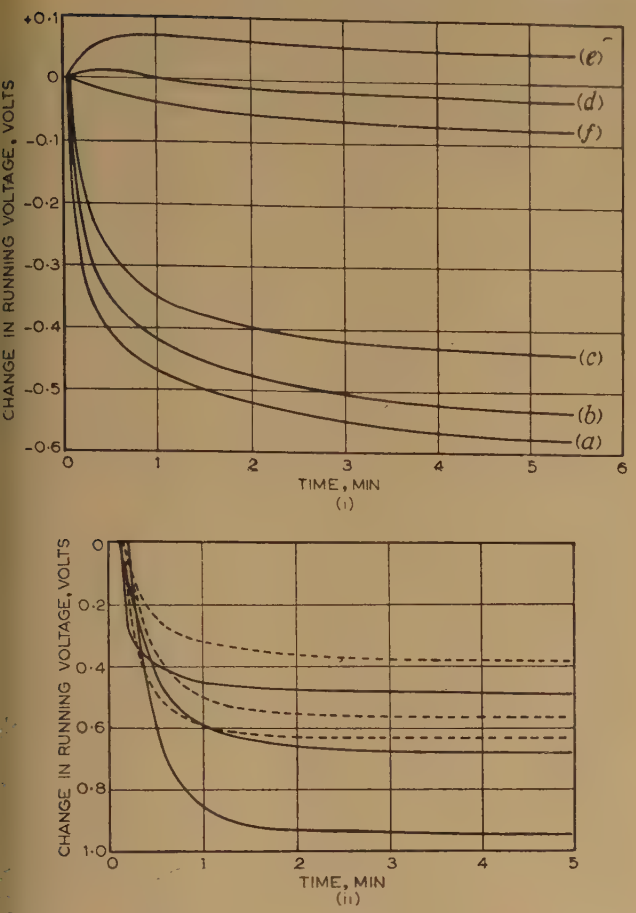

Fig. 6.—Initial running-voltage drift.

(i) *Argon contents up to* 1·0%.
(*a*) pure neon. (*d*) 10^{-1}%.
(*b*) 10^{-3}%. (*e*) 0·5%.
(*c*) 10^{-2}%. (*f*) 1·0%.

(ii) *Argon contents greater than* 1·0%.
——— 3·0%.
– – – – – 10·0%

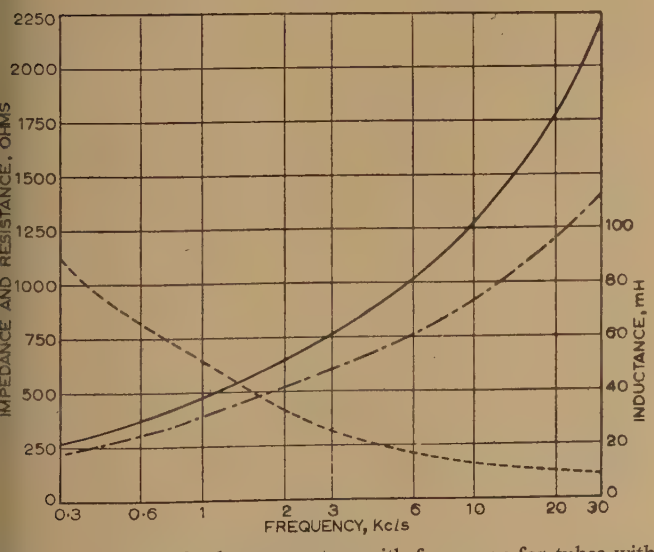

Fig. 7.—Variation of tube parameters with frequency for tubes with 0·25% argon.

——— Impedance.
– – – – Resistance.
– – – – – Inductance.

perature for different argon contents. Only one tube characteristic has been drawn, as the spread in the characteristics for tubes of the same type was small for argon contents up to 1%. Fig. 5 shows a plot of average voltage/temperature coefficient against argon content for the temperature range 20–50° C. Typical initial running-voltage drifts are shown in Fig. 6. As mentioned in Section 1, measurements of impedance and noise in neon-argon tubes with cerium cathodes containing more than 0·5% argon were not possible, because the tubes oscillated. Such oscillations were not observed in the present tubes, except for the samples containing 10% argon, which showed a tendency to oscillate at low tube currents during the warming-up periods. These oscillations died out, however, after running the tubes for a few seconds. Figs. 7 and 8 show typical impedance, inductance and resistance variations with frequency. In Fig. 9

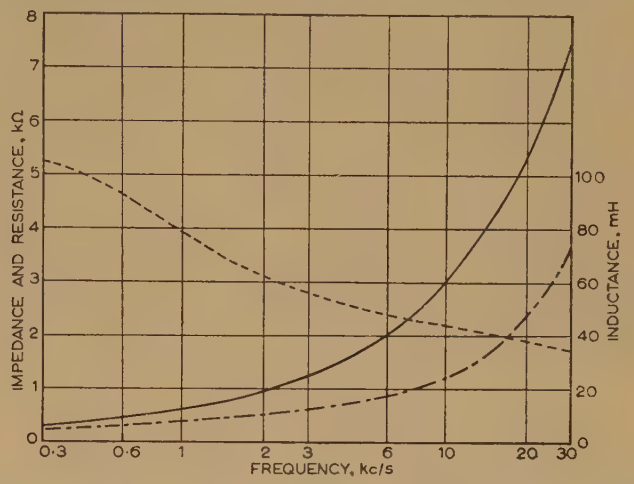

Fig. 8.—Variation of tube parameters with frequency for tubes with 1·0% argon.

——— Impedance.
– – – – Resistance.
– – – – – Inductance.

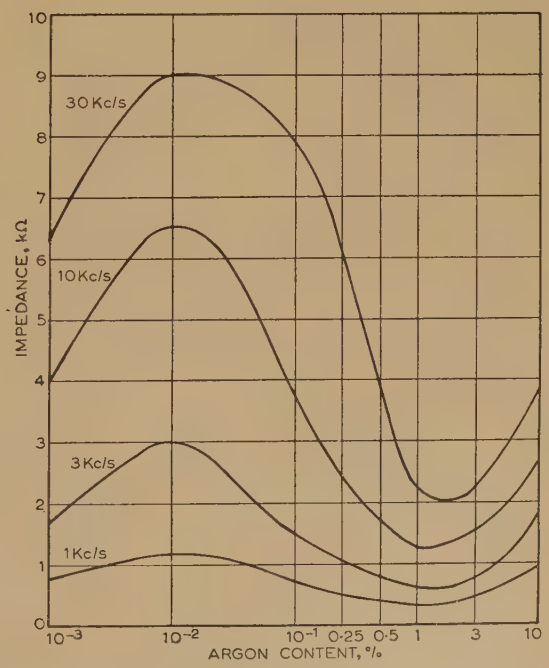

Fig. 9.—Impedance as a function of argon content for various frequencies.

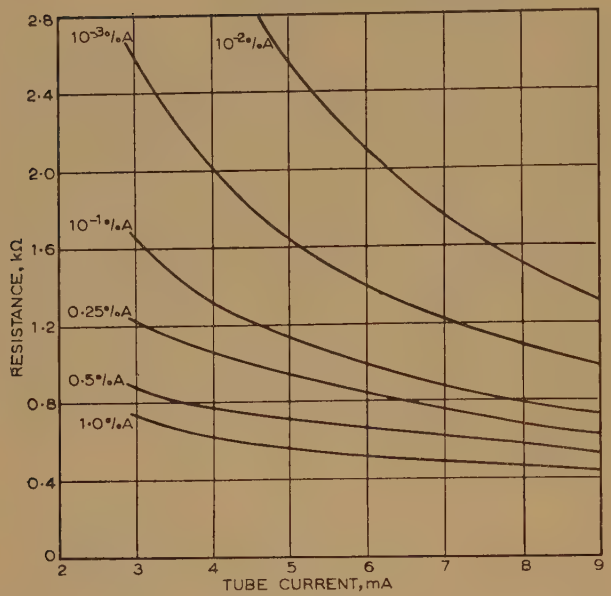

Fig. 10.—Variation of resistance at 10 kc/s with tube current and argon content.

the average tube impedance has been plotted against argon content for various frequencies. Figs. 10 and 11 depict the variation of resistance and inductance with direct tube current for various argon contents.

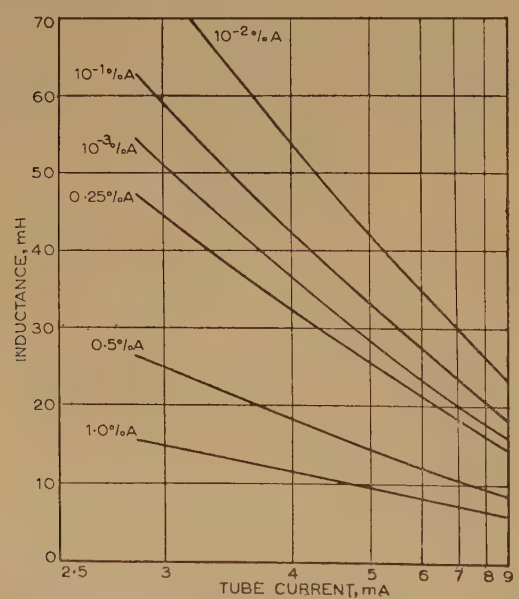

Fig. 11.—Variation of inductance at 10 kc/s with tube current and argon content.

Typical noise-voltage/current curves for various argon contents are illustrated in Fig. 12, while Fig. 13 shows the variation of noise with argon content for a direct current of 3 mA. The equivalent noise impedance z_n and voltage e_n are also shown.

(4) DISCUSSION OF RESULTS

(4.1) Running Voltages

The results showing the minimum voltage as a function of argon content agree fairly well with those obtained by Jurriaanse, Penning and Moubis,[9] as illustrated in Fig. 2. The shift between

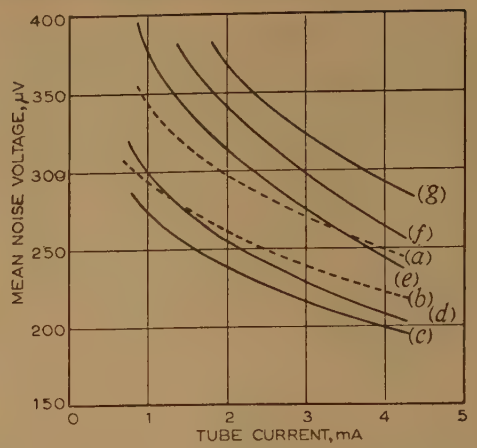

Fig. 12.—Mean noise voltage/current characteristics.

(*a*) 10^{-3}% argon.
(*b*) 10^{-2}% argon.
(*c*) 10^{-1}% argon.
(*d*) 0·25% argon.
(*e*) 0·5% argon.
(*f*) 1·0% argon.
(*g*) 10% argon.

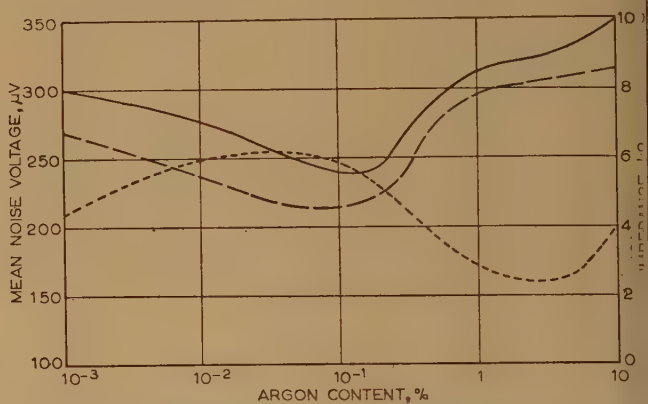

Fig. 13.—Mean noise voltage as a function of argon content.

——— Noise voltage for a load resistance of 37·5 kilohms.
— — — Equivalent noise voltage e_n.
- - - - - Equivalent noise impedance z_n.

the curves is possibly due to the fact that these authors used plane cathode and anode, while during the present studies cylindrical cathode and rod anode were used. A minimu running voltage occurs at about 0·3% argon, and it is interesti to note that there is a minimum spread in the characteristics tubes having this argon content. This may, of course, be due the difficulty of measuring and controlling the amount of add argon in the case of the very low contents, or, for argon conte greater than 1%, to the inability to age and sputter the tub adequately. The high current densities in these tubes, in co junction with the electrode configuration, may have caus incomplete or uneven cleaning of the cathode surface a prevented total coverage of the glass walls with a molybden layer. It was found that the area of cathode covered by gl in these tubes contracted at lower currents after ageing. This probably responsible for the observed form of runnin voltage/current curves at low currents. The minimum runni voltage occurs at much higher values of tube current, where discharge has a cleaning influence which offsets the spoili effect due to impurities.[9]

(4.2) Running-Voltage/Current Curves

For tubes with low argon contents, the minimum runn voltage occurs at higher currents than for tubes containing argon, and the subnormal-glow region appears to be great when 0·01% argon is present. This is not attributed

mpurities, because the characteristics are reproducible and the ow expands uniformly over the cathode surface with increasing rrent. It was observed that with the 0·01% argon tubes, at rrents below 4 mA, the glow appeared as a diffused region ling most of the anode-cathode space, and at higher currents hen the discharge was almost abnormal, the glow formed a fined negative-glow region near the cathode. These pheno-ena[8, 15] seem to be associated with the ionization process in e gas.

If the argon content in a neon glow-discharge tube is increased om slightly above zero, reductions of striking voltage (called e Penning effect[16]), normal current-density and running voltage cur. These decreases can be explained by an increase in the nization of argon atoms caused by collisions with neon atoms the metastable state. The probability that this process curs increases with increasing argon content, until all the etastable neon atoms are active. Then, with further argon ditions, the probability of excitation of argon atoms is pre-minant, so the ionization coefficient decreases. Kruithof and nning[15] found that the maximum value of the ionization efficient is attained when the argon content is about 0·1%.

The electric-field-strength distribution between the electrodes r maintenance of the glow discharge is such that least energy used to form an ion pair. For argon contents between 10^{-3} nd 10^{-1}%, since the ionization coefficient is a maximum at w field strengths, excitation and ionization at low currents will ke place in most of the anode-cathode space, giving the glow diffuse appearance. As the tube current increases, a positive-n space charge builds up in the cathode region, the negative-ow region contracts towards the cathode, and the discharge ould become normal. Meissner[8] points out, however, that the rmal-glow region cannot be recognized in gas mixtures with $)^{-1}$–10^{-2}% argon. This is because the running voltage falls owly with increasing current, but before the negative glow ntracts completely to form a normal region, the discharge comes abnormal, and the running voltage again increases.

With increasing argon content above 0·25%, the subnormal ow recedes and the normal glow becomes more easily definable, nd with 1% argon the running-voltage/current curves are nsibly flat over the current range 1–5 mA.

It is difficult to draw conclusions from the tests on tubes with % and 10% argon, because at currents below 15 mA the con-action phenomenon was prevalent, although the hysteresis hich usually accompanies this[17] was small. No voltage steps jumps were observed in the running-voltage/current curves the normal operating range. This may seem surprising in ew of previous reports[7] of steps having occurred in the charac-ristics of neon-argon tubes with cerium cathodes. These steps, though affected by the argon content, are, however, now ought to be due to an unevenly-prepared cathode surface, for hich the sputtering and preparation procedures were influenced the amount of argon to differing extents.

The small steps in running voltage which are observed at gh currents occur when the glow jumps to the outer surface the cathode cylinder. Previous to this the running voltage es with increasing current, owing to the edge effect at the thode. At the boundary of the glow area the current density less than in the centre of the glow.[18, 19] When the glow reads towards the edge of the cathode, the current density the glow boundary is further decreased, since the field at the ge is smaller, so the normal current density at the centre of e glow increases and consequently the maintaining voltage es. The running voltage continues to rise with further crease of current, until the discharge can be more favourably aintained on the outside surface of the cathode, so the glow oves there. This movement causes a small decrease in current density on the inner cathode surface, and thus there is a small sudden decrease in maintaining voltage.

The general form of the full-glow current curve of Fig. 2 is similar to the current-density/argon-content characteristics of hydrogen-neon gas mixtures in tubes with iron cathodes,[20] and neon-argon mixtures in tubes with nickel cathodes.[8]

(4.3) Running-Voltage/Temperature Curves

The reduction of normal running voltage for a given increase in temperature gets smaller as the argon content is increased. The running-voltage/temperature curves are fairly linear at low argon contents, but for tubes with more than 0·5% argon, there is a decrease in the voltage/temperature coefficient at temperatures above 60° C.

Jurriaanse[21] has explained theoretically the variation of running voltage with temperature and concludes that a negative temperature coefficient should be obtained. Most of the change in voltage between the anode and cathode in a glow-discharge stabilizer tube appears in the cathode-fall region, and is dependent on the gas density in this region. If the tube-envelope temperature increases, heating of the gas near the envelope will cause it to expand, and will increase the gas density near the cathode. Jurriaanse calculated the temperature coefficient of running voltage for the case of a helium-argon-filled tube, by considering a density change in the cathode region of the tube and relating this to the slope of the running-voltage/pressure curve at the initial tube pressure. He also found that, with neon tubes, the decrease of running voltage with increasing pressure was reduced when a small percentage of argon was added to the gas filling, although he only gives results for pure neon and neon with 0·5% argon.

Calculations indicate that the temperature coefficients of running voltage obtained from Jurriaanse's expressions are too small by a factor of 10 for pure-neon and pure-argon tubes. There are also a number of minor errors in Jurriaanse's paper. It appears that, since it is necessary to use running-voltage/pressure characteristics to determine temperature coefficients, it is better first to estimate the change in gas pressure, and not density, with varying tube-wall temperature. A modified form of Jurriaanse's theory is therefore presented in the Appendix, from which the decrease in voltage/temperature coefficient with increasing argon content can be explained. From the theory given, it is seen that the temperature coefficient should be proportional to the slope of the running-voltage/pressure curve. Hence, the temperature coefficient will decrease with increasing argon content if at the same time the slope of the running-voltage/pressure curve also decreases. Further work is necessary to confirm that this is true over the wide range of argon contents used in the present investigations. It is shown in the Appendix, however, that the calculated temperature coefficients using the modified theory, for pure-neon and neon + 0·5% argon tubes, agree closely with the observed values over the temperature range 30–50° C. The theory also shows that the temperature coefficient should decrease with increasing temperature, but the sudden reversal of temperature coefficient observed in some tubes with the higher argon contents is not easily explained. It has sometimes been assumed[11, 12] that observed positive temperature-coefficients were due to impurities and/or adsorbed gases. Further tests will need to be made, however, to see if the voltage/temperature curves of these tubes are reversible, before the phenomenon can be attributed to release of impurities. Positive temperature-coefficients are, of course, possible provided the slopes of the running-voltage/pressure curves are positive.

The large spread in the results for tubes with argon contents greater than 1% may be ascribed to impurities affecting the cathode-surface conditions.

(4.4) Initial Drifts

The initial drift of running voltage was found to be negative for most tubes and, for small argon contents, to decrease with increasing amounts of argon. The drift was very small (less than 0·04 volt) for argon contents between 0·1 and 1% and in all cases was complete after 3 min. The increase in initial drift for argon contents greater than 1% may possibly be due to impurities.

It is thought that there is a connection between initial drift and running-voltage/temperature coefficient as the results tend to suggest. The initial drift can be ascribed to a gradual increase in gas pressure as the gas in the cathode region reaches an equilibrium temperature determined by the heating effect in the cathode region; this increase in gas pressure would result in a lowering of the running voltage as explained in Section 4.3.

(4.5) Impedance/Frequency Curves

It is difficult to compare the impedance/frequency characteristics in the normal-glow region at a fixed tube current, since no one current can be chosen where the discharge is normal in all tubes. The following general conclusions on the effect of the amount of argon on tube impedance can, however, be drawn from the results.

With decreasing argon content the effective inductance and resistance increase rapidly, and reach a maximum when the argon content is about 0·01%; the impedance then falls and approaches the value of pure-neon tubes. The effects of argon are greatest at low tube currents and high frequencies.[7]

The impedance/frequency characteristics had the same form as those observed by previous investigators,[5] the impedance increasing with frequency as predicted by the theory of Van Geel[23] and Verhagen.[24] A detailed study of the impedance characteristics of glow discharges is in progress, to determine whether experimental results agree with a more recent theory due to Van Geel,[25] and to confirm whether there is a correlation between the transit time of ions in the cathode-fall region and the frequency at which the tube reactance changes from an inductive to a capacitive value as observed by Yeh.[26] The results of this work will be reported in a future paper.

(4.6) Noise Characteristics

A comparison of the noise-voltage/argon-content curve of Fig. 13 with the current-density/argon-content curve of Fig. 2 shows that minimum noise occurs with about 0·1% argon, corresponding to the region of minimum current density. Benson and Gillespie[7] have pointed out that the noise is probably largely due to collisions of electrons with gas atoms, and the probability of excitation and ionization by electron collision is a function of electron energy. Thus, the noise generated will also be a function of electron energy. The minimum noise was found to coincide with the minimum of electron energy discussed in Section 4.2. The variation of equivalent-noise impedance with argon content showed the same form as that of impedance at high frequencies, when plotted against argon content.

(5) CONCLUSIONS

The most desirable characteristics of neon tubes with molybdenum cathodes are obtained when the argon content is about 1·0%. Minimum impedance and zero voltage/temperature coefficient, however, can be realized for argon contents between 1% and 3%, but it is difficult to prepare tubes which have similar and reproducible characteristics when the argon content is greater than 1·0%.

(6) ACKNOWLEDGMENTS

The work recorded has been carried out in the Departm of Electrical Engineering at the University of Sheffield. authors wish to thank Professor A. L. Cullen for facili afforded in the laboratories of this Department, and for constant encouragement and advice; also Mr. G. P. Burdi for carrying out many careful examinations of runni voltage/current and running-voltage/temperature characteris and initial drifts of tubes. They also wish to acknowledge kindness of the English Electric Valve Co., Ltd., in supply all the special tubes for examination, for financial assista with the work, for the loan of equipment, and for the ma helpful discussions and valuable suggestions.

(7) REFERENCES

(1) Townsend, M. A., and Depp, W. A.: 'Cold-Cathode Tu for Transmission of Audio-Frequency Signals', *System Technical Journal*, 1953, **32**, p. 1371.

(2) Benson, F. A.: 'Voltage Stabilized Supplies' (MacDon London, 1956).

(3) Benson, F. A., and Mayo, G.: 'Impedance-Freque Variations of Glow-Discharge Voltage-Regulator Tub *Electronic Engineering*, 1954, **26**, p. 206, and 'Impeda Frequency Characteristics of some Glow-Discha Tubes', *ibid.*, 1956, **28**, p. 124.

(4) Bache, H., and Benson, F. A.: 'Mean Noise Char teristics of Glow-Discharge Voltage-Regulator Tub *ibid.*, 1952, **24**, p. 328.

(5) Benson, F. A., and Bental, L. J.: 'Glow-Discha Stabilizers', *Wireless Engineer*, 1955, **32**, p. 330, a 'Glow-Discharge Tubes', *ibid.*, 1956, **33**, p. 33.

(6) Benson, F. A.: 'Gas-Filled Voltage Stabilizers', *Electro and Radio Engineer*, 1957, **34**, p. 16.

(7) Benson, F. A., and Gillespie, E. F. F.: 'Influence Argon Content on the Characteristics of Glow-Discha Tubes', *Proceedings I.E.E.*, Paper No. 2394 R, Septemb 1957 (**104** B, p. 498).

(8) Meissner, J.: 'Über den Einfluss der metastabi Anregungszustände auf die normale Stromdichte u den normalen Kathodenfall der Glimmentladung Edelgasen und Edelgasgemischen', *Zeitschrift für Phys* 1941, **117**, p. 325.

(9) Jurriaanse, T., Penning, F. M., and Moubis, J. H. 'The Normal Cathode Fall for Molybdenum and Z conium in the Rare Gases', *Philips Research Repo* 1946, **1**, p. 225.

(10) Benson, F. A.: 'Initial Drifts in Running Voltage of Glo Discharge Regulator Tubes', *Journal of Scientific Inst ments*, 1950, **27**, p. 71.

(11) Benson, F. A., and Mayo, G.: 'Effects of Ambie Temperature Variations on Glow-Discharge Tube Char teristics', *ibid.*, 1954, **31**, p. 118.

(12) Smith, J.: 'Temperature Coefficient of Maintenance Pot tial of Glow-Discharge Voltage-Stabilizer and Regula Tubes', *British Journal of Applied Physics*, 1958, **9**, p. 1

(13) 'The Impedance of Voltage-Stabilizer and Reference Tube *Mullard Technical Communications*, 1954, **1**, p. 219.

(14) Williams, M. O.: 'Inertia Effects in Cold-Cathode Tube *Strowger Journal*, 1952, **8**, p. 106.

(15) Kruithof, A. A., and Penning, F. M.: 'Townsend Ioni tion Coefficient α for Neon-Argon Mixtures', *Physi* 1937, **4**, p. 430.

(16) Penning, F. M.: 'Über die Zundspannung von Ar– Gemischen', *Zeitschrift für Physik*, 1931, **72**, p. 338.

7) PENNING, F. M., and MOUBIS, J. H. A.: 'The Contraction Phenomenon in a Neon Glow Discharge with Molybdenum Cathode', *Philips Research Reports*, 1946, **1** p. 119.
8) SEELIGER, R., and REGER, M.: 'Über die Stromdichte des normalen Kathodenfalles', *Annalen der Physik*, 1927, **83**, p. 535.
9) VON MURALT, A.: 'Über die normale Stromdichte bei der Glimmentladung', *ibid.*, 1928, **85**, p. 1117.
10) ULRICH, I. G.: 'Kathodenfall, Stromdichte und Dunkelraumdicke der normalen Glimmentladung in Edelgas-Wasserstoff Gemischen', *Wissenshaftliche Zeitschrift der Hochschule für Elektrotechnik, Ilmenau*, 1956, **2**, p. 145.
11) JURRIAANSE, T.: 'The Influence of Gas Density and Temperature on the Normal Cathode Fall of a Gas Discharge in Rare Gases', *Philips Research Reports*, 1949, **1**, p. 407.
12) BENSON, F. A., and BACHE, H.: 'A Note on Temperature Coefficient of Running Voltage of Glow-Discharge Tubes', *Journal of Scientific Instruments*, 1952, **29**, p. 25.
13) VAN GEEL, C.: 'Untersuchungen von Gasenladungen mit Rüchsicht aug ihre dynamischen Eigenschaften und ihre Stabilität', *Physica*, 1939, **6**, p. 806.
14) VERHAGEN, C. J. D. M.: 'Impedanzmessungen an Gasentladungs-röhen', *ibid.*, 1941, **8**, p. 361.
15) VAN GEEL, C.: 'Influence of Self-Induction and After-Effect in Gas Discharges on their Stability', *Applied Scientific Research*, Part B, 1955, **5**, p. 79.
16) YEH, C.: 'Note on Positive-Ion Transit Time in Glow-Discharge Tubes', *Journal of Applied Physics*, 1956, **27**, p. 98.

(8) APPENDIX

nfluence of Ambient-Temperature Variations on the Running Voltage of a Glow-Discharge Tube

The change of running voltage with temperature can be ccounted for by a change of pressure in the tube, and f the running-voltage/pressure characteristic is known, the oltage/temperature coefficient can be estimated.

Consider a discharge tube of total volume v divided into wo regions as shown in Fig. 14, one in the neighbourhood of

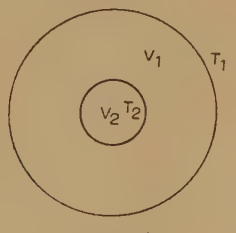

Fig. 14

ie cathode, of volume v_2 and temperature T_2, and the other, ie rest of the tube, of volume v_1 and temperature T_1 (the glass-nvelope temperature).

Neglecting any heat transfer due to radiation and conduction rough the electrode leads, the heat flow from the cathode to ie walls is

$$W = -Ka(dT/dx) \quad . \quad . \quad . \quad . \quad . \quad (1)$$

T/dx being the temperature gradient in a direction x.

For a cylindrical cathode and tube envelope as illustrated in ction in Fig. 15, the heat flow per second from the cylindrical rface to the walls at radius r is

$$W = -2\pi hrK(dT/dr) \quad . \quad . \quad . \quad . \quad . \quad (2)$$

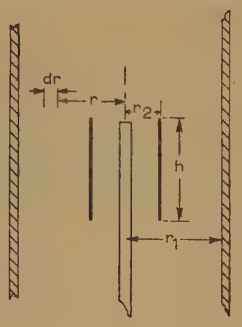

Fig. 15

For inert gases, $K = AT^N \quad . \quad . \quad . \quad . \quad . \quad . \quad . \quad (3)$

so that $W = -2\pi hrAT^N(dT/dr) \quad . \quad . \quad . \quad . \quad (4)$

Integrating from r_2 to r_1:

$$W = \frac{2\pi hA(T_2^{N+1} - T_1^{N+1})}{(N+1)\log_e \frac{r_1}{r_2}} \quad . \quad . \quad . \quad . \quad (5)$$

W can be estimated from the electrical power input, i.e.

$$W = \eta IV/4{\cdot}2 \text{ cal/sec} \quad . \quad . \quad . \quad . \quad . \quad (6)$$

In this expression, η is the fraction of the power converted to heat per second. (A small heat flow takes place from the ends of the cylinders which was reduced in Jurriaanse's measurements[21] by confining the discharge between quartz plates.) In the calculations which follow, η has been taken as 0·7. Initially, the tube is filled with gas at room temperature, so that

$$P_0 = k\rho_0 T_0 \quad . \quad . \quad . \quad . \quad . \quad . \quad (7)$$

where k is a constant.

Also $$P_1 = k\rho T = k\rho_2 T_2 \quad . \quad . \quad . \quad . \quad . \quad (8)$$

Further, since the total mass of gas is unaltered,

$$\rho_2 v_2 + \int_{v_1} \rho dv = \rho_0 v \quad . \quad . \quad . \quad . \quad . \quad (9)$$

From eqns. (8) and (9),

$$\rho_2 v_2 + \rho_2 T_2 \int_{v_1} dv/T = \rho_0 v \quad . \quad . \quad . \quad (10)$$

Now, $\int_{v_1} dv/T$ is difficult to evaluate for the case of a cylindrical structure, so consider a simpler case in rectangular co-ordinates (Fig. 16).

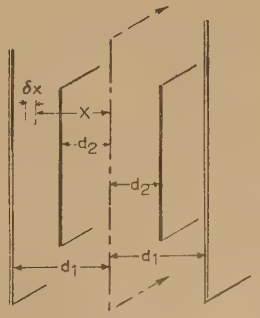

Fig. 16

Eqn. (5) now becomes

$$W = \frac{aA(T_2^{N+1} - T_1^{N+1})}{(d_1 - d_2)(N+1)} \quad . \quad . \quad . \quad . \quad (11)$$

At any point distance x from the axis where the temperature is T,

$$W = \frac{aA(T_2^{N+1} - T^{N+1})}{(x - d_2)(N+1)} \quad . \quad . \quad . \quad . \quad (12)$$

and eqn. (10) becomes

$$\rho_2 v_2 + \rho_2 T_2 \int_{d_2}^{d_1} \frac{adx}{[T_2^{N+1} - W(x - d_2)(N+1)/aA]^{1/(N+1)}} = \rho_0 v \quad . \quad . \quad . \quad . \quad (13)$$

i.e.

$$\rho_2 v_2 + \frac{\rho_2 T_2 v_1 (N+1)(T_2^N - T_1^N)}{N(T_2^{N+1} - T_1^{N+1})} = \rho_0 v \quad . \quad . \quad (14)$$

Using eqns. (7) and (8) this gives

$$P_1 = \frac{P_0 v T_2}{T_0\left[v_2 + \frac{v_1 T_2 (N+1)(T_2^N - T_1^N)}{N(T_2^{N+1} - T_1^{N+1})}\right]} \quad . \quad . \quad (15)$$

or

$$P_1 = \frac{P_0 T_2}{T_0\left[\frac{v_2}{v} + \frac{v_1 T_2 (N+1)(T_2^N - T_1^N)}{vN(T_2^{N+1} - T_1^{N+1})}\right]} \quad . \quad . \quad (16)$$

For small temperature variations, say T_2 from 20 to 40° C, such that dV/dP_1 is approximately constant for varying P_1,

$$\frac{dP_1}{dT_1} = \frac{P_0\left[\frac{v_2}{v}\left(\frac{T_1}{T_2}\right)^N + \frac{v_1(N+1)T_1^{N-1}T_2(T_2 - T_1)}{v(T_2^{N+1} - T_1^{N+1})}\right]}{T_0\left[\frac{v_2}{v} + \frac{v_1(N+1)(T_2^{N+1} - T_1^N T_2}{vN(T_2^{N+1} - T_1^{N+1})}\right]^2} \quad . \quad (17)$$

If $v_1/v \gg v_2/v$ (in the present investigations $v_1/v \simeq 0{\cdot}97$ and $v_2/v \simeq 0{\cdot}03$) eqn. (17) simplifies to

$$\frac{dP_1}{dT_1} \simeq \frac{P_0 N^2 (T_2^{N+1} - T_1^{N+1}) T_1^{N-1}(T_2 - T_1)}{T_0 T_2 (N+1)(T_2^N - T_1^N)^2} \quad . \quad (18)$$

and so

$$\frac{dV}{dT_1} = \frac{dV}{dP}\left[\frac{P_0 N^2 (T_2^{N+1} - T_1^{N+1}) T_1^{N-1}(T_2 - T_1)}{T_0 T_2 (N+1)(T_2^N - T_1^N)^2}\right] . \quad (19)$$

The changes of running voltage with temperature have be calculated for pure neon and neon with 0·5% argon usi eqn. (19) and Jurriaanse's running-voltage/pressure curves. the calculations the figures for the gas constants A and N quot by Jurriaanse have been used and T_1 has been taken as 30° In the case of pure neon at a pressure of 40 mm Hg Jurriaans curves give $dV/dP = -0{\cdot}127$ volts/mm, and so, from eqn. (1 $dV/dT_1 = -17{\cdot}0$ mV/°C.

Jurriaanse's measured value for this tube was −16·5 mV p deg C, and the measured value for a pure-neon tube used duri the present studies was −17·2 mV per deg C. For neon ar 0·5% argon mixtures, $dV/dP = -0{\cdot}034$ volts/mm. The c culated value of dV/dT_1 is −4·7 mV per deg C, and the measur value recorded during the present investigations was −5·0m per deg C.

For pure-argon tubes, $dV/dT_1 \simeq -4{\cdot}7$ mV per deg C, ar Jurriaanse's measured value was −4·3 mV per deg C.

For larger temperature changes when P_1 varies so th dV/dP_1 is no longer constant, the change in running voltage c still be estimated if the form of the equation for the runnin voltage/pressure curve is known. For example, with pure-ne tubes Jurriaanse found that the following empirical relationsh holds:

$$V = 124 - 12 \log_{10} P \quad . \quad . \quad . \quad . \quad (2$$

Substituting eqn. (16) in eqn. (20) and assuming $v_1/v \gg v_2/v$,

$$V = 124 - 12 \log_{10} \frac{P_0 N (T_2^{N+1} - T_1^{N+1})}{T_0 (N+1)(T_2^N - T_1^N)} \quad . \quad (2$$

Suppose T_1 is varied from 20° C (T_1') to 100° C (T_1'') and th running voltages at these temperatures are V_1 and V_2 respe tively; then

$$V_1 - V_2 \simeq 12 \log_{10} \frac{(T_2')^N - (T_1')^N}{(T_2'')^N - (T_1'')^N} \quad . \quad . \quad (22$$

Over the temperature range 20–100° C, $V_1 - V_2 = 1{\cdot}18$ volt The corresponding measured value is 1·21 volts. It is difficu to fit a curve to Jurriaanse's results for the neon-argon mixtur but it is interesting to note that at pressures around 40 mm H the slope of the running-voltage/pressure curve decreases fo increasing pressure.

[The discussion on the above paper will be published in the September, 1959, issue of this Part of the *Proceedings*.]

621.376.2/.3

The Institution of Electrical Engineers
Monograph No. 322 R
Dec. 1958

A COMPARISON OF THE TRANSIENT RESPONSE OF AMPLITUDE-MODULATED AND FREQUENCY-MODULATED SIGNALS

By S. J. COTTON, B.Sc., Associate Member.

(*The paper was first received* 2nd *June, and in revised form* 9th *September*, 1958. *It was published as an* INSTITUTION MONOGRAPH *in December*, 1958.)

SUMMARY

The paper is an analytical investigation of the transient response of resistance-capacitance and resistance-inductance circuits, filters and transmission lines to a frequency-modulated voltage, using a unit-step function as modulating signal. The transient response is compared with that which is known to occur when the voltage is amplitude modulated, using the same modulating signal. The effects, on the response, of the bandwidth of circuits subsequent to the detector stage of a receiver are compared for the two types of modulation.

LIST OF PRINCIPAL SYMBOLS

t, τ = Time.
p = Complex angular frequency.
$z(p)$ = Complex impedance.
$\tilde{\omega}$ = Instantaneous angular frequency.
ω_0 = Resonant angular frequency.
$\tilde{x} = \tilde{\omega} - \omega_0$.
ω_1 = Initial angular frequency.
$x_1 = \omega_1 - \omega_0$.
ω_2 = Final angular frequency.
$x_2 = \omega_2 - \omega_0$.
ω_3, ω_4 = Intermediate angular frequencies.
a = Decay factor.
Y = Amplitude of signal of resonant frequency and considered as of the form $A\varepsilon^{-at}$.
X = Amplitude of signal of angular frequency ω_2.
ϕ = Phase angle of signal of resonant frequency relative to that of angular frequency ω_2.
θ = Phase angle of resultant signal with respect to that of angular frequency ω_2.
Δx = Small angular frequency jump.

(1) INTRODUCTION

The problem of the distortion of f.m. signals by linear passive networks has received increasing attention over the past fifteen years. The response of the network has usually been given in two parts, the quasi-steady-state response and the transient response. Most of the workers on the problem have limited themselves to the quasi-steady-state response, but for time-division multiplex systems and television transmission the modulating signal is in the form of pulses and the transient response becomes of importance. The paper is therefore devoted to this latter response.

Salinger,[1] Bell[2] and Gumowski[3] have investigated the transient response of filters to f.m. signals, assuming an instantaneous jump in the signal frequency, but each obtains a different result. Salinger and Bell compare their results with the transient response to a.m. signals.

Salinger considers an ideal filter, the sole effect of which is to restrict the range of frequencies transmitted. He obtains the result that the response to unit transient has already reached half-amplitude at the instant the transient occurs, the first half of the response appearing to take place prior to the transient. This is obviously impossible, and the anomaly is due to using an ideal filter which has properties inconsistent with those of real filters.

Bell, therefore, uses a simple *LRC* circuit and, by the method of the Laplace transform, finds there are two signals produced, one having a frequency equal to the final frequency of the applied signal, and the other having a frequency equal to the natural frequency of the circuit. He then finds the resultant frequency from an equation which assumes that the amplitudes of both of these signals remain constant, whereas, in fact, the signal of natural frequency is decaying exponentially. This variation, he says, can be neglected for high-Q circuits, but in the subsequent Sections of the paper it will be shown that the effect of this variation cannot be neglected. From his equation, Bell finds that the resultant frequency is made up of one component that varies exponentially with time and a number of components which are varying sinusoidally and produce a 'frequency flutter'. He assumes that this flutter component will be eliminated by subsequent circuits, and shows that the component that is left makes a sudden jump in frequency at the instant of the transient and then varies exponentially, tending to reach the new frequency of the applied signal. According to this result, if the response from the filter were applied to a perfect detector, the output would be as shown in Fig. 1, whereas the output from the detector if the applied signal had been amplitude modulated would be as shown in Fig. 2, which has no sudden jump, but a gradual exponential rise all the way.

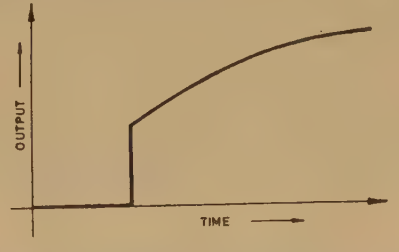

Fig. 1.—Demodulated response of *LRC* circuit to f.m. signal according to Bell's result.

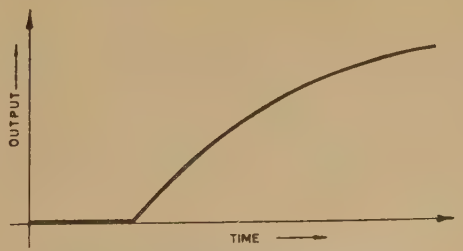

Fig. 2.—Demodulated response of *LRC* circuit to a.m. signal.

Correspondence on Monographs is invited for consideration with a view to publication.
Mr. Cotton is Senior Lecturer in Electrical Engineering at the Nottingham and District Technical College.

Gumowski tackles the problem using the Fourier transform, but finds that, for a unit-step modulating function, the Fourier transform does not exist in the Riemann sense because of the divergent integrals produced. He overcomes this difficulty by considering these integrals in the sense of the distribution theory, instead of in the Riemann sense, and gives curves of the output from a perfect detector, which in shape are similar to that of Fig. 2; i.e. there is no sudden jump but an exponential rise, as in the case of the a.m. signal.

It is the purpose of the succeeding Sections to determine which conclusion is correct, and to compare the responses of other types of circuit to a.m. and f.m. signals.

(2) ENERGY STORED IN ELECTRIC AND MAGNETIC FIELDS DURING THE PASSAGE OF AMPLITUDE-MODULATED AND FREQUENCY-MODULATED SIGNALS

If we consider an alternating current to be passing through an inductor and capacitor in series, the total energy stored in the magnetic and electric fields remains constant if the amplitude of the current remains constant, although it is continuously being interchanged between the two fields. If now there is a sudden jump in the amplitude of the current, as will occur in pulsed-a.m., there will also be a jump in the energy stored in the fields; but, owing to the resistance that is necessarily present in a practical circuit if it is passive, this change will be accompanied by a transient which will produce envelope distortion in the p.d.'s across the inductor and capacitor.

If the frequency of the current, instead of the amplitude, is made to jump, there will also be a variation in the amplitude of the p.d. produced across the capacitor, due to the change in circuit impedance, so that this voltage will possess a hybrid modulation. If pure frequency modulation is to be preserved, some form of limiter must be incorporated in the circuit. If the limiter is applied directly across the capacitor, the amplitude of the voltage across the capacitor will be constant, so that the energy stored in the fields will remain constant, and there will not be any transient. This may also be considered as due to the fact that the limiter will have a damping effect on the circuit, and it will be seen that it would make the Q-factor of the circuit so small that it would not be of any practical value.

The case when there is not any limiter will now be considered. A transient will be produced, which may or may not be oscillatory; its effect on the resultant instantaneous frequency of the voltage will be discussed in Section 4.

If we are to compare the response of a circuit to an a.m. voltage with its response to an f.m. voltage, we must have identical conditions. For this comparison, therefore, the circuit must be considered without a limiter, and in the case of the f.m. voltage the current produced will have a hybrid modulation.

(3) EFFECTS ON THE SIGNAL FREQUENCY OF TRANSIENT OSCILLATIONS IN A FILTER CIRCUIT

If a train of damped oscillations at the natural frequency of the circuit is set up by a sudden change in signal frequency, and if the final frequency of the applied voltage is different from the natural frequency of the circuit, there will be present, for an interval of time, two signals, which will give a resultant of varying amplitude and frequency. The theory for the resultant of two signals of constant amplitude but different frequencies has already been published.*

The subject is treated more fully in the Appendix, where the effect of the amplitude of one signal dying away exponentially and also the effect of a phase displacement of the two signals the time origin are considered. Bell[2] ignores the latter po and assumes the former to be negligible for high-Q circuits.

The resultant instantaneous angular frequency is given [see eqn. (21) in the Appendix]

$$\tilde{\omega} = \frac{\omega_0 Y^2 + \omega_2 X^2 + (\omega_2 + \omega_0) XY \cos(-x_2 t + \phi) - aXY \sin(-x_2 t +}{X^2 + Y^2 + 2XY \cos(-x_2 t + \phi)} \quad . \quad . \quad . \quad . \quad ($$

Since $\omega_2 = \omega_0 + x_2$, this equation could be written

$$\omega = \omega_0 + \frac{x_2 X^2 + XY[x_2 \cos(-x_2 t + \phi) - a \sin(-x_2 t + \phi}{X^2 + Y^2 + 2XY \cos(-x_2 t + \phi)} \quad . \quad . \quad ($$

or

$$\tilde{\omega} = \omega_0 + \tilde{x} \quad . \quad . \quad . \quad . \quad . \quad . \quad . \quad ($$

so that $\tilde{x}$ gives the difference between the resultant frequen and the natural frequency of the circuit.

Since Bell did not consider the phase angle ϕ and neglect the decay factor a, his expression for the instantaneous frequen of the response to the f.m. signal was

$$\tilde{\omega} = \frac{\omega_0 Y^2 + \omega_2 X^2 + (\omega_2 + \omega_0) XY \cos x_2 t}{X^2 + Y^2 + 2XY \cos x_2 t} \quad . \quad ($$

He points out that this expression will give a slowly-varyi mean frequency owing to the terms containing ω_0, ω_2, X and only, together with a frequency 'wobble' or 'flutter' produc by the cosine terms.

In an f.m. receiver, the demodulated signal after the detect will have a frequency governed by the rate of change of frequen of the r.f. signal. These cosine terms will therefore produ angular frequencies of x_2 in the demodulated signal. The flutter terms may be of quite high frequency if x_2 is large, a they may produce frequencies after the detector of a receiv which are outside the pass-band of the audio or video amplifi To get a fair comparison between the a.m. and f.m. respons however, we must not introduce any constraint from a subs quent part of the circuit. We shall therefore first investiga the response containing these flutter frequencies and compa it for a.m. and f.m. signals. The effect of removing the flutt frequencies can then be investigated. We can write

$$\tilde{x} = \frac{x_2 X^2 + XY[x_2 \cos(-x_2 t + \phi) - a \sin(-x_2 t + \phi)]}{(X^2 + Y^2)\left[1 + \frac{2XY}{X^2 + Y^2} \cos(-x_2 t + \phi)\right]}$$

and since

$$X^2 + Y^2 > 2XY \quad \text{if } X \neq Y$$

$$\tilde{x} = \{x_2 X^2 + XY[x_2 \cos(-x_2 t + \phi) - a \sin(-x_2 t + \phi)]\}$$

$$(X^2 + Y^2)^{-1} \times \left[1 + \frac{2XY}{X^2 + Y^2} \cos(-x_2 t + \phi)\right]^{-1} \quad .$$

If this is expanded, we shall obtain an infinite series of flut terms of angular frequency x_2 and its higher harmonics, an flutterless series given by

$$\tilde{x} = \frac{x_2 X^2}{X^2 + Y^2} - \frac{(x_2 - 2a \sin\phi \cos\phi) X^2 Y^2}{(X^2 + Y^2)^2}$$

$$\left[1 + \frac{X^2 Y^2}{2(X^2 + Y^2)^2} + \frac{X^4 Y^4}{4(X^2 + Y^2)^4} + \ldots\right.$$

* See *Wireless Engineer*, 1943, 20, p. 233.

Since the infinite series in square brackets is convergent, it will have a sum to infinity equal to

$$\frac{2(X^2+Y^2)^2}{2X^4+3X^2Y^2+2Y^4}$$

so that the instantaneous frequency component without flutter will be given by

$$\tilde{x} = \frac{x_2X^2}{X^2+Y^2} - \frac{2X^2Y^2(x_2 - 2a\sin\phi\cos\phi)}{2X^4+3X^2Y^2+2Y^4} \quad . \quad (6)$$

It will be seen that this frequency component is affected both by the decay factor and the initial phase angle.

Bell, to obtain the mean frequency from eqn. (4) without the flutter components, just ignores the cosine terms, which gives

$$\tilde{\omega} = \frac{\omega_0Y^2+\omega_2X^2}{X^2+Y^2}$$

or

$$\tilde{x} = \frac{x_2X^2}{X^2+Y^2} \quad . \quad . \quad . \quad . \quad . \quad . \quad (7)$$

This is wrong, since if eqn. (4) is expanded in the same way as eqn. (5), the equation corresponding to eqn. (6) will be

$$\tilde{x} = \frac{x_2X^2}{X^2+Y^2} - \frac{2x_2X^2Y^2}{2X^4+3X^2Y^2+2Y^4} \quad . \quad . \quad (8)$$

Thus eqn. (7) is wrong and differs from eqn. (6) because

(*a*) The cosine terms of eqn. (4) have been neglected before this expression has been expanded.

(*b*) The decay factor a and the phase angle ϕ have been neglected.

Thus, because eqn. (7) has been used instead of the correct equation (6), Bell's result for the instantaneous frequency of the response to the f.m. signal is wrong. Furthermore, by using the instantaneous frequency of the f.m. response when $t = 0$, obtained from eqn. (7), and comparing it with the a.m. response when $t = 0$, Bell is adding the further constraint of the detector and a.f. amplifier in removing the effect of the flutter frequencies. To have made a fair comparison he ought to have used eqn. (5); when $t = 0$ this becomes

$$\tilde{x} = \frac{x_2X^2 + XY(x_2\cos\phi - a\sin\phi)}{X^2+Y^2+2XY\cos\phi} \quad . \quad . \quad . \quad (9)$$

(4) INVESTIGATION OF THE TRANSIENT RESPONSE OF ACTUAL CIRCUITS TO A FREQUENCY-MODULATED SIGNAL

Since the transient response of circuits to a.m. signals is well known, only the response to f.m. signals will be investigated in this Section.

(4.1) Resistance-Capacitance and Resistance-Inductance Circuits

If the transfer function $F(p)$ of the *RC* or *RL* circuit contains two or more poles, the transient produced by such a circuit when the applied signal is suddenly changed in amplitude or frequency may be oscillatory, in which case the problem can be dealt with in a way similar to that explained in Section 4.2. If, however, there is only one pole, as there would normally be for a simple coupling circuit where a typical transfer function would be $F(p) = p/(p + 1/RC)$, the transient would be of the form $A\varepsilon^{-(1/RC)t}$. This is non-oscillatory and dies away exponentially.

If eqn. (21) is now used to find the resultant instantaneous frequency, ω_0 and ϕ must be made equal to zero, when

$$\tilde{\omega} = \omega_2 + \frac{Y}{X}(\omega_2\cos\omega_2t + a\sin\omega_2t)\left(1+\frac{2Y}{X}\cos\omega_2t\right)^{-1} . \quad (10)$$

Of the two expressions on the right-hand side of this equation, the first gives the final steady angular frequency ω_2, while the second gives the transient-frequency term which dies away. If this transient expression is expanded, two distinct series in Y/X will be obtained, one without any trigonometrical terms which gives the steadily decaying part, and the second with sine and cosine terms of the angles ω_2t, $2\omega_2t$, $3\omega_2t$, etc., which gives the flutter-frequency component. Since the flutter frequencies are either equal to or an integral multiple of the signal frequency, they show how the instantaneous frequency varies over one cycle of the signal. The steadily decaying part is due to the fact that the successive periodic times T_1, T_2, T_3, etc., of Fig. 3

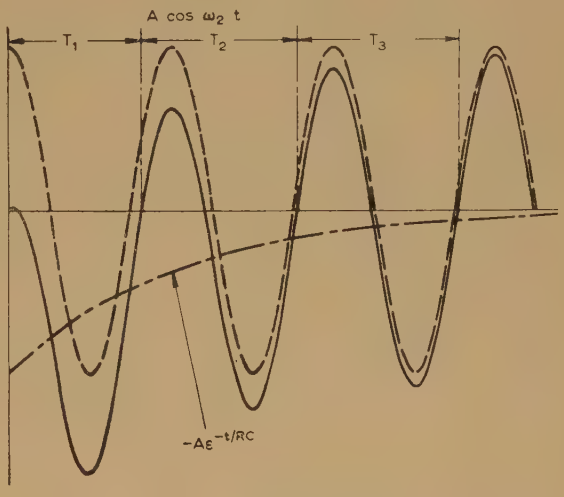

Fig. 3.—Cosine curve added to exponential curve.

(which is merely a cosine curve added to an exponentially decaying curve) are varying.

In practice the exponential transient can be almost removed, leaving only the final steady-state cosine signal, which then will not suffer any appreciable frequency distortion.

(4.2) Single-Tuned Circuits

Since the responses of parallel- and series-tuned circuits are almost identical if we consider dual quantities, only the series circuit will be considered.

Let the circuit impedance be given by

$$Z(p) = R + pL + \frac{1}{pC} \quad . \quad . \quad . \quad . \quad (11)$$

and let the p.d. across the circuit have an angular frequency ω_1, so that, considering the positive frequency component only, we can write

$$v(t) = \varepsilon^{j\omega_1t} \quad . \quad . \quad . \quad . \quad . \quad . \quad (12)$$

If the amplitude of this p.d. remains constant but its angular frequency suddenly changes to ω_2 at time $t = \tau$, the Laplace transform of $v(t)$ is

$$v(p) = \int_0^\tau \varepsilon^{(j\omega_1-p)t}dt + \int_\tau^\infty \varepsilon^{(j\omega_2-p)t}dt$$

$$\text{or } v(p) = \frac{1}{p - j\omega_1} - \frac{1}{p - j\omega_1}\varepsilon^{(j\omega_1 - p)\tau} + \frac{1}{p - j\omega_2}\varepsilon^{(j\omega_2 - p)\tau} \quad . \quad (13)$$

The first term on the right-hand side of this equation represents the application of a signal of angular frequency ω_1 at time $t = 0$, the second term represents its removal at time $t = \tau$, and the third term represents the application of a signal of equal amplitude and angular frequency ω_2 at time $t = \tau$. Since the circuit is linear, each of these terms can be applied separately and their responses summed. The current due to the first term is

$$i_1(p) = \left(\frac{1}{p - j\omega_1}\right)\frac{1}{Z(p)}$$

Now $$Z(p) = \frac{L}{p}(p - p_1)(p - p_2)$$

where $$p_1 = -a + \sqrt{(a^2 - \omega_0^2)}$$

$$p_2 = -a - \sqrt{(a^2 - \omega_0^2)}$$

$$a = \frac{R}{2L}, \qquad \omega_0^2 = \frac{1}{LC}$$

If $$a < \omega_0$$

then $$p_1 = -a + j\sqrt{(\omega_0^2 - a^2)}$$

$$p_2 = -a - j\sqrt{(\omega_0^2 - a^2)}$$

Therefore, by partial fractions,

$$i_1(p) = \frac{1}{L(p_1 - p_2)}\left[\frac{p_1}{p_1 - j\omega_1}\left(\frac{1}{p - p_1} - \frac{1}{p - j\omega_1}\right) - \frac{p_2}{p_2 - j\omega_1}\left(\frac{1}{p - p_2} - \frac{1}{p - j\omega_1}\right)\right]$$

Assuming that $a \ll \omega_0$ so that the natural frequency can be taken as ω_0,

then $$p_1 \simeq -a + j\omega_0 \text{ and } p_2 = -a - j\omega_0$$

By the inverse transform,

$$i_1(t) = \frac{1}{2j\omega_0 L}\left[\frac{-a + j\omega_0}{-a - j(\omega_1 - \omega_0)}(\varepsilon^{p_1 t} - \varepsilon^{j\omega_1 t}) + \frac{a + j\omega_0}{-a - j(\omega_1 + \omega_0)}(\varepsilon^{p_2 t} - \varepsilon^{j\omega_1 t})\right] \quad . \quad (14)$$

The terms containing $\varepsilon^{p_1 t}$ and $\varepsilon^{p_2 t}$ are transient terms produced when the original signal was applied, so that when these have died away we are left with

$$i_1(t) = \frac{\varepsilon^{j\omega_1 t}}{2j\omega_0 L}\left[\frac{a + j\omega_0}{a + j(\omega_1 + \omega_0)} - \frac{a - j\omega_0}{a + j(\omega_1 - \omega_0)}\right] \quad . \quad (15)$$

If we now measure time from the instant the frequency jump occurs, by making $\tau = 0$, the second term of eqn. (13) becomes $-1/(p - j\omega_1)$ and produces a current similar to that of eqn. (14) but negative, so that

$$i_2(t) = -\frac{1}{2j\omega_0 L}\left[\frac{-a + j\omega_0}{-a - j(\omega_1 - \omega_0)}(\varepsilon^{p_1 t} - \varepsilon^{j\omega_1 t}) + \frac{a + j\omega_0}{-a - j(\omega_1 + \omega_0)}(\varepsilon^{p_2 t} - \varepsilon^{j\omega_1 t})\right] \quad . \quad (16)$$

Adding eqns. (15) and (16), we are left with only the transient terms, so that

$$i_1(t) + i_2(t) = \frac{1}{2j\omega_0 L}\left[\frac{-a + j\omega_0}{a + j(\omega_1 - \omega_0)}\varepsilon^{p_1 t} + \frac{a + j\omega_0}{a + j(\omega_1 + \omega_0)}\varepsilon^{p_2 t}\right]$$

. . . . . (17)

The third term of eqn. (13) will also produce a current given by an expression similar to that of eqn. (14) with ω_1 changed to ω_2, so that the total current, if we write $\varepsilon^{p_1 t} = \varepsilon^{-at}\varepsilon^{j\omega_0 t}$ and $\varepsilon^{p_2 t} = \varepsilon^{-at}\varepsilon^{-j\omega_0 t}$, will be given by

$$i(t) = \frac{1}{2j\omega_0 L}\left\{\left[\left(\frac{1 - j\frac{\omega_0}{a}}{1 + j\frac{\omega_2 - \omega_0}{a}} - \frac{1 - j\frac{\omega_0}{a}}{1 + j\frac{\omega_1 - \omega_0}{a}}\right)\varepsilon^{+j\omega_0 t} + \left(\frac{1 + j\frac{\omega_0}{a}}{1 + j\frac{\omega_1 + \omega_0}{a}} - \frac{1 + j\frac{\omega_0}{a}}{1 + j\frac{\omega_2 + \omega_0}{a}}\right)\varepsilon^{-j\omega_0 t}\right]\varepsilon^{-at} + \left(\frac{1 + j\frac{\omega_0}{a}}{1 + j\frac{\omega_2 + \omega_0}{a}} - \frac{1 - j\frac{\omega_0}{a}}{1 + j\frac{\omega_2 - \omega_0}{a}}\right)\varepsilon^{+j\omega_2 t}\right\} \quad . \quad (18)$$

If ω_1 and ω_2 are both nearly equal to ω_0, $\omega_2 + \omega_0 \gg \omega_2 - \omega_0$ and $\omega_1 + \omega_0 \gg \omega_1 - \omega_0$, so that the value of the $\varepsilon^{-j\omega_0 t}$ term is negligible and the value of the $\varepsilon^{j\omega_2 t}$ term is approximately

$$-\frac{1 - j\frac{\omega_0}{a}}{1 + j\frac{\omega_2 - \omega_0}{a}}$$

Also $\omega_0/a = 2Q$, so that if Q is large, e.g. 100 or more,

$$1 - j\frac{\omega_0}{a} \simeq -2jQ$$

and therefore

$$i(t) \simeq \frac{Q}{\omega_0 L}\left[\left(\frac{1}{1 + j\frac{\omega_1 - \omega_0}{a}} - \frac{1}{1 + j\frac{\omega_2 - \omega_0}{a}}\right)\varepsilon^{-at}\varepsilon^{j\omega_0 t} + \frac{1}{1 + j\frac{\omega_2 - \omega_0}{a}}\varepsilon^{j\omega_2 t}\right]$$

Now $Q/\omega_0 L = 1/R$, so that writing $\omega_1 - \omega_0 = x_1$ and $\omega_2 - \omega_0 = x_2$,

$$i(t) \simeq \frac{\varepsilon^{j\omega_0 t}}{R\left(1 + j\frac{x_2}{a}\right)}\left[\frac{j\frac{x_2 - x_1}{a}}{1 + j\frac{x_1}{a}}\varepsilon^{-at} + \varepsilon^{jx_2 t}\right] \quad . \quad (19)$$

This agrees with eqn. (16) of the paper by Gumowski.[3]

Determining the instantaneous frequency from eqn. (2) we get, for time $t = 0$,

$$\tilde{\omega}_{t=0} = \omega_0 + \frac{a^2 x_2 + x_1^2 x_2 + (x_2 - x_1)(x_2 x_1 - a^2)}{x_2^2 + a^2}$$

$$= \omega_0 + x_1$$

so that $\tilde{\omega}_{t=0} = \omega_1$

This shows that there is not any sudden frequency jump, but a smooth change from ω_1 to ω_2. The detected output would therefore be similar to the detected output using an a.m. signal.

One point may be of interest in passing. If $\omega_2 = \omega_0$, i.e. $x_2 = 0$, both components of the response, as given by eqn. (19), have the same angular frequency ω_0, and it might be thought that the instantaneous frequency would always be ω_0, i.e. that there would be an instantaneous jump from ω_1 to ω_0. However, owing to the initial phase angle between the two components and the decaying amplitude of the transient term, the frequency at $t = 0$ is still ω_1.

(4.2.1) Effect of Bandwidth of Circuits Subsequent to the Detector.

If these circuits eliminate the effect of the frequency-flutter components, we can find the instantaneous frequency from eqn. (6) and the result will be affected by the values of ω_1 and ω_2. Several particular cases will therefore be taken.

Case (a). A frequency jump between the two half-power frequencies of the circuit response curve.

In this case $x_1 = -a$ and $x_2 = +a$, so that at time $t = 0$, the value of Y of eqn. 6 is $\sqrt{2}$. Substituting these values in eqn. (6) gives $\tilde{x}_{t=0} = -a/6$.

The removal of some of the frequency components has therefore resulted in an instantaneous frequency jump from $(\omega_0 - a)$ to $(\omega_0 - a/6)$.

Case (b). A small frequency jump near to one half-power frequency of the circuit response curve.

Let $x_1 = a$ and $x_2 = a + \Delta x$ so that when $t = 0$ $Y^2 = \Delta x^2/2a^2$.

Then, when $t = 0$,

$$\tilde{x}_{t=0} = a + \Delta x - \frac{\Delta x^2}{2a} - \frac{\Delta x^3}{a^2} \cdots$$

Thus the smaller the value of Δx compared with a, the closer are the instantaneous frequency jumps from ω_1 to ω_2.

Case (c). Final frequency equal to the resonant frequency of the circuit.

Here $\omega_2 = \omega_0$, so that x_2 is now zero and there will not be any frequency flutter. The bandwidth of any subsequent circuit will not affect the response by removing any flutter terms, so that the response will be as given in Section 4.2.

Case (d). Frequency jump from the resonant frequency of the circuit to one of the half-power frequencies of the circuit response curve.

Let the frequency jump from ω_0 to $\omega_0 + a$. Then $x_1 = 0$ and $x_2 = a$, so that when $t = 0$, $Y = 1$ and $\tilde{x}_{t=0} = 3a/14$. There is thus an instantaneous frequency jump from ω_0 to $(\omega_0 + 3a/14)$.

(4.2.2) Effects of Limiter.

As Brown[5] points out in the conclusion to his paper, it is often tacitly assumed in the literature that the amplitude-limiting process does not of itself introduce f.m. distortion, but in general this is not true, and there is need for further investigation into this problem.

It would appear that the effect of the limiter depends on its position in the overall circuit. If the limiter were in the filter circuit so that the limiter characteristic modified the filter characteristic, it would damp out any oscillatory transient but would also lower the Q-factor of the circuit. If, on the other hand, it were separated from the filter in such a way that its effect would not be reflected on to the filter characteristic, the oscillatory transient would develop and affect the resultant frequency in the way that has been shown. The limiter would then control the amplitude of the resultant signal but would not affect its frequency. It would be interesting to investigate these two cases in practice.

(4.3) Lines With Discontinuity

If a constant-voltage constant-frequency signal is considered to be applied to an open-circuited line, the voltage applied is equal to the vector sum of the voltage of the incident wave and that of the reflected wave at the input terminals. If now the angular frequency jumps from its initial value (say ω_1) to a higher value ω_2, but the amplitude remains the same, then for a time τ, equal to that taken by the wave to travel down the line and back again, the reflected wave will still have a frequency ω_1. This means that the frequency of the incident wave must assume a value ω_3, such that, when the incident and reflected waves are added, we get a resultant frequency [as given by an equation similar to eqn. (2) with $a = 0$] equal to ω_2. This means that ω_3 will be greater than ω_2. After the time τ, the reflected wave arriving at the input terminals will have this new frequency ω_3. The incident wave will therefore suddenly jump to a new value ω_4, less than ω_2, so that the resultant input-terminal voltage will still have a frequency ω_2. Thus the incident-wave frequency will experience sudden jumps of decaying value about ω_2, until it eventually attains the value ω_2.

If, instead of the line being open-circuited, it is connected to another line of different characteristic impedance, there will still be a reflected wave in the first line, so that the theory outlined above will hold. The voltage wave travelling down the second line will be some fraction of the incident voltage wave of the first line and will therefore have the same frequency transients as this wave.

It will be observed that, owing to the flutter components of eqn. (2), frequencies such as ω_3 and ω_4 will be continuously variable. During this transient period, also, the incident wave will possess amplitude modulation at the flutter frequency.

(5) CONCLUSIONS

(*a*) *RC and RL circuits.*—The response of these types of circuit to an f.m. wave, unlike their response to an a.m. wave, may not suffer any transient distortion since the transient term can be removed; so that for amplifier circuits, if the transient response only is considered, it would appear that frequency modulation would be preferable to amplitude modulation.

(*b*) *Filter circuits.*—The response of this type of circuit to an f.m. wave is similar to its response to an a.m. wave. Subsequent circuits, however, can modify the final response. For a.m. waves, restriction of the bandwidth of the circuits after the detector stage of a receiver will reduce the higher harmonics of any pulses and produce pulse distortion. For f.m. waves, such a restriction will not only reduce the higher harmonics but will also reduce the components produced by the frequency flutter. It has been shown that the removal of these latter components improves the transient response for a pulse by giving an instantaneous jump at the beginning of the pulse. If, therefore, the frequency deviation of the f.m. wave is large, so that the restriction of the bandwidth of the amplifier after the detector is sufficient to remove these flutter components without affecting the significant harmonics of the pulse, the final response of a receiver to an f.m. wave will be better than its response to an a.m. wave.

(*c*) *Lines.*—If the line is incorrectly matched, or if there is a sudden variation of impedance such as may occur at a junction, so that reflection takes place, the transient responses to both f.m. and a.m. waves will be similarly affected.

(6) REFERENCES

(1) SALINGER, H.: 'Transients in Frequency Modulation', *Proceedings of the Institute of Radio Engineers*, 1942, **30**, p. 378.
(2) BELL, D. A.: 'Transient Response in Frequency Modulation', *Philosophical Magazine*, 1944, **35**, p. 143.
(3) GUMOWSKI, I.: 'Transient Response in FM', *Proceedings of the Institute of Radio Engineers*, 1954, **42**, p. 819.
(4) BELL, D. A.: 'Theory of Ideal Filters', *Wireless Engineer*, 1943, **20**, p. 323.
(5) BROWN, R. F.: 'Frequency-Modulation Distortion in Linear Networks', *Proceedings I.E.E.*, Paper No. 2196 R, January, 1957 (**104** B, p. 52).

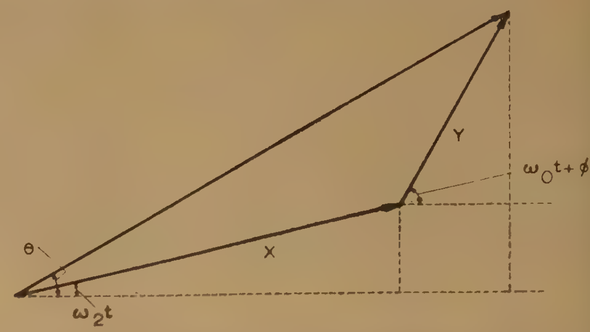

Fig. 4.—Vector addition of two signals of different frequencies.

(7) APPENDIX: FREQUENCY OF RESULTANT OF TWO SIGNALS OF DIFFERENT FREQUENCIES

X is assumed constant while Y is assumed to be of the form $A\varepsilon^{-at}$

$$\tan\theta = \frac{Y\sin(\omega_0 t+\phi) + X\sin\omega_2 t}{Y\cos(\omega_0 t+\phi) + X\cos\omega_2 t} \quad . \quad . \quad . \quad (20)$$

Differentiating with respect to t,

$$\sec^2\theta\frac{d\theta}{dt} = \frac{\omega_0 Y\cos(\omega_0 t+\phi) - aY\sin(\omega_0 t+\phi) + \omega_2 X\cos\omega_2 t}{Y\cos(\omega_0 t+\phi) + X\cos\omega_2 t}$$

$$+ \frac{[\omega_0 Y\sin(\omega_0 t+\phi) + aY\cos(\omega_0 t+\phi) + \omega_2 X\sin\omega_2 t][Y\sin(\omega_0 t+\phi) + X\sin\omega_2 t]}{[Y\cos(\omega_0 t+\phi) + X\cos\omega_2 t]^2}$$

Now

$$\sec^2\theta = \frac{[X\cos\omega_2 t + Y\cos(\omega_0 t+\phi)]^2}{[X\cos\omega_2 t + Y\cos(\omega_0 t+\phi)]^2 + [X\sin\omega_2 t + Y\sin(\omega_0 t+\phi)]^2}$$

and $d\theta/dt = \tilde{\omega}$, the instantaneous angular frequency, so that

$$\tilde{\omega} = \frac{\omega_0 Y^2 + \omega_2 X^2 + (\omega_2+\omega_0)XY\cos[(\omega_0-\omega_2)t+\phi] - aXY\sin[(\omega_0-\omega_2)t+\phi]}{X^2+Y^2+2XY\cos[(\omega_0-\omega_2)t+\phi]} \quad . \quad . \quad . \quad (21)$$

621.385.13:621.317.34

The Institution of Electrical Engineers
Monograph No. 323 R
Jan. 1959

A FILAMENT NOISE SOURCE FOR 3 Gc/s

By E. W. COLLINGS, M.Sc., Ph.D.

(*The paper was first received* 23*rd December*, 1957, *and in revised form* 25*th September*, 1958. *It was published as an* INSTITUTION MONOGRAPH *in January*, 1959.)

SUMMARY

The construction of an incandescent filament lamp and suitable tuned waveguide mounting for use as a noise source at 3 Gc/s is described. Methods of measuring filament temperature are outlined and the procedure for assessing mounting losses is described. Also, results of some noise measurements on a 6-watt fluorescent lamp and some cold-cathode argon discharges are outlined.

(1) INTRODUCTION

A standard noise generator is an ideal instrument for measuring both the noise figures of amplifiers and the noise ratios of 2-terminal networks. The superiority of the noise generator over the continuous-wave signal generator has been discussed by Moxon.[1] For measurements at low radio frequencies a noise diode used in a high-impedance circuit is a satisfactory noise generator, and with low-impedance coaxial-cable output the usual noise diode (e.g. CV172) may be used up to frequencies near 200 Mc/s. For use at higher frequencies (e.g. 1 Gc/s) Kompfner and others[2] have constructed a special noise diode in the form of a coaxial line; and Moxon has suggested a method for converting noise from a diode at an intermediate frequency into u.h.f. noise, by using a local oscillator and crystal mixer.

The expression kTB, for the available power within a bandwidth B from a resistor at temperature T°K, shows that, in principle at least, a heated load should be a very convenient standard noise generator. Ullrich and Rogers[3] have described the use of thermal noise sources consisting of heated filaments. A thermal noise source consisting of a section of waveguide heated to 450°K has been used by Davies and Cowcher[4] when measuring the noise temperatures of some gaseous discharge tubes at 3 Gc/s; and recently, Knol[5] has described a thermal noise standard for 10 Gc/s consisting of a section of waveguide containing a lossy wedge heated to the melting-point of gold.

In an effort to obtain a noise standard of higher temperature than usual, and suitable for 3 Gc/s, an incandescent filament lamp and suitable waveguide mounting were designed; the output noise temperature was about 1 300°K.

(2) DESCRIPTION OF THE NOISE SOURCE

(2.1) The Lamp Mounting

Fig. 1 shows the lamp mounting, the form of which was suggested by the tri-tuner mounts used for power measurement with bolometer lamps[6] and bead thermistors.[7]

The lamp was fitted between coaxial side-arms mounted on the broad faces of a waveguide, and the external surface of the glass envelope was kept at approximately room temperature by a blast of air through the small tubular side-arm shown in the drawing.

The lamp itself was an evacuated lead-glass cylinder with end-caps and axial filament of coiled 15-micron tungsten wire (Fig. 2).

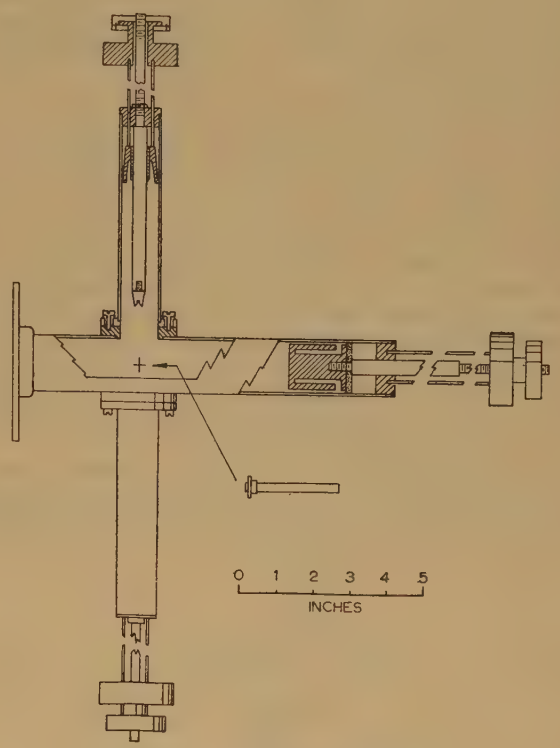

Fig. 1.—The lamp mounting.

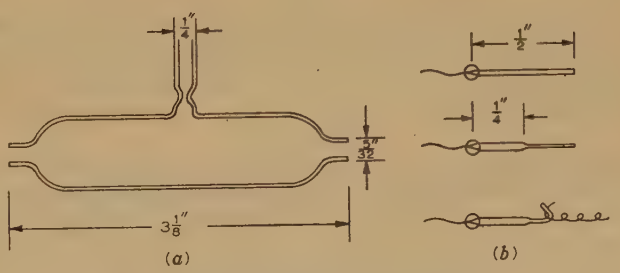

Fig. 2.—The incandescent filament lamp.
(*a*) Glass bulb.
(*b*) Method of attaching the filament.

The filament was one-eighth of a 60-watt coiled-coil lamp filament which had been stretched to about eight times its original length. The stretching operation removed all the 'secondary' coiling, so that in the finished lamp the filament was a spiral under tension.

The several pieces comprising the lamp (Fig. 2) were fitted together on a jig, based on the one described by Bleaney[6] for bolometer lamps. The lamps were attached to a manifold and processed in groups of four. Processing consisted of baking

Correspondence on Monographs is invited for consideration with a view to publication.

Dr. Collings was in the Department of Physics, Victoria University of Wellington, New Zealand, and is now in the Department of Physics, University of Ottawa, Canada.

them under vacuum for half an hour at 400° C and running their filaments at about 2500° C for a quarter of a minute prior to sealing off.

(2.2) Filament Temperature

It was decided to operate the filament at a temperature in the vicinity of 2800° K. Using a portable colour-temperature meter, an arbitrary temperature, namely 2790° K, near this value was chosen and the filament current required to give this reading was measured. A current value was thus assigned to each lamp and it provided a convenient means of maintaining constant filament temperature during the useful life of a given lamp and of ensuring that all the lamps used were being operated at the same temperature.

Finally, before any results could be calculated, it was necessary to determine the true absolute temperature of a filament corresponding to a reading of 2790° K on the colour-temperature meter. Langmuir and Jones[8] have tabulated (hot resistance)/(resistance at 293° K) against true temperature for any filament within the temperature range 1000–3500° K. Using a pair of similar lamps, resistance ratios were measured and filament temperatures of 2838° K and 2832° K were calculated from the data of Langmuir and Jones. Another, but probably less accurate, check on filament temperature was made with the aid of a National Physical Laboratory colour-temperature substandard. This yielded a true temperature of 2813° K at the reference current. Based on these figures, the value taken for the true filament temperature was 2830° K.

The noise measurements using the lamp required a knowledge of 'excess temperature' (or temperature in excess of room temperature, T_r, taken as 290° K); the accepted excess temperature of the filament was therefore 2540° K. Table 1, which shows

Table 1

DEVIATIONS OF THE MEASURED EXCESS FILAMENT TEMPERATURES FROM THE ACCEPTED VALUE

	Excess temperature deg K	Deviation deg K
Accepted value	2540	
(i)	2548	8 (0·3%)
(ii)	2542	2 (0·08%)
(iii)	2523	17 (0·7%)

the deviations of the measured values from this figure, suggests that, allowing for slight increase in filament temperature with age, it would be fair to allow ± 1% for uncertainty in excess filament temperature.

(3) MEASUREMENT OF LOSSES IN THE LAMP MOUNTING AND CALCULATION OF THE NOISE TEMPERATURE

The complete noise source comprised the incandescent filament, the glass envelope and the waveguide mounting. Ideally, the noise temperature of the source should be the absolute temperature of the filament; but because of absorption of energy, possibly in the tuning elements and certainly in the glass bulb, the noise temperature would be expected to be less than this value. Because of losses, the noise source becomes equivalent to a network consisting of a resistance at the filament temperature together with resistances at the temperatures of the various losses. A calculation showed the temperature gradient in the glass walls of the lamp to be negligibly small, with the inner wall at a temperature no more than 0·2° C above that of the external surface. Since the air jet kept the external surface at room temperature, the whole bulb could be represented, from the point of view of dielectric loss, by a resistance at that temperature. The waveguide itself was at room temperature, and therefore only two temperatures needed to be considered when calculating the noise temperature of the mounting—the filament temperature, T_l, and the room temperature, T_r. The procedure employed for measuring the losses was first used by Davies and Cowcher[4] for assessing loss in waveguide discharge-tube mountings.

(3.1) Equivalent Circuits

The lamp can be represented by a resistance R' and a reactance X, and the purpose of the mounting is to match these to the waveguide. The procedure is equivalent to (*a*) introducing a transformer to transform both R' and X so that the transformed value of the resistance is approximately equal to the characteristic resistance of the waveguide; (*b*) adding a reactance to cancel the transformed X, which is equivalent to setting up the parallel-resonant circuit of Fig. 3(*a*). In this diagram, R_s is

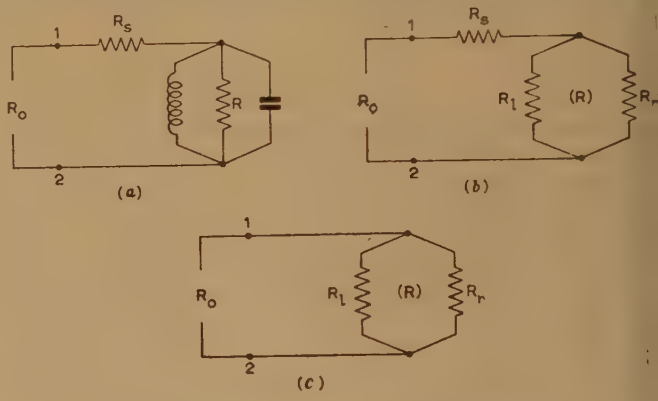

Fig. 3.—Equivalent circuits of the lamp mounting.

small series resistance to represent losses in the tuning elements. At the matching frequency, the reactances resonate and may be removed from the circuit, leaving $R_0 = R_s + R$.

Because the lamp was in the form of a glass cylinder with filament down the axis, it was represented by a pair of parallel resistances placed across the waveguide, such that $R = R_l R_r/(R_l + R_r)$. One resistance, R_l, was at the filament temperature; the other, R_r, represented the loss in the glass envelope and other shunt losses and was at room temperature because of the air cooling. Fig. 3(*b*) shows the equivalent circuit at the matching frequency.

In order to assess the noise temperature of the network it was necessary to investigate R_s and R_r. Accordingly a dummy lamp was made, similar in all respects to the noise lamps but with the filament, R_l, absent. After a real lamp had been matched and noise readings taken, it was replaced by the dummy lamp without altering the tuner settings, and measurements were made on the mounting by means of a standing-wave machine.

(3.2) Standing-Wave Measurements on the Lossy Resonator

At a frequency remote from resonance, the impedance seen is mainly a resistance R_s. The resulting voltage standing-wave ratio (v.s.w.r.), which, by convention, is greater than unity, is R_0/R_s. This is indefinitely large when R_s is practically zero, which was shown to be the case for the lamp mounting. At the resonant frequency, the standing wave is due to a termination consisting of R_s and R_r in series. Of these, R_r was by far the greater so that the resonant v.s.w.r. was practically R_r/R_0.

If the impedance seen upon looking into terminals 1, 2 is measured at various frequencies, all values of impedance assumed by the circuit can be represented by a circle on a Smith chart. Fig. 4 illustrates this, and shows the two alternative resonant

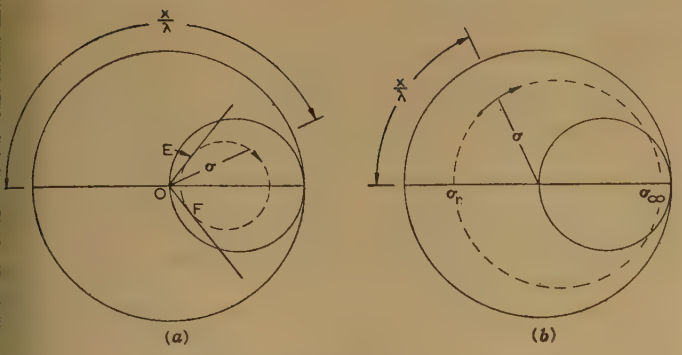

Fig. 4.—Loci of impedances assumed by the mounting as the frequency is swept through resonance.

conditions which can occur. If $R_r + R_s < R_0$, the cavity is said to be 'undercoupled' [Fig. 4(*a*)] and the movement of the standing-wave pattern with change of frequency is confined between the tangents OE and OF. On the other hand, if $R_r + R_s > R_0$ [and the standing-wave minimum is $(R_r + R_s)/R_0 = \sigma_r$], the impedance circle encloses the centre of the chart, the cavity is said to be 'over-coupled', and the reference minimum sweeps through $\lambda/2$ on passing through resonance.

Thus the value of the resonant standing-wave ratio, or standing-wave minimum, σ_r, is not sufficient to enable the normalized value of R_r to be deduced; for σ_r may equal either $(R_r + R_s)/R_0$ or $R_0/(R_r + R_s)$, whichever is greater than unity. But the two cases can be readily distinguished by observing the manner in which the standing-wave pattern shifts as the frequency is swept through resonance.

Since R_r represented the glass losses, and a filament R_l placed in parallel with this reduced the resistance of the combination to R_0, R_r must always have been greater than R_0, and $R_r + R_s > R_0$. Therefore only the over-coupled case gives a meaningful result in the waveguide lamp problem, and only such cavities were used as noise sources.

(3.3) Specimen Measurement

A noise lamp was placed in the mounting and matched. After a set of noise measurements had been made, the lamp was replaced by a dummy, the mounting transferred to the standing-wave bench and the v.s.w.r. and position of minimum were measured at wavelength intervals of 0·05cm between $\lambda = 9{\cdot}8$ and 10·4cm. Having found the position of resonance, it was investigated in greater detail by taking readings of v.s.w.r. and relative position of minimum, x, with respect to the resonant position every two megacycles. V.S.W.R. versus frequency, and x/λ versus frequency, in the vicinity of resonance, were then plotted as in Fig. 5.

In all experiments on losses it was found that the standing wave remote from resonance was immeasurably large (greater than 200); the series resistance, R_s, was therefore practically zero. The equivalent circuit of the noise lamp in its mounting, at resonance, is therefore given by Fig. 3(*c*).

(3.4) Calculation of the Noise Temperature

At the matching frequency, the noise source consisted of a resistance R_r, at room temperature T_r, in parallel with R_l at the filament temperature T_l. Working in terms of conductance, the noise temperature of the network was therefore:

$$T_n = \frac{G_l}{G_0} T_l + \frac{G_r}{G_0} T_r$$

During the loss measurements the resonant v.s.w.r., σ_r, was

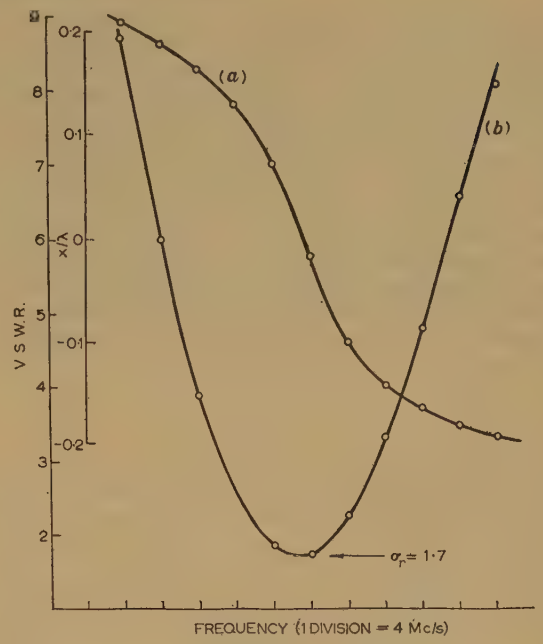

Fig. 5.—Frequency response of the mounting and glass bulb (filament absent).

(*a*) Relative position of the standing-wave minimum.
(*b*) Voltage standing-wave ratio.

measured looking into a circuit from which R_l had been removed; thus:

$$\sigma_r = \frac{R_r}{R_0} = \frac{G_0}{G_r}$$

Therefore

$$T_n = \frac{\sigma_r - 1}{\sigma_r} T_l + \frac{T_r}{\sigma_r} \quad . \quad . \quad . \quad . \quad . \quad (1)$$

or, in terms of 'excess noise temperature',

$$(T_n - T_r) = \frac{\sigma_r - 1}{\sigma_r}(T_l - T_r) \quad . \quad . \quad . \quad (2)$$

which is the form most suitable for noise calculations.

As an example, the minimum v.s.w.r. of Fig. 5 was 1·70, so that $T_n - T_r = 1046°\text{K}$, and $T_n = 1336°\text{K}$.

(3.5) Measurement of the Voltage Standing-Wave Ratio at Resonance

Eqn. (2) shows that the accuracy of noise temperature assessment depends heavily on the accuracy with which the resonant v.s.w.r., σ_r, can be measured.

$$T_n - T_r \propto \frac{\sigma_r - 1}{\sigma_r}$$

therefore

$$\frac{d(T_n - T_r)}{T_n - T_r} = \frac{d\sigma_r}{(\sigma_r - 1)\sigma_r}$$

so that with

$$\sigma_r = 1{\cdot}7$$

$$\frac{d(T_n - T_r)}{T_n - T_r} \simeq 1\tfrac{1}{2} \frac{d\sigma_r}{\sigma_r}$$

The error in excess noise temperature is thus $1\frac{1}{2}$ times that of the v.s.w.r. measurement. For example, to keep the error below 1% due to this cause, the v.s.w.r. in the vicinity of 1·7 should be measured to the nearest 0·01 of a unit. This is unusually

high accuracy for the conventional standing-wave measurement using slotted waveguide detector; moreover it is difficult to assess the accuracy of such a measurement. Some thought was therefore given to devising an alternative method for measuring v.s.w.r., which would have greater accuracy than usual, and would also allow an estimation of the error to be made.

First, over a small range of frequencies passing through resonance, a set of maximum and minimum readings of a conventional standing-wave machine were noted. The lamp mounting was then replaced by an attenuator short-circuited at the far end. This was adjusted, in conjunction with the output level of the test oscillator, to give the same set of readings as before. The respective v.s.w.r.'s were then read from a graph based on the relationship

$$A = 10 \log_{10}\left(\frac{\sigma + 1}{\sigma - 1}\right)$$

where A is the attenuation in decibels.

This can be regarded as a substitution method in which the device setting up the known standing wave replaces the mounting under test to produce the same external conditions. The accuracy of this method is discussed elsewhere.[10]

Owing to uncertainty in the attenuation values, the accuracy of v.s.w.r. measurement by this method was $\pm 0{\cdot}8\%$. The resulting error in excess noise temperature was therefore $1\frac{1}{2}$ times this; i.e. approximately $1\frac{1}{2}\%$.

(3.6) Uncertainty in the Noise Temperature of the Mounting

If about 1% is allowed for uncertainty in the excess filament temperature, and $1\frac{1}{2}\%$ for the error in $(\sigma_r - 1)/\sigma_r$, the error in the excess noise temperature of the standard is approximately $\pm 2\frac{1}{2}\%$.

(4) MEASUREMENT OF THE NOISE TEMPERATURES OF GASEOUS DISCHARGES

(4.1) The 3Gc/s Receiver used for Noise Comparisons

A discharge tube under test was placed in a '90° H-plane' mounting, in which its axis was perpendicular to the narrow side-walls of the waveguide arranged to propagate in the TE_{01} mode. The receiver had two input waveguides, one mounted above the other. The noise standard was placed at the end of the upper waveguide, and the discharge tube mounting was applied to the lower. By means of a hand-operated waveguide switch, either of these two inputs could be presented to the receiver.

The frequency band over which the lamp mounting was matched (with a v.s.w.r. less than, say, 1·1) did not include both the signal and image frequencies, whereas a discharge tube, matched at the signal frequency, was matched (approximately) at the image frequency as well. The effect of differing amounts of mismatch of the two noise sources at the image frequency was eliminated by a coaxial tuner inserted in the output line from the waveguide. The use of selected crystals in a balanced mixer gave a receiver noise figure, with tuner, of 9·8dB. The output from the intermediate-frequency amplifier (at 24Mc/s) was displayed on a square-law voltmeter.

(4.2) Assessed Experimental Error

The excess noise temperature of the lamp mounting was known to an accuracy within $\pm 2\frac{1}{2}\%$; whilst the comparison error was $\pm 3\frac{1}{2}\%$. Possible error in the measurement of the noise temperature of the lamp under test was therefore $\pm 6\%$.

Using three noise lamps in turn, measurements were performed on a 6-watt fluorescent lamp passing a current of 40mA. The average of six measurements was $9{\cdot}55(8) \times 10^3$°K with probable error of $\pm 6\%$.

(4.3) Noise Temperature of a Six-Watt Fluorescent Lamp

The average noise temperature agrees well with that estimated by Houlding and Miller[11] for a 6-watt fluorescent tube, but is lower than the noise temperatures obtained by Mumford[12] and Hughes.[13] However, it is known that the noise temperatures of 6-watt fluorescent tubes differ amongst themselves by as much as 20% (Chinnock,[14] and Maxwell and Leon[15]).

It was therefore felt that the figure of $9{\cdot}56 \times 10^3$°K for the noise temperature of the fluorescent tube was satisfactory. This conclusion was later substantiated by the results of measurements on some pure argon discharges by comparison with the calibrated fluorescent lamp.

(4.4) Noise Temperatures of Some Argon Discharges

Using the standardized fluorescent lamp, noise measurements were made on six cold-cathode discharge tubes containing argon at a pressure of 15mmHg and six filled to 7·5mmHg. Both sets were run at 40mA. Measuremsnts were also made on a pair of argon tubes filled to 30mmHg.

Theoretically the noise temperature of a gas discharge should equal the electron temperature,[16] which can be measured by the Langmuir probe method or calculated from data provided by von Engel and Steenbeck.[17] The results of a set of noise-temperature measurements and accompanying electron temperature measurements and calculations showed good agreement between the noise and electron temperatures.[18]

(5) CONCLUSION

An incandescent-filament noise source has been described and shown to be suitable for the measurement of the noise temperatures of gaseous discharge tubes. The standard has a noise temperature somewhat higher than usual, but possesses the disadvantage of narrow bandwidth (width of response curve at v.s.w.r. = 2 is 55Mc/s), so that in noise comparisons an image rejection tuner is required.

(6) REFERENCES

(1) MOXON, L. A.: 'Recent Advances in Radio Receivers' (Cambridge University Press, 1949), Chap. 5.

(2) KOMPFNER, R., HATTON, J., SCHNEIDER, E. E., and DRESEL, L. A. G.: 'The Transmission Line Diode as a Noise Source at Centimetre Wavelengths', *Journal I.E.E.*, 1946, **93**, Part IIIA, p. 1436.

(3) ULLRICH, E. H., and ROGERS, D. C.: 'An Absolute Method of Measurement of Receiver Noise Factor', *ibid.*, 1946, **93**, Part IIIA, p. 1347.

(4) DAVIES, L. W., and COWCHER, E.: 'Microwave and Metre Wave Radiation from the Positive Column of a Gas Discharge', *Australian Journal of Physics*, 1955, **8**, p. 108.

(5) KNOL, K. S.: 'A Thermal Noise Standard for Microwaves', *Philips Research Report*, 1957, **12**, p. 123.

(6) BLEANEY, B.: 'Radio-Frequency Power Measurements by Bolometer Lamps at Centimetre Wavelengths', *Journal I.E.E.*, 1946, **93**, Part IIIA, p. 1378.

(7) GRIESHEIMER, R. N.: 'Technique of Microwave Measurements', M.I.T. Radiation Laboratory Series, Volume 1 (McGraw-Hill, 1947), p. 149.

(8) LANGMUIR, I., and JONES, H. A. (1927): see PARKER, P.: 'Electronics' (Arnold, 1955), p. 1010.

(9) MALTER, L., and BREWER, G. R.: 'Microwave Q Measurements in the Presence of Series Losses', *Journal of Applied Physics*, 1949, **20**, p. 918.

(10) COLLINGS, E. W.: 'Voltage Standing-Wave Ratio Measurement', *Electronic and Radio Engineer*, 1958, **35**, p. 287.
(11) HOULDING, N., and MILLER, L. C.: 'Discharge Tube Noise Sources', Telecommunications Research Establishment Memo. No. 593, October, 1953.
(12) MUMFORD, W. W.: 'A Broad-Band Microwave Noise Source', *Bell System Technical Journal*, 1949, **28**, p. 608.
(13) HUGHES, V. A.: 'Absolute Calibration of a Standard Temperature Noise Source for use with S-Band Radiometers', Radio Research Establishment Technical Note No. 543, 1955.
(14) CHINNOCK, E. L.: 'A Portable Direct-Reading Microwave Noise Generator', *Proceedings of the Institute of Radio Engineers*, 1952, **40**, p. 160.
(15) MAXWELL, E., and LEON, B. J.: 'Absolute Measurement of Receiver Noise Figures at UHF', *Transactions of the Institute of Radio Engineers*, 1956, **MTT-4**, p. 81.
(16) VAN DER ZIEL, A.: 'Noise' (Prentice-Hall, New York, 1954), p. 16.
(17) COBINE, J. D.: 'Gaseous Conductors' (McGraw-Hill, New York), p. 239.
(18) COLLINGS, E. W.: 'Noise and Electron Temperatures of Some Cold Cathode Argon Discharges', *Journal of Applied Physics*, 1958, **29**, p. 1215.

621.317.79

The Institution of Electrical Engineers
Monograph No. 324 M
Jan. 195

QUADRATIC INTERPOLATION IN TAPPED-POTENTIOMETER FUNCTION GENERATORS

By E. M. DEELEY, B.Sc., Ph.D., Graduate.

(*The paper was first received* 21*st May, and in revised form* 20*th October*, 1958. *It was published as an* INSTITUTION MONOGRAPH *in January* 1959.)

SUMMARY

The paper describes a method of obtaining quadratic interpolation in a tapped-potentiometer generator for functions of a single variable. The method depends on the quadratic form of the variation of resistance to earth at the slider, across which is developed the voltage necessary to reproduce correctly the first three terms of the Taylor's series. The supply to the tapping points from voltage sources of zero and finite resistance is analysed, and the problem of supplying these voltages is examined. The application of the method to the generation of functions of two variables is briefly discussed.

LIST OF PRINCIPAL SYMBOLS

$V_1, V_2 \ldots V_n$ = Voltages at tapping points of potentiometer.
V_r, V_s, V_t = Voltages at sliders A, B and C with load resistances disconnected.
V_a, V_b, V_c = Voltages at sliders A, B and C with load resistances connected.
V_{1b}, V_{2b}, V_{3b} = Voltages at slider B when coincident with tapping points 1, 2 or 3.
V_{out} = Output voltage.
V'_a, V'_b, V'_c = Correcting voltages generated at sliders A, B and C.
α = Distance of a slider past a tapping point, expressed as a fraction of the distance between taps.
R = Resistance of one section of potentiometer.
R_0 = Voltage-source resistance.
R_z = Characteristic resistance.
x = Distance along potentiometer.

(1) INTRODUCTION

The use of tapped potentiometers to generate the voltage analogue of functions of a single variable is a well-known technique in analogue computation.[1] In principle, voltages representing values of the function at several fixed values of the input variable are applied to the tapping points of the potentiometer, the slider of which provides linear interpolation between these points. Readily-adjustable voltages and a high-quality servomechanism controlling the position of the slider result in an adaptable device capable of giving a highly reproducible output. These advantages, however, are offset by limited accuracy, dependent on the form of the function generated and on the number of tapping points available.

The accuracy available is adequate for many applications, especially those in which the function to be generated is not precisely known. In other applications, however, a higher accuracy would be welcome without a large increase in the number of tapping points. This may generally be obtained by using quadratic interpolation in place of linear interpolation, i.e. by calculating the value of the function at any point from the first three terms of the Taylor's series, which in terms of the voltages at distances x and $(x + \delta x)$ along the potentiometer becomes:

$$V_{out} = V_{x+\delta x} = V_x + \delta x \frac{dV_x}{dx} + \frac{\delta x^2}{2} \frac{d^2V_x}{dx^2} \quad . \quad . \quad (1$$

In the following Sections a method is described for approximating to quadratic interpolation in potentiometers provided with equally-spaced tapping points.*

(2) QUADRATIC INTERPOLATION WITH ZERO-RESISTANCE SOURCES

(2.1) Theory

Writing the derivatives of voltage in terms of finite differences using the voltages at the tapping points, eqn. (1) becomes

$$V_{out} = V_n + \frac{\alpha}{2}(V_{n+1} - V_{n-1}) + \frac{\alpha^2}{2}(V_{n+1} + V_{n-1} - 2V_n) \quad . \quad (2$$

Assuming for simplicity that the slider lies between tapping points 2 and 3, the required output may be written

$$V_{out} = V_2 + \alpha(V_3 - V_2) + (\alpha^2 - \alpha)\frac{(V_3 + V_1 - 2V_2)}{2} \quad . \quad (3$$

The first two terms on the right-hand side of this equation give the voltage which would normally appear on the unloaded potentiometer slider using linear interpolation, and therefore a means must be sought to introduce a further voltage at the slider corresponding to the last term in eqn. (3). To generate this voltage, use is made of the quadratic expression for the resistance to earth at the slider of the potentiometer when all the tapping points are connected to zero-resistance sources. This resistance is $R(\alpha - \alpha^2)$. If a current equal to $-(V_1 + V_3 - 2V_2)/2R$ is allowed to flow into the potentiometer at the slider, the required correcting voltage will be generated.

The voltage $-(V_1 + V_3 - 2V_2)$ may be computed by conventional analogue methods, but in practice this approach would involve the switching of voltages as the slider passes from one section of the potentiometer to another, and would therefore be impracticable. A modified form of quadratic interpolation, which possesses certain advantages over pure quadratic interpolation between the tapping points, may be obtained by deriving the voltages used in the correcting term from two additional sliders on the potentiometer. These sliders, A and C, are mounted on each side of the existing slider, B, and are separated from it by a distance equal to the distance between the tapping points. If the voltages on the unloaded sliders are V_r, V_s and V_t,

$$V_r = V_1 + \alpha(V_2 - V_1) \quad . \quad . \quad . \quad . \quad (4$$

$$V_s = V_2 + \alpha(V_3 - V_2) \quad . \quad . \quad . \quad . \quad (4$$

$$V_t = V_3 + \alpha(V_4 - V_3) \quad . \quad . \quad . \quad . \quad (4$$

* Patent applied for

Correspondence on Monographs is invited for consideration with a view to publication.

Dr. Deeley is in the Electrical Engineering Department, King's College, University of London.

If now a current $-(V_r + V_t - 2V_s)/2R$ is introduced at slider B the additional generated voltage becomes

$$(\alpha^2 - \alpha)\frac{(V_1 + V_3 - 2V_2)}{2} + \alpha(\alpha^2 - \alpha)\frac{(V_4 - 3V_3 + 3V_2 - V_1)}{2}$$

The third derivative of voltage is thus contained in the last term of this expression, which has the desirable effect of removing discontinuities in the first and second derivatives that would otherwise exist at the tapping points.

In the practical circuits used to generate the correcting current, the unloaded voltage V_s is not available, since slider B carries correcting current, which generates a correcting voltage V_b'. In order that the expression $(V_r + V_t - 2V_s)$ may be correctly evaluated from the corrected value of V_s, additional currents must be arranged to flow in sliders A and C, to produce correcting voltages V_a' and V_c' such that $V_a' + V_c' = 2V_b'$.

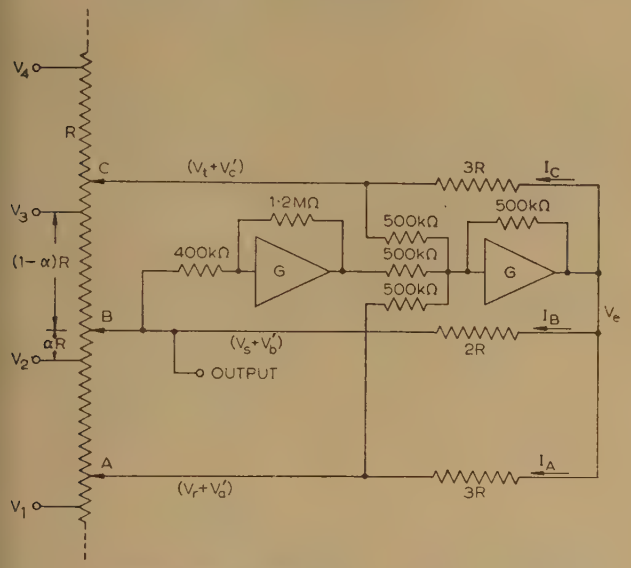

Fig. 1.—Quadratic interpolator for low-resistance voltage sources.
Slider B is assumed to lie between taps 2 and 3.
G. High-gain d.c. amplifiers.

The complete system is illustrated in Fig. 1. It may be shown (Appendix 10.1) that such a system in fact generates the required voltages according to the requirements stated above.

(2.2) Measurements

In a practical function generator the position of the slider is linearly related to the input variable, x. In testing the performance of the quadratic interpolator, the value of x was measured by disconnecting the slider load resistances and applying a known voltage across the potentiometer terminals. Under these conditions the unloaded voltage at slider B was itself linearly related to x.

Voltages were measured by a dial-box potentiometer and a null-reading meter, the system having a sensitivity and accuracy of the order of 0·01%.

The potentiometer used for test experiments was provided with ten tapping points (excluding the terminals) which were nominally equally spaced. The number of turns per section was approximately 100, and the mean resistance per section was 930 ohms. (Extreme values of 914 and 938 ohms were obtained.) The tappings were taken from the side of the card remote from the slider, with the result that there was a small minimum resistance of 3–8 ohms between the slider and each tapping point. The relative positions of the three sliders were adjustable, and each made contact with not more than two turns of the winding at any setting. It was possible to adjust the sliders so that, when the resistance of one slider to any one tapping point was a minimum, the resistances between the other sliders and their nearest tapping points were less than 30 ohms.

The slider load resistances were adjusted to within 0·5% of the value required by theory, using the mean value of R as stated above. Commercial d.c. amplifiers provided with continuous zero-drift correction (as used for analogue computation) were used in the interpolating circuit, and also as the voltage sources for the tapping points in order to ensure low source resistance. The only initial adjustment made before setting up test functions was to trim the transfer functions of the linear units (Fig. 1) so that no current flowed into slider B when all the tapping points were connected to the same voltage source.

(2.3) Results

An interesting test function is the square-law relationship $V = Ax^2$, since all derivatives beyond the second vanish and the function should be generated without error. The error curve, obtained when part of this function (symmetrical about zero) is generated using linear interpolation between seven tapping points, is illustrated in Fig. 2. The percentage error obtained

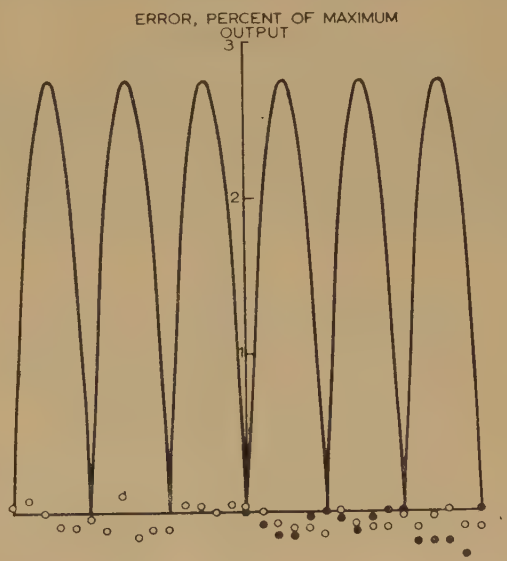

Fig. 2.—Interpolator performance: square-law function.
——— Error using linear interpolation.
○ Error using quadratic interpolation.
● Error using voltage source of finite impedance.

using quadratic interpolation in the manner described is also shown, and is less than 0·2% of the maximum value of the function. (Note that two more sections are required to allow for the excursion of sliders A and C.)

The result of a similar test using the function $V = A\cos\mu$ in the interval $0 < \mu < \pi/2$, and defined at four points ($\mu = 0$, $\pi/6$, $\pi/3$, $\pi/2$), is illustrated in Fig. 3. The solid curve again represents the error for linear interpolation, while the broken curve indicates the error to be expected with this function using quadratic interpolation. The percentage errors measured are seen to lie close to this curve.

(3) QUADRATIC INTERPOLATION USING FINITE-RESISTANCE SOURCES

In the foregoing it has been assumed that the tapping points were supplied from voltage sources of zero or very small resis-

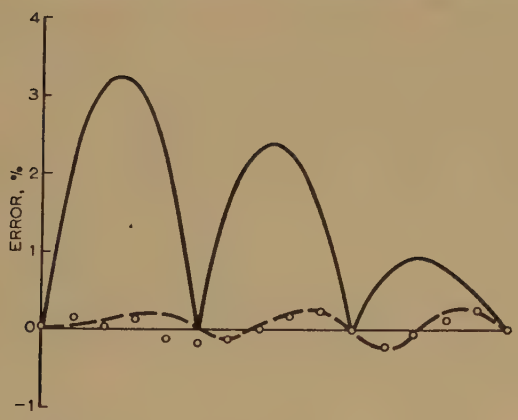

Fig. 3.—Interpolator performance: cosine function.

———— Error using linear interpolation.
— — — — Expected error using quadratic interpolation.
○ Measured error using quadratic interpolation.

tance. In general, however, any simple and readily adjustable voltage source will not be of low resistance. The effect of source resistance is therefore examined in the following Sections.

(3.1) Representation of the Potentiometer

The voltage sources connected to each tapping point are assumed to have a finite resistance R_0, represented by resistances in series with each tapping point (Fig. 4). The potentiometer thus resembles a lumped-constant transmission line, for which a characteristic resistance R_z can be calculated. The value of R_z for such a system, calculated at the tapping point with the source resistance at the tapping point connected, may readily be shown to be

$$\sqrt{(\tfrac{1}{4}R^2 + R_0R)} - \tfrac{1}{2}R \quad . \quad . \quad . \quad . \quad . \quad (5$$

Thus, if the potentiometer is terminated at each end by R instead of R_0, the resistance at any tapping point looking in one direction along the potentiometer with the source resistance connected is also R_z. The resistance to earth at the slider is therefore

$$R_E = \frac{(R_z + \alpha R)[R_z + (1 - \alpha)R]}{2R_z + R}$$

$$= \frac{R_z(R + R_z)}{2R_z + R} + \frac{R^2}{2R_z + R}(\alpha - \alpha^2) \quad . \quad (6$$

(3.2) Interaction between Sections

Since R_0 is common to adjacent sections of the potentiometer there is interaction between the voltages at the tapping points. In the case of the simple tapped potentiometer employing linear interpolation, this is reflected merely in an added difficulty in setting up the potentiometer for any given function. In the present instance, however, there is a further modification of the tapping-point voltages when the sliders are connected, due to the current introduced at the sliders. In order to calculate the effect of this interaction, the approximate voltage change at each relevant tapping point due to each slider is calculated. It is shown in Appendix 10.2 that if the slider load resistances are $3R_p$, $2R_p$ and $3R_p$ respectively (Fig. 4), and if [eqn. (25)]

$$R_p = R\frac{R}{2R_z + R}\left(1 + \frac{2R_z}{R_z + R}\right) + \frac{R_z^2}{2R_z + R}$$

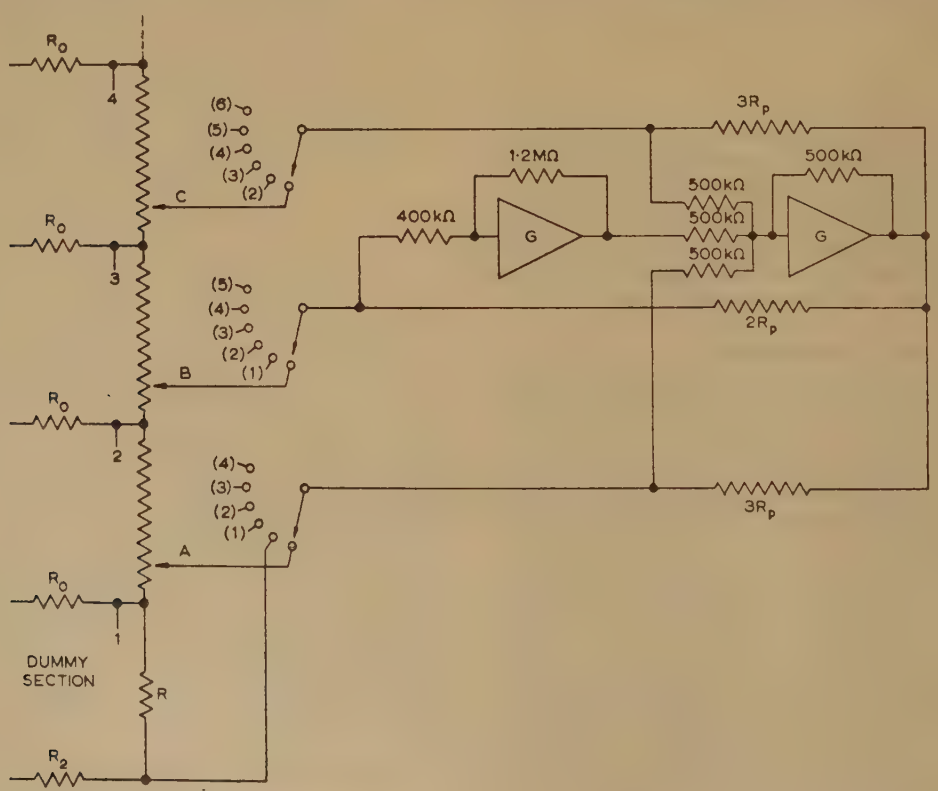

Fig. 4.—Quadratic interpolator and setting-up circuit for finite-resistance voltage sources.

Slider B is assumed to lie between taps 2 and 3.
G. High-gain d.c. amplifiers.

then V_b, the output voltage, is approximately given by

$$V_b \simeq V_{2b} + \alpha\left(\frac{dV_{2b}}{dx}\right) + \frac{\alpha^2}{2}\left(\frac{d^2V_{2b}}{dx^2}\right) - \frac{(\alpha-\alpha^2)}{2}\left[\alpha\frac{d^3V_{(z-3)}}{dx^3} + \beta\frac{d^4V_{2b}}{dx^4} + \ldots\right]$$

Thus the first three terms of the Taylor's series are correctly produced, so that theoretically a square-law function is generated without error. A larger number of higher derivatives, whose coefficients are not those of Taylor's series, appear in the equation, however, so that more complex functions may not be generated so accurately as when zero-resistance sources are used.

(3.3) The Equation for R_p

When $R_z \ll R$, eqn. (25) may be written

$$R_p = R\left[1 - \left(\frac{R_z}{R}\right)^2 + 2\left(\frac{R_z}{R}\right)^4\right] \quad \ldots \quad (7)$$

Thus the value of R_p does not deviate appreciably from R until quite large values of R_z/R are employed (e.g. for $R_z/R = 0{\cdot}1$, R_p is $0{\cdot}993R$). The approximate equation above gives values for R_p within 1% of those calculated from the more exact equation, for values of R_z/R up to $0{\cdot}2$.

(3.4) Setting Up the Potentiometer

The voltage at each tapping point must be set up with slider B connected to that tapping point and sliders A and C connected to the neighbouring points, as this is the situation when the function is being generated. Owing to interaction, successive approximations are required to adjust each voltage. A 3-pole multi-way rotary switch is therefore used in the setting-up procedure, so that the slider load resistances can be readily connected to any group of three tapping points (Fig. 4).

A further difficulty remains in setting up the voltages at the ends of the potentiometer, since either slider A or slider C will not then be connected to any point. Using the rotary switch, this difficulty is overcome by switching into the circuit resistances representing an extra, or dummy, section of the potentiometer at each end (Fig. 4). The voltages at the two artificial tapping points so produced are adjusted to represent the values of the function at those points, and the voltages at the real ends of the potentiometer are then set up. This process involves an approximation, so that the voltages at the ends of the potentiometer will not behave in precisely the correct way, but since, in practice, those voltages are involved only in the quadratic correction term, the effect of such an approximation is small.

(3.5) Results

The error curve obtained for a square-law function using voltage sources of finite impedance (approximately $0{\cdot}29R$) is shown in Fig. 2. The error is seen to be not significantly greater than for zero source resistance.

(4) CONTROL OF THE SOURCE VOLTAGES

It has been shown in the previous Section that the alteration required in the slider load resistances for correct quadratic interpolation depends on the source resistance only in a second order term. Thus, for instance, if the source resistances are $0{\cdot}2R$, and the load resistances are retained at $3R$, $2R$ and $3R$ respectively, the error in the quadratic term of the Taylor's series is only 2·4%. Since the quadratic term is generally not more than a small percentage of the whole function, it follows that this represents an error of not more than about 0·1% of the maximum value of the function. Thus, for a sacrifice in accuracy of this order, the tapping points can be supplied from a number of simple potentiometers, each of resistance $0{\cdot}8R$, and connected across a single stable d.c. supply.

More complicated supply systems, in which the variation of source resistance with supply voltage was small, would enable even larger source resistances to be employed, with appropriate values chosen for the slider load resistances.

(5) OUTPUT LOADING

The foregoing analysis and tests have assumed no-load conditions, whereas the function generator is in general used with a load connected to the output, slider B. The effect of such a load on the potentiometer slider can be removed by the action of the well-known 'bootstrap' circuit,[1] which in the present device involves the addition of one more inverting unit to generate a voltage proportional to V_b, and of the same sign.

If, however, the output is taken from the linear unit connected to slider B (Figs. 1 and 4), a voltage proportional to V_b is obtained without loading the slider. The change of sign and amplitude introduced by the linear unit can be allowed for by changing the signs and magnitudes of the voltages applied to the tapping points of the potentiometer.

(6) QUADRATIC INTERPOLATION IN TWO-VARIABLE FUNCTION GENERATORS

It is appropriate briefly to consider the possible extension of the method to the generation of functions of two variables. The most obvious extension is to the type of generator using a number of single-variable tapped-potentiometer generators set up at finite intervals of the second variable.[1] Such a function generator would possess the advantages of the single-variable device, but would involve the use of a large number of linear units.

In another form of two-variable function generator,[2] separate tapped potentiometers are replaced by a resistive sheet provided with an array of inset studs to act as tapping points. In the simplest form of this device the variation of resistance at the slider with respect to changes in position in the x- and y-directions cannot be separated from one another, so that the method described can only provide interpolation based on the average of the x- and y-derivatives. It can be shown, however, that such 'averaged' quadratic interpolation can be of benefit in correcting the form of the output from the resistive-sheet device.[3]

(7) CONCLUSIONS

The simple tapped potentiometer, used as a function generator in an analogue computer or simulator, provides linear interpolation between the voltages applied to the tapping points, so that a given continuous function can be generated with only limited accuracy. A method has been described for obtaining quadratic interpolation in such a device, with a corresponding improvement in accuracy depending on the form of the function being generated.

The method makes use of the quadratic form of the resistance variation to earth at the slider of the potentiometer as it moves between tapping points, across which resistance is developed a voltage proportional to the second difference of the function. This difference is derived by using two correctly-positioned sliders in addition to the original slider and two computing amplifiers, so that the use of subsidiary potentiometers and gears, which have been used in previous devices providing higher-order interpolation, is avoided.

For the special case of a square-law function, which should be generated without error using quadratic interpolation, an

error of the order of $\pm 0{\cdot}2\%$ of maximum output is obtained with a relatively low-grade potentiometer. It has been shown that the internal resistance of the voltage sources supplying the tapping points can be of the same order as that of the sections of the potentiometer, and that the variation of these resistances has only a second-order effect on the quadratic term in the output voltage.

In a modified form, the method can also be of use in improving the accuracy of certain types of generator for functions of two variables.

(8) ACKNOWLEDGMENTS

The paper is a result of a vacation consultancy with the Royal Aircraft Establishment, Farnborough.

The author would like to express his grateful thanks to Dr. S. H. Hollingdale for providing facilities for this work, and to Mr. G. C. Tootill for valuable discussion and suggestions. He would also like to thank Mr. H. D. S. Faulder, Mr. J. J. Gait and Mr. K. H. Treweek for discussion and co-operation, and Mr. R. G. Anderson for arranging certain mechanical assistance.

(9) REFERENCES

(1) KORN, G. A., and KORN, T. M.: 'Electronic-Analogue Computers (McGraw-Hill, 1956), Chapter 6.

(2) GAIT, J. J., and GARVEY, R. G.: 'An Electrical Analogue Equipment for Generating Functions of Two Variables'. Unpublished Ministry of Supply report.

(3) DEELEY, E. M.: 'Quadratic Interpolation in Tapped-Potentiometer Type Function Generators'. Unpublished Ministry of Supply report.

(10) APPENDICES

(10.1) Operation of the Quadratic Interpolation Circuit

Two linear units (high-gain amplifiers provided with feedback networks) are employed to derive the necessary correcting voltages (Fig. 1). One such unit has a gain of 3 with sign reversal, while the other acts simply as a summing unit with unity gain and sign reversal. The output V_e of the summing amplifier is thus

$$V_e = 3(V_s + V_b') - (V_r + V_a') - (V_t + V_c') \quad . \quad . \quad (8)$$

The currents in the slider load resistances are therefore given by

$$I_A = \frac{3(V_s + V_b') - 2(V_r + V_a') - (V_t + V_c')}{3R} \quad . \quad (9a)$$

$$I_B = \frac{2(V_s + V_b') - (V_r + V_a') - (V_t + V_c')}{2R} \quad . \quad . \quad (9b)$$

$$I_C = \frac{3(V_s + V_b') - (V_r + V_a') - 2(V_t + V_c')}{3R} \quad . \quad (9c)$$

The voltages developed at the slider may now be found by multiplying these currents by $R(\alpha - \alpha^2)$. Thus

$$V_a' + V_c' = (I_A + I_c)R(\alpha - \alpha^2)$$
$$= (\alpha - \alpha^2)[2(V_s + V_b') - (V_r + V_a') - (V_t + V_c')] \quad . \quad (10)$$

and $V_b' = I_B R(\alpha - \alpha^2)$

$$= \frac{(\alpha - \alpha^2)}{2}[2(V_s + V_b') - (V_r + V_a') - (V_t + V_c')]$$
$$. \quad . \quad . \quad . \quad (11)$$

Therefore $$(V_a' + V_c') = 2V_b' \quad . \quad . \quad . \quad . \quad . \quad (12)$$

Substituting for $(V_a' + V_c')$ in eqn. (11),

$$V_b' = \frac{(\alpha - \alpha^2)}{2}(2V_s - V_r - V_t) \quad . \quad . \quad . \quad (13)$$

which is the required expression.

(10.2) Effect of Interaction between Sections due to Finite Source Resistance

Let V_a, V_b and V_c be the voltages which normally exist at sliders A, B, and C, when connected to the potentiometer. Suppose for the purpose of analysis that the sliders are effectively disconnected from the potentiometer by the switches S_1, S_2 and S_3 (Fig. 5), and connected to alternative sources of

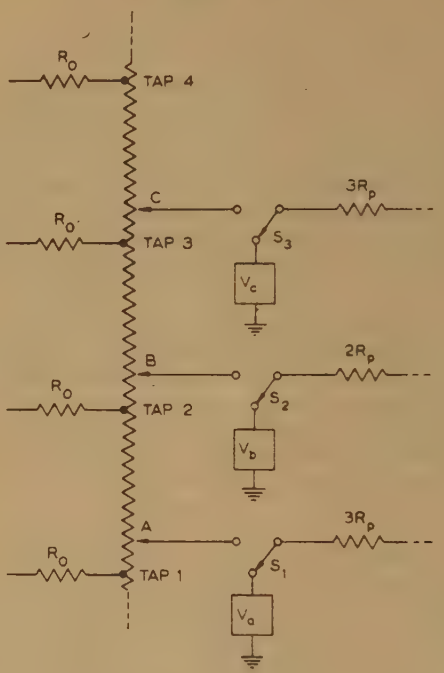

Fig. 5.—Alternative slider voltages.

voltage, V_a, V_b and V_c, and suppose that the voltages at the tapping points 2 and 3 then become V_2 and V_3.

If now sliders A and C are reconnected to the potentiometer the voltage increases, V_a' and V_c', at the sliders due to the current in the load resistances (each $3R_p$) are

$$V_a' = \frac{R_E}{3R_p}(3V_b - 2V_a - V_c) \quad . \quad . \quad . \quad (14a)$$

$$V_c' = \frac{R_E}{3R_p}(3V_b - V_a - 2V_c) \quad . \quad . \quad . \quad (14b)$$

where [eqn. (6)] $$R_E = R_Y + \frac{R^2}{R + 2R_z}(\alpha - \alpha^2) \quad . \quad . \quad . \quad (15)$$

and $$R_Y = \frac{R_z(R + R_z)}{R + 2R_z} \quad . \quad . \quad . \quad . \quad . \quad (16)$$

We can therefore write down the approximate increase in voltage at the tapping points 2 and 3 as a result of connecting sliders A and C.

Increase in voltage at tap 2 due to slider A

$$\simeq V_a' \frac{R_z}{R_z + R(1 - \alpha)}$$

Increase in voltage at tap 3 due to slider A

$$\simeq V'_a \frac{R_z}{R_z + R(1-\alpha)} \frac{R_z}{R_z + R}$$

Increase in voltage at tap 3 due to slider C

$$\simeq V'_c \frac{R_z}{R_z + \alpha R}$$

Increase in voltage at tap 2 due to slider C

$$\simeq V'_c \frac{R_z}{R_z + \alpha R} \frac{R_z}{R_z + R}$$

(The approximation is a result of the finite resistance connected to the sliders themselves.)

Thus, if slider B is now reconnected to the appropriate point between tap 2 and tap 3, the slider voltage is given by

$$V_b \simeq (1-\alpha)\left[V_2 + V'_a \frac{R_z}{R_z + (1-\alpha)R} + V'_c \frac{R_z}{R_z + \alpha R} \frac{R_z}{R_z + R}\right]$$

$$+ \alpha\left[V_3 + V'_c \frac{R_z}{R_z + \alpha R} + V'_a \frac{R_z}{R_z + (1-\alpha)R} \frac{R_z}{R_z + R}\right] + V'_b \quad . \quad . \quad . \quad . \quad (18)$$

where

$$V'_b = \frac{R_E}{2R_p}(2V_a - V_b - V_c) \quad . \quad . \quad . \quad . \quad (19)$$

Eqn. (18) simplifies to

$$V_b \simeq [V_2 + \alpha(V_3 - V_2)] + 2V'_b\left(\frac{R_z}{R_z + R}\right) + V'_b \quad . \quad (20)$$

Similar equations can be derived for V_a and V_c. Substituting for V_a, V_b and V_c in eqn. (19), an expression is derived for V'_b in terms of V_1, V_2, V_3 and V_4, which on substituting in eqn. (20) gives

$$V_b = [V_2 + \alpha(V_3 - V_2)] + \frac{R_E}{2R_p} \frac{\left(1 + \frac{2R_2}{R_z + R}\right)}{\left(1 - \frac{R_z}{R_z + R}\frac{R_E}{R_p}\right)}$$

$$\{2V_2 - V_1 - V_3) + \alpha[2(V_3 - V_2) - (V_2 - V_1) - (V_4 - V_3)]\} \quad . \quad . \quad . \quad . \quad (21)$$

From this expression we can find the voltage at tap 2 when slider B coincides with it, by putting α equal to zero. This voltage must therefore represent one of the points on the function being generated. This voltage is given by

$$V_{2b} = V_2 + \beta(2V_2 - V_1 - V_3) \quad . \quad . \quad . \quad (22)$$

where

$$\beta = \frac{2R_p}{R_Y} \frac{\left(1 - \frac{2R_z}{R_z + R}\right)}{\left(1 + \frac{R_Y}{R_p}\frac{R_z}{R_z + R}\right)}$$

Similar equations can be obtained for V_{1b} and V_{3b}, the voltages at tap 1 and tap 3 when slider B coincides with these taps. Expressing the higher-order differences of these voltages (V_{1b}, V_{2b}, V_{3b}, etc.) as derivatives, the following series can be derived from these equations:

$$(V_1 + V_3 - 2V_2) = \frac{d^2V_{2b}}{dx^2} + \beta\frac{d^4V_{2b}}{dx^4} + \beta^2\frac{d^6V_{2b}}{dx^6} + \ldots \quad (23)$$

$$(V_3 - V_2) = (V_{3b} - V_{2b}) + \beta\frac{d^3V_{(2-3)}}{dx^3} + \beta^2\frac{d^5V_{(2-3)}}{dx^5} \quad (24)$$

where subscript 2–3 refers to a value between that at tap 2 and tap 3.

Using eqns. (22), (23) and (24), and also further equations for the differences $(V_2 - V_1)$ and $(V_4 - V_3)$, eqn. (21) can be rewritten in terms of the above derivatives. In order that the coefficient of the second derivative in this expression shall be that of the Taylor's series, R_p must be chosen so that

$$R_p = R\frac{R}{(2R_z + R)}\left(1 + \frac{2R_z}{R_z + R}\right) + \frac{R_z^2}{2R_z + R} \quad . \quad (25)$$

in which case eqn. (21) reduces to

$$V_b \simeq V_{2b} + \alpha\left(\frac{dV_{2b}}{dx}\right) + \frac{\alpha^2}{2}\left(\frac{d^2V_{2b}}{dx^2}\right)$$

$$- \frac{(\alpha - \alpha^2)}{2}\left[\alpha\frac{d^3V_{(2-3)}}{dx^3} + \beta\frac{d^4V_{2b}}{dx^4} + \ldots\right] \quad . \quad (26)$$

which gives the first three terms of the Taylor's series correctly.

621.319.7.011.4

The Institution of Electrical Engineers
Monograph No. 325
Jan. 19

THE CALCULATION OF THE ELECTRIC FIELD IN A SPHERE-GAP BY MEANS OF DIPOLAR CO-ORDINATES

By Professor G. W. CARTER, M.A., Member, and S. C. LOH, B.Sc., Ph.D., Student.

(*The paper was first received* 3*rd September, and in revised form* 29*th October*, 1958. *It was published as an* INSTITUTION MONOGRAPH *in January*, 1959.)

SUMMARY

The problem of calculating the electric field in a sphere-gap, usually attacked by means of an infinite series of image charges, is here approached through the direct solution of Laplace's equation. This solution is obtained in dipolar co-ordinates, which are suitable for problems in which boundary conditions are specified on two non-intersecting spherical surfaces. The result is given as an infinite series, from which is derived a curve, universally applicable, for the maximum voltage gradient in the field between two equal spheres. The alternative method of solution by image charges is briefly outlined for comparison.

(1) INTRODUCTION

The electric field in a sphere-gap has been investigated by a number of writers, including Kelvin,[1] Kirchhoff,[2] Maxwell[3] and Alexander Russell.[4,5] They concentrated chiefly on the calculation of the coefficients of capacity and induction, and employed the method of images, which led to a solution in the form of an infinite series. The possibility of an alternative solution by means of dipolar co-ordinates was pointed out by Kelvin,[6] and the coefficients of capacity and induction were calculated in these terms by Jeffery.[7]

In the present-day application of the sphere-gap as a voltage-measuring device, the maximum value of the electric field intensity is a quantity of more importance than the capacitance. It is calculated in the paper with the aid of dipolar co-ordinates, a method which is shown to lead to a more convenient form of solution than is obtained by the method of images.

(2) DIPOLAR CO-ORDINATES

The co-ordinate system known as dipolar co-ordinates is obtained by the rotation of two orthogonal systems of coaxal circles about the line of symmetry which passes through the (real) limiting points of one system[7] (Fig. 1). If the cylindrical polar co-ordinates of a point are ρ (radial), z (axial), and χ (azimuth angle), the dipolar co-ordinates (u, v, w) are related with (ρ, z, χ) by the equations

$$\left.\begin{aligned} u + jv &= \log_\varepsilon \frac{\rho + j(z+a)}{\rho + j(z-a)} \\ w &= \chi \end{aligned}\right\} \quad \ldots\ldots \quad (1)$$

from which

$$\left.\begin{aligned} \rho &= \frac{a \sin v}{\cosh u - \cos v} \\ z &= \frac{a \sinh u}{\cosh u - \cos v} \\ \chi &= w \end{aligned}\right\} \quad \ldots\ldots \quad (2)$$

Dipolar co-ordinates are closely analogous to the toroidal co-ordinates discussed in another paper by the present authors;[8] the latter are obtained by rotating the same system of coaxal circles about their other axis of symmetry.

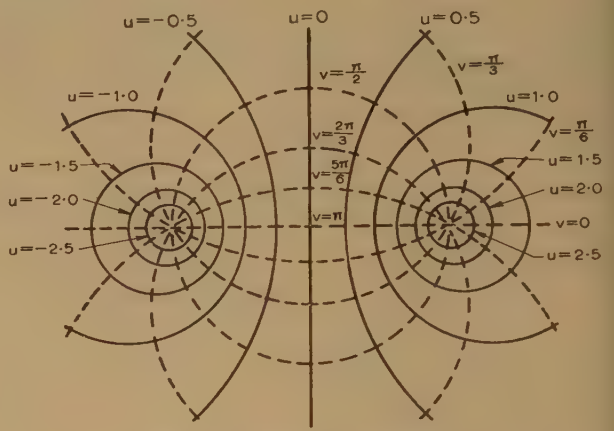

Fig. 1.—Dipolar co-ordinates.

The surfaces u = (a constant) are seen to be a series of non-intersecting coaxal spheres. The origin and the value of a can be so chosen that any two given non-intersecting spheres are included in the system. The relevance of dipolar co-ordinates to the sphere-gap problem is evident.

When a point is displaced so that its co-ordinates change by δu, δv, δw, its linear displacements in the three co-ordinate directions are δs_u, δs_v, δs_w, where

$$\left.\begin{aligned} \delta s_u &= \frac{a\delta u}{\cosh u - \cos v} \\ \delta s_v &= \frac{a\delta v}{\cosh u - \cos v} \\ \delta s_w &= \frac{a \sin v \delta w}{\cosh u - \cos v} \end{aligned}\right\} \quad \ldots\ldots$$

If r is the radius of any sphere of the system and d the distance of its centre from the origin,

$$\left.\begin{aligned} r &= \frac{a}{|\sinh u|} \\ d &= a \coth u \end{aligned}\right\} \quad \ldots\ldots$$

(3) SOLUTION OF LAPLACE'S EQUATION

The potential, ϕ, of an electrostatic field must satisfy the differential equation known as Laplace's equation, which must be expressed, for purposes of solution, in terms of the co-ordinates appropriate to the problem in hand. In the present case Laplace's equation takes the form

$$\frac{\partial}{\partial u}\left(\frac{\sin v}{\cosh u - \cos v}\frac{\partial \phi}{\partial u}\right) + \frac{\partial}{\partial v}\left(\frac{\sin v}{\cosh u - \cos v}\frac{\partial \phi}{\partial v}\right) = 0 \quad \ldots$$

The co-ordinate w does not appear, since we are solely concerned with problems having cylindrical symmetry.

The substitution

$$\phi = \psi (\cosh u - \cos v)^{1/2} \quad \ldots\ldots$$

Correspondence on Monographs is invited for consideration with a view to publication.

Professor Carter is, and Dr. Loh was formerly, in the Electrical Engineering Department, Leeds University. Dr. Loh is now with the National Research Council of Canada.

educes eqn. (5) to

$$\frac{\partial^2\psi}{\partial u^2}+\frac{\partial^2\psi}{\partial v^2}+\cot v\frac{\partial\psi}{\partial v}-\tfrac{1}{4}\psi=0 \quad . \quad . \quad . \quad (7)$$

Let $\psi = UV$, where U and V are respectively functions of u and v only. Eqn. (7) now becomes

$$\frac{1}{U}\frac{d^2U}{du^2}+\frac{1}{V}\left(\frac{d^2V}{dv^2}+\cot v\frac{dV}{dv}-\tfrac{1}{4}V\right)=0$$

and since the first term cannot contain v and the second cannot contain u, both must be constants, and can therefore be written as $+(n+\frac{1}{2})^2$ and $-(n+\frac{1}{2})^2$ respectively. Thus the separate equations for U and V are

$$\frac{d^2U}{du^2}-(n+\tfrac{1}{2})^2U=0 \quad . \quad . \quad . \quad . \quad . \quad (8)$$

and

$$\frac{d^2V}{dv^2}+\cot v\frac{dV}{dv}+n(n+1)V=0 \quad . \quad . \quad . \quad (9)$$

Write μ for $\cos v$; eqn. (9) then reduces to

$$(1-\mu^2)\frac{d^2V}{d\mu^2}-2\mu\frac{dV}{d\mu}+n(n+1)V=0 \quad . \quad . \quad (10)$$

which is the best-known form of Legendre's equation. The solution is expressed as

$$V=aP_n(\mu)+bQ_n(\mu) \quad . \quad . \quad . \quad . \quad (11)$$

Here $P_n(\mu)$ and $Q_n(\mu)$ are known as Legendre functions of order n, of the first and second kind. A particular solution of eqn. (5) may therefore be written as

$$\phi=(\cosh u-\cos v)^{1/2}[A\cosh(n+\tfrac{1}{2})u+B\sinh(n+\tfrac{1}{2})u]$$
$$[aP_n(\mu)+bQ_n(\mu)] \quad . \quad (12)$$

We shall find that, for physical applications, it is sufficient to confine our attention to integral values of n. Moreover, the solution corresponding to $n=-(m+1)$ is identical in form with that corresponding to $n=+m$. It will therefore be sufficient to consider only positive integral values of n, and we may write the general solution for the potential as

$$\phi=(\cosh u-\cos v)^{1/2}\sum_{n=0}^{\infty}[A_n\cosh(n+\tfrac{1}{2})u$$
$$+B_n\sinh(n+\tfrac{1}{2})u]\times[a_nP_n(\mu)+b_nQ_n(\mu)] \quad . \quad (13)$$

The function ϕ and its first differential coefficients must be finite and continuous at all points of the field except at those which correspond to some special physical conditions such as a source or a charge. $P_n(\mu)$ is finite and continuous for all real values of v, but $Q_n(\mu)$ becomes infinite when $v=0$ or π, and hence cannot occur in the expression for ϕ which is to hold throughout the region, including any point on the axis of z. It is to such cases that we confine our attention in the paper, so that

$$\phi=(\cosh u-\cos v)^{1/2}\sum_{n=0}^{\infty}[A_n\cosh(n+\tfrac{1}{2})u$$
$$+B_n\sinh(n+\tfrac{1}{2}u]P_n(\cos v) \quad . \quad (14)$$

(4) MAXIMUM VOLTAGE GRADIENT IN A SPHERE-GAP

The sphere-gap may be used in two distinct ways: as a symmetrical gap, in which the spheres carry equal and opposite charges and are at equal and opposite potentials to earth, and as an unsymmetrical gap, in which one sphere is earthed. The theories of these two must be considered separately.

(4.1) The Symmetrical Gap

The surfaces $u=u_1$, $u=-u_1$ (where $u_1>0$) are equal, non-intersecting spheres, and will be taken as the electrodes. The potential ϕ is constant over each of these spheres, and will be taken as $+V/2$ on $u=u_1$ and $-V/2$ on $u=-u_1$. ϕ will be of the form

$$\phi=(\cosh u-\cos v)^{1/2}\sum_{n=0}^{\infty}B_n\sinh(n+\tfrac{1}{2})uP_n(\cos v) \quad . \quad (15)$$

from which, writing $u=u_1$,

$$\frac{V}{2}(\cosh u_1-\cos v)^{-1/2}=\sum_{n=0}^{\infty}B_n\sinh(n+\tfrac{1}{2})u_1P_n(\cos v) \quad . \quad (16)$$

The left-hand side of this equation may be written

$$\frac{V}{\sqrt{2}}\varepsilon^{-u_1/2}(1-2\varepsilon^{-u_1}\cos v+\varepsilon^{-2u_1})^{-1/2}$$
$$=\frac{V}{\sqrt{2}}\sum_{n=0}^{\infty}\varepsilon^{-(n+\frac{1}{2})u_1}P_n(\cos v) \quad . \quad (17)$$

since $u_1>0$. Equating the coefficients of $P_n(\cos v)$, we obtain the value of B_n, and the potential function then becomes

$$\phi=\frac{V}{\sqrt{2}}(\cosh u-\cos v)^{1/2}\sum_{n=0}^{\infty}\varepsilon^{-(n+\frac{1}{2})u_1}\frac{\sinh(n+\frac{1}{2})u}{\sinh(n+\frac{1}{2})u_1}P_n(\cos v)$$
$$. \quad . \quad . \quad . \quad . \quad (18)$$

We are chiefly interested in the maximum value of the voltage gradient at the surface of the spheres. Since u is constant on those surfaces, the gradient E_u is $-\partial\phi/\partial s_u$, where δs_u is given by eqns. (3); i.e.

$$E_u=-\left(\frac{\cosh u-\cos v}{a}\right)\frac{\partial\phi}{\partial u}$$

The maximum is on the line $v=\pi$, where

$$E_u=-\left(\frac{1+\cosh u}{a}\right)\frac{\partial\phi}{\partial u} \quad . \quad . \quad . \quad . \quad (19)$$

Evaluating this by differentiating eqn. (18), we find, when $u=u_1$,

$$E_{max}=\frac{V}{a}\cosh^2\frac{u_1}{2}\sum_{n=0}^{\infty}(-1)^n\varepsilon^{-(n+\frac{1}{2})u_1}$$
$$\times\left[\sinh\frac{u_1}{2}+(2n+1)\coth(n+\tfrac{1}{2})u_1\cosh\frac{u_1}{2}\right] \quad . \quad (20)$$

Eqn. (20) may be simplified as follows. Since the series $\sum_{n=0}^{\infty}(-1)^n\varepsilon^{-(u+\frac{1}{2})u_1}$ is a geometrical progression, it may be proved that

$$\sum_{n=0}^{\infty}(-1)^n\varepsilon^{-(n+\frac{1}{2})u_1}=\frac{1}{2\cosh\frac{u_1}{2}} \quad . \quad . \quad . \quad (21)$$

whence, by differentiation,

$$\sum_{n=0}^{\infty}(-1)^n(2n+1)\varepsilon^{-(n+\frac{1}{2})u_1}=\frac{\sinh\frac{u_1}{2}}{2\cosh^2\frac{u_1}{2}} \quad . \quad . \quad (22)$$

The summation in eqn. (20) is equivalent to

$$\sum_{n=0}^{\infty}(-1)^n\varepsilon^{-(n+\frac{1}{2})u_1}\left\{\sinh\frac{u_1}{2}+(2n+1)\cosh\frac{u_1}{2}\right.$$
$$\left.\times\left[-1+\frac{\varepsilon^{(n+\frac{1}{2})u_1}}{\sinh(n+\frac{1}{2})u_1}\right]\right\}$$

and eqns. (21) and (22) enable this to be reduced to

$$\sum_{n=0}^{\infty}(-1)^n\frac{(2n+1)\cosh\frac{u_1}{2}}{\sinh(n+\frac{1}{2})u_1}$$

so that $$E_{max}=\frac{V}{a}\cosh^3\frac{u_1}{2}\sum_{n=0}^{\infty}(-1)^n\frac{(2n+1)}{\sinh(n+\frac{1}{2})u_1} \quad . \quad (23)$$

A more rapidly convergent expression is obtained by using the identity

$$\frac{1}{\sinh\theta}\equiv 2\sum_{m=0}^{\infty}\varepsilon^{-(2m+1)\theta}$$

which transforms eqn. (23) into

$$E_{max}=\frac{2V}{a}\cosh^3\frac{u_1}{2}\sum_{n=0}^{\infty}\sum_{m=0}^{\infty}(-1)^n(2n+1)\varepsilon^{-(2m+1)(n+\frac{1}{2})u_1}$$

Performing the summation in n with the aid of eqn. (22) we obtain

$$E_{max}=\frac{V}{a}\cosh^3\frac{u_1}{2}\sum_{m=0}^{\infty}\frac{\sinh(m+\frac{1}{2})u_1}{\cosh^2(m+\frac{1}{2})u_1} \quad . \quad . \quad (24)$$

This expression tends to infinity as the spacing of the spheres tends to zero ($d\to r$, or $a\to 0$, $u_1\to 0$). It is therefore desirable to plot the ratio E_{max}/E_{mean}, where $E_{mean}[=V/2(d-r)]$ is the mean voltage gradient between the spheres along the line joining their points of nearest approach. From eqns. (4),

$$E_{mean}=\frac{V}{2a}\coth\frac{u_1}{2}$$

Therefore

$$\frac{E_{max}}{E_{mean}}=2\sinh\frac{u_1}{2}\cosh^2\frac{u_1}{2}\sum_{m=0}^{\infty}\frac{\sinh(m+\frac{1}{2})u_1}{\cosh^2(m+\frac{1}{2})u_1} \quad . \quad (25)$$

(4.2) The Unsymmetrical Gap

The solution in this case has the form

$$\phi=(\cosh u-\cos v)^{1/2}\sum_{n=0}^{\infty}C_n\sinh[(n+\tfrac{1}{2})(u+u_1)]P_n(\cos v) \quad . \quad . \quad . \quad . \quad (26)$$

which makes $\phi=0$ when $u=-u_1$. The coefficients C_n are obtained by writing $\phi=V$ and $u=u_1$, the method being similar to that employed for the symmetrical gap; the result is

$$\phi=\sqrt{2}V(\cosh u-\cos v)^{1/2}\sum_{n=0}^{\infty}\varepsilon^{-(n+\frac{1}{2})u_1}\times\frac{\sinh[(n+\frac{1}{2})(u+u_1)]}{\sinh(2n+1)u_1}P_n(\cos v) \quad . \quad (27)$$

The charge on the sphere of potential V exceeds that on the earthed sphere, since some of the flux from the former will terminate on charges on 'earth'. Thus the point of maximum voltage gradient will occur on the sphere $u=u_1$. By the method already used, we obtain

$$E_{max}=\frac{2V}{a}\cosh^2\frac{u_1}{2}\sum_{n=0}^{\infty}(-1)^n\varepsilon^{-(n+\frac{1}{2})u_1}\times\left[\sinh\frac{u_1}{2}+(2n+1)\coth(2n+1)u_1\cosh\frac{u_1}{2}\right] \quad . \quad (28)$$

This corresponds with eqn. (20) derived for the symmetrical gap. Pursuing the same algebraic process as before, we can reduce eqn. (28) to

$$E_{max}=\frac{2V}{a}\cosh^3\frac{u_1}{2}\sum_{m=0}^{\infty}\frac{\sinh(2m+\frac{1}{2})u_1}{\cosh^2(2m+\frac{1}{2})u_1} \quad . \quad . \quad (29)$$

whence

$$\frac{E_{max}}{E_{mean}}=4\sinh\frac{u_1}{2}\cosh^2\frac{u_1}{2}\sum_{m=0}^{\infty}\frac{\sinh(2m+\frac{1}{2})u_1}{\cosh^2(2m+\frac{1}{2})u_1} \quad . \quad (3$$

It will be observed that the terms in the series in eqn. (30) a the even terms in the series in eqn. (25).

The ratio E_{max}/E_{mean} is plotted in Fig. 2 as a function spacing/sphere diameter, for each form of gap.

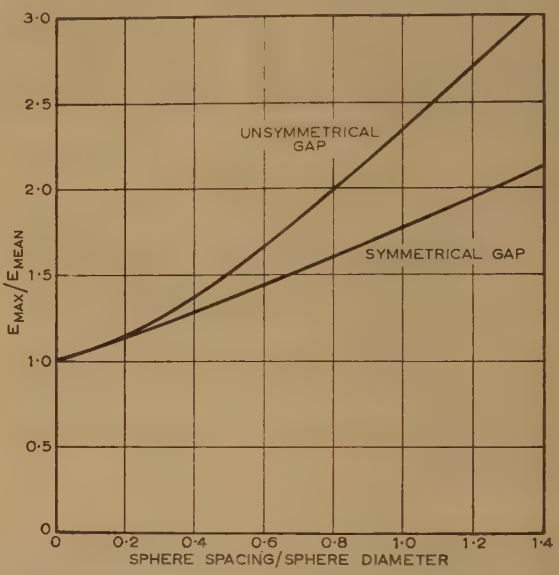

Fig. 2.—Maximum voltage gradient, equal spheres.

(5) SOLUTION BY THE METHOD OF IMAGES

The details of this method are given in textbooks on electr magnetism,[9] so only an outline is necessary here.

If S is a spherical surface of radius r, having its centre at point O, and q is a point charge at a distance $l(>r)$ from it is possible to make S into an equipotential surface by placi a charge $-qr/l$ at the point on the line Oq which is distant r^2 from O. This point is called the 'inverse point' of the poi where q is located, and the charge $-qr/l$ is an 'inverse charge'.

Consider now a pair of spherical surfaces S_1 and S_2, havi radii r_1, r_2 and centres at O_1, O_2, the distance O_1O_2 being (Fig. 3). We shall find a system of charges which will ma

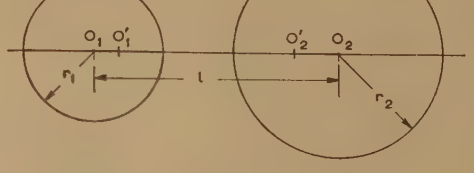

Fig. 3.—Image charges in spheres.

the potentials of S_1, S_2, uniform and equal to V and zero respe tively. A charge of $(4\pi\varepsilon_0 r_1)V$, placed at O_1, will raise S_1 potential V, but S_2 is not an equipotential in its field; to ma it so, a charge $-(4\pi\varepsilon_0 r_1)Vr_2/l$ must be placed at O_2', dista r_2^2/l from O_2. This disturbs the potential of S_1, necessitating t placing of an inverse charge to the last-named at O_1', the inver point of O_2' with respect to the surface S_1.

The process is non-terminating, but the successive ima charges diminish, so that a finite number of terms will give

Table 1

Sphere S_1		Sphere S_2	
Charge	Distance from O_1	Charge	Distance from O_2
1	0	$-\frac{r_2}{l}$	$\frac{r_2^2}{l} = l_2$
$\frac{r_1 r_2}{l(l-l_2)}$	$\frac{r_1^2}{l-l_2} = l_1'$	$\frac{-r_1 r_2^2}{l(l-l_1')(l-l_2)}$	$\frac{r_2^2}{l-l_1'} = l_2'$
$\frac{r_1^2 r_2^2}{l(l-l_1')(l-l_2)(l-l_2')}$	$\frac{r_1^2}{l-l_2'} = l_1''$	$\frac{-r_1^2 r_2^3}{l(l-l_1')(l-l_1'')(l-l_2)(l-l_2')}$	$\frac{r_2^2}{l-l_1''} = l_2''$
. . .	. . .	. . .	. . .
$\frac{r_1^n r_2^n}{l(l-l_1')\ldots[l-l_1^{(n-1)}]\times(l-l_2)\ldots[l-l_2^{(n-1)}]}$	$\frac{r_1^2}{l-l_2^{(n-1)}} = l_1^{(n)}$	$\frac{-r_1^n r_2^{n+1}}{l(l-l_1')\ldots[l-l_1^{(n)}]\times(l-l_2)\ldots[l-l_2^{(n-1)}]}$	$\frac{r_2^2}{l-l_1^{(n)}} = l_2^{(n)}$

sufficient approximation to the field. The relative values of the successive charges, and their locations, are given in Table 1.

As an example, Table 2 gives the numerical values for the case $r_1 = r_2 = 10\,\text{cm}$, $l = 40\,\text{cm}$.

Table 2

Sphere S_1		Sphere S_2	
Charge	Distance from O_1	Charge	Distance from O_2
1	0	−0·2500	2·500
0·0667	2·667	−0·0179	2·679
0·0048	2·680	−0·0013	2·680
0·0003	2·680	−0·0001	2·680

The totals of the charges in the two columns, when multiplied by $(4\pi\varepsilon_0 r_1)V$, are the charges which appear on the two spheres when S_1 is raised to potential V while S_2 is earthed. Thus the figures as they stand refer to an unsymmetrical gap; from them the maximum voltage gradient may be calculated, and it will be found that $E_{max}/E_{mean} = 2{\cdot}34$. For the symmetrical gap it is necessary to superimpose two unsymmetrical charge systems, namely S_1 raised to potential $V/2$ with S_2 earthed, and S_2 raised to potential $-V/2$ with S_1 earthed. The result is quickly deducible from the tabulated figures, and it is found that $E_{max}/E_{mean} = 1{\cdot}77$. These figures agree with values derived from eqns. (30) and (25) respectively.

(6) CONCLUSIONS

The solution by the method of images, given above, is not in a general form and must be performed afresh for each new set of values of r_1, r_2, l. Several of the writers cited have generalized it and converted it into various forms of infinite series, adapted (as has been stated) to the calculation of capacitance coefficients. Doubtless the method of images could also yield an expression for the voltage gradient in series form. The use of dipolar co-ordinates, however, leads directly to such a form [eqns. (25) or (30)], and one, moreover, which proves convenient in calculation.

The physical process of sparkover in a sphere-gap is a complex one,[10] and the sparkover voltage is consequently not related to the voltage gradient in a simple manner. Nevertheless, the process of sparkover is initiated at the most intense part of the field; the calculation of the voltage gradient is therefore of some importance.

(7) ACKNOWLEDGMENTS

The authors wish to express their gratitude to Professor B. Hague of Glasgow University for his encouragement and helpful criticism in the preparation of the paper; also to Mr. Michael Erdei for assistance in the computation.

(8) REFERENCES

(1) Lord Kelvin: 'On the Mutual Attraction or Repulsion between Two Electrified Spherical Conductors', Reprint of Papers on Electrostatics and Magnetism, 2nd edition (Macmillan, 1884), p. 88.

(2) Kirchhoff, G.: 'Ueber die Vertheilung der Elektricität auf Zwei Leitenden Kugeln', Gesammelte Abhandlungen (Barth, Leipzig, 1882), p. 78.

(3) Maxwell, J. Clerk: 'A Treatise on Electricity and Magnetism', 3rd edition (Clarendon Press, Oxford, 1892) vol. I, p. 270.

(4) Russell, A.: 'The Coefficients of Capacity and the Mutual Attractions or Repulsions of Two Electrified Spherical Conductors when Close Together', *Proceedings of the Royal Society*, A, 1909, **82**, p. 524.

(5) Russell, A.: 'The Capacity Coefficients of Spherical Electrodes', *Proceedings of the Physical Society*, 1911, **23**, p. 352.

(6) Lord Kelvin: 'Extraits de deux lettres addressées à M. Liouville par M. William Thomson', Reprint of Papers on Electrostatics and Magnetism, p. 146.

(7) Jeffery, G. B.: 'On a Form of the Solution of Laplace's Equation suitable for Problems relating to Two Spheres', *Proceedings of the Royal Society*, A, 1912, **87**, p. 109.

(8) Carter, G. W., and Loh, S. C.: 'The Approximate Calculation of the Electric Field between a Rod and a Concentric Ring by means of Toroidal Functions', *Proceedings I.E.E.*, Monograph No. 247 M, June, 1958 (**105** C, p. 13).

(9) Jeans, J. H.: 'The Mathematical Theory of Electricity and Magnetism' (Cambridge University Press, 1951), p. 196.

(10) Meek, J. M., and Craggs, J. D.: 'Electrical Breakdown of Gases' (Clarendon Press, Oxford, 1953), p. 251.

621.372.5

The Institution of Electrical Engineers
Monograph No. 326
Jan. 195

A NEW SYNTHESIS PROCEDURE FOR TWO-TERMINAL-PAIR NETWORKS USING THE SYMMETRICAL LATTICE STRUCTURE

By S. S. FORTE, B.Sc., Ph.D., Graduate.

(*The paper was first received* 26*th November*, 1955, *in revised form* 17*th June and* 29*th September, and in final form* 10*th November*, 1958. *It was published as an* INSTITUTION MONOGRAPH *in January*, 1959.)

SUMMARY

A new synthesis procedure for the realization of 2-terminal-pair networks without ideal transformers is given. A new theorem is formulated concerning the necessary and sufficient conditions to be satisfied by a prescribed set of impedance or admittance functions for it to be realized as a symmetrical lattice network with series impedances (or shunt admittances) at either end of the structure, without ideal transformers.

A numerical example is included to illustrate the synthesis procedure.

SYMBOLS AND DEFINITIONS

z_{11}, z_{22}, z_{12} = Driving-point and transfer open-circuit impedances of 2-terminal-pair.

Z = Driving-point impedance.

$r_{11}, r_{22}, r_{12}, R$ = Real parts of z_{11}, z_{22}, z_{12} and Z, respectively, on the boundary.

$\mathscr{R}f(j\omega)$ = Real part of $f(\lambda)$ on the boundary.

$p_{11}, p_{22}, p_{12}, p_z$ = Residues of any poles of z_{11}, z_{22}, z_{12} and Z, respectively, on the boundary.

ω = Angular frequency.

λ = The complex frequency variable $v + j\omega$.

The boundary.—The complex frequency variable is defined as $v + j\omega$. Network behaviour in terms of zeros and poles can be depicted on an Argand diagram, with v as the real axis, and $j\omega$ as the imaginary axis. This forms the complex frequency plane, and the imaginary axis is known as the boundary.

p.r. function.—A positive real function, i.e. one whose real part is $\geqslant 0$ for all real frequencies (i.e. everywhere on the boundary), which has no poles to the right of the boundary, and in which poles occurring on the boundary are simple with positive residues. A necessary and sufficient condition for the realizability of a driving-point impedance (or admittance) function is that it be positive real.

(1) INTRODUCTION

Gewertz[1] first gave the necessary and sufficient conditions for the realization of a 2-terminal-pair network containing all three kinds of network element. This realization involves the use of ideal transformers which are not physically realizable, and suffers from the disadvantage of introducing infinite quantities into an otherwise finite system. A considerable body of research has been and is being conducted to try to exclude the ideal transformer from the synthesis of 2-terminal-pair networks; this has been directed along two main channels, namely

(*a*) The special cases of networks containing only two kinds of element (Darlington,[2] Fialkow and Gerst,[3] Talbot[4] and others).

(*b*) The synthesis starting from prescribed transfer or insertion function rather than the complete set of driving-point and transfer functions (Darlington, Weinberg[5] and others).

A new solution is offered in the paper for the synthesis of a prescribed impedance or admittance matrix as a simple structure without ideal transformers; the necessary and sufficient conditions for this realization are formulated. Because of their relative simplicity, these conditions are readily applied to a prescribed set of functions to determine whether or not a realizable solution exists, before any lengthy computation need be undertaken.

(2) THE SYNTHESIS PROCEDURE

In order to realize a symmetrical network from an unsymmetrical set of functions, it is necessary to extract series impedances in the case of an impedance family, or shunt admittances in the case of an admittance family, at either end of the network so that the resultant set of functions is symmetrical. The entire work which now follows is on an impedance basis, but all remarks and results apply equally to admittances.

The necessary and sufficient conditions for the realizability of such a network, with reference to Fig. 1, are that the required

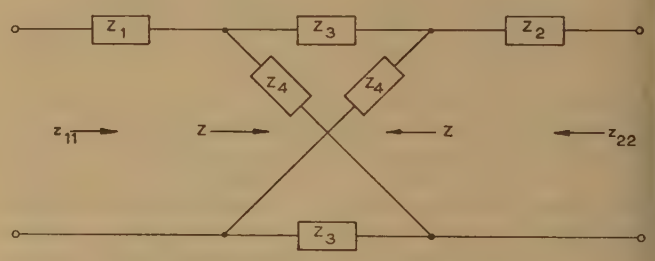

Fig. 1.—Schematic of 2-terminal-pair network.

arbitrary function Z (the open-circuit driving-point impedance of the symmetrical network) is so chosen that

$$\left.\begin{aligned} Z_1 &= z_{11} - Z \\ Z_2 &= z_{22} - Z \\ Z_3 &= Z - z_{12} \\ Z_4 &= Z + z_{12} \end{aligned}\right\} \quad \ldots\ldots \quad (1)$$

and all are p.r. functions. It follows that, irrespective of the choice of the arbitrary function Z, necessary conditions for the realization of the lattice are

$$\left.\begin{aligned} z_{11} \pm z_{12} &\text{ must be p.r.} \\ z_{22} \pm z_{12} &\text{ must be p.r.} \end{aligned}\right\} \quad \ldots\ldots \quad (2)$$

This implies that, for all real frequencies, ω,

$$\left.\begin{aligned} r_{11} \pm r_{12} &\geqslant 0 \\ r_{22} \pm r_{12} &\geqslant 0 \end{aligned}\right\} \quad \ldots\ldots \quad (3)$$

Correspondence on Monographs is invited for consideration with a view to publication.

Dr. Forte is with Marconi's Wireless Telegraph Co., Ltd.

nd that at any pole on the boundary the residues satisfy

$$\left.\begin{aligned} p_{11} \pm p_{12} &\geqslant 0 \\ p_{22} \pm p_{12} &\geqslant 0 \end{aligned}\right\} \quad \ldots\ldots \quad (4)$$

ondition (4) need be considered only for poles on the boundary hich are common to z_{11} and z_{12} and/or to z_{22} and z_{12}, for any ole in z_{11} or z_{22} not contained in z_{12} can be extracted as a eries reactive network at the appropriate end of the structure, rior to the application of the synthesis procedure.

In the discussion which follows it is assumed that the extraction f any such poles has been effected and that the functions under onsideration will be the remainder functions.

The arbitrary function Z must first be determined. The real art of Z $(=R)$ must be chosen so that the real parts of the riving-point impedances of the component branches of the net- ork be positive for all real frequencies. Thus, R must be hosen so as to satisfy, for all real frequencies,

$$\left.\begin{aligned} R &\geqslant 0 \\ r_{11} - R &\geqslant 0 \\ r_{22} - R &\geqslant 0 \\ R - r_{12} &\geqslant 0 \\ R + r_{12} &\geqslant 0 \end{aligned}\right\} \quad \ldots\ldots \quad (5)$$

It follows that if r_{11}, say, contains a real frequency zero, e.g. $\omega^2 - \omega_1^2)^2$, then R must contain the same zero factor and will enerally be of form $R_1(\omega^2 - \omega_1^2)^2$. However, unless $(\omega^2 - \omega_1^2)^2$ s also a factor of r_{12}, conditions (5) will not be satisfied.

If conditions (3) are observed, however, this will always e the case, for if either r_{11} or r_{22} has a zero at some real requency $\omega = \omega_1$, then r_{12} must of necessity have a zero of t least the same order at $\omega = \omega_1$. It is therefore evident that value of R can always be found to lead to a realizable network f, for all real frequencies,

$$\left.\begin{aligned} R &\geqslant |r_{12}| \\ R &\leqslant r_{11} \\ R &\leqslant r_{22} \end{aligned}\right\} \quad \ldots\ldots \quad (6)$$

where $|r_{12}|$ is defined as the magnitude of r_{12} over the frequency ange.

After plotting r_{11}, r_{22} and $|r_{12}|$ as functions of ω^2, the arbitrary unction R can be represented by any curve lying between the imits given by conditions (6), and can be determined as a ational function of ω^2 by any suitable method of approximation.

Using Gewertz's method, for example, Z' is determined as a .r. function in λ from the real part of $R(\omega^2)$.

Z' derived in this manner contains no boundary poles. It is herefore necessary to add poles on the boundary to Z' so as to atisfy at each boundary pole of z_{11} and z_{12} and/or z_{22} and z_{12} he residue conditions

$$\left.\begin{aligned} p_{11} - p_z &\geqslant 0 \\ p_{22} - p_z &\geqslant 0 \\ p_z \pm |p_{12}| &\geqslant 0 \end{aligned}\right\} \quad \ldots\ldots \quad (7)$$

aking $p_z = |p_{12}|$ at every boundary pole ensures that condi- ions (7) are satisfied, with the residues in the poles of one of he functions Z_3 or Z_4 vanishing each time, thereby reducing the umber of elements required.

The derived function Z, consisting of Z' with added boundary oles, will therefore satisfy conditions (1), so that, so long as onditions (2) are observed, a realizable solution is always ossible. Conditions (2) are therefore both necessary and ufficient, and a new theorem can therefore be formulated, as ollows:

Theorem.—The necessary and sufficient conditions for a set of driving-point and transfer impedance or admittance functions f_{11}, f_{22} and f_{12} to be realizable as a 2-terminal pair network without ideal transformers, consisting of a symmetrical lattice network with series reactances or shunt susceptances at either end of the structure, are

$f_{11} \pm f_{12}$ must be p.r.
$f_{22} \pm f_{12}$ must be p.r.

(3) CONCLUSION

A new synthesis procedure has been described for prescribed impedance or admittance matrices, leading to a realizable structure without ideal transformers. Use of the Bott and Duffin[6] synthesis procedure, for example, for the driving-point impedances of the component branches of the structure will lead finally to a realization entirely free of mutual coupling.

(4) ACKNOWLEDGMENTS

The paper forms part of the work for a thesis[7] accepted by the University of Leeds in 1955 for the degree of Doctor of Philosophy. The author wishes to express his gratitude to Dr. G. S. Brayshaw, of the Electrical Engineering Department at the university, for his continued assistance and encouragement, and to the Chief of Research, Marconi's Wireless Telegraph Co., Ltd., for permission to publish the paper.

(5) REFERENCES

(1) GEWERTZ, C. M.: 'Synthesis of a Finite 4-Terminal Network', *Journal of Mathematics and Physics*, 1933, **12**, p. 1.
(2) DARLINGTON, S.: 'Synthesis of Reactance Fourpoles which produce prescribed Insertion-Loss Characteristic', *ibid.*, 1939, **18**, p. 257.
(3) FIALKOW, A. D., and GERST, I.: 'The Transfer Function of Networks without Mutual Reactance', *Quarterly of Applied Mathematics*, 1954, **12**, p. 117.
(4) TALBOT, A.: 'A New Method of Synthesis of Reactance Networks', *Proceedings I.E.E.*, Monograph No. 77 R, 1953 (**101**, Part IV, p. 73).
(5) WEINBERG, L.: 'A General *RLC* Synthesis Procedure', *Convention Record of the Institute of Radio Engineers*, 1953, **1**, Part 5, p. 2.
(6) BOTT, R., and DUFFIN, R. J.: 'Impedance Synthesis without the use of Transformers', *Journal of Applied Physics*, 1929, **20**, p. 816.
(7) FORTE, S. S.: 'The Synthesis of Electrical Networks to Satisfy Prescribed Conditions', Ph.D. Thesis, Leeds University, 1955.

(6) APPENDIX: ILLUSTRATIVE NUMERICAL EXAMPLE

Prescribed functions:

$$z_{11} = \frac{6\lambda^3 + 15\lambda^2 + 15\lambda + 6}{\lambda^2 + 2\lambda + 2}$$

$$z_{22} = \frac{9\lambda^3 + 24\lambda^2 + 24\lambda + 3}{\lambda^2 + 2\lambda + 2}$$

$$z_{12} = \frac{4\lambda^3 + 10\lambda^2 + 10\lambda - 2}{\lambda^2 + 2\lambda + 2}$$

The real parts are then obtained as

$$r_{11} = \frac{3\omega^4 - 6\omega^2 + 12}{\omega^4 + 4}$$

$$r_{22} = \frac{6\omega^4 - 3\omega^2 + 6}{\omega^4 + 4}$$

$$r_{12} = \frac{2\omega^4 + 2\omega^2 - 4}{\omega^4 + 4}$$

These functions obey the necessary and sufficient conditions given in the new theorem, so that the synthesis can proceed.

Fig. 2 shows r_{11}, r_{22} and $|r_{12}|$ as functions of ω^2. The function

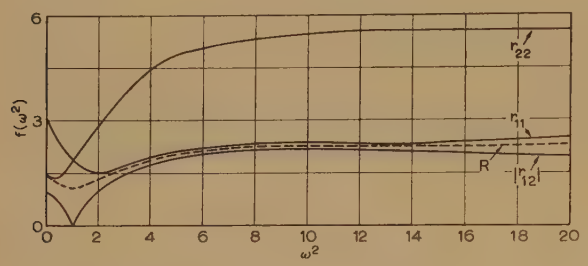

Fig. 2.—r_{11}, r_{22} and $|r_{12}|$ as functions of ω^2.

$R(\omega^2)$ must fit between the curves in any manner satisfying conditions (6). As shown by the broken curve in Fig. 2, the function

$$R(\omega^2) = \frac{\frac{21}{8}\omega^4 - 3\omega^2 + 6}{\omega^4 + 4}$$

is found to satisfy the requirements.

The corresponding p.r. impedance function is readily determined by Gewertz's method as

$$Z' = \frac{3}{8}\,\frac{7\lambda^2 + 7\lambda + 8}{\lambda^2 + 2\lambda + 2}$$

The poles of z_{11}, z_{22} and z_{12} on the boundary must be added. There is only one pole, and therefore a pole $p_z = |p_{12}| = 4\lambda$ is added. Whence

$$Z = 4\lambda + \frac{3}{8}\,\frac{7\lambda^2 + 7\lambda + 8}{\lambda^2 + 2\lambda + 2}$$

The driving-point impedance of the component 2-terminal networks are determined as

$$Z_1 = 2\lambda + \frac{3}{8}\,\frac{\lambda^2 + \lambda + 8}{\lambda^2 + 2\lambda + 2}$$

$$Z_2 = 5\lambda + \frac{3}{8}\,\frac{9\lambda^2 + 9\lambda}{\lambda^2 + 2\lambda + 2}$$

$$Z_3 = \frac{1}{8}\,\frac{5\lambda^2 + 5\lambda + 40}{\lambda^2 + 2\lambda + 2}$$

$$Z_4 = 8\lambda + \frac{1}{8}\,\frac{37\lambda^2 + 37\lambda + 8}{\lambda^2 + 2\lambda + 2}$$

Z_1–Z_4 are readily shown to be p.r. functions, and can be realized as 2-terminal networks without mutual inductance using the Bott and Duffin synthesis procedure, for instance, so that the synthesis is complete, leading to a realization entirely free of mutual coupling.

DISCUSSION ON

'THE STATISTICAL BASIS OF IMPULSE TESTING'*

Mr. W. Baumann (*Germany: communicated*): In Section 8, the author states that rather large errors can occur with small numbers of trials. This may be correct statistically, but it does not give the right impression of the accuracy that is normal in impulse testing.

It should not be overlooked that the ultimate result desired in a test is a measure of the impulse voltage. We would like to know, therefore, the probable, or otherwise defined, error in this measurement of the voltage for a given flashover probability. It can be inferred from the paper that the steepness of the probability/impulse-voltage curve determines this because with a steep curve, for example, great errors in probability are associated with small errors in voltage. I have investigated this matter in some detail for the 50% flashover voltage† and have found that in almost all practical cases the error is $\leqslant 4\%$. The point may be illustrated by reference to Fig. 5 of Dr. Lewis's paper, which shows the probability of breakdown as a function of impulse voltage for sphere-gaps. Curve (*d*), which is by far the most unfavourable for my argument, shows that a determination of the 50% flashover voltage of the test object with only 10 applied impulses would be unlikely to result in 5 flashovers at a voltage less than 95 kV or greater than 115 kV. Since the 50% flashover voltage is about 105 kV, the maximum possible error in voltage is obviously about 10%, and in fact calculation gives a smaller value than this. For the test object corresponding to curve (*a*), the error in a measured 50% flashover voltage (or any other voltage level) would be almost negligible compared with other errors, since the whole dispersion of voltage between the 0% and 100% levels is only about 1% of the 50% value.

* Lewis, T. J.: Monograph No. 249 M, July, 1957 (see 105 C, p. 27).
† Baumann, W.: *Electrotechnische Zeitschrift* (A), 1957, 11, p. 369.

Dr. T. J. Lewis (*in reply*): Dr. Baumann's comments may be summarized in the following way:

If, for a particular test object, ΔV is the range of voltage required to change the probability of impulse breakdown from zero to unity, then the error in determining the 50% breakdown probability on the voltage scale (or indeed any other point except 0% or 100%) must be less than $\Delta V/\bar{V}$, where $\bar{V}$ is the 50% point. If ΔV is very small or $\bar{V}$ large, it is meaningless to inquire about the 50% point, because the voltage error will always be satisfactorily small at *any* point. This result does not require any statistical argument. As Dr. Baumann has shown, the flashover of a simple high-voltage spark-gap in air is in this category.

Consider, however, a more general case not confined to high-voltage spark-gaps in air, to which Section 8 of the paper is meant to apply. Suppose that p as a function of voltage is unknown for a particular object. There is no *a priori* way of knowing whether $\Delta V/\bar{V}$ is small or large, and therefore no immediate way of knowing what the maximum error on the voltage scale might be. If a test is performed by making N trials which result in S_N breakdowns, the apparent value of p for that voltage is S_N/N and, Section 8 permits the accuracy of this determination, i.e. the error $S_N/N - p$, to be estimated. For any N, the error is always greatest when $p = 0{\cdot}5$, i.e. estimated values of p from S_N/N can be taken with greater confidence as p moves away from the 50% point.

Not only is the width ΔV important in these matters, but dp/dV, the slope of the probability curve, also influences the result, as reference to a previous discussion† will show.

† *Proceedings I.E.E.*, 1958, 105 C, p. 553.

DISCUSSION ON

'ON THE AMPLIFICATION FACTOR OF A TRIODE VALVE: PART 2'*

Prof. F. G. Heymann (*South Africa: communicated*): It appears that the penultimate set of equations in Section 5 should read as follows:

$$\delta V_A = \delta Q/C_{GA} = C_{GB}\delta V_G/C_{GA}$$

$$C_{GA} = 1\Big/\left(2\log_e \frac{a}{R}\right)$$

From this follows the amplification factor:

$$\mu = C_{GB}/C_{GA}$$

This factor is therefore dimensionless and is not the product of two capacitances as derived in the paper.

A more serious criticism relates to Sections 2 and 3. The calculations in Section 2 indicate that amplification factor μ decreases with increase in g, but the author states that the opposite is indicated. This error is repeated in Section 3 in an attempt to explain the behaviour of the experimental triode. Contrary to the author's claim, therefore, the theory of a previous paper† fails to explain the measured variation of μ.

It seems that the approximate theory† is only valid when g is large compared with S. When g is small, some other approach is called for since the grid no longer acts as an almost complete shield between anode and cathode but only controls electron motion near the grid wires. Midway between grid wires the grid will have little control so that reduced amplification factor is to be expected with reduced grid-to-cathode spacing.

Several ordinary triodes exhibit variations of μ similar to those found by Prof. Moullin, and it seems that a reasonable test of the theory will only be possible if a special triode is used with guard anodes to eliminate end-effects.

* Moullin, E. B.: Monograph No. 270 R, December, 1957 (105 C, p. 196.)

† Moullin, E. B.: 'On the Amplification Factor of the Triode', *Proceedings I.E.E.*, Monograph No. 211 R, November, 1956 (104 C, p. 222).

DISCUSSION ON

'CONDITIONS FOR THE IMPEDANCE AND ADMITTANCE MATRICES OF *n*-PORTS WITHOUT IDEAL TRANSFORMERS'*

Mr. P. R. Bryant (*communicated*): I should like first to point out three small errors in Dr. Cederbaum's Monograph. The first occurs in Section 6. Condition (*b*) of Theorem (i) should read: '(*b*) In each column of Q there occurs either a single non-zero element (+1 or −1) or one +1 and one −1'.

The second error also occurs in Section 6: the form of eqn. (12) is incorrect; it should be

$$C = [I, R] = [I, L'(K^{-1})'] \quad . \quad . \quad . \quad (A)$$

The third error occurs in the second paragraph of Section 8. The condition that the network should remain planar 'if all the *n*-ports are short-circuited' is rather ambiguous. This condition should be that the network remains planar *if n fictitious branches are connected, one between the terminals of each port.*

The following theorem concerning necessary and sufficient conditions for an impedance matrix of a resistive *n*-port is similar to Cederbaum's.

THEOREM

The necessary and sufficient condition for an $n \times n$ matrix Z of real numbers, to be the impedance matrix of a resistive *n*-port is that Z should be of the form

$$Z = S'G^{-1}S \quad . \quad . \quad . \quad . \quad . \quad . \quad (B)$$

where (*a*) S is of order $(\tau - 1) \times n$ for some τ satisfying $(n + 1) \leqslant \tau \leqslant 2n$, and is a submatrix of a $(\tau - 1) \times (\tau - 1)$ reduced-incidence matrix K of a tree.

(*b*) G is a $(\tau - 1) \times (\tau - 1)$ non-singular 'dominant matrix'† having non-positive off-diagonal elements.

We require the following lemma:

Lemma.—The admittance matrix of a resistive *n*-port, every port having a common terminal, is a non-singular dominant matrix having non-positive off-diagonal elements.

Proof.—If the network contains only $(n + 1)$ nodes, the matrix in question is in fact the nodal-admittance matrix of the network, and the property is well known for such matrices.[A,B] If the network contains more than $(n + 1)$ nodes, star-mesh transformations on those nodes which are not being used as accessible terminals will give us an equivalent network containing only $(n + 1)$ nodes. The result then follows from the first part.

PROOF OF THEOREM

Necessity.—Let the *n*-port be described on τ accessible terminals. Then

$$(n + 1) \leqslant \tau \leqslant 2n \quad . \quad . \quad . \quad . \quad . \quad (C)$$

If each port is represented by a fictitious branch, the resulting set of *n* fictitious branches must be *part* of a tree-like structure T, say, of $(\tau - 1)$ fictitious branches on the set of τ terminals. Let the reduced-incidence matrix of T be the $(\tau - 1) \times (\tau - 1)$ matrix K. Then the *n*-ports will define a $(\tau - 1) \times n$ submatrix S, say, of K. Let us suppose that current $(I_1 + I_2 + \ldots + I_{\tau-1})$ is extracted from the reference terminal, currents $I_1, I_2, \ldots, I_{\tau-1}$ being injected at the remaining $(\tau - 1)$ terminals. Let the resulting potentials of the terminals relative to the reference terminal, be $V_1, V_2, \ldots, V_{\tau-1}$. Denote by I and V the corresponding $(\tau - 1) \times 1$ column vectors, and suppose that

$$I = GV \quad . \quad . \quad . \quad . \quad . \quad . \quad . \quad (D)$$

Then by the lemma, G is a non-singular dominant matrix having non-positive off-diagonal terms. Let the port currents and voltages be denoted by the $n \times 1$ column vectors i and v. Then

$$v = S'V \quad . \quad . \quad . \quad . \quad . \quad . \quad . \quad (E)$$

and

$$I = Si \quad . \quad . \quad . \quad . \quad . \quad . \quad . \quad (F)$$

Hence, from eqns. (E), (D) and (F),

$$v = S'V = S'G^{-1}I = (S'G^{-1}S)i \quad . \quad . \quad . \quad (G)$$

Sufficiency.—G satisfies the well-known necessary and sufficient conditions to be the nodal admittance matrix of a resistive network containing τ nodes.[A,B] Realize this resistive network and define on the τ nodes a set of n independent ports by means of the $(\tau - 1) \times n$ matrix S. By considerations similar to those used in the necessity part of the proof, the impedance matrix of this *n*-port will be $(S'G^{-1}S)$, as required.

REFERENCES

(A) BOXALL, F. S.: 'Synthesis of Multiterminal Two-Element Kind Networks', Technical Report No. 95, Electronics Research Laboratory, Stanford University, November 1955.

(B) SLEPIAN, P., and WEINBERG, L.: 'Synthesis Applications of Paramount and Dominant Matrices' (to be published).

Dr. I. Cederbaum (*in reply*): The first two remarks of Mr. Bryant are correct. With respect to his third remark, the following may be said: from the topological point of view, short-circuiting of a port by an impedanceless connection is identical with connecting a fictitious branch between the terminals of the port. However, short-circuiting of a port may alternatively be interpreted as identifying the nodes of the network on which the port is described. With this interpretation the condition on page 24 is wrong. Thus, I think, the expression proposed by Mr. Bryant '. . . if *n* fictitious branches are connected, one between the terminals of each port', should be preferred.

There is another small error which I find in my paper. The system I of Section 5 consists of $(f + s)$ links of $\bar{N}$ and not of $(b + s)$.

Mr. Bryant's theorem is very interesting. My only criticism is directed against the wording of the lemma. The latter is correct under the tacit assumption that the port voltage V_k is defined as the voltage rise from the common terminal to terminal k for every port of the *n*-port, this being implicit in its use for the proof of Bryant's theorem. However, if for some ports V_k is defined as the voltage rise and for others as the voltage drop, then the corresponding admittance matrix, being always dominant, may well have positive off-diagonal elements.[B]

* CEDERBAUM, I.: Monograph No. 276 R, January, 1958 (see 105 C, p. 245).

† Following Slepian and Weinberg,[B] we call a matrix of real numbers a 'dominant matrix' if the following conditions hold:

(*a*) The matrix is square and symmetric.

(*b*) Each element on the main diagonal is not less than the sum of the absolute values of all the other elements in the same row.

† See Section 2, Theorem (ii), of the Monograph.

PROCEEDINGS OF
THE INSTITUTION OF ELECTRICAL ENGINEERS

PART C—MONOGRAPHS, MARCH 1959

CONTENTS

Bibliographical References.—It is requested that bibliographical reference to an Institution paper should always include the serial number of the paper and the month and year of publication, which will be found at the top right-hand corner of the first page of the paper. This information should precede the reference to the Volume and Part.

Example.—SMITH, J.: 'Reflections from the Ionosphere', *Proceedings, I.E.E.*, Paper No. 3001 R, December, 1954 (102 B, p. 1234).

Published by The Institution, Savoy Place, London, W.C.2. *Telephone:* Temple Bar 7676. *Telegrams:* 'Voltampere, Phone, London.'
Printed by Unwin Brothers Limited, Woking and London.